Phase Domain Modelling and Simulation of Large-scale Power Systems with VSC-based FACTS Equipment

By
César Angeles-Camacho

B.Eng. Instituto Tecnológico de Morelia, México, 1992
M.Sc. Instituto Tecnológico de Morelia, México, 2000

A Thesis submitted to the
Department of Electronics and Electrical Engineering
of
The University of Glasgow
For the degree of Doctor of Philosophy

March 2005

Blank Page

Abstract

The commercial use of electricity began in the late 1870's when arc lamps were used for lighthouse illumination and street lighting. The first complete electric power system (comprising a generator, cable, fuse, meter and loads) was built in 1882. This was the beginning of what would develop into one of the largest industries in the world. Nowadays electrical power systems worldwide vary in size and structure. However, they all have the same basic characteristics: they are three-phase AC systems operating at constant voltage and frequency. Generation and transmission facilities use three-phase equipment. Industrial loads are invariably three-phase; single-phase residential and commercial loads are distributed among the phases so as to try to keep the three-phase system as well balanced as possible. Nevertheless, a perfect balancing is impossible to achieve owing to the asymmetrical nature of the power network due to electromagnetic and electrostatic coupling between transmission lines, unbalanced loads and transformers.

Most of the analysis techniques available for planning and operation of multiphase power systems are based upon the assumption that the network operates under perfectly balanced conditions. The advantage of this assumptions from the modelling viewpoint is that only one phase of the three phase system needs to be considered for analysis, resulting in a reduced size of the problem at hand. However, the phase frame of reference offers a more general representation for the solution of power system problems than the frame of reference provided by the sequences. The former can accommodate networks containing any degree of unbalance whilst the latter is only applicable to power networks exhibiting perfect or near-perfect impedance balance between phases.

The thesis reports on the development of steady state and time domain models of Flexible AC Transmission System (FACTS) controllers in the natural framework of electric systems, i.e. namely the phase co-ordinates domain. The FACTS equipment selected for analytical development in this research are: the static synchronous compensator (STATCOM), the static synchronous series compensator (SSSC), the unified power flow controller (UPFC) and the high-voltage direct current (HVDC). These power electronics-based controllers have the voltage source converter as their main constituent. The combined solution of both steady state and dynamic power flow equations pertaining to the VSC-based FACTS controllers and the power network are fully described in the thesis.

The steady-state mathematical models of VSC-based FACTS controllers are formulated in nodal form using the frame of reference of the phases. Guidelines for their implementation into two distinct power flows algorithm namely, the Newton-Raphson in polar co-ordinates and the Newton-Raphson in rectangular coordinates are given. For the purpose of long-term dynamic assessment, a simultaneous solution using implicit trapezoidal integration method with Newton iteration is used to solve the set of differential-algebraic equations of generating plants and network components. In order to assess both the steady state and the dynamic behaviour of the models developed, a comprehensive, newly developed integrated software environment is used.

A mis padres quienes me han enseñado el valor del trabajo y la dedicación.

A mis hermanos por todo su apoyo durante estos años lejos de ustedes, disculpas por no estar a su lado.

A mi esposa Angélica por todo el amor, su ilimitada paciencia, comprensión y ayuda durante estos años de trabajo y sacrificios: sin ti no lo hubiera logrado, te amo.

A mi hija Leti a quien agradezco el animo que me da el solo verla crecer cada día, gracias; También gracias por ser la compañera de mama durante estos años y gracias por ayudarme a olvidarme de mis problemas cuando estas conmigo.

A todo ustedes, como podré compensarlos por el tiempo que no les dedique durante esto años?

Acknowledgements

The Consejo Nacional de Ciencia y Tecnología of México (CONACYT) is gratefully acknowledgement for the financial support provided to the overall research project.

I would like to thank to my supervisor Prof. Enrique Acha, he has supervised me form the very first day at Glasgow. He taught me how to look at thinks and cope with problems in a different way. I am most grateful for all his efforts, time, patient and many other thinks that I may have missed now, but chiefly I would express many thanks for his sincere friendship.

I would also thank my examiners Prof. Malcolm Irving (Brunel University) and Dr. David Dorrell (University of Glasgow) for valuable comments, fruitful discussions and for persistently revising the manuscript.

I greatly appreciate the many fruitful talks and helpful suggestions from my colleges; I have enjoyed the working environment at the power systems group at the department of electronic and electrical engineering and extend my thanks to its entire staff.

Finally, I would like to thank to the Glaswegian people for the hospitality and friendly treat to my family and myself.

Table of Contents

Abstract iii
Acknowledgements v
Table of Contents vi
List of Figures xi
List of Tables xiv
Symbols xv
Subscripts and superscripts xvi
Abbreviations xviii

Chapter 1 Introduction

1.1 Overview 1
1.2 Objectives of the Project 2
1.3 Motivation 3
1.4 Achievements 3
1.5 Publications 5
1.6 Outline of the Thesis 6
1.7 References 7

Chapter 2 Modelling of VSC-based FACTS Controllers and Conventional Power System Components in Phase Domain

2.1 Introduction 9
2.2 Phase-domain Modelling Philosophy 11
2.2.1 Conventional element models of an electrical power system 11
2.3 Controllers Based on Conventional Thyristors 12
2.4 Power Electronic Controllers Phased on Fully Controlled Semiconductor Devices 12
2.5 The Voltage Source Converter 13
2.5.1 Principles of VSC operation 15
2.5.2 The Static Synchronous Compensator 16
2.6 The Static Synchronous Series Compensator 18
2.7 The Unified Power Flow Controller 19
2.8 The High Voltage Direct Current based on Voltage Source Converters 21
2.9 Control Capabilities of VSC-based Controllers 22

2.10 Summary 24
2.11 References 24

Chapter 3 Phase-domain Power Flows Polar Co-ordinates Frame of Reference Including VSC-based FACTS

3.1 Introduction 27
3.2 General Phase-domain Power Flows 27
3.2.1 Power Flow equations 29
3.2.2 Newton-Raphson power flow algorithm 30
3.2.3 Three-Phase numerical example 32
3.3 Static Synchronous Compensator 37
3.3.1 Power flow equations 38
3.3.2 Linearised system of equations 38
3.3.3 STATCOM three-phase numerical example 40
3.4 Static Synchronous Series Compensation 43
3.4.1 Power flow model 43
3.4.2 Linearised system of equations 44
3.4.3 SSSC Three-Phase Numerical Example 47
3.5 Unified Power Flow Controller 49
3.5.1 Power flow model 50
3.5.2 Numerical example of power flow control using a UPFC 54
3.6 High-Voltage Direct Current VSC-based 56
3.6.1 Power flow model 57
3.6.2 Numerical example of power flow control using a HVDC VSC-based 59
3.7 Effective Initialisation of VSC-based FACTS Controllers 61
3.7.1 UPFC modelling 61
3.7.2 SSSC modelling 62
3.8 Summary 62
3.9 References 63

Chapter 4 Phase-domain Power Flows Rectangular Co-ordinates Frame of Reference Including VSC-based FACTS Controllers

4.1 Introduction 66

4.2 Power Flows using Rectangular Co-ordinates 66
4.2.1 Power flow equations 67
4.2.2 Form the Jacobian matrix 68
4.2.3 Voltage controlled bus 70
4.3 Static Synchronous Compensator 71
4.3.1 Reactive power flow model 72
4.4 Static Synchronous Series Compensation 75
4.4.1 Power flow model 75
4.4.2 Linearised system of equations 75
4.5 Unified Power Flow Controller 77
4.5.1 Power flow model 78
4.6 High-Voltage Direct Current VSC-based 80
4.6.1 Power flow model 81
4.7 Evaluation of Power Flow Algorithms in Polar and Rectangular Co-ordinates Including FACTS VSC-based Controllers 83
4.8 Solution of Large-scale Multiphase Power Network with Embedded VSC-based FACTS Controllers 86
4.8.1 IEEE 118-node system 86
4.8.2 New England test system 87
4.9 Summary 92
4.10 References 92

Chapter 5 Dynamic Phase-domain Modelling of Power Plant Components

5.1 Introduction 95
5.2 Power System Stability 95
5.3 Dynamic Modelling Philosophy 97
5.4 Power Plant Components Dynamic Modelling 98
5.4.1 Synchronous generator model 99
5.4.2 Automatic voltage regulator model 102
5.4.3 Governor model 103
5.4.4 Turbine model 105
5.5 Power System Components Dynamic Models 106
5.6 Dynamic Power Flow Algorithm 107
5.7 Differential Equations Discretization 107

5.7.1 Synchronous generator 109
5.7.2 Automatic voltage regulator 114
5.7.3 Governor 115
5.7.4 Steam turbine 116
5.8 Dynamic Power Flow Formulation 118
5.8.1 Jacobian matrix formation 119
5.8.2 Mismatch vector 120
5.9 Power Disturbances and Network Topological Changes 122
5.10 Case Studies for Dynamic Power Flows 122
5.11 Load Related Transient Events 123
5.12 Unbalance Load Disturbance 127
5.13 Transmission Line Outages 131
5.14 Unbalanced Transmission Lines Events 135
5.15 Generator Transients Events 139
5.16 Summary 143
5.17 References 143

Chapter 6 Dynamic Phase-domain Modelling of VSC-based FACTS Controllers

6.1 Introduction 146
6.2 Static Synchronous Compensator 146
6.2.1 Voltage magnitude control using STACTCOMs in dynamic power flows 148
6.3 Static Synchronous Series Compensator 153
6.3.1 Power flow control using SSSCs in dynamic power flows 154
6.4 High-Voltage Direct Current VSC-based 159
6.4.1 Power flow control using an HVDC-VSC 161
6.5 Unified Power Flow Controller 166
6.6 Dynamic Power Flow Analysis of a Larger Multiphase Power Systems with VSC-based Controllers 168
6.7 Summary 170
6.8 References 170

Chapter 7 Conclusions and Future Work

7.1 Conclusions 172

7.2 Future Work 173

Appendix I Mathematical Derivation of Active and Reactive Power Equations

I.1 Conventional Power Plant Components 175

I.1.1 Polar co-ordinates 175

I.1.2 Rectangular co-ordinates 178

I.2 FACTS devices power equations 181

I.2.1 Polar co-ordinates 181

I.2.2 Rectangular co-ordinates 183

Appendix II Networks Test Data

II.1 Five-bus System Test 186

II.2 New England Reduced System Test 186

II.3 IEEE 57 Buses System Test 188

Appendix III Jacobian Matrix Elements

III.1 Unified Power Flow Controller 191

III.2 High-voltage Direct Current VSC-based 193

III.3 Unified Power Flows Controller 194

III.4 High-voltage Direct Current VSC-based 197

Appendix IV Jacobian Matrix Elements

IV.1 Implicit Trapezoidal Integration Method with Newton Iteration 199

List of Figures

Figure 1.1 Integrated software for the electronic control of large-scale power systems 4

Figure 2.1 A simplified one-line diagram of a power system [3] 10

Figure 2.2 Circuit symbols for: (a) GTO; (b) IGBT 12

Figure 2.3 Topology of a three-phase, two-level VSC using IGBTs 14

Figure 2.4 Basic VSC operation: (a) VSC connected to a system bus; Space vector representation for (b) Lagging operation and (c) Leading operation 15

Figure 2.5 STATCOM system: (a) VSC connected to the AC network via a shunt-connected transformer; (b) Shunt solid-state voltage source 17

Figure 2.6 SSSC system: (a) VSC connected to the AC network using a series transformer; (b) Series solid-state voltage source 18

Figure 2.7 UPFC system: (a) Two back-to-back VSCs with one VSC connected to the AC network using a shunt transformer and the second VSC connected to the AC network using a series transformer; (b) Equivalent circuit based on solid state voltage sources 20

Figure 2.8 HVDC-VSC system: (a) The VSC at the sending end performs the role of rectifier and the VSC at the receiving end performs the role of inverter; (b) Equivalent circuit 22

Figure 2.9 Phasor diagram illustrating the general concept of: (a) Magnitude voltage control; (b) Impedance line compensation; (c) Phase angle regulation; and (d) Simultaneous control 23

Figure 3.1 Three-phase transmission line 28

Figure 3.2 Five-bus test network and power flow results 33

Figure 3.3 Three-phase power flows, (a) phase *a*, (b) phase *b*, and (c) phase *c* 36

Figure 3.4 Three-phase STATCOM equivalent circuit 37

Figure 3.5 STATCOM upgraded test network and power flows 42

Figure 3.6 Three-phase SSSC equivalent circuit 43

Figure 3.7 SSSC upgraded test network and power flow 48

Figure 3.8 Three-phase UPFC equivalent circuit 49

Figure 3.9 UPFC upgraded test network and power flow 55

Figure 3.10 Three-phase HVDC VSC-based equivalent 57

Figure 3.11 HVDC upgrade test network and power flows 60

Figure 4.1 Convergence rate for (a) active and (b) reactive power absolute mismatches in both polar and rectangular co-ordinates 85

Figure 4.2 Nodal voltage profile in the 118-node IEEE test system 87

Figure 4.3 New England test network 88

Figure 4.4 Network voltage profile 89

Figure 4.5 Transmission lines power flows, sending end 91
Figure 5.1 Classification of power system stability 97
Figure 5.2 Power plant block diagram [12] 99
Figure 5.3 Diagram of the power balance of a generator 100
Figure 5.4 Synchronous machine: (a) Schematic representation and (b) equivalent five winding model 101
Figure 5.5 Automatic Voltage Regulator block diagram 102
Figure 5.6 Steam turbine block diagram 103
Figure 5.7 Hydro governor block diagram 104
Figure 5.8 Steam turbine; (a) System configuration, (b) approximate linear model ... 105
Figure 5.9 Simple linear model for hydro turbines 106
Figure 5.10 Dynamic power flow algorithm 108
Figure 5.11 Generator equivalent circuit 109
Figure 5.12 Generating plant responses to a three-phase load disturbance; (a) frequency; (b) load angle difference; (c) excitation voltage; (d) active power 124
Figure 5.13 Generating plant responses to a three-phase load disturbance; (a) governor power; steam turbine (b) HP; (c) IP; (d) LP 125
Figure 5.14 Nodal voltage responses of the system to a three-phase load disturbance; (a) magnitude; (b) phase angle 126
Figure 5.15 Generating plant variable responses due to an unbalanced loading condition; (a) frequency; (b) load angle; (c) excitation voltage; (d) electrical active power 128
Figure 5.16 Generating plant variable responses due to an unbalanced loading condition; (a) governor power; steam turbine (b) HP; (c) IP; (d) LP 129
Figure 5.17 Three-phase nodal voltage in the system for the case of an unbalanced three-phase load disturbance; (a) magnitude; (b) phase angle 130
Figure 5.18 Generating plant response of the system to a line outage; (a) frequency; (b) load angle; (c) excitation voltage; (d) active power 132
Figure 5.19 Generating plant response of the system to a line outage; (a) governor power; steam turbine (b) HP; (c) IP; (d) LP 133
Figure 5.20 System nodal voltages for the case of a three-phase transmission line outage; (a) magnitude and (b) phase angle 134
Figure 5.21 Generating plants responses due to an unbalanced transmission line disturbance; (a) frequency; (b) load angle; (c) excitation voltage; (d) active power 136
Figure 5.22 Generating plants responses due to an unbalanced transmission line disturbance; (e) governor power; steam turbine (f) HP; (g) IP; (h) LP 137
Figure 5.23 System nodal voltages for the case of an unbalanced transmission line disturbance; (a) magnitude and (b) phase angle 138

Figure 5.24 Generating plants responses to a generator disturbance; (a) frequency; (b) load angle; (c) excitation voltage; (d) active power 140
Figure 5.25 Generating plants responses to a generator disturbance; (a) governor power; steam turbine (b) HP; (c) IP; (d) LP 141
Figure 5.26 Nodal voltage of the system following a generator disturbance; (a) magnitude and (b) phase angle..... 142
Figure 6.1 STATCOM linear model for voltage magnitude control 147
Figure 6.2 Generating plant responses of the system with one STATCOM; (a) frequency; (b) load angle; (c) excitation voltage; (d) active power..... 150
Figure 6.3 Generating plant responses of the system with one STATCOM; (a) governor power; steam turbine (b) HP; (c) IP; (d) LP 151
Figure 6.4 Nodal voltage responses of the system with one STATCOM; (a) magnitude and (b) phase angle..... 152
Figure 6.5 STATCOM internal parameters following a load disturbance; voltage (a) magnitude; (b) phase angle and (c) reactive power 153
Figure 6.6 SSSC linear model for active and reactive power flow control 154
Figure 6.7 Generating plant responses of the system with a SSSC embedded; (a) frequency; (b) load angle; (c) excitation voltage; (d) active power..... 156
Figure 6.8 Generating plant responses of the system with a SSSC embedded; (a) governor power; steam turbine (b) HP; (c) IP; (d) LP 157
Figure 6.9 Nodal voltage responses of the system with a SSSC embedded; (a) magnitude and (b) phase angle..... 158
Figure 6.10 SSSC parameter responses to a load disturbance; Voltage (a) magnitude and (b) phase angle..... 159
Figure 6.11 HVDC-VSC block diagram for (a) inverter and (b) rectifier converter..... 160
Figure 6.12 Generating plant responses of the system with a BTB HVDC embedded; (a) frequency; (b) load angle; (c) excitation voltage; (d) electrical active power..... 163
Figure 6.13 Generating plant responses of the system with a BTB HVDC embedded; (a) governor power; steam turbine (b) HP; (c) IP; (d) LP..... 164
Figure 6.14 Nodal voltage responses of the system with HVDC-VSC embedded; (a) magnitude and (b) phase angle..... 165
Figure 6.15 VSCs parameters to a load tripped out; voltage (a) magnitude; (b) phase angle and (c) reactive power..... 166
Figure 6.16 Block diagram of (a) shunt-connected and (b) series connected converters of the UPFC controller 167
Figure 6.17 Frequency responses of generating plants in the system IEEE57-buses system 169
Figure 6.18 Nodal voltage magnitude in the system IEEE57-buses system..... 169

List of Tables

Table.3.1 Three-phase nodal voltages for the balanced case 34

Table 3.2 Five-bus unbalance loading ∓ 34

Table 3.3 Three-phase nodal voltages in the unbalanced network-phase voltages 35

Table 3.4 Nodal voltage in the three-phase unbalanced network with a STATCOM – phase voltages 41

Table 3.5 Nodal voltage in the three-phase unbalanced network with a SSSC – phase voltages 47

Table 3.6 Nodal voltages in the three-phase unbalanced network with a UPFC – phase voltages 54

Table 4.1 CPU times in seconds 84

Table 4.2 Source voltages in the IEEE118-node system 86

Table 4.3 Power flow exchange between the two subsystems 90

Table 4.4 Internal voltage sources parameters 90

Symbols

B	Susceptance
C	Capacitance
Deg.	Degrees
E	Controlled voltage or source voltage
e	Real component voltage
f	Imaginary component voltage
G	Conductance
I	Complex current
I	Magnitude current
j	Complex operator $\sqrt{-1}$
L	Inductance
m_a	Amplitude modulation ratio
nb	Number of buses
P	Active power
p.u.	Per unit
Q	Reactive power
S	Complex power
V	Nodal complex voltage
V	Magnitude voltage
X	Reactance
Y	Admittance
Z	Impedance
Δ	A small change in...
δ	Phase angle voltage in source voltage
θ_s	Nodal angles phase voltage
γ	Phase angle current

Dynamic Power Flows

D	Damping coefficient
E	Excitation voltage or voltage behind the generator's impedance
E_{fd}	Applied voltage
F_{HP}	HP turbine power fraction
F_{IP}	IP turbine power fraction

F_{LP}	LP turbine power fraction
f_0	Synchronous frequency
I_d	Direct axis current
I_q	Quadrature axis current
K_A	Excitation gain
K	Governor gain
M	Inertia moment
P_e	Electrical power of the generator
P_{m}	Equivalent generator input mechanical power
r	Armature resistance
$T_{d0}^{'}$	Open-circuit field transient time constant
T_{CH}	Steam chest time constant (including the high pressure (HP) stage of the turbine time constant)
T_{RH}	Re-heater time constant (including the intermediate-pressure (IP) stage of the turbine time constant)
T_{CO}	Steam storage of the cross-over time constant (including the low-pressure (LP) stage of the turbine time constant)
T_c	Governor time constant
T_{W}	Water time constant
T_{vR}	Transient time constant
T_{cR}	Transient time constant
V_t	Terminal voltage of phase
V_{ref}	Pre-specified reference voltage
x_d	Direct reactance
x_q	Quadrature axis reactance

Subscripts and superscripts

0	Initial value of...
a, b, c	The three phases of the power system
cal	Calculated value of...
cR	Series-connected converter
d	Direct axis
DC	Direct current value of...
GV	Governor value of...
Im	Imaginary component or reactive component
it	Iteration

k, l, m	Buses
max	Maximum value of...
min	Minimum value of ...
q	Quadrature axis
r	Receiving end
Re	Real or resistive component
ref	Reference value of...
s	Sending end
set	Set point of...
sp	Specified value of...
t	Time
T	Transpose of...
vR	Shunt-connected converter
x	Reactive component
ρ	Phase quantities
*	Complex conjugation

Abbreviations

AC	Alternating Current
AVR	Automatic voltage regulators
BTB	Back-to-back arrangement
CIGRÉ	International council on large electric systems
DC	Direct current
D-Statcom	Distribution static synchronous compensator
DVR	Dynamic voltage restorer
ETAP®	Electrical transient analyzer program
FACTS	Flexible AC transmission Systems
GTO	Gate-turn off thyristor
HP	Steam high pressure stage
HVDC	High voltage direct current
HVDC-VSC	High-voltage direct current-voltage source converter
IASTED	The international association of science and technology for development
IEE	The institution of electrical engineers
IEEE	Institute of electrical and electronics engineers
IGBT	Insulated gate bipolar transistor
IP	Steam inter-mediate pressure stage
kHz	Kilo hertz (equal to one cycle per second)
kW	Kilo watts
LP	Steam low pressure stage
OLTC	On-load-changing transformer
OOP	Object oriented philosophy
PWM	Pulse-width modulation
SSR	Sub-synchronous resonance's
SSSC	Static synchronous series compensator
STATCOM	Static synchronous compensator
SVC	Static VAR controllers
TCSC	Thyristor-controlled series compensator
UPFC	Unified power flow controller
VAR	Volt-ampere reactive
VSC	Voltage source converter

Chapter 1

INTRODUCTION

1.1 Overview

The electric power industry is undergoing major technological and organizational changes. The increasing presence of cost-effective, small and flexible power generating plants, customer automation, electronic control and the revolutionary changes in communications and computing all offer possibilities for safer and more economically run electric power systems. At the same time, the industry has moved from a top-down, system-wide decision making into active, decentralized decision-making [1].

Such a pace of change presents power systems control engineers and designers with the need to revise the methods by which the system is operated today and to develop control paradigms more amenable to a decentralized operation.

The key objective of power system control is to balance time-varying load demand so that the power at the customer side is of sufficiently high quality and largely independent of system disturbances. The quality of the AC power is measured with respect to variations in voltage magnitude and frequency of its sinusoidal waveform. More recently, the increased presence of higher-order harmonics in the basic sinusoidal waveform of voltage, current and instantaneous power have also become problems of much concern [2,3].

Flexible AC Transmission Systems (FACTS) controllers introduce additional degrees of freedom to control power flow over desired transmission routes, enabling secure loadings of transmission lines up to their thermal capacities. They also provide a more effective utilisation of available generation and prevent outages from spreading to wider areas. A **FACTS controller** is a power electronic-based system, which provides control of one or more AC transmission system parameters [1,4-6].

The thyristor, the gate-turn off thyristor (GTO) and the insulated gate bipolar transistor (IGBT) are key basic components of the FACTS technology. High current, high voltage power semiconductors and control engineering have had a profound effect on electric power transmission over the last three decades. Example areas include high-voltage direct current (HVDC) and Static Var Compensator (SVC) installations. Thanks to the experience gained in the construction, design and operation of this technology, there has been rapid progress in the deployment and operation of FACTS controllers [4-13].

Owing to the rapid development and general acceptance of FACTS technology as means of alleviating a host of long standing operational problems in the electrical power network, the open literature has become populated with FACTS-oriented research work. However, most of the research reported on FACTS has been oriented to modelling and

simulation of power systems operating under steady-state and balanced conditions. The assessment of electromechanical oscillations of FACTS-upgraded power networks has also received attention but limited to balanced operation.

As far as this author is aware, the more complex task of modelling the network and FACTS controllers in the phase frame of reference, where equipment and operational imbalances can be explicitly represented, has been left, to large extent, unattended. Only preliminary work on modelling of FACTS controllers in the phase domain has been reported [14-16]. The research work presented in this thesis gives a comprehensive and systematic treatment of FACTS models and their incorporation into power networks represented in its natural frame of reference the phases.

Issues such as the social cost of transmission outages, problems of congestions, the opportunity to exercise market power and connection of independent producer to the grid are certainly impacted by FACTS technology. This is an additional motivation to explore the capabilities of FACTS in a more flexible modelling environment.

1.2 Objectives of the Project

The main objective of this PhD project is to conduct research on the steady-state and dynamic modelling and analysis of large-scale electrical power networks with embedded FACTS controllers.

In this research project, an aspect of paramount importance is the development of new mathematical models and methods coded into software to carry out effective analysis of large-scale, FACTS-controlled electrical power systems. The software should be robust and flexible enough to model and solve power networks with any kind and number of FACTS controllers. It should also make previsions to cater for future additions in the form of added functionality and future FACTS equipment.

The aim is to realise mathematical models and software for both steady-state and long-term dynamic analyses of electrical power systems. The FACTS equipment selected for analytical development in this research work are: the Static Compensator (STATCOM), the Static Synchronous Series Compensator (SSSC), the Unified Power Flow Controller (UPFC) and the High-Voltage Direct Current-Voltage Source Converter (HVDC-VSC). All these equipment have the VSC as their basic building block [1,5,6,17-18].

In this project, the three-phase power systems modelling philosophy, using rectangular co-ordinates, will be applied to develop a method for analysing dynamic power flows with FACTS devices. The method take into account the characteristics of power systems components in the phase domain, leading to more versatile analyses than that allowed by symmetrical-components-based studies. The phase domain frame of reference allows the study of practically any abnormal network condition and the inclusion of multi-phase components such as power electronics equipment and conventional equipment, which may exhibit imbalances.

A key goal of this project is to develop an integrated software environment for the solution of large-scale power networks, where long-term dynamic power flows can be

conducted alongside steady-state power flows and, generalised fault analysis. This longer-term vision is illustrated graphically in Figure 1.1.

1.3 Motivation

With the ever increasing complexity of electrical power networks, its planning, management and operation has had to rely more and more on advanced computer algorithms. Apart from electromagnetic transient studies and harmonic studies, almost any other power system study assumes that the transmission network is geometrically balanced. In this situation, the positive sequence frame of reference is used to model the entire power network. Short-circuit fault studies are the exception, where the negative and zero sequences are also used in addition to the positive sequence frame-of-reference.

Over the years, a great deal of research work has been conducted on individual modelling of power plant components using the phase domain frame of reference. More recently, with the widespread availability of powerful computing resources, this modelling philosophy has been used to develop power systems application software such as load flows and short-circuit fault analysis. The attraction of this more demanding modelling approach is the ability to take into account all the natural imbalances and the operational imbalances that exist in the power system. So far, multi-phase power flows have received the most attention, with iterative solution techniques based on either Newton-type techniques or the current injection method [19,20]. It should be pointed out that so far the multi-phase software reported in the literature has been intended for research purposes and that no commercial power systems software in the phase domain seems to exist, except for DINIS which uses a multiphase nodal impedance matrix and current injections method. The extensive literature survey carried out reveals that little representation exists for power electronics controllers suitable for multi-phase load flows and transient stability studies [14-16].

The motivation behind this PhD research is to develop an integrated, highly efficient software package suitable for the solution of large-scale, multi-phase power networks, which incorporate power electronic controllers. These are the power networks that will be in operation in the near future and for which there are no suitable tools for their planning, management and operation. The research effort will be on the mathematical modelling of power electronics controllers suitable for large-scale power systems operating under the steady-state and dynamic regimes.

As far as the author is aware, the software developed under this research project on three phase power flows and three-phase dynamic power flows is the first of its kind: capable of solving large-scale power systems with various kinds and any number of VSC-based FACTS controllers.

1.4 Achievements

The first practical step taken in this research project has been to develop mathematical models for various controllers using the phase domain modelling techniques in both

frames of reference polar and rectangular co-ordinates and to code them. A power flow computer program written in C++ has been upgraded to achieve this. The software is fast and reliable and is entirely adequate for the analysis and control of large-scale power networks containing FACTS-controlled buses and transmission lines. The power flow algorithm is a full Newton-Raphson method exhibiting quadratic convergence characteristics. Sparse matrix techniques have been incorporated for the efficient handling of large-scale power networks [21-22].

In order to carry out dynamic power flow assessments in the phase frame of reference a simultaneous algorithm for positive sequence networks, reported in a classical publications [23-24], has been adopted and coded. Moreover, models of VSC-based FACTS controllers have been included in the multiphase dynamic power flow algorithm in order to assess the impact of these controllers on large-scale electric power network.

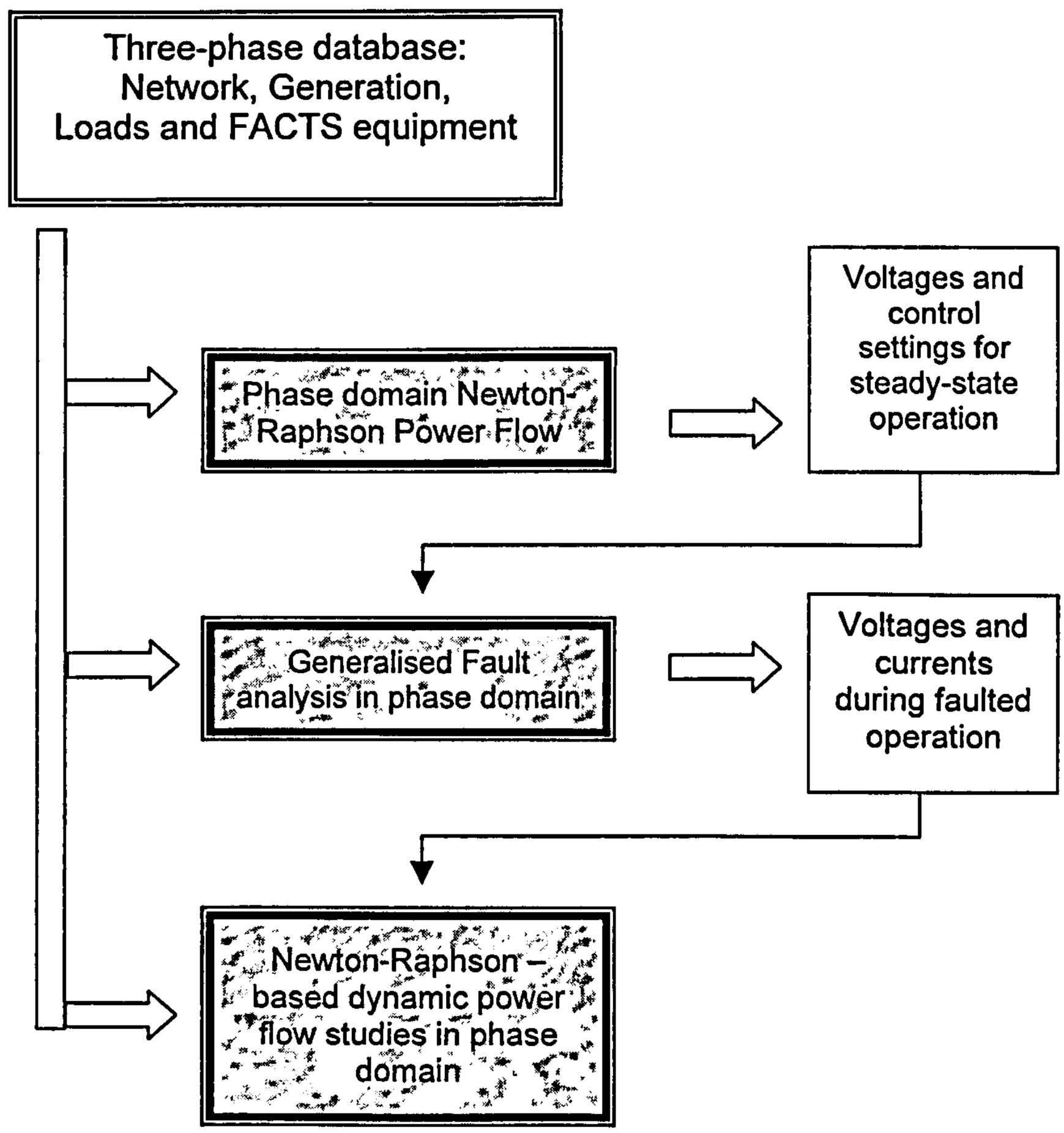

Figure 1.1 Integrated software environment for the electronic control of large-scale power systems

The three-phase software would offer a unique and powerful tool to power systems designers and operators with which to assess the technical benefits afforded by the FACTS technology in network wide applications. Moreover, the range of power systems analysis offered by the three-phase software has been greatly expanded by combining the power flow algorithm with the dynamic power flow algorithm in a single simulation environment. In future this capability will be further enhanced by the addition of generalised fault analysis module as shown in Figure 1.1.

Concerning large signal analysis, the standard power systems tool is termed the dynamic power flow. In this research the algorithm used is a simultaneous solution using the implicit trapezoidal integration method with Newton iteration. Arguably, the trapezoidal algorithm is the most powerful and accurate means of simulating transient events, which has shown to produce fast and reliable solutions [25-27].

1.5 Publications

The following publications have been generated as part of this research:

Transaction-grade paper

- **Angeles-Camacho, C.**, Tortelli, O. L., Acha, E. Fuerte-Esquivel, C. R., "Inclusion of a high voltage DC-voltage source converter model in a Newton-Raphson power flow algorithm," IEE Proc.-Gen. Trans. & Dist., Vol. 150, No. 6, Nov. 2003. pp. 691-695.

Prepared transaction-grade paper

- Angeles-Camacho, C., Acha, E., "Generalised modelling of VSC-based FACTS controllers in a three-phase Newton-Raphson method in rectangular co-ordinates", IEEE Trans. Power Systems

Conference papers

- Acha, E., **Angeles-Camacho, C.**, Tortelli, O. L., Fuerte-Esquivel, C. R., "Reactive Power Tracking in FACTS Upgraded Power Network" IASTED, Proc-of the Third IASTED International Conference on Power and Energy Systems, Marbella, Spain, Sep. 2003.

- Tortelli, O. L., **Angeles-Camacho, C.**, Acha, E., Anesio Santos, Jr., "Recommendations for the effective initialisation of FACTS controllers in Newton-Raphson power flow algorithms," IASTED, Proc-of the Third IASTED International Conference on Power and Energy Systems, Marbella, Spain, Sep. 2003.

Book

- FACTS: Modelling and Simulation in Power Networks by Acha, E., Fuerte-Esquivel, C.R., Ambriz-Perez, H. **Angeles-Camacho, C.** John Wiley & Sons, ltd., Chichester, England, February 2004, ISBN 0-470-852712.

1.6 Outline of the Thesis

Apart from the introductory chapter and conclusions, this thesis consists of five chapters, divided in two main parts: Chapter 2 to Chapter 4 comprise the work carried out for steady-state modelling and simulation, whereas Chapter 5 and Chapter 6 address aspects of dynamic modelling and simulation.

Chapter 1 introduces the current research work where the background and motivation to the project are stated.

Chapter 2 gives a general overview of power electronic equipment principles and its application in electric power systems. Flexible models of FACTS equipment, which use synchronous voltage source converters as their main constituent, are derived in the form of nodal admittance matrices. Control capabilities of the VSC-based controllers are analysed for the purpose of voltage regulation, active and reactive power flow control, and power quality enhancement.

In **Chapter 3,** mathematical models of the most common VSC-based FACTS controllers are developed. The proposed models are suitable for performing power flow analysis in the frame of reference of the phases for both balanced and unbalanced operation. An existing three-phase Newton-Raphson program has been upgraded to include these models. Guidelines and methods for implementing the FACTS controllers as well as their adjustments within the Newton-Raphson algorithm are also described. Simulation results for the various VSC-based FACTS controllers are presented.

A more efficient alternative to solve power flows using the Newton-Raphson is presented in **Chapter 4**. Instead of using polar co-ordinates, mathematical models of conventional power networks and VSC-based controllers are obtained using rectangular co-ordinates. A rectangular co-ordinates three-phase power flow algorithm has been written which include VSC-based FACTS controllers. A comparative analysis between polar and rectangular analysis is presented, with the rectangular co-ordinates method showing a superior performance, and with simulation results coinciding with each other.

Simple models of the generating plant components, suitable for long term dynamic assessment of large-scale power systems in both balanced and unbalanced operation are given in **Chapter 5.** Guidelines and methods for implementing the dynamic power flow algorithm are described here. Case studies for different transient scenarios, which produce step voltages on power systems, are also given here.

Chapter 6 reports on research carried out to assess the impact of VSC-based FACTS controllers on long-term power systems dynamics. The application tool termed in

Chapter 5, dynamic power flows is upgraded to include models of VSC-based FACTS controllers and several test cases are carried out, including a large power system.

The most important conclusions of this research work are presented in **Chapter 7**. The chapter also contains suggestions for future work.

1.7 References

[1] Hingorani, N. G.: "Flexible AC Transmission Systems", IEEE *Spectrum*, April 1993. pp. 40-45.

[2] Anderson, P. M. and Fouad, A. A.: "*Power system stability and control*" (Revised Printing). New York: IEEE Press. 1994. INSB 0-87942-264-5.

[3] Kundur, P.: "*Power System Stability and Control*". New York, McGraw-Hill. 1994. INSB 007035958X.

[4] IEEE Power Engineering Society: "FACTS applications", special Issue, 96TP116-0, IEEE *Service Centre*, Piscataway, N.J., 1996.

[5] Song, Y. H. and Johns, A. T.: "*Flexible AC Transmission Systems (FACTS)*", The Institution of Electrical Engineers, London, U K, 1999, INSB 0852967713.

[6] CIGRE: "FACTS Technology for open access", JWG 14/37/38/39-24. Final draft report, Aug. 2000.

[7] Hingorani, N.G. and Gyugyi, L.: "*Understanding FACTS: concepts and technology of flexible AC transmission systems*", the Institute of Electrical and Electronics Engineers, Inc., New York, 2000. ISNB 0-780334558.

[8] Nelson, R. J.: "Transmission power flow control: electronic vs. electromagnetic alternatives for steady-state operation", IEEE *Trans. On Power Delivery*, Vol. 9, No. 3, July 1994. pp. 1678-1684.

[9] Fuerte-Esquivel, C. R.: "Modelling and analysis of FACTS devices", PhD Thesis, University of Glasgow, Scotland, UK, 1997.

[10] Ledu, A., Tontini, G. and Winfield, M.: "Which FACTS equipment for which need?", *International Conference on Large High Voltage Electric Systems* (CIGRÉ), paper 14/37/38-08, Paris, Sept. 1992.

[11] Larsen, E., Bowler, C., Damsky, B. and Nilsson, S.: "Benefits of thyristor controlled series compensation", *International Conference on Large High Voltage Electric Systems* (CIGRÉ), paper 14/37/38-04, Paris, Sept. 1992.

[12] Christl, N., Hedin, R., Sadek, K., Lützelberger, P., Krause, P. E., McKenna, S. M., Montoya, A. H. and Togerson, D.: "Advanced series compensation (ASC) with thyristor controlled impedance", *International Conference on Large High Voltage Electric Systems* (CIGRÉ), paper 14/37/38-05, Paris, Sept. 1992.

[13] Kinney, S. J., Mittelstadt, W. A. and Suhrbier, R. W.: "Test results and initial experience for the BPA 500 kV thyristor controlled series capacitor unit at Slat substation, part I- design, operation, and fault test results", Flexible AC Transmission Systems (FACTS 3): The Future in High Voltage Transmission Conference, EPRI, Baltimore Maryland, Oct. 1994.

[14] Zhang, X.-P.; Xue, C.-F. and Godfrey, K.R.; "Modelling of the static synchronous series compensator (SSSC) in three-phase Newton power flow", IEE *Proc. Gen. Trans. And Dist.* Vol. 151, No. 4, July 2004, pp.486-494.

[15] Venegas T., and Fuerte-Esquivel C.R.: "Steady-state modelling of an advanced series compensator for power flow analysis of electric networks in phase co-ordinates", IEEE *Trans. Power Syst.*, Vol. 16, No. 4, Oct. 2001, pp. 758-765.

[16] Angeles Camacho, C.: "Steady-state modelling of the unified power flow controller for three phase power flow analysis of electric systems" M.Sc. Thesis (in Spanish), Department of Electrical and Electronics Engineering, Instituto Tecnológico de Morelia, Aug. 2000.

[17] Sen, K. K., "SSSC-Static synchronous series compensator: theory, modelling, and applications", IEEE *Trans. Power Delivery,* vol. 3, Jan. 1998 pp. 241-246.

[18] Sen, K. K., "STATCOM-Static synchronous compensator: theory, modelling, and applications", IEEE *Power Eng. Soc. Winter Meeting*, 1999, pp. 1177-1183.

[19] Stagg, G. W., and El-Abiad, A. H.: "*Computer methods in power system analysis*". McGraw-Hill, Kogakusha, Ltd. New York, 1968. ISNB 67-129963-07-060658-7.

[20] Arrillaga, J. and Watson, N. R.: "*Computer modelling of electrical power system*", Second Ed. Wiley and Sons Ltd., Sussex, England, 2001. INSB 0-471-87249-0.

[21] Buzzi-Ferraris, G.: "*Scientific C++, building numerical libraries the object oriented way*", Ed. Addison-Wesley, 1994. ISBN 0-201-63192-X.

[22] Capper, D.M.: "*Introducing C++ for scientist, engineers and mathematicians*", 2nd edition, Springer-Verlag, London, UK, 2001.

[23] Rafian, M., Sterling, M.J.H, and Irving, M. R.: "Real-time power systems simulation", *IEE Proc.* Vol. 134. Pt. C. No. 3, May 1987. pp. 206-223.

[24] Rafian, M., Sterling, M.J.H. and Irving, M. R.: "Parallel processor algorithm for power system simulation", *IEE Proc.* Vol. 135. Pt. C. No. 4, July 1988. pp. 285-290.

[25] Dommel, H. W. and Sato, N.: "Fast transient stability solutions", IEEE *Trans PAS-91*, No. 4, July/Aug. 1972. pp. 1643-1650.

[26] Stott, B.: "Power system dynamic response calculations", *Proc.*, IEEE, Vol. 67, Feb. 1979. pp. 219-241.

[27] Byerly, R.T. and Kimbark, E.W.: "Stability of large electric power systems", IEEE press, New York, USA, 1974, ISNB 0-87942-037-5.

Chapter 2

MODELLING OF VSC-BASED FACTS CONTROLLERS AND CONVENTIONAL POWER SYSTEM COMPONENTS IN PHASE DOMAIN

2.1 Introduction

Two kinds of emerging power electronics applications in power systems are already well defined: (i) bulk active and reactive power control; (ii) and power quality improvement [1]. The first application area is known as FACTS, where the latest power electronic devices and methods are used to electronically control the high-voltage side of the network [2]. The second application area is custom power, which focuses on low voltage distribution and is a technology created in response to reports of poor power quality and reliability of supply affecting factories, offices and homes. It is expected that when widespread deployment of the technology takes place, the end-user will see tighter voltage regulation, minimum power interruptions, low harmonic voltages, and acceptance of rapidly fluctuating and other non-linear loads in the vicinity [3].

The one-line diagram shown in Figure 2.1 illustrates the connection of power plants in an interconnected transmission system, where the boundary between the high-voltage transmission and the low-voltage distribution is emphasised. The former benefits from the installation of FACTS equipment whereas the latter benefits from the installation of custom power equipment.

To a greater or lesser extent, high-voltage transmission systems are highly meshed. For many decades the trend has been towards interconnection, linking generators and loads into large integrated systems. The motivation has been to take advantage of load diversity, enabling a better utilisation of primary energy resources.

From the outset, interconnection was aided by breakthroughs in high-current, high-power semiconductor valve technology [4]. Thyristor-based High Voltage Direct Current converter installations provided a means for interconnecting power systems with different operating frequencies, e.g. 50/60 Hz, for interconnecting power systems of different frequency and for interconnecting weak and strong power systems and asynchronized systems [5]. The most recent development in HVDC technology is the HVDC system based on solid-state voltage source converters, which enables independent, fast control of active and reactive powers, HVDC also provides a means to transmit power in unbalanced conditions [6].

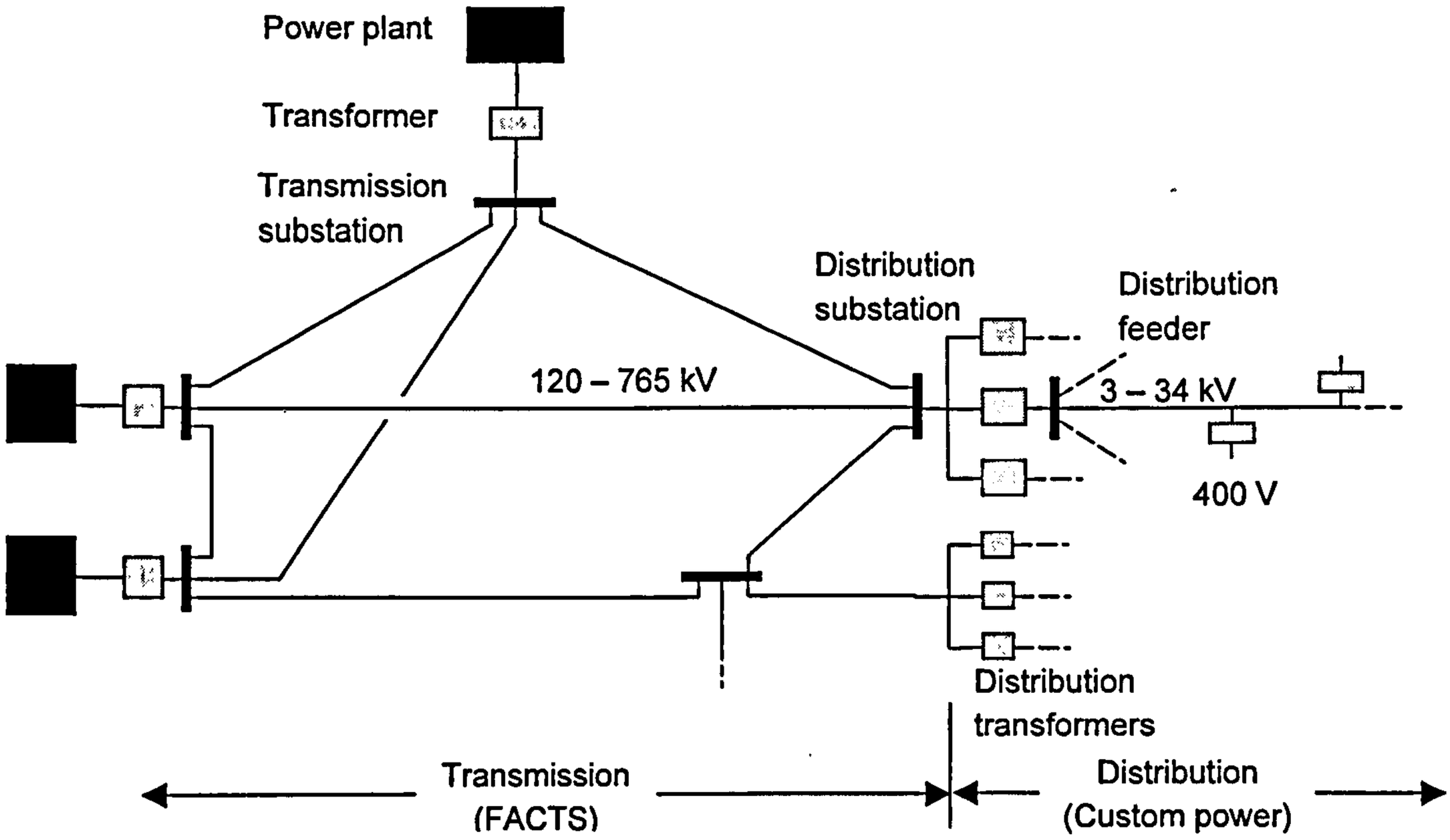

Figure 2.1 A simplified one-line diagram of a power system [3]

Power electronics is a ubiquitous technology which has affected every aspect of electrical power networks, not just HVDC transmission but also AC transmission, distribution and utilisation. Deregulated markets are imposing further demands on generating plants, increasing their wear and tear and the likelihood of generator instabilities of various kinds. To help to alleviate such problems, power electronic controllers have recently been developed to enable generators to operate more reliably in the new market place. The Thyristor-Controlled Series Compensator (TCSC) is used to mitigate sub-synchronous resonance's (SSR) and to damp power systems oscillations [7]. However, it may be argued that the primary function of the TCSC, like that of its mechanically controlled counterpart, the series capacitor bank, is to reduce the electrical length of the compensated transmission line. Hence, the aim is still to increase power transfers significantly, but with increased transient stability margins. With reference to the schematic network of Figure 2.1, the TCSC is deployed on the FACTS side.

For most practical purposes the thyristor-based Static VAR Compensator has made the rotating synchronous compensator redundant, except where an increase in the short-circuit level is required along with fast-acting reactive power support [8]. However, as the power electronic technology continues to develop further, the replacement of the SVC by a new breed of static compensators based on the use of voltage source converters (VSCs) is looming. They are known as STATCOMs, and provide all the functions that the SVC can provide, but at a higher speed [9]; it is more compact and requires only a fraction of the land required by an SVC installation. The STATCOM is essentially a VSC interfaced to the AC system through a shunt-connected transformer. The VSC is the basic building block of the new generation of power electronic

controllers that have emerged from the FACTS and custom power initiatives [1]. In high-voltage transmission, the most popular FACTS VSC-based equipment are: the STATCOM, the SSSC, the UPFC and the HVDC-VSC. At the low-voltage distribution level, the SVC provides the core of the following custom power equipment: the distribution STATCOM, the dynamic voltage restorer and active filters.

This Chapter presents the detailed mathematical modells of the most recent generation of FACTS controllers based on the voltage source converter. Also a brief description of conventional components of the electrical power system is given.

2.2 Phase-domain Modelling Philosophy

In this Chapter the development of models and procedures are described which are used to assess the three-phase steady-state operation of electrical power systems at the fundamental frequency. All models may be developed from first principles, with strong reference to the physical structure of the equipment. Such an approach is amenable to flexible modelling which is useful for assessing the operation of plant components in network-wide applications, taking due care of equipment design imbalances, which are naturally present in all power plant equipment.

The application tool used to assess the steady-state operation of power systems exhibiting a considerable degree of geometric unbalance or load unbalance is known as three-phase power flow. In this application all operations are carried out on a per- phase basis and all power plant components making up the power system are modelled in the frame of reference of the phases [10,12].

2.2.1 Conventional element models of an electrical power system

Three-phase synchronous generators are used to produce most of the electricity consumed worldwide [3] and except for a small percentage, which is transported in DC form using HVDC links, all electricity is brought to the points of demand using AC three-phase transmission lines and cables. More often than not, long distance transmission circuits consist of more than one three-phase circuit, and contain series and shunt compensation to enable stable operation. Nevertheless, it has long been recognised that remote generating stations, which are mostly of the hydroelectric type, are only weakly interconnected and that the non-uniform nature of their rotors, i.e. saliency, increases the overall system unbalance. It should also be remarked that the windings of three-phase transformers can be connected in a variety of ways to suit specific requirements, and that transformer connections should be modelled explicitly when system imbalances cannot be ignored in power systems studies [5]. The bulk load points associated with transmission systems may be taken to be highly balanced but such an assumption is no longer valid in low voltage distribution systems, where load points may be highly unbalanced owing to an abundance of individual single-phase loads within a distribution load point.

2.3 Controllers Based on Conventional Thyristors

Power electronic circuits using conventional thyristors have been widely used in power transmission applications since the early seventies [4]. The first applications took place in the area of HVDC transmission but shunt reactive power compensation using fast controllable inductors and capacitors soon gained general acceptance [8]. More recently, fast acting series compensators using thyristors have been used to vary the electrical length of key transmission lines, with almost no delay, instead of the classical series capacitor, which is mechanically controlled. In distribution system applications, solid-state transfer switches using thyristors are now being used to enhance the reliability of the supply to critical customer loads [15].

2.4 Power Electronic Controllers Phased on Fully Controlled Semiconductor Devices

Modern power system controllers based on power electronic converters are capable of generating reactive power with no need for large reactive energy storage elements, such as in SVC systems. This is achieved by making the currents circulate through the phases of the AC system with the assistance of fast switching devices [1].

Power electronic controllers are based on an assembly of AC/DC and/or DC/AC converters and/or high power AC switches, and supporting devices. The converters, switches and devices are connected in series or parallel, to achieve the desired Controller; a Controller in some cases may also be separated into single-phase assemblies. The semiconductor devices employed in the new generation of power electronic converters are of the fully controlled type, such as the IGBT (Integrated Gate Bipolar Transistor) and the GTO (Gate Turn-Off). Nominal rating of power electronics controllers is in the range of 8-10 KV for thyristor, 5-8 KV for GTOs and 3-5 for IGBTs. Their respective circuit symbols are shown in Figure 2.2 [19].

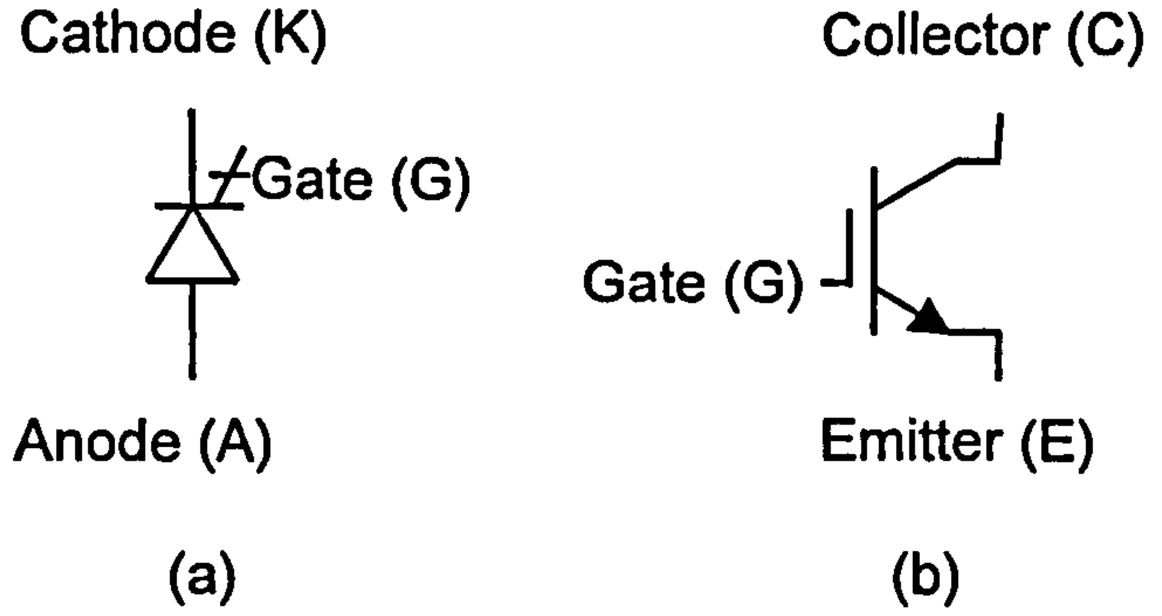

Figure 2.2 Circuit symbols for: (a) GTO; (b) IGBT

The GTO is a more advanced version of the conventional thyristor, with a similar switched on characteristic but with the ability to switch off at a time different from when the forward current falls naturally below the holding current level. Such added

functionality has enabled new application areas in industry to be developed, even at bulk power transmission where levels it is now possible to re-direct active power at the MW level. However, there is room for improvement in GTO construction and design, since large negative pulses are still required to turn it off. At present, the maximum switching frequency attainable is in the order of 1 kHz [19].

The IGBT is one of the most well developed members of the power transistor family. It is the most popular device used in the area of AC and DC motor drives, reaching power levels of a few hundred kW. Power converters aimed at power systems applications are beginning to make use of IGBTs owing to their increasing power handling capability and relatively low conduction losses. Further progress is expected in IGBT and GTO technology and applications [20].

In DC-AC converters that use fully controlled semiconductors rather than conventional thyristors, the DC input can be either a voltage source (typically a capacitor) or a current source (typically a voltage source in series with an inductor). With reference to this basic operational principle, converters can be classified as either voltage source converters or current source converters. For economic and performance reasons, most reactive power controllers are based on the former VSC topology. The availability of modern semiconductors with relatively high-voltage and current ratings, such as GTOs or IGBTs, has made the concepts of reactive compensation based on switching converters a certainty, even for substantial high-power applications.

A number of power system controllers that use VSCs as their basic building block are in operation in various parts of the world. The most popular are: STATCOM, SSSC, the UPFC, and the HVDC-VSC [9].

2.5 The Voltage Source Converter

There are several VSC topologies currently in use in actual power systems operation, and some others that hold great potential, including the single-phase full bridge (H-bridge), the conventional three-phase two-level converter, and the three-phase three-level converter based on the neutral-point-clamped converter. Other VSC topologies are based on combinations of the neutral-point-clamped topology and multilevel-based systems [19]. Common aims of these topologies are to minimise the operating frequency of the semiconductors inside the VSC and to produce a high-quality sinusoidal voltage waveform with minimum or no filtering requirements. By way of example, the topology of a conventional two-level VSC using IGBT switches is illustrated in Figure 2.3 [19].

The VSC shown in Figure 2.3 comprises six IGBTs, with two IGBTs placed on each leg. Moreover, each IGBT is provided with a diode connected in anti-parallel to make provisions for possible voltage reversals due to external circuit conditions. Two equally sized capacitors are placed on the DC side to provide a source of reactive power.

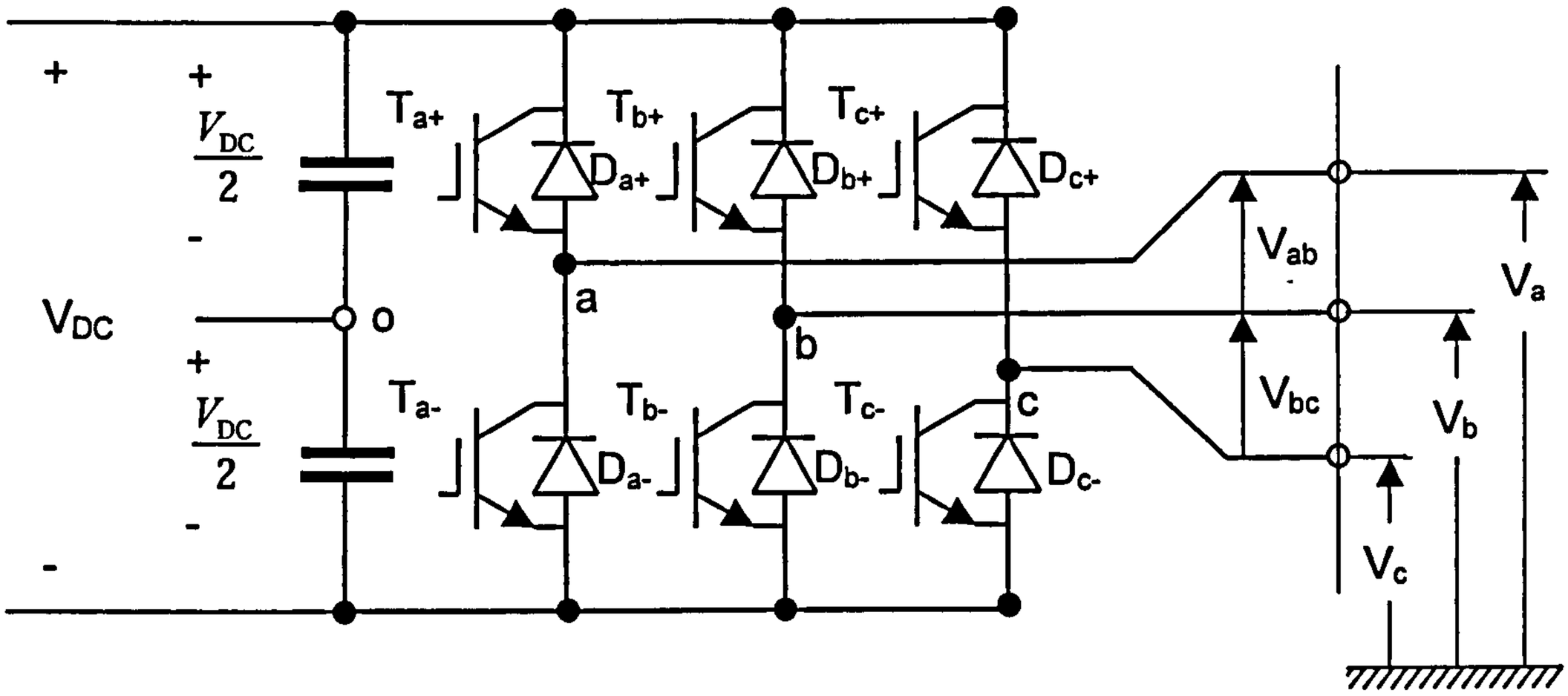

Figure 2.3 Topology of a three-phase, two-level VSC using IGBTs

Although not shown in the circuit of Figure 2.3, the switching control module is an integral component of the VSC [19]. Its task is to control the switching sequence of the various semiconductor devices in the VSC, aiming at producing an output voltage waveform, which is as near to a sinusoidal waveform as possible, with high power controllability and minimum switching loss.

Current VSC switching strategies aimed at utility applications may be classified into two main categories [21]:

Fundamental frequency switching: The switching of each semiconductor device is limited to one turn-on and one turn-off per power cycle. The basic VSC topology shown in Figure 2.3. With fundamental frequency switching it yields a quasi-square-wave output, which has an unacceptable high harmonic content. It is current practice to use several six-pulse VSCs, arranged to form a multi-pulse structure, to achieve better waveform quality and higher power ratings [1].

Pulse-width modulation (PWM): This control technique enables the switches to be turned on and off at a rate considerably higher than the fundamental frequency. The output waveform is chopped and the width of the resulting pulses is modulated. Undesirable harmonics in the output waveform are shifted to the higher frequencies, and filtering requirements are much reduced. Over the years, various PWM control techniques have been published but the sinusoidal PWM scheme remains one of the most popular owing to its simplicity and effectiveness [19].

From the viewpoint of utility applications, both switching techniques are far from perfect. The fundamental frequency switching technique requires of complex transformer arrangements to achieve an acceptable level of waveform distortion. Such a drawback is offset by its high semiconductor switch utilization and low switching losses; and it is, at present, the switching technique used in high-voltage, high-power applications. The PWM technique incurs high switching loss, but it is envisaged that future semiconductor devices would reduce this by a significant margin; making PWM the universally

preferred switching technique, even at high- and extra-high-voltage transmission applications.

2.5.1 Principles of VSC operation

The interaction between the VSC and the power system may be explained in simple terms by considering a VSC connected to the AC mains through a loss less reactor, as illustrated in the single-line diagram shown in Figure 2.4(a). The premise is that the amplitude and the phase angle of the voltage drop, ΔV_x, across the reactor, X_l, can be controlled; defining the amount and direction of active and reactive power flows through X_l. The voltage at the supply bus is taken to be sinusoidal, of value $V_s\angle 0°$, and the fundamental frequency component of the SVC's AC voltage is taken to be $V_{vR}\angle\delta_{vR}$. The positive sequence, fundamental frequency vector representation is shown in Figure 2.4(b) and (c) for leading and lagging VAR compensation, respectively.

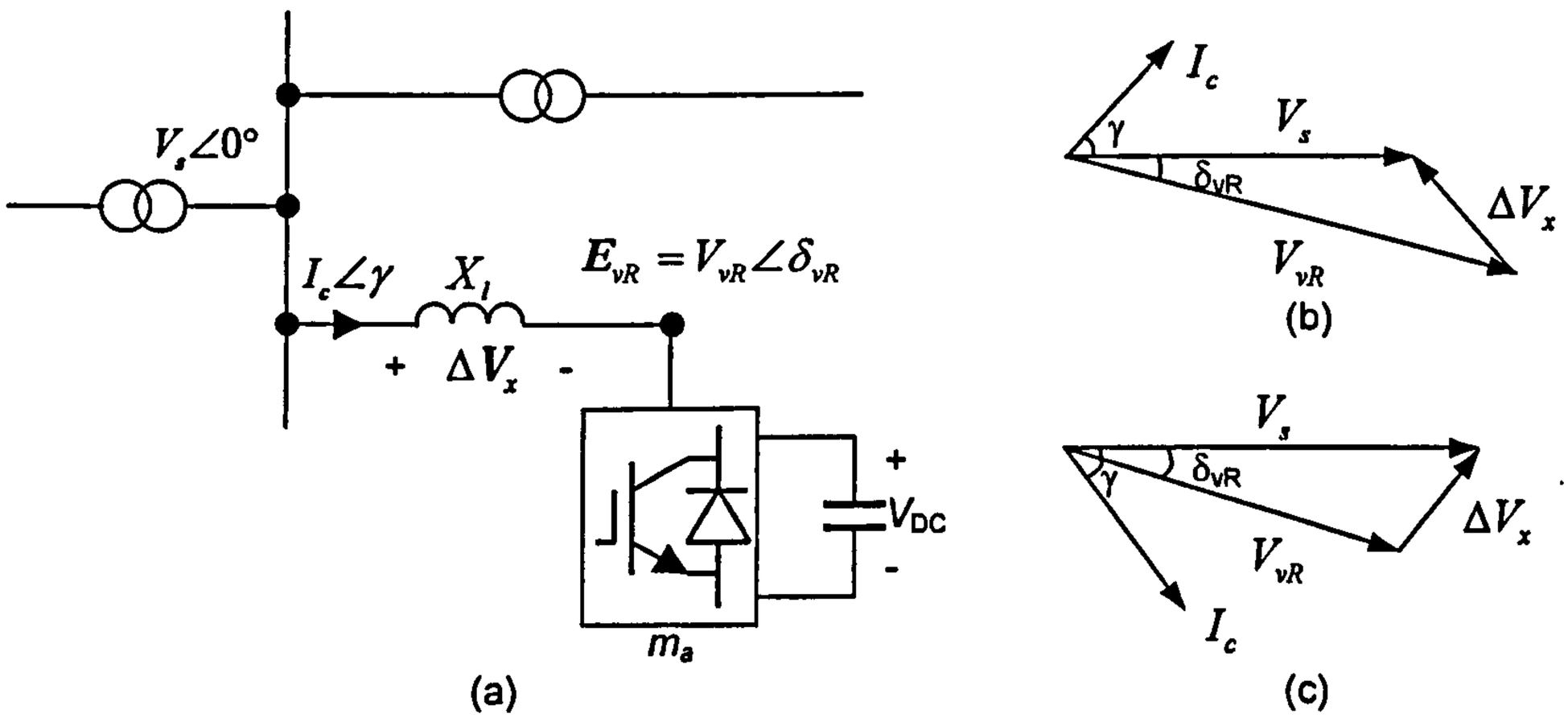

Figure 2.4 Basic VSC operation: (a) VSC connected to a system bus; Space vector representation for (b) Lagging operation and (c) Leading operation

According to Figure 2.4, for both leading and lagging VAR, the active and the reactive powers can be expressed as

$$P = \frac{V_s V_{vR}}{X_l}\sin\delta_{vR}$$
$$Q = \frac{V_s^2}{X_l} - \frac{V_s V_{vR}}{X_l}\cos\delta_{vR} \qquad (2.1)$$

With reference to Figure 2.4 and (2.1), the following observations are derived:

The VSC output voltage E_{vR} lags the AC voltage source V_s by an angle δ_{vR}, and the input current lags the voltage drop across the reactor ΔV_x by 90°.

The active power flow between the AC source and the VSC is controlled by the phase angle δ_{vR}. Active power flows into the VSC from the AC source at lagging δ_{vR} $(\delta_{vR} > 0)$, and *vice versa* for leading δ_{vR} $(\delta_{vR} < 0)$.

The reactive power flow is determined mainly by the magnitude of the voltage source, V_s, and the VSC output fundamental voltage, V_{vR}. For $V_{vR} > V_s$, the VSC generates reactive power and consumes reactive power when $V_{vR} < V_s$.

The DC capacitor voltage V_{DC} is controlled by adjusting the active power flow that goes into the VSC. During normal operation, a small amount of active power must flow into the VSC to compensate for the power losses inside the VSC, and δ_{vR} is kept slightly larger than 0° (lagging).

The various power system controllers that use the VSC as their basic building block are addressed in the next sections below with reference to key three-phase steady-state operational characteristics and their impact on system voltage and power flow control.

2.5.2 The Static Synchronous Compensator

The Static Synchronous Compensator (STATCOM or SSC) consists of one VSC and its associated shunt-connected transformer. It is the static counterpart of the rotating synchronous condenser but it generates/absorbs reactive power at a faster rate because no moving parts are involved. In principle, it performs the same voltage regulation function as the SVC but in a more robust manner because unlike the SVC, its operation is not impaired by the presence of low voltages [9].

The schematic representation of the STATCOM and its equivalent circuit are shown in Figure 2.5. The equivalent circuit corresponds to the Thevenin equivalent as seen from bus *k*, with the voltage source E_{vR} being the fundamental frequency component of the VSC output voltage, resulting from the product of V_{DC} and m_a.

In steady-state, fundamental frequency studies the STATCOM may be represented in the same way as a synchronous condenser, which in most cases is the model of a synchronous generator with zero active power generation. A more flexible model may be realised by representing the STATCOM as a variable voltage source E_{vR}, whose magnitude and phase angle may be adjusted using a suitable iterative algorithm to satisfy a specified voltage magnitude at the point of connection with the AC network. The shunt voltage source of the three-phase STATCOM may be represented by:

$$E_{vR}^{\rho} = V_{vR}^{\rho}\left(\cos\delta_{vR}^{\rho} + \mathrm{j}\sin\delta_{vR}^{\rho}\right) \tag{2.2}$$

where ρ indicates phase quantities, *a*, *b* and *c*.

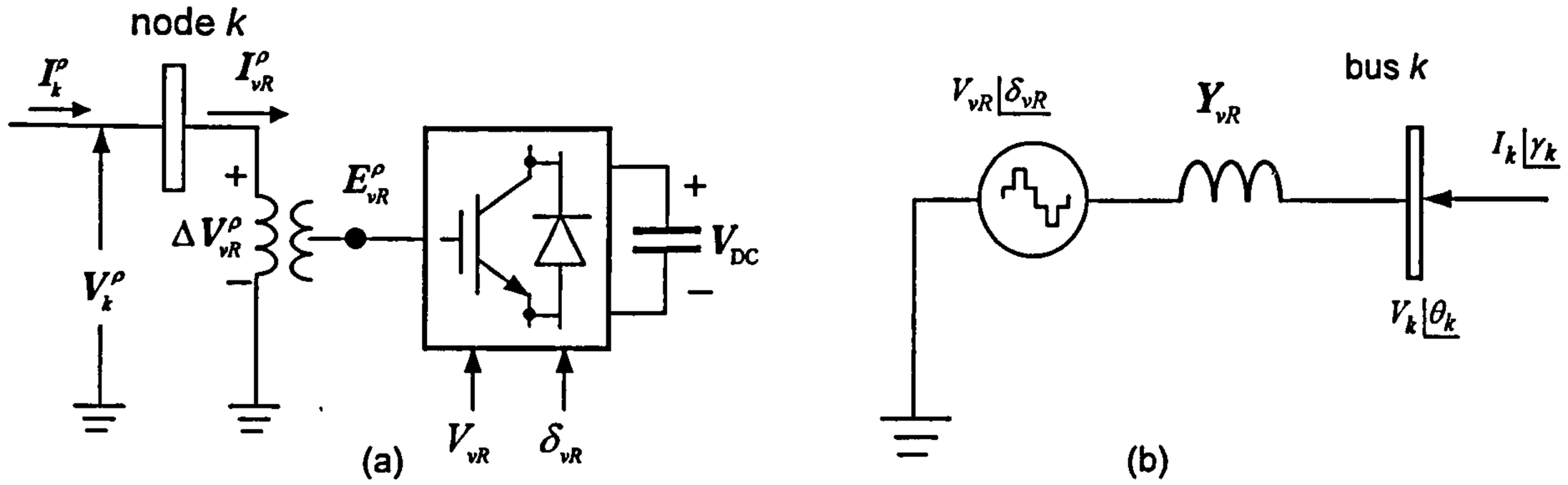

Figure 2.5 STATCOM system: (a) VSC connected to the AC network via a shunt-connected transformer; (b) Shunt solid-state voltage source

The voltage magnitude, V_{vR}^ρ, is given maximum and minimum limits, which are a function of the STATCOM capacitor rating. On the other hand, δ_{vR}^ρ may take any value between 0 and 2π radians.

With reference to the equivalent circuit shown in Figure 2.5(b), and assuming three-phase parameters, the following transfer admittance equation can be written:

$$[\boldsymbol{I}_k] = [\boldsymbol{Y}_{vR} \quad -\boldsymbol{Y}_{vR}] \begin{bmatrix} \boldsymbol{V}_k \\ \boldsymbol{E}_{vR} \end{bmatrix} \tag{2.3}$$

where

$$\boldsymbol{I}_k = \left[I_k^a \angle \gamma_k^a \quad I_k^b \angle \gamma_k^b \quad I_k^c \angle \gamma_k^c \right]^T \tag{2.4}$$

$$\boldsymbol{V}_k = \left[V_k^a \angle \theta_k^a \quad V_k^b \angle \theta_k^b \quad V_k^c \angle \theta_k^c \right]^T \tag{2.5}$$

$$\boldsymbol{E}_{vR} = \left[V_{vR}^a \angle \delta_{vR}^a \quad V_{vR}^b \angle \delta_{vR}^b \quad V_{vR}^c \angle \delta_{vR}^c \right]^T \tag{2.6}$$

$$\boldsymbol{Y}_{vR}^\rho = \begin{bmatrix} \boldsymbol{Y}_{vR}^{aa} & 0 & 0 \\ 0 & \boldsymbol{Y}_{vR}^{bb} & 0 \\ 0 & 0 & \boldsymbol{Y}_{vR}^{cc} \end{bmatrix} \tag{2.7}$$

2.6 The Static Synchronous Series Compensator

For the purpose of steady-state operation, the Static Synchronous Series Compensator or Solid State Series Compensator (SSSC) performs a similar function to the static phase shifter; it injects voltage in quadrature with one of the line end voltages in order to regulate active power flow. However, the SSSC is a far more versatile controller than the phase shifter because it does not draw reactive power from the AC system; it has its own reactive power provisions in the form of a DC capacitor. This characteristic makes the SSSC capable of regulating not only active but also reactive power flow or nodal voltage magnitude. This functionality is addressed further in Section 2.8. The schematic representation of the SSSC and its equivalent circuit are shown in Figure 2.6.

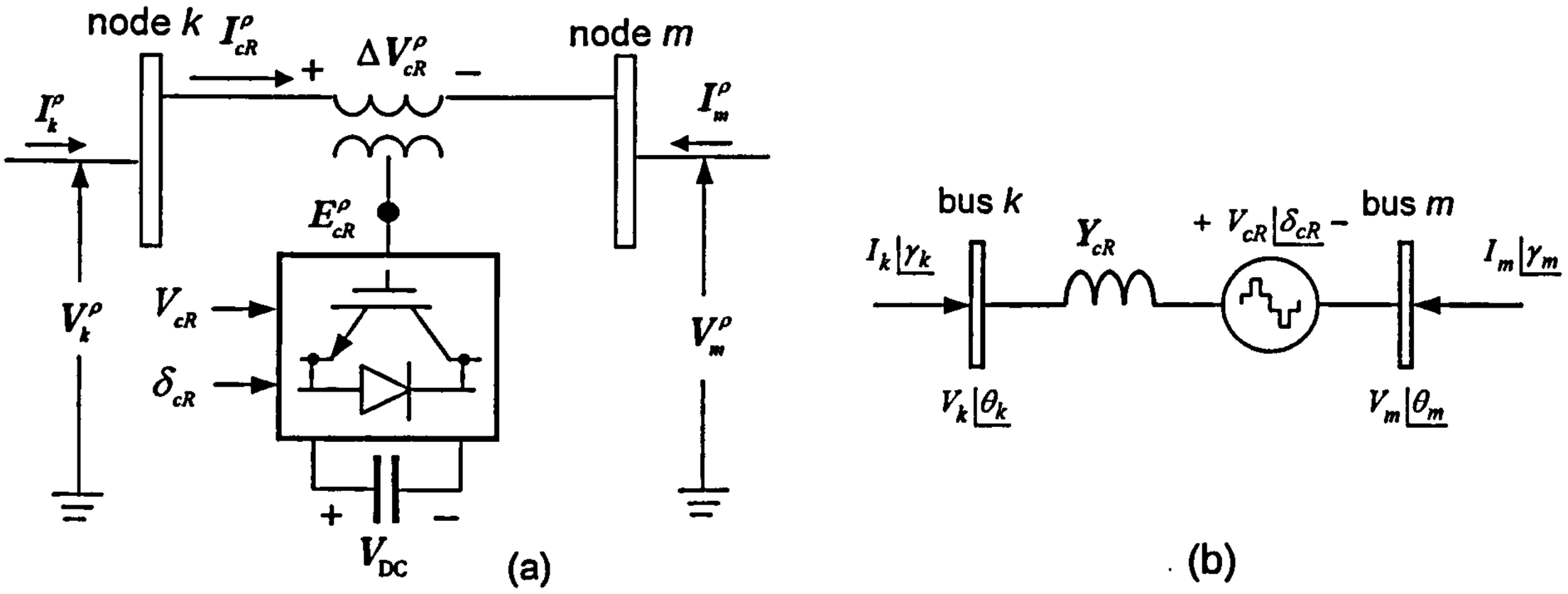

Figure 2.6 SSSC system: (a) VSC connected to the AC network using a series transformer; (b) Series solid-state voltage source

The series voltage source of the three-phase SSSC may be represented by,

$$E_{cR}^{\rho} = V_{cR}^{\rho}\left(\cos\delta_{cR}^{\rho} + \mathrm{j}\sin\delta_{cR}^{\rho}\right) \tag{2.8}$$

where ρ indicates phase quantities, *a*, *b* and *c*.

The magnitude and phase angle of the SSSC model are adjusted using any suitable iterative algorithm to satisfy a specified active and reactive power flow across the SSSC. Similarly to the STATCOM, maximum and minimum limits will exist for the voltage magnitude V_{cR}, which are a function of the SSSC capacitor rating. On the other hand, the voltage phase angle δ_{cR} can take any value between 0 and 2π radians. The control capabilities of the SSSC are addressed in Section 2.8.

Based on the equivalent circuit shown in Figure 2.6 (b), and assuming three-phase parameters, the following transfer admittance equation can be written:

$$\begin{bmatrix} I_k \\ I_m \end{bmatrix} = \begin{bmatrix} Y_{cR} & -Y_{cR} & -Y_{cR} \\ -Y_{cR} & Y_{cR} & Y_{cR} \end{bmatrix} \begin{bmatrix} V_k \\ V_m \\ E_{cR} \end{bmatrix} \tag{2.9}$$

In addition to parameters used in (2.4)-(2.7) the following quantities are defined,

$$I_m^{\rho} = \begin{bmatrix} I_m^a \angle \gamma_m^a & I_m^b \angle \gamma_m^b & I_m^c \angle \gamma_m^c \end{bmatrix}^T \tag{2.10}$$

$$V_m^{\rho} = \begin{bmatrix} V_m^a \angle \theta_m^a & V_m^b \angle \theta_m^b & V_m^c \angle \theta_m^c \end{bmatrix}^T \tag{2.11}$$

$$E_{cR}^{\rho} = \begin{bmatrix} V_{cR}^a \angle \delta_{cR}^a & V_{cR}^b \angle \delta_{cR}^b & V_{cR}^c \angle \delta_{cR}^c \end{bmatrix}^T \tag{2.12}$$

$$Y_{cR}^{\rho} = \begin{bmatrix} Y_{cR}^{aa} & 0 & 0 \\ 0 & Y_{cR}^{bb} & 0 \\ 0 & 0 & Y_{cR}^{cc} \end{bmatrix} \tag{2.13}$$

2.7 The Unified Power Flow Controller

The UPFC may be seen to consist of two VSCs, one shunt and one series connected, sharing a common capacitor on their DC side and a unified control system. A simplified schematic representation of the UPFC is given in Figure 2.7 together with its equivalent circuit [22].

The UPFC allows simultaneous control of active power flow, reactive power flow and voltage magnitude at the UPFC terminals. Alternatively, the controller may be set to control one or more of these parameters in any combination or to control none of them [23].

The active power demanded by the series converter is drawn by the shunt converter from the AC network and supplied to bus *m* through the DC link. The output voltage of the series converter is added to the nodal voltage, at say bus *k*, to boost the nodal voltage at bus *m*. The voltage magnitude of the output voltage V_{cR} provides voltage regulation and the phase angle δ_{cR} determines the mode of power flow control [1].

In addition to providing a supporting role in the active power exchange that takes place between the series converter and the AC system, the shunt converter may also generate or absorb reactive power in order to provide independent voltage magnitude regulation at its point of connection with the AC system.

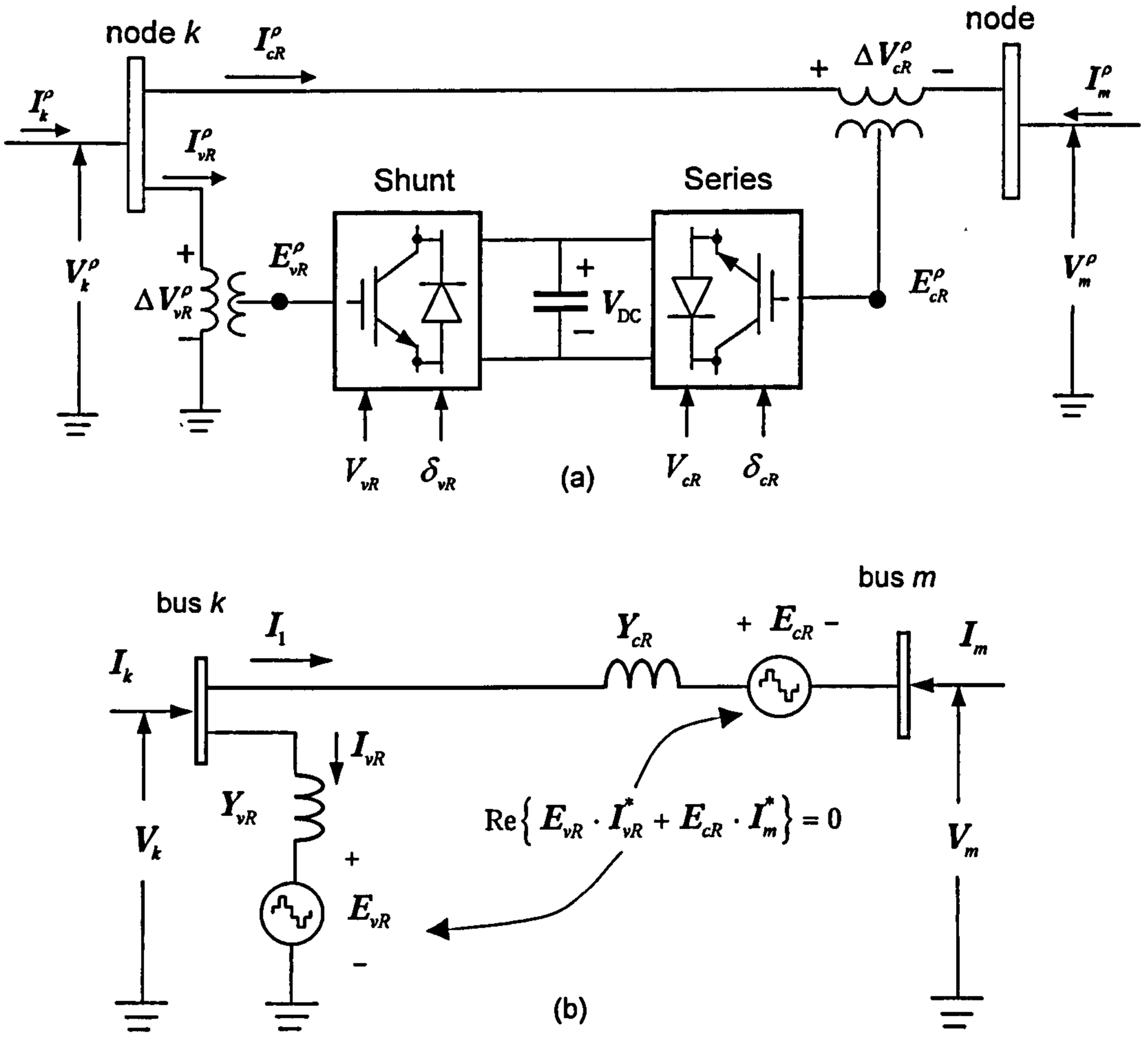

Figure 2.7 UPFC system: (a) Two back-to-back VSCs with one VSC connected to the AC network using a shunt transformer and the second VSC connected to the AC network using a series transformer; (b) Equivalent circuit based on solid state voltage sources

The UPFC equivalent circuit shown in Figure 2.7(b), consists of a shunt connected voltage source, a series connected voltage source and an active power constraint equation which links the two voltage sources. The two voltage sources are connected to the AC system through inductive reactances representing the VSC transformers. In a three-phase UPFC, suitable expressions for the two voltage sources and constraint equation would be:

$$E_{vR}^{\rho} = V_{vR}^{\rho}\left(\cos\delta_{vR}^{\rho} + \mathrm{j}\sin\delta_{vR}^{\rho}\right) \tag{2.14}$$

$$E_{cR}^{\rho} = V_{cR}^{\rho}\left(\cos\delta_{cR}^{\rho} + \mathrm{j}\sin\delta_{cR}^{\rho}\right) \tag{2.15}$$

$$\mathrm{Re}\left\{ -E_{vR}^{\rho}\left(I_{vR}^{\rho}\right)^{*} + E_{vR}^{\rho}\left(I_{m}^{\rho}\right)^{*} \right\} = 0 \tag{2.16}$$

where ρ indicates phase quantities, *a*, *b* and *c*.

Similarly to the shunt and series voltage sources used to represent the STATCOM and the SSSC, respectively, the voltage sources used in the UPFC application would also have limits.

Based on the equivalent circuit shown in Figure 2.7(b), and assuming three-phase parameters, the following transfer admittance equation can be written as:

$$\begin{bmatrix} I_k \\ I_m \end{bmatrix} = \begin{bmatrix} (Y_{cR} + Y_{vR}) & -Y_{cR} & -Y_{cR} & -Y_{vR} \\ -Y_{cR} & Y_{cR} & Y_{cR} & 0 \end{bmatrix} \begin{bmatrix} V_k \\ V_m \\ E_{cR} \\ E_{vR} \end{bmatrix} \tag{2.17}$$

where all the parameters have been defined in (2.4)-(2.7) and (2.10)-(2.13).

2.8 The High Voltage Direct Current based on Voltage Source Converters

The HVDC-VSC comprises two VSCs, one operating as a rectifier and the other as an inverter. The two converters are connected either back-to-back or joined together by a DC cable, depending on the application. Its main function is to transmit constant DC power from the rectifier to the inverter station, with high controllability. The schematic representation of the HVDC-VSC and its equivalent circuit are shown in Figure 2.8.

One VSC controls DC voltage and the other the transmission of active power through the DC link. Assuming lossless converters, the active power flow entering the DC system must equal the active power reaching the AC system at the inverter end minus the transmission losses in the DC cable. During normal operation, both converters have independent reactive power control [24].

Based on the equivalent circuit shown in Figure 2.8(b), and assuming three-phase parameters, the following transfer admittance equation can be written as:

$$E_{vR1}^{\rho} = V_{vR1}^{\rho}\left(\cos\delta_{vR1}^{\rho} + \mathrm{j}\sin\delta_{vR1}^{\rho}\right) \tag{2.18}$$

$$E_{vR2}^{\rho} = V_{vR2}^{\rho}\left(\cos\delta_{vR2}^{\rho} + \mathrm{j}\sin\delta_{vR2}^{\rho}\right) \tag{2.19}$$

$$\mathrm{Re}\left\{-E_{vR1}^{\rho}\left(I_{vR1}^{\rho}\right)^{*} + E_{vR2}^{\rho}\left(I_{m}^{\rho}\right)^{*}\right\} = 0 \tag{2.20}$$

where ρ indicates phase quantities, *a*, *b* and *c*.

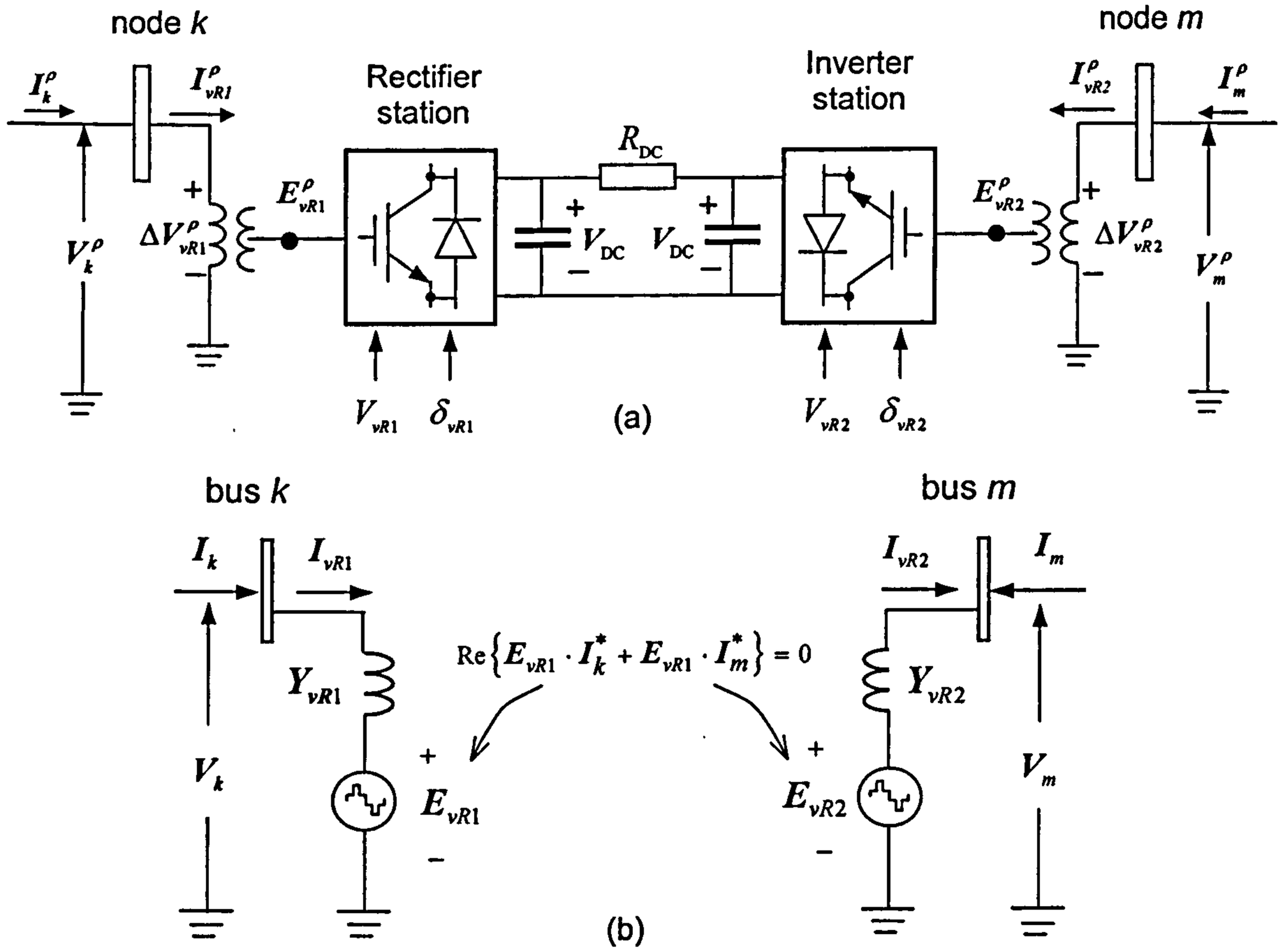

Figure 2.8 HVDC-VSC system: (a) The VSC at the sending end performs the role of rectifier and the VSC at the receiving end performs the role of inverter; (b) Equivalent circuit

Based on the equivalent circuit shown in Figure 2.8(b), and assuming three-phase parameters, the following transfer admittance equation can be written:

$$\begin{bmatrix} I_k \\ I_m \end{bmatrix} = \begin{bmatrix} Y_{vR1} & -Y_{vR1} & 0 & 0 \\ 0 & 0 & Y_{vR2} & -Y_{vR2} \end{bmatrix} \begin{bmatrix} V_k \\ E_{vR1} \\ V_m \\ E_{vR2} \end{bmatrix} \tag{2.21}$$

where all the parameters have been defined in (2.4)-(2.7) and (2.10)-(2.13).

2.9 Control Capabilities of VSC-based Controllers

To a greater or lesser extent, the three "series" VSC-based controllers, namely the SSSC, the UPFC and the HVDC-VSC, share similar power system control capabilities. They are able to regulate either nodal voltage magnitude or injection of reactive power

at one of its terminals, and active power flow through the controller. The UPFC and the HVDC-VSC employ two converters and are able to regulate nodal voltage magnitude with one of them and reactive power injection with the other. From the perspective of fundamental frequency power system studies, there is little difference between the control flexibility afforded by the three controllers, except that the UPFC and HVDC-SVC do it more robustly than the SSSC. The individual control functions are illustrated in Figure 2.9, with reference to the operating regions of the SSSC.

The equivalent circuit of the SSSC shown Figure 2.6(b) is used as the basis for the analysis. The voltage magnitude of $V_m\underline{|\theta_m}$, can be controlled at a specified value by injecting an in-phase/anti-phase voltage increment $\Delta V_{cR}\underline{|\delta_{cr} = \theta_m}$, as illustrated in Figure 2.9(a). Notice that for the purpose of drawing the phasor diagrams in Figure 2.9, the phase angle θ_m is taken to have a value of 0°. Series reactive compensation can be achieved by injecting a complex voltage, $\Delta V_{cR}\underline{|\delta_{cR} = \gamma_m \pm 90°}$, which is in quadrature with the line current, $I_m\underline{|\gamma_m}$, as illustrated in Figure 2.9(b). Pure phase angle control is also possible, as shown in Figure 2.9(c), by injecting an angular quantity, $1\underline{|\pm\delta_{cR}}$, to the otherwise unaffected voltage, $V_m\underline{|\theta_m}$. Furthermore, all three functions can be applied simultaneously by injecting an incremental complex voltage $\Delta V_{cR}\underline{|\delta_{cR}}$ to $V_m\underline{|\theta_m}$, as shown in Figure 2.9(d), a characteristic, which adds unrivalled flexibility in power system operation.

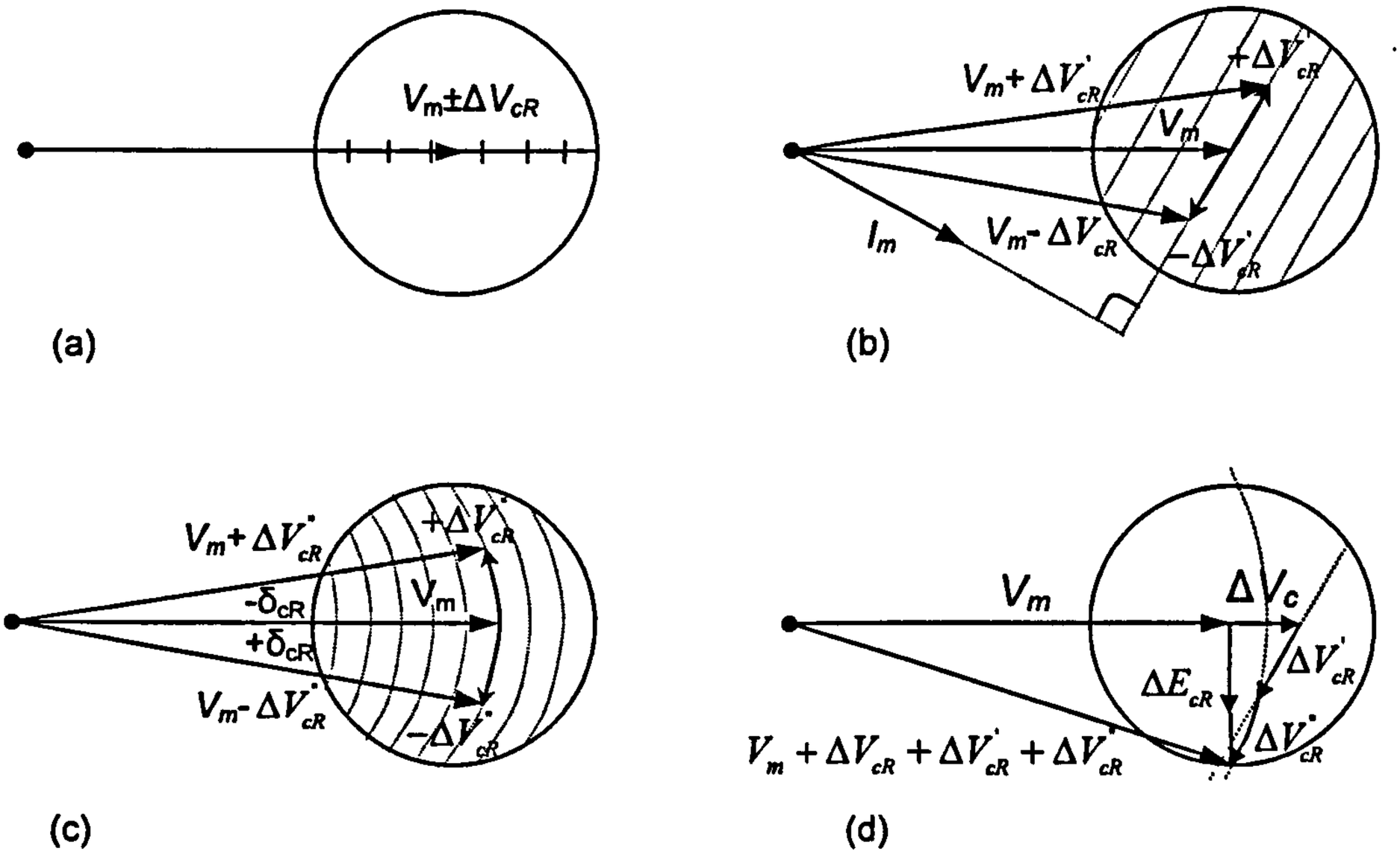

Figure 2.9 Phasor diagram illustrating the general concept of: (a) Magnitude voltage control; (b) Impedance line compensation; (c) Phase angle regulation; and (d) Simultaneous control

2.10 Summary

This chapter has presented an overview of the most salient characteristics of the power electronic equipment currently used in the electricity supply industry for the purpose of voltage regulation; active and reactive power flow control; and power quality enhancement. The emphasis has been on steady-state operation, and a distinction has been made between power electronic equipment, which use conventional power semiconductor devices, i.e. thyristors, and the new generation of power system controllers, which use fully controllable semiconductor devices such as GTOs and IGBTs. The latter devices work on well with fast switching control techniques, such as the sinusoidal PWM control scheme; and, from the power system perspective, operate like voltage sources having an almost delay-free response. Equipment based on thyristors have a slower speed of response, greater than one cycle of the fundamental frequency, and use phase control as opposed to PWM control. From the power system perspective, thyristor-based controllers behave like controllable reactances as opposed to voltage sources.

The STATCOM, SSSC, UPFC and HVDC-VSC use the VSC as their basic building block. It has been emphasised that all these power electronic controllers produce harmonic distortion, which is an undesirable side effect, as part of their normal operation. The various means of harmonic cancellation open to system engineers have been mentioned, such as switching control, multi-level configurations, three-phase connections and, as a last resort, filtering equipment. The emphasis has been on deriving flexible models, in the form of nodal admittance matrices that use the frame of reference of the phases, which is a frame of reference closely associated with the physical structure of the actual power system plant. A major strength of this frame of reference is that all the design and operational imbalances present in the power system are incorporated quite straightforwardly in to the model. Nevertheless, it is acknowledged that very often it is desirable to reduce the comprehensiveness of the power system solution, and to carry out the study in the frame of reference of the sequences, rather than in the phases. This has the advantage of speedier calculations, but key information becomes unavailable, since sequence domain modelling assumes that no imbalances are present in the plant being modelled. When such an assumption is incorporated in to the phase domain nodal admittance models, it yields simpler models expressed in the frame of reference of the sequences.

2.11 References

[1] Hingorani, N.G. and Gyugyi, L.: "*Understanding FACTS concepts and technology of Flexible AC Transmission Systems*", The Institute of Electrical and Electronics Engineers, NY, 2000. ISBN 0780334558.

[2] Hingorani, N.G.: "*Flexible AC Transmission Systems*", IEEE *Spectrum*, Vol. 30, No. 4, April 1993, pp. 41-48.

[3] Hingorani, N.G.: "Introducing custom power", *IEEE Spectrum*, Vol. 32, No. 6, June 1995, pp. 41-48.

[4] Arrillaga, J.: "*High voltage direct current transmission*", The Institution of Electrical Engineers, 2nd Edition, London UK, 1998. INSB 0906048974

[5] Hingorani, N.G.: "High voltage DC transmission: a power electronics work-horse", *IEEE Spectrum*, Vol. 33, No.4, April 1996, pp. 63-72.

[6] McMurray, W.: "Feasibility of GTO thyristors in a HVDC transmission System", *EPRI EL-5332*, Project 2443-5, Final Report, Aug. 1987.

[7] Larsen, E.V., Bowler, C., Damsky, B. and Nilsson, S.: "Benefits of thyristor controlled series compensation", *International Conference on Large High Voltage Electric Systems* (CIGRE), Paper 14/37/38-04, Paris, Sep. 1992.

[8] Miller, T.J.E.: "*Reactive power control in electric systems*", John Wiley Interscience, 1982. INSB 0471869333.

[9] IEEE/CIGRE: "FACTS overview", Special Issue, 95TP108, IEEE *Service Center*, Piscataway, N.J., 1995.

[10] Stagg, G.W. and El-Habiad, H.: "*Computer methods in power systems analysis*", McGraw-Hill, 1968. ISNB 67-129963-07-060658-7.

[11] Wollenberg, B. and Wood, A.J.: "*Power generation, operation and control*", John Wiley & Sons, 2nd Edition, 1984. INSB 0471169218.

[12] Arrillaga, J., Watson, N. R.: "*Computer modelling of electrical power system*", Second Ed. Wiley and Sons Ltd, Sussex, Eng., 2001. INSB 0-471-872490.

[13] Acha, E. and Madrigal, M.: "*Power system harmonics: computer modelling and analysis*", John Wiley & Sons, Chichester, Eng., 2001. INSB 0471521752

[14] Kundur, P.: "*Power system stability and control*", McGraw-Hill, NY, 1994. INSB 007035958X

[15] Anaya-Lara, O. and Acha, E.: "Modelling and analysis of custom power systems by PSCAD/EMTDC", IEEE *Trans. Power Del*, Vol. 7, No. 1, Jan. 2002, pp 266-272.

[16] Fuerte-Esquivel, C. R., Acha, E. and Ambriz-Perez, H.: "A thyristor controlled series compensator model for the power flow solution of practical power networks", IEEE *Trans. Power Syst.*, Vol. 15, No. 1, Feb. 2000, pp. 58-64.

[17] Kinney, S.J., Mittelstadt, W.A. and Suhrbier, R.W.: "The Results and initial experience for the BPA 500 kV thyristor controlled series capacitor unit at Slatt substation, part I – design, operation and fault test results", *Flexible AC Transmission Systems: The Future in High Voltage Transmission Conference*, EPRI, Baltimore, Maryland, Oct. 1994.

[18] Christl, N., Hedin R., Sadek, K., Lutzelberger, P., Krause, P.E., McKenna, S.M., Montoya, A.H. and Torgerson, D.: "Advanced series compensation (ASC) with thyristor controlled impedance", *International Conference on Large High Voltage Electric Systems* (CIGRE), Paper 14/37/38-05, Paris, Sep. 1992.

[19] Mohan, N., Undeland, T. M. and Robbins, W. P.: "*Power electronics: converter applications and design*", John Wiley & Sons, 3rd Edition, 2003. INSB 0471429082.

[20] Hingorani, N.G.: "High power electronics and flexible AC transmission systems", IEEE *Power Eng. Review*, July 1998, pp. 3-4.

[21] Raju, N.R., Venkata, S.S. and Sastry, V.V.: "The use of decoupled converters to optimise the power electronics of shunt and series AC system controllers", IEEE *Trans. Power Del*, Vol. 12, No. 2, April 1997, pp. 895-900.

[22] Nabavi-Niaki, A. and Iravani, M.R.: "Steady-state and dynamic models of unified power flow controller (UPFC) for power system studies", IEEE *Trans. Power Syst.*, Vol. 11, No. 4, Nov. 1996, pp. 1937-1943.

[23] Fuerte-Esquivel, C.R., Acha, E. and Ambriz-Perez, H.: "A comprehensive UPFC model for the quadratic load flow solution of power networks", IEEE *Trans. Power Syst.*, Vol. 15, No. 1, Feb. 2000, pp. 102-109.

[24] Asplund, G.: "Application of HVDC light to power system enhancement", IEEE *Winter Meeting*, Session: Development and Application of Self-Commutated Converters in Power Systems, Singapore, Jan. 2000.

Chapter 3

PHASE-DOMAIN POWER FLOWS POLAR CO-ORDINATES FRAME OF REFERENCE INCLUDING VSC-BASED FACTS

3.1 Introduction

The main difference between FACTS controllers and conventional power system plant components is that the former have time-varying topologies, which in turn interact with the power system to produce voltage and current distortions as well as imbalanced operating conditions. This together with any asymmetry in transmission lines, loads and sources calls for the necessity to carry out power flow analysis in the phase reference frame. A comprehensive theory covering the steady-state modelling and analysis of power systems in phase co-ordinates was developed and published in the late sixties [1]. From early 1970s onwards, a long list of extensions and applications of this theory to power flow analysis have been reported [2-15]. However, only a few papers take into account controllable components [6,8,16-17]. Additionally, in this context, little progress has been reported on power flow models taking into account power-electronics-based controllers [9,11,16-18]. Bearing this in mind, this chapter presents the latest generation of Synchronous Voltage Source Converter-based Controllers. It's include the Static Synchronous Compensator (STATCOM or SSC), the Static Synchronous Series Compensator (SSSC), the Unified Power Flow Compensator (UPFC), and the High Voltage DC (HVDC-VSC).

Using the mathematical models developed on Chapter 2, the present chapter focuses on the extension of the controller models to be suitable to include them in a three-phases power flow algorithm including the whole networks components. For the operational point of view, the power flow analysis has been traditionally performed in the assumption that three-phase networks operate under perfect balanced network components, i.e. a single, positive sequence network is involved. Newton-Raphson method to solve the power flow in positive sequence has shown possesses good characteristics to treat with power flow analysis [19-23]. Based in these considerations Newton-Raphson has been adopted to solve the three-phase power flow analysis.

3.2 General Phase-domain Power Flows

Using the Newton-Raphson method in polar co-ordinates to solve for the power flow for each plant component making up the network, the relevant power flow and Jacobian equations are chosen based up on the types of bus to which the plant component is connected. These buses determine the location of the individual active and reactive

power contributions to the mismatch vector as well as the Jacobian terms in the overall Jacobian matrix. Based up on this idea, and because transmission lines are responsible for introducing considerable geometric unbalance, only the power flow equations and Jacobian terms associated to the three-phase transmission line in power flow model are presented in this section to illustrate the technique. Figure 3.1 shown a schematic representation of the three-phase transmission line, where the phases are electrically coupled [1-3].

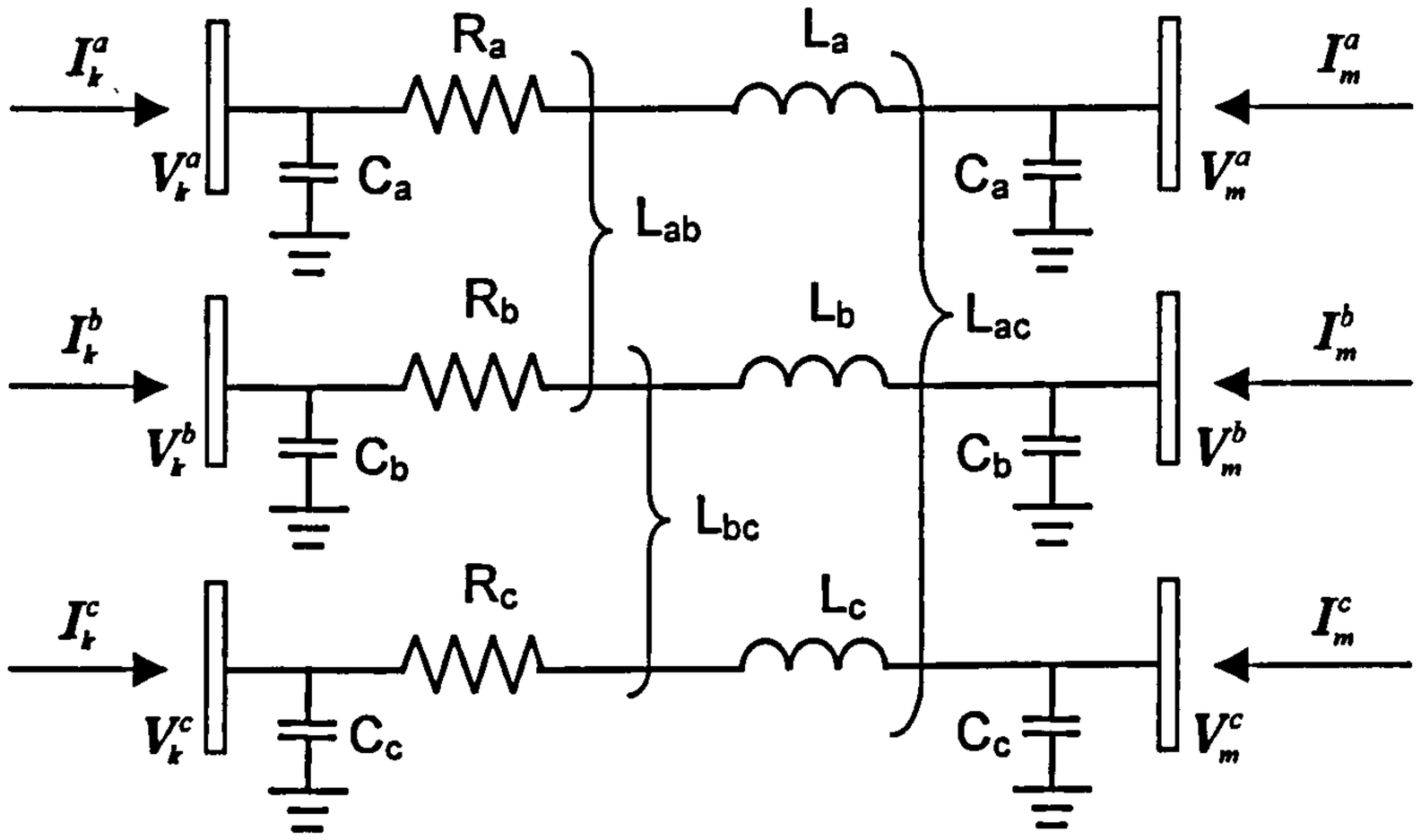

Figure 3.1 Three-phase transmission line

Accord in Figure 3.1 the power balance equation for a three-phase transmission line at each node can be written as,

$$\boldsymbol{S}^{a,b,c} = P^{a,b,c} + \mathrm{j}Q^{a,b,c} = \boldsymbol{V}^{a,b,c}\left(\boldsymbol{I}^{a,b,c}\right)^{*} \tag{3.1}$$

where

$\boldsymbol{S}^{a,b,c}$ is the complex power injected into the three-phase bus

$P^{a,b,c}$ is the real power injected into the three-phase bus

$Q_k^{a,b,c}$ is reactive power injected into the three-phase bus

$\boldsymbol{V}^{a,b,c}$ are the complex voltages of the three-phase bus

$\boldsymbol{I}^{a,b,c}$ are the complex currents injected into the three-phase bus

and *a*, *b* and *c* refer to the three-phases.

Assuming $\rho = a, b$ and c, the three-phase currents injected into one node may be expressed as a function of the currents flowing in the branches connected to the node:

$$\boldsymbol{I}_{bus}^{\rho} = \boldsymbol{Y}_{bus}^{\rho}\boldsymbol{V}_{bus}^{\rho} \tag{3.2}$$

Substitution of Equation (3.2) in (3.1), the complex power at bus *k* becomes

$$S_k^\rho = P_k^\rho + \mathrm{j}Q_k^\rho = V_k^\rho \sum_{i=k,m} \left(Y_{ki}^\rho\right)^* \left(V_i^\rho\right)^* \tag{3.3}$$

In polar co-ordinate analysis, the bus voltages are expressed as a function of the voltage magnitude and phase angle. Hence, the voltage matrix at node *k* is,

$$V_k^\rho = \begin{bmatrix} V_k^a \angle \theta_k^a \\ V_k^b \angle \theta_k^b \\ V_k^c \angle \theta_k^c \end{bmatrix} \tag{3.4}$$

The transmission line admittances matrix is expressed in complex form [2] as

$$Y_{km}^{\rho\rho} = \begin{bmatrix} Y_{km}^{aa} & Y_{km}^{ab} & Y_{km}^{ac} \\ Y_{km}^{ba} & Y_{km}^{bb} & Y_{km}^{bc} \\ Y_{km}^{ca} & Y_{km}^{cb} & Y_{km}^{cc} \end{bmatrix} = \begin{bmatrix} G_{km}^{aa} + \mathrm{j}B_{km}^{aa} & G_{km}^{ab} + \mathrm{j}B_{km}^{ab} & G_{km}^{ac} + \mathrm{j}B_{km}^{ac} \\ G_{km}^{ba} + \mathrm{j}B_{km}^{ba} & G_{km}^{bb} + \mathrm{j}B_{km}^{bb} & G_{km}^{bc} + \mathrm{j}B_{km}^{bc} \\ G_{km}^{ca} + \mathrm{j}B_{km}^{ca} & G_{km}^{cb} + \mathrm{j}B_{km}^{cb} & G_{km}^{cc} + \mathrm{j}B_{km}^{cc} \end{bmatrix} \tag{3.5}$$

3.2.1 Power Flow equations

Substitution of equation (3.4) and (3.5) in (3.3). After some arduous algebra, the expressions for active and reactive powers injected into phases *a*, *b* and *c* of bus *k*, are arrived at, where

$$P_k^\rho = V_k^\rho \left\{ \sum_{i=k,m} \sum_{j=a,b,c} V_i^j \left[G_{ki}^{\rho j} \cos\left(\theta_k^\rho - \theta_i^j\right) + B_{ki}^{\rho j} \sin\left(\theta_k^\rho - \theta_i^j\right) \right] \right\} \tag{3.6}$$

$$Q_k^\rho = V_k^\rho \left\{ \sum_{i=k,m} \sum_{j=a,b,c} V_i^j \left[G_{ki}^{\rho j} \sin\left(\theta_k^\rho - \theta_i^j\right) - B_{ki}^{\rho j} \cos\left(\theta_k^\rho - \theta_i^j\right) \right] \right\} \tag{3.7}$$

The superscript ρ is used to denote phases *a*, *b* and *c*. The complete process to derivate the power equations for the transmission line is show in Appendix I. A similar process is used to derivate power equations for all over power plants components.

As expected, the expressions for calculating the active and reactive powers injected into bus *m* are of the same form as (3.6) and (3.7), with the subscript *m* replacing *k* and *vice versa*:

$$P_m^\rho = V_m^\rho \left\{ \sum_{i=m,k} \sum_{j=a,b,c} V_i^j \left[G_{mi}^{\rho j} \cos\left(\theta_m^\rho - \theta_i^j\right) + B_{mi}^{\rho j} \sin\left(\theta_m^\rho - \theta_i^j\right) \right] \right\} \tag{3.8}$$

$$Q_m^\rho = V_m^\rho \left\{ \sum_{i=m,k} \sum_{j=a,b,c} V_i^j \left[G_{mi}^{\rho j} \sin\left(\theta_m^\rho - \theta_i^j\right) - B_{mi}^{\rho j} \cos\left(\theta_m^\rho - \theta_i^j\right) \right] \right\} \tag{3.9}$$

3.2.2 Newton-Raphson power flow algorithm

In order to perform the Newton-Raphson method to carry out large-scale power flow analysis in the phase frame of reference under polar co-ordinates for a three-phase balanced or unbalanced network, the power flow equations given by equations (3.6)-(3.9) can be expanded into Taylor series [21] and the following first order approximation can be obtained.

$$\begin{bmatrix} \Delta P_k^{a,b,c} \\ \Delta P_m^{a,b,c} \\ \Delta Q_k^{a,b,c} \\ \Delta Q_k^{a,b,c} \end{bmatrix} = \begin{bmatrix} \frac{\partial P_k^{a,b,c}}{\partial \theta_k^{a,b,c}} & \frac{\partial P_k^{a,b,c}}{\partial \theta_m^{a,b,c}} & \frac{\partial P_k^{a,b,c}}{\partial V_k^{a,b,c}} V_k^{a,b,c} & \frac{\partial P_k^{a,b,c}}{\partial V_m^{a,b,c}} V_m^{a,b,c} \\ \frac{\partial P_m^{a,b,c}}{\partial \theta_k^{a,b,c}} & \frac{\partial P_m^{a,b,c}}{\partial \theta_m^{a,b,c}} & \frac{\partial P_m^{a,b,c}}{\partial V_k^{a,b,c}} V_k^{a,b,c} & \frac{\partial P_m^{a,b,c}}{\partial V_m^{a,b,c}} V_m^{a,b,c} \\ \frac{\partial Q_k^{a,b,c}}{\partial \theta_k^{a,b,c}} & \frac{\partial Q_k^{a,b,c}}{\partial \theta_m^{a,b,c}} & \frac{\partial Q_k^{a,b,c}}{\partial V_k^{a,b,c}} V_k^{a,b,c} & \frac{\partial Q_k^{a,b,c}}{\partial V_m^{a,b,c}} V_m^{a,b,c} \\ \frac{\partial Q_m^{a,b,c}}{\partial \theta_k^{a,b,c}} & \frac{\partial Q_m^{a,b,c}}{\partial \theta_m^{a,b,c}} & \frac{\partial Q_m^{a,b,c}}{\partial V_k^{a,b,c}} V_k^{a,b,c} & \frac{\partial Q_m^{a,b,c}}{\partial V_m^{a,b,c}} V_m^{a,b,c} \end{bmatrix} \begin{bmatrix} \Delta \theta_k^{a,b,c} \\ \Delta \theta_m^{a,b,c} \\ \frac{\Delta V_k^{a,b,c}}{V_k^{a,b,c}} \\ \frac{\Delta V_m^{a,b,c}}{V_m^{a,b,c}} \end{bmatrix} \tag{3.10}$$

where the elements are a 3x1 or 3x3 matrices with vectors and matrix elements. The various matrices in the Jacobian matrix now may consist of 3×3 elements of the form:

$$\begin{matrix} \frac{\partial P_{k,m}^{\rho 1}}{\partial \theta_{k,m}^{\rho 2}} & \frac{\partial P_{k,m}^{\rho 1}}{\partial V_{k,m}^{\rho 2}} V_{k,m}^{\rho 2} \\ \frac{\partial Q_{k,m}^{\rho 1}}{\partial \theta_{k,m}^{\rho 2}} & \frac{\partial Q_{k,m}^{\rho 1}}{\partial V_{k,m}^{\rho 2}} V_{k,m}^{\rho 2} \end{matrix} \tag{3.11}$$

where ρ refers to *a*, *b* and *c* phases and k=1,..,nb and m=1,..,nb but omitting the *slack* bus entries. Each one of above elements is a 3×3 matrix which is symmetric if the network is balanced and asymmetric if matrix is unbalanced.

Consider the i^{th} transmission element connected between buses k and m in (3.10), for which self and mutual Jacobian terms are given below.

For k ≠ m

$$\frac{\partial P_{k,i}^{\rho 1}}{\partial \theta_{m,i}^{\rho 2}} = V_k^{\rho 1} V_m^{\rho 2} \left[G_{km}^{\rho 1 \rho 2} \sin\left(\theta_k^{\rho 1} - \theta_m^{\rho 2}\right) - B_{km}^{\rho 1 \rho 2} \cos\left(\theta_k^{\rho 1} - \theta_m^{\rho 2}\right) \right] \tag{3.12}$$

$$\frac{\partial P_{k,i}^{\rho 1}}{\partial V_{m,i}^{\rho 2}} V_{m,i}^{\rho 2} = V_k^{\rho 1} V_m^{\rho 2} \left[G_{km}^{\rho 1 \rho 2} \cos\left(\theta_k^{\rho 1} - \theta_m^{\rho 2}\right) + B_{km}^{\rho 1 \rho 2} \sin\left(\theta_k^{\rho 1} - \theta_m^{\rho 2}\right) \right] \tag{3.13}$$

$$\frac{\partial Q_{k,i}^{\rho 1}}{\partial \theta_{m,i}^{\rho 2}} = -V_k^{\rho 1} V_m^{\rho 2} \left[G_{km}^{\rho 1 \rho 2} \cos\left(\theta_k^{\rho 1} - \theta_m^{\rho 2}\right) + B_{km}^{\rho 1 \rho 2} \sin\left(\theta_k^{\rho 1} - \theta_m^{\rho 2}\right) \right] \tag{3.14}$$

$$\frac{\partial Q_{k,i}^{\rho 1}}{\partial V_{m,i}^{\rho 2}} V_{m,i}^{\rho 2} = V_k^{\rho 1} V_m^{\rho 2} \left[G_{km}^{\rho 1 \rho 2} \sin\left(\theta_k^{\rho 1} - \theta_m^{\rho 2}\right) - B_{km}^{\rho 1 \rho 2} \cos\left(\theta_k^{\rho 1} - \theta_m^{\rho 2}\right) \right] \tag{3.15}$$

For $k = m$:
For $\rho 1 = \rho 2$

$$\frac{\partial P_{k,i}^{\rho 1}}{\partial \theta_{k,i}^{\rho 2}} = -Q_k^{\rho 1 \,\mathrm{cal}} - \left(V_k^{\rho 1}\right)^2 B_{kk}^{\rho 1 \rho 1} \tag{3.16}$$

$$\frac{\partial P_{k,i}^{\rho 1}}{\partial V_{k,i}^{\rho 2}} V_{k,i}^{\rho 1} = P_k^{\rho 1 \,\mathrm{cal}} + \left(V_k^{\rho 1}\right)^2 G_{kk}^{\rho 1 \rho 1} \tag{3.17}$$

$$\frac{\partial Q_{k,i}^{\rho 1}}{\partial \theta_{k,i}^{\rho 2}} = P_k^{\rho 1 \,\mathrm{cal}} - \left(V_k^{\rho 1}\right)^2 G_{kk}^{\rho 1 \rho 1} \tag{3.18}$$

$$\frac{\partial Q_{k,i}^{\rho 1}}{\partial V_k^{\rho 2}} V_k^{\rho 2} = Q_k^{\rho 1 \,\mathrm{cal}} - \left(V_k^{\rho 1}\right)^2 B_{kk}^{\rho 1 \rho 1} \tag{3.19}$$

For $\rho 1 \neq \rho 2$

$$\frac{\partial P_{k,i}^{\rho 1}}{\partial \theta_{k,i}^{\rho 2}} = V_k^{\rho 1} V_k^{\rho 2} \left[G_{kk}^{\rho 1 \rho 2} \sin\left(\theta_k^{\rho 1} - \theta_k^{\rho 2}\right) - B_{kk}^{\rho 1 \rho 2} \cos\left(\theta_k^{\rho 1} - \theta_k^{\rho 2}\right) \right] \tag{3.20}$$

$$\frac{\partial P_{k,i}^{\rho 1}}{\partial V_{k,i}^{\rho 2}} V_{k,i}^{\rho 2} = V_k^{\rho 1} V_k^{\rho 2} \left[G_{kk}^{\rho 1 \rho 2} \cos\left(\theta_k^{\rho 1} - \theta_k^{\rho 2}\right) + B_{kk}^{\rho 1 \rho 2} \sin\left(\theta_k^{\rho 1} - \theta_k^{\rho 2}\right) \right] \tag{3.21}$$

$$\frac{\partial Q_{k,i}^{\rho 1}}{\partial \theta_{k,i}^{\rho 2}} = -V_k^{\rho 1} V_k^{\rho 2} \left[G_{kk}^{\rho 1 \rho 2} \cos\left(\theta_k^{\rho 1} - \theta_k^{\rho 2}\right) + B_{kk}^{\rho 1 \rho 2} \sin\left(\theta_k^{\rho 1} - \theta_k^{\rho 2}\right) \right] \tag{3.22}$$

$$\frac{\partial Q_{k,i}^{\rho 1}}{\partial V_{k,i}^{\rho 2}} V_{k,i}^{\rho 1} = V_k^{\rho 1} V_k^{\rho 2} \left[G_{kk}^{\rho 1 \rho 2} \sin\left(\theta_k^{\rho 1} - \theta_k^{\rho 2}\right) - B_{kk}^{\rho 1 \rho 2} \cos\left(\theta_k^{\rho 1} - \theta_k^{\rho 2}\right) \right] \tag{3.23}$$

The mutual elements given by equations (3.12)-(3.15) remain the same whether we have one transmission element or *n* transmission elements terminating at bus *k*.

The Jacobian matrix is evaluated at $V^{\rho} = \left(V^{\rho}\right)^{it}$ and $\theta^{\rho} = \left(\theta^{\rho}\right)^{it}$ and the generic power mismatch equations at bus *k* are:

$$\Delta P_{k,m}^{\rho} = \left(P_{k,m}^{\rho}\right)^{\text{sp}} - \left(P_{k,m}^{\rho}\right)^{\text{cal}}$$
$$\Delta Q_{k,m}^{\rho} = \left(Q_{k,m}^{\rho}\right)^{\text{sp}} - \left(Q_{k,m}^{\rho}\right)^{\text{cal}} \tag{3.24}$$

$\left(P_k^{\rho}\right)^{\text{sp}}$ and $\left(Q_k^{\rho}\right)^{\text{sp}}$ are the specified net power active and reactive power injections and are determinated by the complex generation and load power connected to the bus, whereas $\left(P_k^{\rho}\right)^{\text{cal,it}}$ and $\left(Q_k^{\rho}\right)^{\text{cal,it}}$ are the calculated net active and reactive power injection vectors at iterations evaluated using $\left(V^{\rho}\right)^{\text{it}}$ and $\left(\theta^{\rho}\right)^{\text{it}}$. Voltage magnitude and phase angle initialized equal to the unit and zero respectively for phase *a* and the unit and -2π/3 and 2π/3 for phases *b* and *c*, and are updated after each iteration using,

$$\left(V_{k,m}^{\rho}\right)^{it+1} = \left(\frac{\Delta V_{k,m}^{\rho}}{V_{k,m}^{\rho}}\right)^{it} \left(V_{k,m}^{\rho}\right)^{it} + \left(V_{k,m}^{\rho}\right)^{it}$$
$$\left(\theta_{k,m}^{\rho}\right)^{it+1} = \left(\Delta\theta_{k,m}^{\rho}\right)^{it} + \left(\theta_{k,m}^{\rho}\right)^{it} \tag{3.25}$$

Notice that, in polar co-ordinates, when the transmission line is connected to the slack node, ΔV^{ρ} and Q^{ρ} are set equal to zero. Whereas for PV-type nodes, ΔV^{ρ} is set to zero. Notice that for PV-type buses the reactive power generation has to be calculated and checked for reactive power limit violations. In the case of limit violations, the bus type has to be switched from PV-type to PQ-type in order to maintain the reactive generation within the specified limits.

3.2.3 Three-Phase numerical example

Digital software for analysis and control of large-scale power networks under both balanced or unbalanced conditions was developed. The software was written in Visual C++ using Object Oriented Programming (OOP). This language and technique was chosen because it makes easier the coding, debugging and maintenance of programs and because of its modularity that easily allows the incorporation of more "Objects" [23]. The three-phase OOP power flow program has been applied to the analysis of a large number of multi phase power networks of different sizes and complexity [24-25]. Power flow solutions converge in five iterations or less to a tolerance of $1e^{-12}$, starting from a flat voltage profile. The accuracies of the solution have been tested against commercial software and single-phase programs [23].

A small traditional network [19] shown in Figure 3.2 is used as the basis for illustrating how the VSC-based models for three-phase power flow performs under both balanced and unbalanced operating conditions. This is a five-bus network containing two generators and seven transmission lines. Appendix II contains all the required data for the five-bus power flow solution. Notice that voltage information is provided explicitly for the three phases, where a balanced set of three-phase voltages means equal voltage

magnitude and phase angles between adjacent phases separated by $2\pi/3$ radians, with the following rotation: 0, $-2\pi/3$, $2\pi/3$.

As expected, the solution given by the three-phase program essentially agrees with that provided by the positive sequence power flow program. More specifically, the nodal voltage magnitudes and phase angles for phase *a* of the network coincide with those for positive sequence. The voltage magnitude for phases *a*, *b* and *c* have equal values, with the phase angles for phases *b* and *c* displaced by 240 and 120 deg, with respect to phase *a*. Table 3.1 summarises the results for the balanced three-phase solution. Convergence was achieved in 5 iterations to a power mismatch tolerance of $1e^{-12}$.

It can be observed from the results presented in Figure 3.2 and Table 3.1 that all nodal voltages are within accepted voltage magnitude limits, i.e. 100 ± 6% in the United Kingdom. The largest power flow takes place in the transmission line connecting the two generator buses: 89.3 MW and 74.2 MVAR leave North and 86.8 MW and 72.9 MVAR arrive at South. This is also the transmission line that incurs higher active power loss, i.e. 2.5 MW. The active power system loss is 6.12 MW per phase, this represent the 3.57 % of the active power generation.

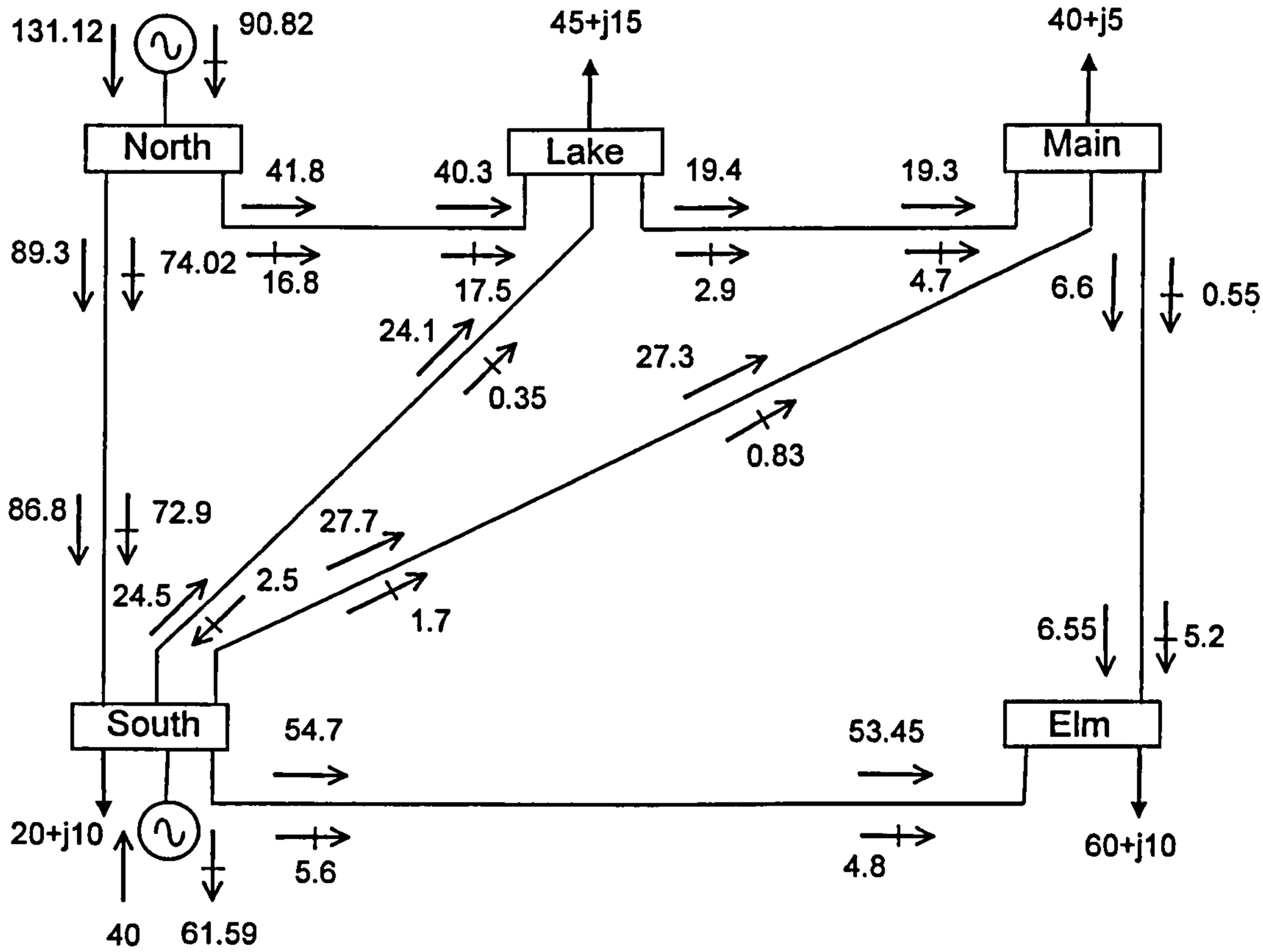

Figure 3.2 Five-bus test network and power flow results

Table.3.1 Three-phase nodal voltages for the balanced case

Voltage	Phase	Network buses				
		North	South	Lake	Main	Elm
Magnitude (p.u.)	*a*	1.06	1.00	0.9872	0.9841	0.9717
	b	1.06	1.00	0.9872	0.9841	0.9717
	c	1.06	1.00	0.9872	0.9841	0.9717
Phase angle (deg)	*a*	0	-2.06	-4.63	-4.95	-5.76
	b	240	237.93	235.36	235.04	234.23
	c	120	117.93	115.36	115.04	114.23

The operating conditions demand a large amount of reactive power generation by the generator connected at North, i.e. 90.82 MVAR. This amount is well in excess of the reactive power drawn by the system loads, i.e. 40 MVAR. The generator at South draws the excess of reactive power in the network, i.e. 61.59 MVAR. This amount includes the net reactive power produced by several of the transmission lines.

Since this is a case of balanced operation and design parameters – all loads are taken to be balanced – neither negative nor zero sequence voltages exist. An altogether different situation arises if imbalances are introduced into the test network, say in the system load. This only requires a straightforward change in the data file. At each bus, active and reactive power loads have been altered arbitrarily by ±15% with respect to the base, balanced case, as shown below.

Table 3.2 Five-bus unbalance loading ₸

Phase	Network buses							
	South		Lake		Main		Elm	
	Active	Reactive	Active	Reactive	Active	Reactive	Active	Reactive
a	20	10	51.75	17.25	34.78	4.35	60	10
b	17.39	8.695	45.0	15.0	46.0	5.75	52.17	8.7
c	23	11.5	39.13	13.04	40.0	5.0	69.0	11.5

₸ Active load in MW and reactive load in MVAR

The impact of unbalanced loading on system performance can be appreciated by comparing the results given in Table 3.3(a), where small amounts of negative and zero sequence voltages are now evident. Power system loss has increased by nearly 2% with respect to the balanced case. It can also be seen from the power flow results in Figure 3.3(a)-(c) that power flows in all three phases are unbalanced. The solution was achieved in 5 iterations to a power mismatch tolerance of 1e-12.

Table 3.3 Three-phase nodal voltages in the unbalanced network-phase voltages

Voltage	Phase	Network buses				
		North	South	Lake	Main	Elm
(a) Phase voltages						
Magnitude (p.u.)	*a*	1.06	1.00	0.9820	0.9811	0.9789
	b	1.06	1.00	0.9881	0.9831	0.9755
	c	1.06	1.00	0.9908	0.9872	0.9599
Phase angle (deg.)	*a*	0	-2.02	-4.67	-4.84	-5.96
	b	240	238.16	235.26	234.95	235.26
	c	120	117.58	115.38	114.88	113.23
(b) Sequence voltages						
Magnitude (p.u.)	Zero	0.00	0.0030	0.0032	0.0027	0.0148
	Positive	1.06	1.0000	0.9870	0.9838	0.9713
	Negative	0.00	0.0030	0.0020	0.0017	0.0070

It should be noted that imbalance generates a fair amount of loss of active power for this condition, i.e. 18.72 MW, which represents the 3.62% of generation against the 3.57% under balanced conditions.

It has been stated in the introduction to this chapter that VSC-based controllers intended for nodal voltage control could perform the role of restoring voltage magnitude balance at the point of connection. It was also argued that a series compensator could provide a useful role in balancing out power flows at the point of compensation.

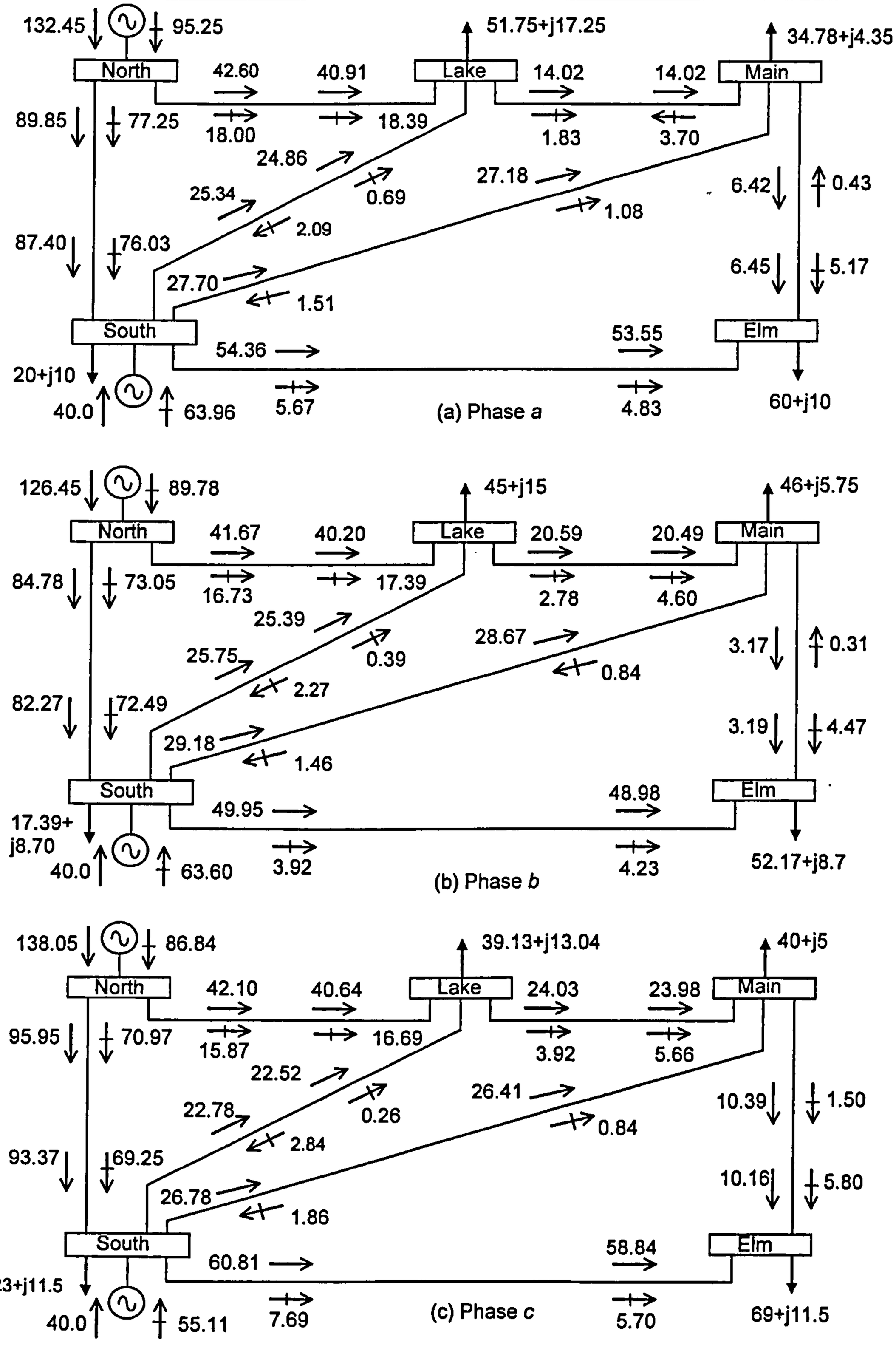

Figure 3.3 Three-phase power flows, (a) phase *a*, (b) phase *b*, and (c) phase *c*

3.3 Static Synchronous Compensator

From the principles of operation outlined at Section 2.5, it follows that for the purpose of fundamental frequency analysis the Static Synchronous Compensator (STATCOM or SSC) consists of a voltage source converter (VSC) in shunt coupling with the bus via a series inductance and series resistance. The primary and main function of the static synchronous compensator (STATCOM) controller is for voltage control by injection or absorption of reactive power at the compensated node [26-30]. The STATCOM is represented in flow power studies as a synchronous generator with zero active power generation and reactive powers limits. Hence, the equivalent circuit shown in Figure 3.4 is used to derive the mathematical model of the STATCOM three-phase in polar co-ordinates for inclusion in the power flow Newton-Raphson method.

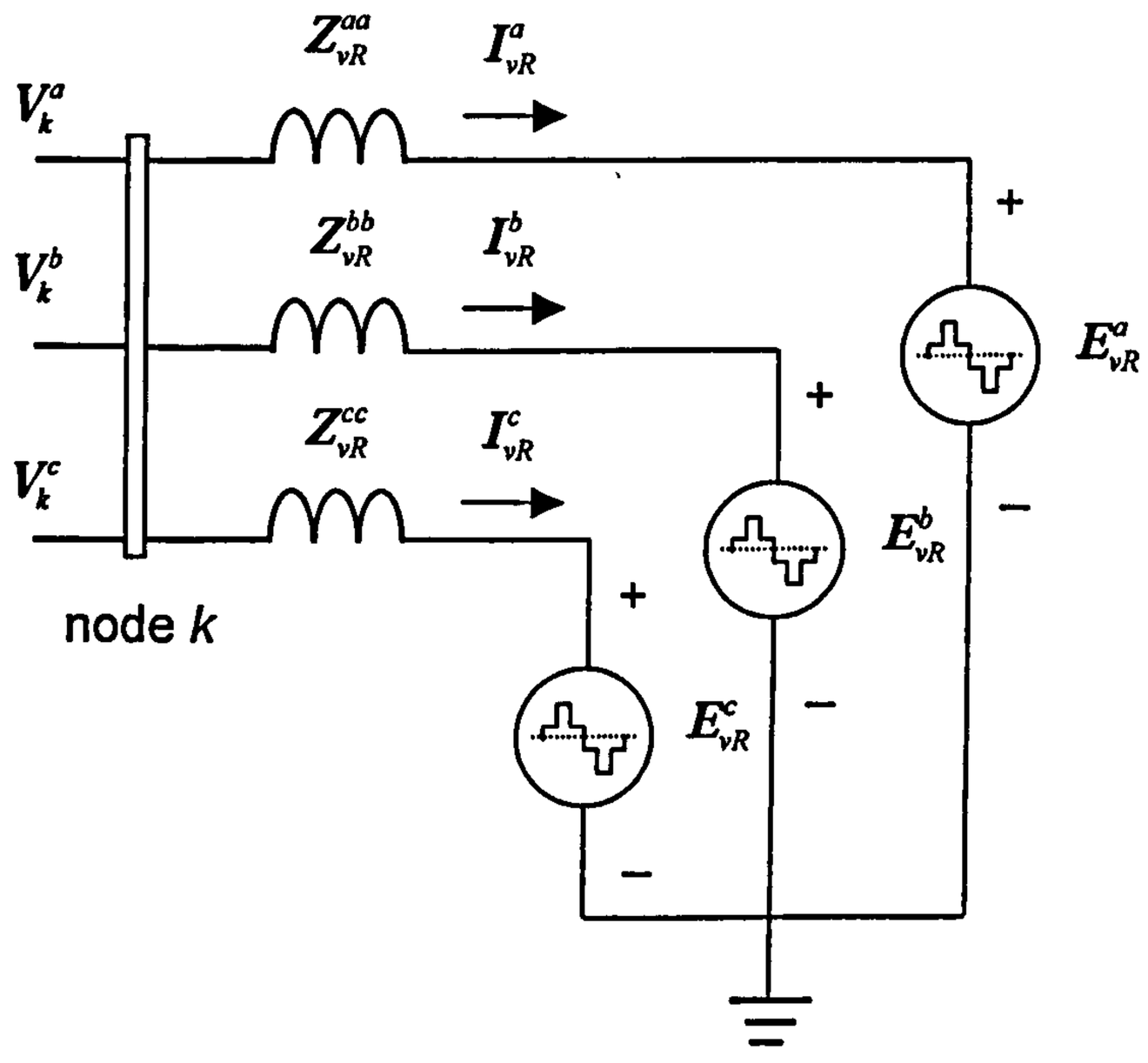

Figure 3.4 Three-phase STATCOM equivalent circuit

The complex voltage sources representing the VSC station in the STATCOM in polar co-ordinates is expressed as,

$$E_{vR}^{\rho} = V_{vR}^{\rho} \angle \delta_{vR}^{\rho} \tag{3.26}$$

In the current application the voltage sources were modelled with the following voltage magnitudes and phase angles limits: $V_{vR,\min}^{\rho} \le V_{vR}^{\rho} \le V_{vR,\max}^{\rho}$ and $0 \le \delta_{vR}^{\rho} \le 2\pi$.

3.3.1 Power flow equations

Based on the equivalent circuit shown in Figure 3.4, and the transfer admittance equation (2.3), the following may be written,

$$S_{vR}^{\rho} = E_{vR}^{\rho} I_{vR}^{\rho *} = E_{vR}^{\rho} \left(Y_{vR}^{\rho}\right)^{*} \left[\left(E_{vR}^{\rho}\right)^{*} - \left(V_{k}^{\rho}\right)^{*}\right] \tag{3.27}$$

After performing some complex operations, the following active and reactive power equations are obtained, at converter,

$$P_{vR}^{\rho} = \left(V_{vR}^{\rho}\right)^{2} G_{vR}^{\rho\rho} - V_{vR}^{\rho} V_{k}^{\rho} \left[G_{vR}^{\rho\rho} \cos\left(\delta_{vR}^{\rho} - \theta_{k}^{\rho}\right) + B_{vR}^{\rho\rho} \sin\left(\delta_{vR}^{\rho} - \theta_{k}^{\rho}\right)\right] \tag{3.28}$$

$$Q_{vR}^{\rho} = -\left(V_{vR}^{\rho}\right)^{2} B_{vR}^{\rho\rho} - V_{vR}^{\rho} V_{k}^{\rho} \left[G_{vR}^{\rho\rho} \sin\left(\delta_{vR}^{\rho} - \theta_{k}^{\rho}\right) - B_{vR}^{\rho\rho} \cos\left(\delta_{vR}^{\rho} - \theta_{k}^{\rho}\right)\right] \tag{3.29}$$

at node *k*

$$P_{k}^{\rho} = \left(V_{k}^{\rho}\right)^{2} G_{vR}^{\rho\rho} - V_{k}^{\rho} V_{vR}^{\rho} \left[G_{vR}^{\rho\rho} \cos\left(\theta_{k}^{\rho} - \delta_{vR}^{\rho}\right) + B_{vR}^{\rho\rho} \sin\left(\theta_{k}^{\rho} - \delta_{vR}^{\rho}\right)\right] \tag{3.30}$$

$$Q_{k}^{\rho} = -\left(V_{k}^{\rho}\right)^{2} B_{vR}^{\rho\rho} - V_{k}^{\rho} V_{vR}^{\rho} \left[G_{vR}^{\rho\rho} \sin\left(\theta_{k}^{\rho} - \delta_{vR}^{\rho}\right) - B_{vR}^{\rho\rho} \cos\left(\theta_{k}^{\rho} - \delta_{vR}^{\rho}\right)\right] \tag{3.31}$$

3.3.2 Linearised system of equations

An n-node power network with no voltage and power flow regulation provisions is described by a 2×(nb-1) non-linear system of equations. Moreover, for each STATCOM that exists in the power network the 2×(nb-1) system of equations is augmented by up to four equations to take account of the converter station. The solution of the combined system of non-linear equations is carried out by iteration using the Newton-Raphson method, enabling quadratic convergent solutions. The elements of the linearised system of equations for the conventional power plant components are included in same way as described in section 3.2.

Although the main function of the STATCOM is for voltage control, the converter station is capable of having control over either the voltage magnitude or reactive power injected at the connecting node. It is capable of drawing real power from an energy source (large capacitor, battery, fuel cell, etc.) at its DC terminals and delivering it as AC power to the system. When both active power and reactive power are regulated, the linearised system of equations for polar co-ordinates, i.e. the voltage magnitude V_{vR}^{ρ} and phase angle δ_{vR}^{ρ} are taken to be the state variables, the system has the following structure:

$$\begin{bmatrix} \Delta P_k^\rho \\ \Delta Q_k^\rho \\ \Delta P_{vR}^\rho \\ \Delta Q_{vR}^\rho \end{bmatrix} = \begin{bmatrix} \frac{\partial P_k^\rho}{\partial \theta_k^\rho} & \frac{\partial P_k^\rho}{\partial V_k^\rho} V_k^\rho & \frac{\partial P_k^\rho}{\partial \delta_{vR}^\rho} & \frac{\partial P_k^\rho}{\partial V_{vR}^\rho} V_{vR}^\rho \\ \frac{\partial Q_k^\rho}{\partial \theta_k^\rho} & \frac{\partial Q_k^\rho}{\partial V_k^\rho} V_k^\rho & \frac{\partial Q_k^\rho}{\partial \delta_{vR}^\rho} & \frac{\partial Q_k^\rho}{\partial V_{vR}^\rho} V_{vR}^\rho \\ \frac{\partial P_{vR}^\rho}{\partial \theta_k^\rho} & \frac{\partial P_{vR}^\rho}{\partial V_k^\rho} V_k^\rho & \frac{\partial P_{vR}^\rho}{\partial \delta_{vR}^\rho} & \frac{\partial P_{vR}^\rho}{\partial V_{vR}^\rho} V_{vR}^\rho \\ \frac{\partial Q_{vR}^\rho}{\partial \theta_k^\rho} & \frac{\partial Q_{vR}^\rho}{\partial V_k^\rho} V_k^\rho & \frac{\partial Q_{vR}^\rho}{\partial \delta_{vR}^\rho} & \frac{\partial Q_{vR}^\rho}{\partial V_{vR}^\rho} V_{vR}^\rho \end{bmatrix} \begin{bmatrix} \Delta \theta_k^\rho \\ \frac{\Delta V_k^\rho}{V_k^\rho} \\ \Delta \delta_{vR}^\rho \\ \frac{\Delta V_{vR}^\rho}{V_{vR}^\rho} \end{bmatrix} \tag{3.32}$$

The Jacobian elements for this application are given below:

$$\frac{\partial P_k^\rho}{\partial \theta_k^\rho} = -Q_k^\rho - \left(V_k^\rho\right)^2 B_{vR}^\rho \tag{3.33}$$

$$\frac{\partial P_k^\rho}{\partial V_k^\rho} V_k^\rho = P_k^\rho + \left(V_k^\rho\right)^2 G_{vR}^\rho \tag{3.34}$$

$$\frac{\partial P_k^\rho}{\partial \delta_{vR}^\rho} = \frac{\partial Q_{vR}^\rho}{\partial V_k^\rho} V_k^\rho = V_{vR}^\rho V_k^\rho \left[G_{vR}^\rho \sin\left(\delta_{vR}^\rho - \theta_k^\rho\right) + B_{vR}^\rho \cos\left(\delta_{vR}^\rho - \theta_k^\rho\right) \right] \tag{3.35}$$

$$\frac{\partial P_k^\rho}{\partial V_{vR}^\rho} V_{vR}^\rho = -\frac{\partial Q_{vR}^\rho}{\partial \theta_k^\rho} = V_k^\rho V_{vR}^\rho \left[G_{vR}^\rho \cos\left(\theta_k^\rho - \delta_{vR}^\rho\right) + B_{vR}^\rho \sin\left(\theta_k^\rho - \delta_{vR}^\rho\right) \right] \tag{3.36}$$

$$\frac{\partial Q_k^\rho}{\partial \theta_k^\rho} = P_k^\rho - \left(V_k^\rho\right)^2 G_{vR}^\rho \tag{3.37}$$

$$\frac{\partial Q_k^\rho}{\partial V_k^\rho} V_k^\rho = Q_k^\rho - \left(V_k^\rho\right)^2 B_{vR}^\rho \tag{3.38}$$

$$\frac{\partial Q_k^\rho}{\partial \delta_{vR}^\rho} = -\frac{\partial P_{vR}^\rho}{\partial V_k^\rho} V_k^\rho = -V_k^\rho V_{vR}^\rho \left[G_{vR}^\rho \cos\left(\theta_k^\rho - \delta_{vR}^\rho\right) + B_{vR}^\rho \sin\left(\theta_k^\rho - \delta_{vR}^\rho\right) \right] \tag{3.39}$$

$$\frac{\partial Q_k^\rho}{\partial V_{vR}^\rho} V_{vR}^\rho = \frac{\partial P_{vR}^\rho}{\partial \theta_k^\rho} = V_k^\rho V_{vR}^\rho \left[G_{vR}^\rho \sin\left(\theta_k^\rho - \delta_{vR}^\rho\right) - B_{vR}^\rho \cos\left(\theta_k^\rho - \delta_{vR}^\rho\right) \right] \tag{3.40}$$

$$\frac{\partial P_{vR}^\rho}{\partial \delta_{vR}^\rho} = -Q_{vR}^\rho - \left(V_{vR}^\rho\right)^2 B_{vR}^\rho \tag{3.41}$$

$$\frac{\partial P_{vR}^\rho}{\partial V_{vR}^\rho} V_{vR}^\rho = P_{vR}^\rho + \left(V_{vR}^\rho\right)^2 G_{vR}^\rho \tag{3.42}$$

$$\frac{\partial Q_{vR}^\rho}{\partial \delta_{vR}^\rho} = P_{vR}^\rho - \left(V_{vR}^\rho\right)^2 G_{vR}^\rho \tag{3.43}$$

$$\frac{\partial Q_{vR}^{\rho}}{\partial V_{vR}^{\rho}} V_{vR}^{\rho} = Q_{vR}^{\rho} - \left(V_{vR}^{\rho}\right)^2 B_{vR}^{\rho} \tag{3.44}$$

When the voltage magnitude is controlled at the node, where a STATCOM is connected, the node becomes a PV-type node and changes to the Jacobian matrix and the mismatches vector take place, i.e. ΔV_k^{ρ} are set equal zero.

Upon solution of the Jacobian matrix, a new set of state variable increments is obtained. The increments are used to update the VSC magnitude and phase angle for each iteration using

$$\begin{aligned} \left(V_{vR}^{\rho}\right)^{it+1} &= \left(\frac{\Delta V_{vR}^{\rho}}{V_{vR}^{\rho}}\right)^{it} \left(V_{vR}^{\rho}\right)^{it} + \left(V_{vR}^{\rho}\right)^{it} \\ \left(\delta_{vR}^{\rho}\right)^{it+1} &= \left(\Delta\delta_{vR}^{\rho}\right)^{it} + \left(\delta_{vR}^{\rho}\right)^{it} \end{aligned} \tag{3.45}$$

Voltage magnitude limits are checked at the end of each iterative step, and if one or more limits is violated, the voltage magnitude is fixed at the violated limit. Notice that, for the STATCOM controlling the reactive power generation, it has to be calculated and checked for reactive power limit violations. For the case of limit violation, the reactive power has to be fixed to the limit violation.

3.3.3 STATCOM three-phase numerical example

The five-bus unbalanced network used in Section 3.2.3 is modified to include a three-phase STATCOM model. It is used to balance the voltage magnitude at Elm to 0.98 p.u. The source impedances are $X_{vR} = 0.1$ p.u. per phase. The power flow results indicate that the STATCOM generates 4.81 MVAR, 8.47 MVAR and 15.25 MVAR in phases *a*, *b* and *c*, respectively, in order to achieve the three-phase voltage magnitude target. The STATCOM parameters associated with this amount of reactive power generation are: V_{vR}=0.9849, 0.9886 and 0.9955 p.u. for *a*, *b* and *c* phases, respectively.

Nodal voltage magnitudes and phase angles are given in Table 3.4(a), and sequence domain voltage magnitudes are given in Table 3.4(b), where it is shown that the STATCOM is effective in regulating and balancing the nodal voltage magnitudes at Elm. As expected, the phase angles at that bus are still unbalanced. It should be mentioned that the power losses now stand at 3.58%, a result that compares favourably with the unbalanced case where no device is used and where power losses stand at 3.62%. Notice that negative sequence voltages have also reduced in magnitude. The power flows within the STATCOM embed are shown in Figure 3.5

Table 3.4 Nodal voltage in the three-phase unbalanced network with a STATCOM – phase voltages

Voltage		Network buses				
	Phase	North	South	Lake	Main	Elm
(a) Phase voltages						
Magnitude (p.u.)	*a*	1.06	1.00	0.9822	0.9810	0.98
	b	1.06	1.00	0.9888	0.9974	0.98
	c	1.06	1.00	0.9947	0.9923	0.98
Phase angle (deg.)	*a*	0	-2.04	-4.64	-4.79	-5.76
	b	240	238.16	235.17	234.84	234.81
	c	120	117.60	115.37	114.86	113.09
(b) Sequence voltages						
Magnitude (p.u.)	Zero	0.00	0.0028	0.0047	0.0050	0.0087
	Positive	1.06	1.0000	0.9886	0.9859	0.9799
	Negative	0.00	0.0028	0.0025	0.0022	0.0086

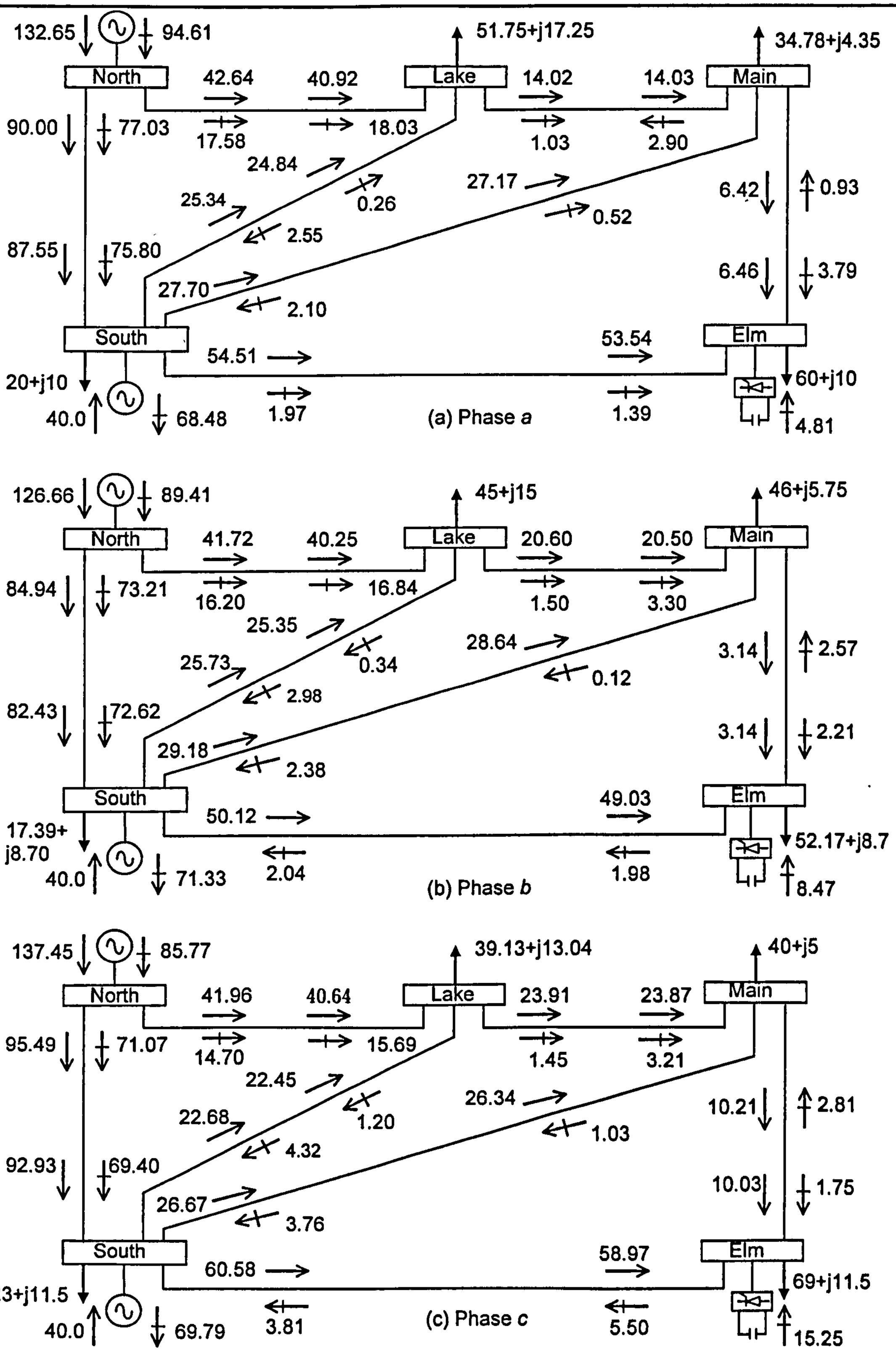

Figure 3.5 STATCOM upgraded test network and power flows

3.4 Static Synchronous Series Compensation

In a SSSC the VSC is connected to the system in series with the transmission line (Section 2.6). The SSSC controller injects voltage in quadrature with one of the line-end voltages in order to regulate active power. However, since the VSC has its own reactive power provision in the form of a DC capacitor, it make the SSSC capable of regulating both active and reactive power flow within the limits imposed by its rating [18, 31-33].

From the principles of operation the SSSC may be adequately represented by a complex voltage source in series with the transformer impedance. Hence, the equivalent circuit shown in Figure 3.6.

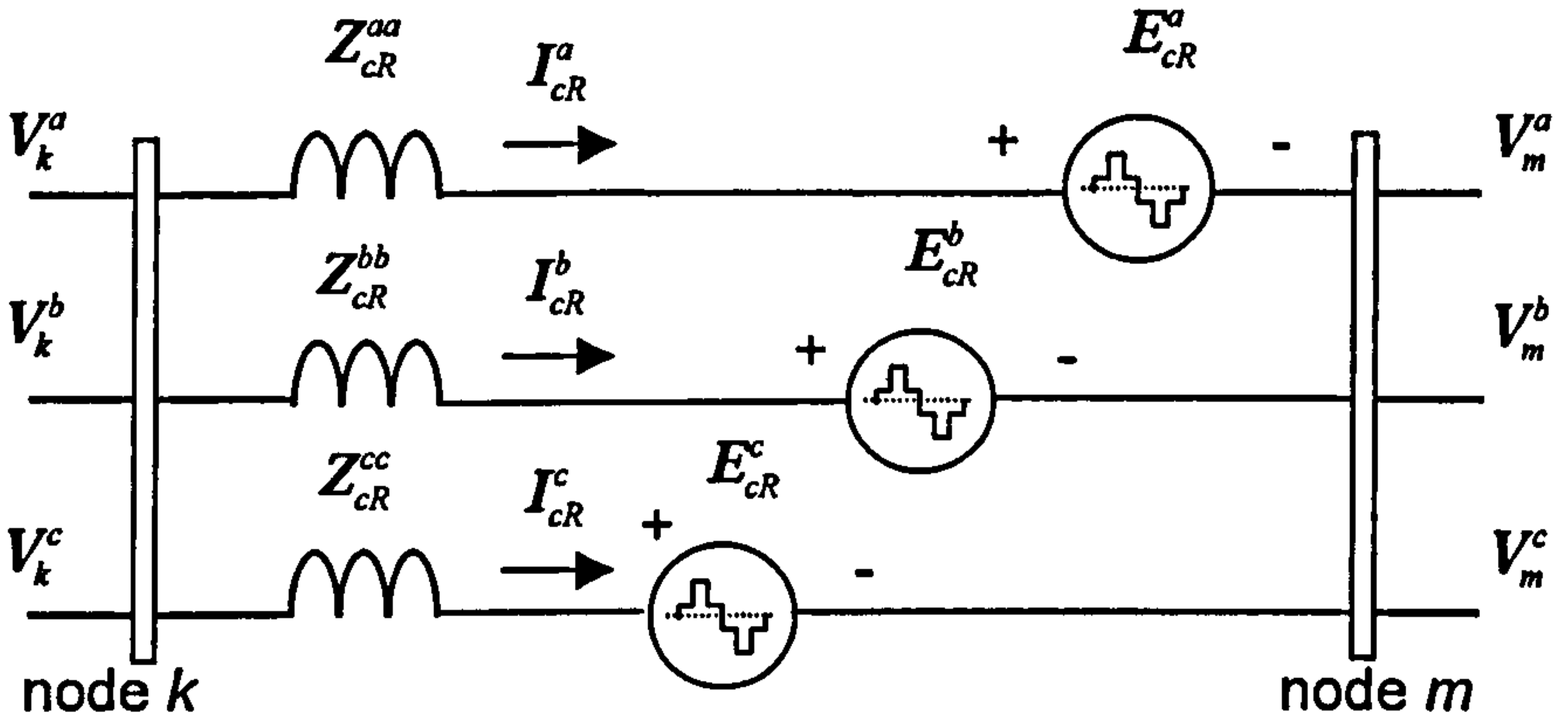

Figure 3.6 Three-phase SSSC equivalent circuit

The complex voltage sources representing the VSC station in the SSSC in polar co-ordinates is expressed as

$$E_{cR}^{\rho} = V_{cR}^{\rho} \angle \delta_{cR}^{\rho} \tag{3.46}$$

In the current application the voltage sources are modelled with the following voltage magnitude and phase angle limits: $V_{cR\ \min}^{\rho} \le V_{cR}^{\rho} \le V_{cR\ \max}^{\rho}$ and $0 \le \delta_{cR}^{\rho} \le 2\pi$. The transfer admittance equation (2.9) is used to derive the mathematical model of the SSSC for inclusion in the three-phase power flow Newton-Raphson method.

3.4.1 Power flow model

Based on the equivalent circuit shown in Figure 3.6 and the transfer admittance equation (2.9) the following may be written

$$S_k^{\rho} = V_k^{\rho} I_k^{\rho *} = V_k^{\rho} \left[\left(Y_{kk}^{\rho}\right)^{*} \left(V_k^{\rho}\right)^{*} - \left(Y_{kk}^{\rho}\right)^{*} \left(E_{cR}^{\rho}\right)^{*} + \left(Y_{km}^{\rho}\right)^{*} \left(V_m^{\rho}\right)^{*} \right] \tag{3.47}$$

After performing some complex operations, the following active and reactive power equations are obtained for node *k*, for the phase *p*= *a*, *b* and *c*

$$P_k^\rho = V_k^\rho \sum_{i=k,m} V_i^\rho \left[G_{ki}^{\rho\rho} \cos\left(\theta_k^\rho - \theta_i^\rho\right) + B_{ki}^{\rho\rho} \sin\left(\theta_k^\rho - \theta_i^\rho\right) \right] - V_k^\rho \, V_{cR}^\rho \left[G_{km}^{\rho\rho} \cos\left(\theta_k^\rho - \delta_{cR}^\rho\right) + B_{km}^{\rho\rho} \sin\left(\theta_k^\rho - \delta_{cR}^\rho\right) \right] \tag{3.48}$$

$$Q_k^\rho = V_k^\rho \sum_{i=k,m} V_i^\rho \left[G_{ki}^{\rho\rho} \sin\left(\theta_k^\rho - \theta_i^\rho\right) - B_{ki}^{\rho\rho} \cos\left(\theta_k^\rho - \theta_i^\rho\right) \right] - V_k^\rho V_{cR}^\rho \left[G_{km}^{\rho\rho} \sin\left(\theta_k^\rho - \delta_{cR}^\rho\right) - B_{km}^{\rho\rho} \cos\left(\theta_k^\rho - \delta_{cR}^\rho\right) \right] \tag{3.49}$$

An identical set of power equations are obtained for node *m*, where the sub-scripts *k* and *m* are interchange.

3.4.2 Linearised system of equations

An n-node power network with no voltage and power flow regulation provisions is described by a 2×(nb-1) non-linear system of equations. Moreover, for each SSSC that exists in the power network the 2×(nb-1) system of equations is augmented by up to two equations to take account of the converter station, i.e. a new node is added to the network.

The main function of the SSSC is to control the active and reactive power injected at the connecting node or the added node. When both active and reactive powers are regulated, the linearised system of equations for polar co-ordinates has the following structure:

$$\begin{bmatrix} \Delta P_k^\rho \\ \Delta P_m^\rho \\ \Delta Q_k^\rho \\ \Delta Q_m^\rho \\ \Delta P_{km}^\rho \\ \Delta Q_{km}^\rho \end{bmatrix}^i = \begin{bmatrix} \frac{\partial P_k^\rho}{\partial \theta_k^\rho} & \frac{\partial P_k^\rho}{\partial \theta_m^\rho} & \frac{\partial P_k^\rho}{\partial V_k^\rho} V_k^\rho & \frac{\partial P_k^\rho}{\partial V_m^\rho} V_m^\rho & \frac{\partial P_k^\rho}{\partial \theta_{cR}^\rho} & \frac{\partial P_k^\rho}{\partial V_{cR}^\rho} V_{cR}^\rho \\ \frac{\partial P_m^\rho}{\partial \theta_k^\rho} & \frac{\partial P_m^\rho}{\partial \theta_m^\rho} & \frac{\partial P_m^\rho}{\partial V_k^\rho} V_k^\rho & \frac{\partial P_m^\rho}{\partial V_m^\rho} V_m^\rho & \frac{\partial P_m^\rho}{\partial \theta_{cR}^\rho} & \frac{\partial P_m^\rho}{\partial V_{cR}^\rho} V_{cR}^\rho \\ \frac{\partial Q_k^\rho}{\partial \theta_k^\rho} & \frac{\partial Q_k^\rho}{\partial \theta_m^\rho} & \frac{\partial Q_k^\rho}{\partial V_k^\rho} V_k^\rho & \frac{\partial Q_k^\rho}{\partial V_m^\rho} V_m^\rho & \frac{\partial Q_k^\rho}{\partial \theta_{cR}^\rho} & \frac{\partial Q_k^\rho}{\partial V_{cR}^\rho} V_{cR}^\rho \\ \frac{\partial Q_m^\rho}{\partial \theta_k^\rho} & \frac{\partial Q_m^\rho}{\partial \theta_m^\rho} & \frac{\partial Q_m^\rho}{\partial V_k^\rho} V_k^\rho & \frac{\partial Q_m^\rho}{\partial V_m^\rho} V_m^\rho & \frac{\partial Q_m^\rho}{\partial \theta_{cR}^\rho} & \frac{\partial Q_m^\rho}{\partial V_{cR}^\rho} V_{cR}^\rho \\ \frac{\partial P_{km}^\rho}{\partial \theta_k^\rho} & \frac{\partial P_{km}^\rho}{\partial \theta_m^\rho} & \frac{\partial P_{km}^\rho}{\partial V_k^\rho} V_k^\rho & \frac{\partial P_{km}^\rho}{\partial V_m^\rho} V_m^\rho & \frac{\partial P_{km}^\rho}{\partial \theta_{cR}^\rho} & \frac{\partial P_{km}^\rho}{\partial V_{cR}^\rho} V_{cR}^\rho \\ \frac{\partial Q_{km}^\rho}{\partial \theta_k^\rho} & \frac{\partial Q_{km}^\rho}{\partial \theta_m^p} & \frac{\partial Q_{km}^\rho}{\partial V_k^\rho} V_k^\rho & \frac{\partial Q_{km}^\rho}{\partial V_m^\rho} V_m^\rho & \frac{\partial Q_{km}^\rho}{\partial \theta_{cR}^\rho} & \frac{\partial Q_{km}^\rho}{\partial V_{cR}^\rho} V_{cR}^\rho \end{bmatrix}^i \begin{bmatrix} \Delta\theta_k^\rho \\ \Delta\theta_m^\rho \\ \frac{\Delta V_k^\rho}{V_k^\rho} \\ \frac{\Delta V_m^\rho}{V_m^\rho} \\ \Delta\theta_{cR}^\rho \\ \frac{\Delta V_{cR}^\rho}{V_{cR}^\rho} \end{bmatrix}^i \tag{3.50}$$

Notice that the voltage, magnitudes and phase angles at the new node are taken to be state variables.

The Jacobian elements for this application are given below:

$$\frac{\partial P_k^\rho}{\partial \theta_k^\rho} = -Q_k^\rho - \left(V_k^\rho\right)^2 B_{kk}^\rho \tag{3.51}$$

$$\frac{\partial P_k^\rho}{\partial \theta_m^\rho} = \frac{\partial Q_m^\rho}{\partial V_k^\rho} V_k^\rho = V_m^\rho V_k^\rho \left[G_{km}^\rho \sin\left(\theta_m^\rho - \theta_k^\rho\right) + B_{km}^\rho \cos\left(\theta_m^\rho - \theta_k^\sigma\right) \right] \tag{3.52}$$

$$\frac{\partial P_k^\rho}{\partial V_k^\rho} V_k^\rho = P_k^\rho + \left(V_k^\rho\right)^2 G_{kk}^\rho \tag{3.53}$$

$$\frac{\partial P_k^\rho}{\partial V_m^\rho} V_m^\rho = -\frac{\partial Q_m^\rho}{\partial \theta_k^\rho} = V_k^\rho V_m^\rho \left[G_{km}^\rho \cos\left(\theta_k^\rho - \theta_m^\rho\right) + B_{km}^\rho \sin\left(\theta_k^\rho - \theta_m^\rho\right) \right] \tag{3.54}$$

$$\frac{\partial Q_k^\rho}{\partial \theta_k^\rho} = P_k^\rho - \left(V_k^\rho\right)^2 G_{kk}^\rho \tag{3.55}$$

$$\frac{\partial Q_k^\rho}{\partial \theta_m^\rho} = -\frac{\partial P_m^\rho}{\partial V_k^\rho} V_k^\rho = -V_k^\rho V_m^\rho \left[G_{km}^\rho \cos\left(\theta_k^\rho - \theta_m^\rho\right) + B_{km}^\rho \sin\left(\theta_k^\rho - \theta_m^\rho\right) \right] \tag{3.56}$$

$$\frac{\partial Q_k^\rho}{\partial V_k^\rho} V_k^\rho = Q_k^\rho - \left(V_k^\rho\right)^2 B_{kk}^\rho \tag{3.57}$$

$$\frac{\partial Q_k^\rho}{\partial V_m^\rho} V_m^\rho = \frac{\partial P_m^\rho}{\partial \theta_k^\rho} = V_k^\rho V_m^\rho \left[G_{km}^\rho \sin\left(\theta_k^\rho - \theta_m^\rho\right) - B_{km}^\rho \cos\left(\theta_k^\rho - \theta_m^\rho\right) \right] \tag{3.58}$$

$$\frac{\partial P_m^\rho}{\partial \theta_m^\rho} = -Q_m^\rho - \left(V_m^\rho\right)^2 B_{mm}^\rho \tag{3.59}$$

$$\frac{\partial P_m^\rho}{\partial V_m^\rho} V_m^\rho = P_m^\rho + \left(V_m^\rho\right)^2 G_{mm}^\rho \tag{3.60}$$

$$\frac{\partial Q_m^\rho}{\partial \theta_m^\rho} = P_m^\rho - \left(V_m^\rho\right)^2 G_{mm}^\rho \tag{3.61}$$

$$\frac{\partial Q_m^\rho}{\partial V_m^\rho} V_m^\rho = Q_m^\rho - \left(V_m^\rho\right)^2 B_{mm}^\rho \tag{3.62}$$

$$\frac{\partial P_k^\rho}{\partial \delta_{cr}^\rho} = -V_m^\rho V_{cr}^\rho \left[G_{kk}^\rho \sin\left(\theta_m^\rho - \delta_{cR}^\rho\right) - B_{kk}^\rho \cos\left(\theta_m^\rho - \delta_{cR}^\rho\right) \right] \tag{3.63}$$

$$\frac{\partial P_k^\rho}{\partial V_{cR}^\rho} V_{cR}^\rho = -V_k^\rho V_{cR}^\rho \left[G_{kk}^\rho \cos\left(\theta_k^\rho - \delta_{cR}^\rho\right) + B_{kk}^\rho \sin\left(\theta_k^\rho - \delta_{cR}^\rho\right) \right] \tag{3.64}$$

$$\frac{\partial Q_k^\rho}{\partial \delta_{cR}^\rho} = -V_m^\rho V_{cR}^\rho \left[G_{kk}^\rho \cos\left(\theta_m^\rho - \delta_{cR}^\rho\right) + B_{kk}^\rho \sin\left(\theta_m^\rho - \delta_{cR}^\rho\right) \right] \tag{3.65}$$

$$\frac{\partial Q_k^\rho}{\partial V_{cR}^\rho} V_{cR}^\rho = -V_k^\rho V_{cR}^\rho \left[G_{cR}^\rho \sin\left(\theta_k^\rho - \delta_{cR}^\rho\right) - B_{cR}^\rho \cos\left(\theta_k^\rho - \delta_{cR}^\rho\right) \right] \tag{3.66}$$

$$\frac{\partial P_m^\rho}{\partial \delta_{cR}^\rho} = -V_m^\rho V_{cR}^\rho \left[G_{km}^\rho \sin\left(\theta_m^\rho - \delta_{cR}^\rho\right) - B_{km}^\rho \cos\left(\theta_m^\rho - \delta_{cR}^\rho\right) \right] \tag{3.67}$$

$$\frac{\partial P_m^\rho}{\partial V_{cR}^\rho} V_{cR}^\rho = -V_m^\rho V_{cR}^\rho \left[G_{km}^\rho \cos\left(\theta_m^\rho - \delta_{cR}^\rho\right) + B_{km}^\rho \sin\left(\theta_m^\rho - \delta_{cR}^\rho\right) \right] \tag{3.68}$$

$$\frac{\partial Q_m^\rho}{\partial \delta_{cR}^\rho} = V_m^\rho V_{cR}^\rho \left[G_{km}^\rho \cos\left(\theta_m^\rho - \delta_{cR}^\rho\right) + B_{km}^\rho \sin\left(\theta_m^\rho - \delta_{cR}^\rho\right) \right] \tag{3.69}$$

$$\frac{\partial Q_m^\rho}{\partial V_{cr}^\rho} V_{cr}^\rho = -V_m^\rho V_{cr}^\rho \left[G_{km}^\rho \sin\left(\theta_m^\rho - \delta_{cR}^\rho\right) - B_{km}^\rho \cos\left(\theta_m^\rho - \delta_{cR}^\rho\right) \right] \tag{3.70}$$

The generic power mismatch equations at nodes *k* and *m* are

$$\begin{aligned} \Delta P_{k,m}^\rho &= \left(P_{k,m}^\rho\right)^{\text{sp}} - \left(P_{k,m}^\rho\right)^{\text{cal}} \\ \Delta Q_{k,m}^\rho &= \left(Q_{k,m}^\rho\right)^{\text{sp}} - \left(Q_{k,m}^\rho\right)^{\text{cal}} \end{aligned} \tag{3.71}$$

$\left(P_k^\rho\right)^{\text{sp}}$ and $\left(Q_k^\rho\right)^{\text{sp}}$ are the specified active and reactive powers to be controlled. $\left(P_k^\rho\right)^{\text{cal,it}}$ and $\left(Q_k^\rho\right)^{\text{cal,it}}$ are the calculated net active and reactive power injection vectors at iteration and they are evaluated using $\left(V^\rho\right)^{\text{it}}$ and $\left(\theta^\rho\right)^{\text{it}}$. The voltage magnitude and phase angle are initialized equal to the unit and zero respectively, and are updated after each iteration using

$$\begin{aligned} \left(V_{k,m}^\rho\right)^{it+1} &= \left(\frac{\Delta V_{k,m}^\rho}{V_{k,m}^\rho}\right)^{it} \left(V_{k,m}^\rho\right)^{it} + \left(V_{k,m}^\rho\right)^{it} \\ \left(\theta_{k,m}^\rho\right)^{it+1} &= \left(\Delta\theta_{k,m}^\rho\right)^{it} + \left(\theta_{k,m}^\rho\right)^{it} \end{aligned} \tag{3.72}$$

During each iteration, after nodal voltage updating, the series source converter voltage is also updated using

$$\begin{aligned} \left(V_{cR}^\rho\right)^{it+1} &= \left(\Delta V_{cR}^\rho\right)^{it} + \left(V_{cR}^\rho\right)^{it} \\ \left(\theta_{cR}^\rho\right)^{it+1} &= \left(\Delta\theta_{cR}^\rho\right)^{it} + \left(\theta_{cR}^\rho\right)^{it} \end{aligned} \tag{3.73}$$

In polar co-ordinates, when the SSSC is connected to the slack node, ΔV^ρ and Q^ρ at the slack are set to zero. Whereas with PV-type nodes, the ΔV^ρ is set to zero. Note that the magnitude and phase angle for the voltage source converter has to be checked for limit violations. If theres is a limit violation, the VSC has to be set to the limit violated.

3.4.3 SSSC Three-Phase Numerical Example

The unbalanced five-bus network is now modified to include the three-phase SSSC model. It is used to balance the three-phase power flow at the transmission line connecting the Lake and Main buses at a specified active power of 20 MW and reactive power of 2 MVAR flowing from Lake to Main. The source impedances are X_{cR}=0.1 p.u. per phase. The SSSC parameters associated with this active and reactive power control are: V_{cR}=0.03565, 0.01978 and 0.02829 p.u. for *a*, *b* and *c* phases, respectively.

Nodal voltage magnitudes and phase angles are given in Table 3.5(a), and sequence domain voltage magnitudes are given in Table 3.4(b), where it is shown that the SSSC is effective in regulating and balancing nodal power flows from Lake to Main. As expected, the phase angles at that bus are still unbalanced. It should be mentioned that power losses now stand at 3.62%, the power flows within the SSSC embed are shown in Figure 3.7.

Table 3.5 Nodal voltage in the three-phase unbalanced network with a SSSC – phase voltages

Voltage		Network buses				
	Phase	North	South	Lake	Main	Elm
(a) Phase voltages						
Magnitude (p.u.)	*a*	1.06	1.00	0.9728	0.9926	0.9834
	b	1.06	1.00	0.9957	0.9737	0.9721
	c	1.06	1.00	0.9942	0.9827	0.9578
Phase angle (deg.)	*a*	0	-1.87	-5.21	-3.96	-5.55
	b	240	238.11	235.11	235.05	235.28
	c	120	117.50	115.93	114.04	112.86
(b) Sequence voltages						
Magnitude (p.u.)	Zero	0.00	0.0028	0.0047	0.0050	0.0087
	Positive	1.06	1.0000	0.9886	0.9859	0.9799
	Negative	0.00	0.0028	0.0025	0.0022	0.0086

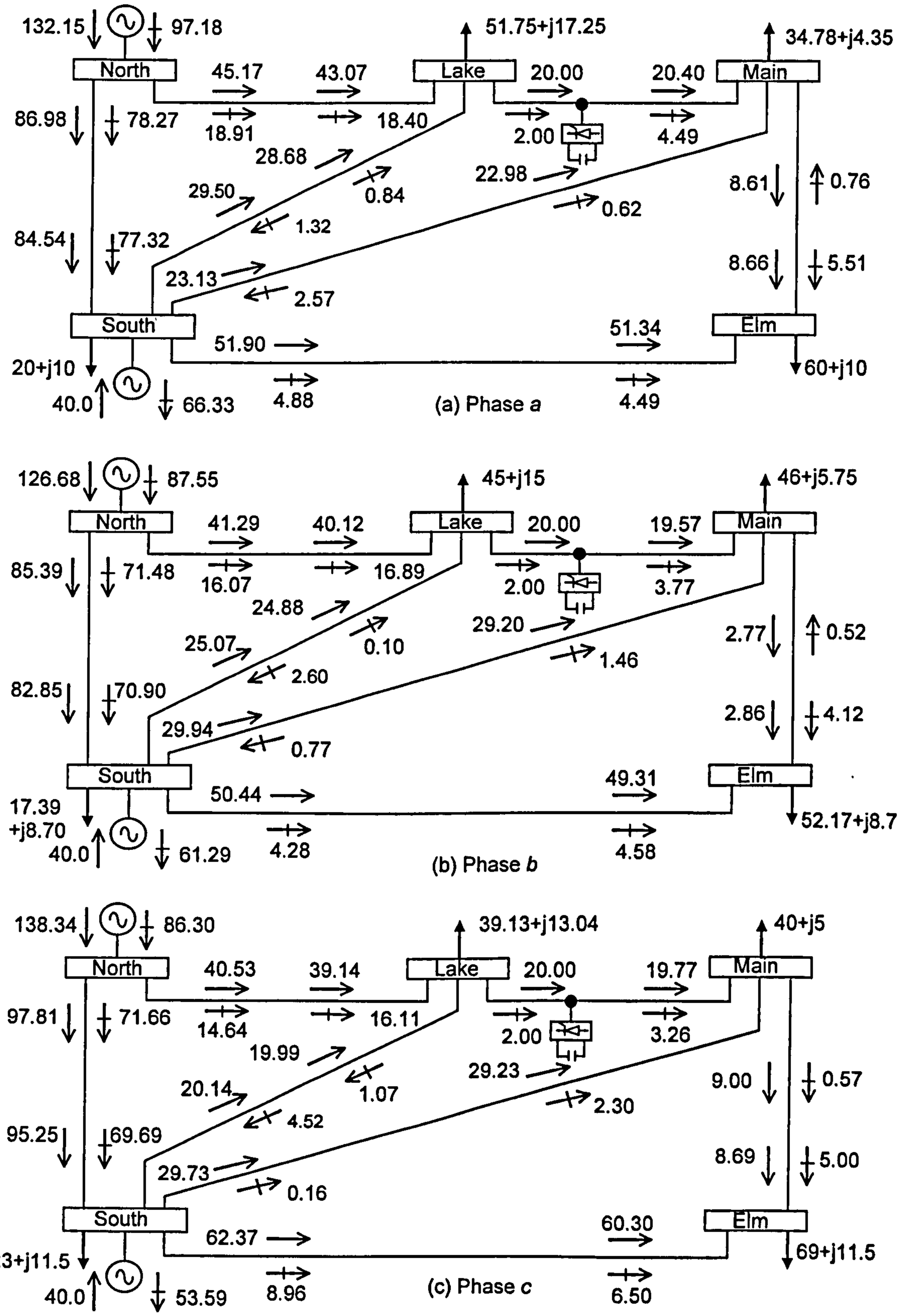

Figure 3.7 SSSC upgraded test network and power flow

3.5 Unified Power Flow Controller

The basic principle of UPFC operation has been discussed in Section 2.7. It follows from that discussion that an equivalent circuit consisting of two coordinated synchronous voltage sources per phase should represent the three-phase UPFC adequately for the purpose of fundamental frequency steady-state analysis. Such an equivalent circuit is shown in Figure 3.8. The synchronous voltage sources represent the fundamental Fourier series component of the switched voltage waveforms at the AC converter terminals of the UPFC [34-37].

Assuming that the equivalent circuit of a three-phase UPFC consist of three single-phase UPFC equivalent circuits, with no couplings between them, as shown in Figure 3.8, and each phase consists of one shunt and one series complex voltage source. The complex voltage sources in polar co-ordinates are expressed as

$$\boldsymbol{E}_{vR}^{\rho} = V_{vR}^{\rho} \angle \delta_{vR}^{\rho} \tag{3.74}$$

$$\boldsymbol{E}_{cR}^{\rho} = V_{cR}^{\rho} \angle \delta_{cR}^{\rho} \tag{3.75}$$

where V_{vR}^{ρ} and δ_{vR}^{ρ} are controllable: $V_{vR\ \min}^{\rho} \le V_{vR}^{\rho} \le V_{vR\ \max}^{\rho}$ and $0 \le \delta_{vR}^{\rho} \le 2\pi$ for the voltage source of the shunt converter. The magnitude V_{cR}^{ρ} and phase angle δ_{cR}^{ρ} of the series converter voltage are controlled between: $V_{cR\ \min}^{\rho} \le V_{cR}^{\rho} \le V_{cR\ \max}^{\rho}$ and $0 \le \delta_{vR}^{\rho} \le 2\pi$, respectively.

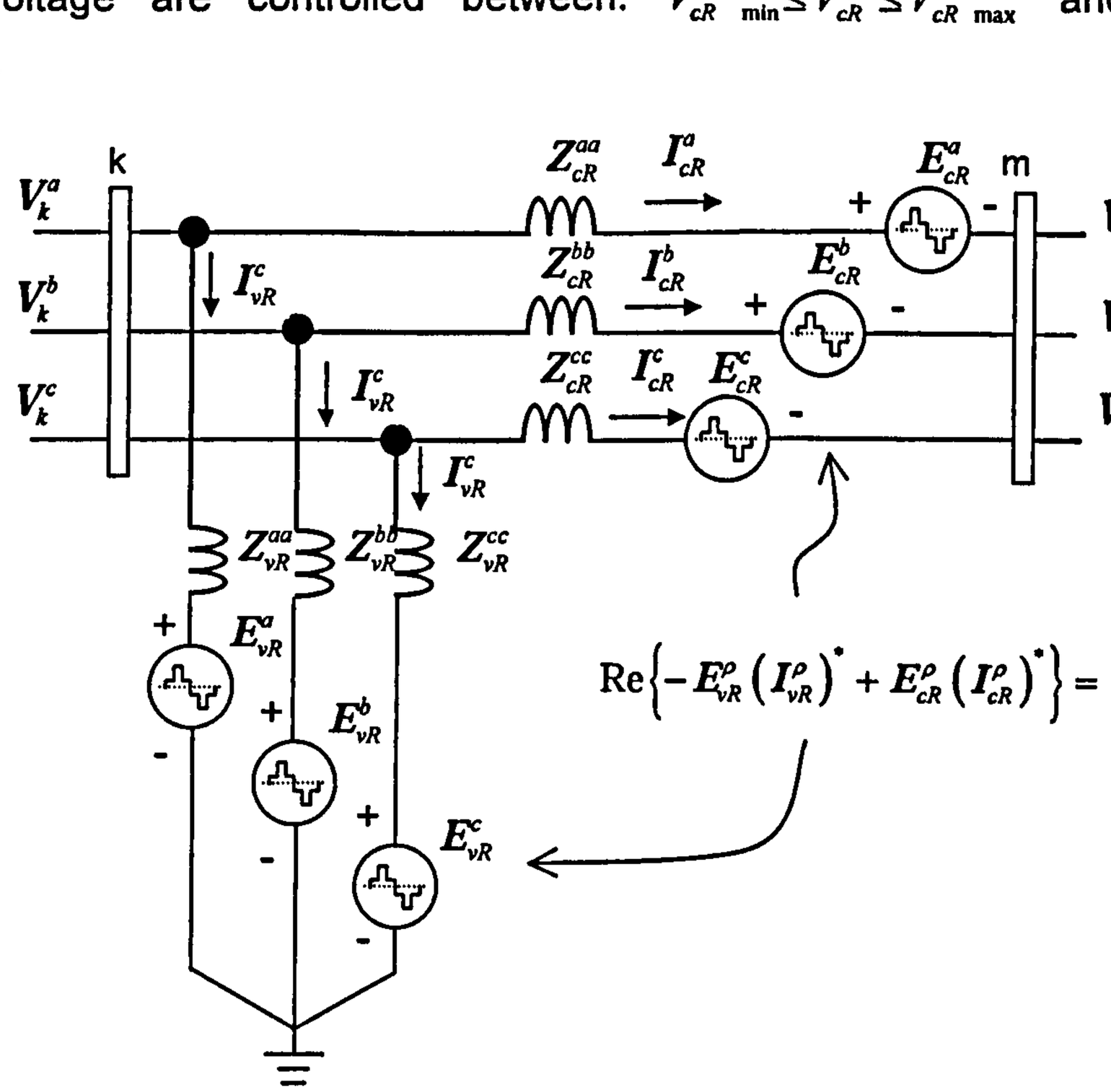

Figure 3.8 Three-phase UPFC equivalent circuit

The phase angle of the series injected voltage determines the mode of power flow control. If δ_{cR}^{ρ} is in phase with the nodal voltage angle θ_k^{ρ}, the UPFC regulates the terminal voltage. If δ_{cR}^{ρ} is in quadrature with respect to θ_k^{ρ}, it controls active power flow, acting as a phase shifter. If δ_{cR}^{ρ} is in quadrature with the line current angle then it controls active power flow, acting as a variable series compensator. At any other value of δ_{cR}^{ρ}, the UPFC operates as a combination of voltage regulator, variable series compensator and phase shifter. The magnitude of the series injected voltage determines the amount of power flow to be controlled.

3.5.1 Power flow model

From Figure 3.8 and the transfer admittance equation (2.17), the power balance equation for the three-phase UPFC at the node can be written as

$$S_k^{\rho} = V_k^{\rho} I_k^{\rho^*} = V_k^{\rho}\left[\left(Y_{kk}^{\rho}\right)^*\left(V_k^{\rho}\right)^* + \left(Y_{km}^{\rho}\right)^*\left(V_m^{\rho}\right)^* + \left(Y_{km}^{\rho}\right)^*\left(E_{cR}^{\rho}\right)^* + \left(Y_{vR}^{\rho}\right)^*\left(E_{vR}^{\rho}\right)^*\right] \tag{3.76}$$

$$S_m^{\rho} = V_m^{\rho} I_m^{\rho^*} = V_k^{\rho}\left[\left(Y_{mk}^{\rho}\right)^*\left(V_k^{\rho}\right)^* + \left(Y_{mm}^{\rho}\right)^*\left(V_m^{\rho}\right)^* + \left(Y_{mm}^{\rho}\right)^*\left(E_{cR}^{\rho}\right)^*\right] \tag{3.77}$$

After performing some complex operations, the following active and reactive power equations are obtained for node *k*, for phase ρ= *a, b* and *c*:

$$\begin{aligned} P_k^{\rho} =& \left(V_k^{\rho}\right)^2 G_{kk}^{\rho\rho} + V_k^{\rho} V_m^{\rho}\left[G_{km}^{\rho\rho}\cos\left(\theta_k^{\rho}-\theta_m^{\rho}\right) + B_{km}^{\rho\rho}\sin\left(\theta_k^{\rho}-\theta_m^{\rho}\right)\right] \\ &+ V_k^{\rho} V_{cR}^{\rho}\left[G_{km}^{\rho\rho}\cos\left(\theta_k^{\rho}-\delta_{cr}^{\rho}\right) + B_{km}^{\rho\rho}\sin\left(\theta_k^{\rho}-\delta_{cR}^{\rho}\right)\right] \\ &+ V_k^{\rho} V_{vR}^{\rho}\left[G_{vR}^{\rho}\cos\left(\theta_k^{\rho}-\delta_{vR}^{\rho}\right) + B_{vR}^{\rho}\sin\left(\theta_k^{\rho}-\delta_{vR}^{\rho}\right)\right] \end{aligned} \tag{3.78}$$

$$\begin{aligned} Q_k^{\rho} =& -\left(V_k^{\rho}\right)^2 B_{kk}^{\rho\rho} + V_k^{\rho} V_m^{\rho}\left[G_{km}^{\rho\rho}\sin\left(\theta_k^{\rho}-\theta_m^{\rho}\right) - B_{km}^{\rho}\cos\left(\theta_k^{\rho}-\theta_m^{\rho}\right)\right] \\ &+ V_k^{\rho} V_{cR}^{\rho}\left[G_{km}^{\rho\rho}\sin\left(\theta_k^{\rho}-\delta_{cR}^{\rho}\right) - B_{km}^{\rho}\cos\left(\theta_k^{\rho}-\delta_{cR}^{\rho}\right)\right] \\ &+ V_k^{\rho} V_{vR}^{\rho}\left[G_{vR}^{\rho}\sin\left(\theta_k^{\rho}-\delta_{vR}^{\rho}\right) - B_{vR}^{\rho}\cos\left(\theta_k^{\rho}-\delta_{vR}^{\rho}\right)\right] \end{aligned} \tag{3.79}$$

At bus *m*:

$$\begin{aligned} P_m^{\rho} =& \left(V_m^{\rho}\right)^2 G_{mm}^{\rho\rho} + V_m^{\rho} V_k^{\rho}\left[G_{mk}^{\rho\rho}\cos\left(\theta_m^{\rho}-\theta_k^{\rho}\right) + B_{mk}^{\rho}\sin\left(\theta_m^{\rho}-\theta_k^{\rho}\right)\right] \\ &+ V_m^{\rho} V_{cR}^{\rho}\left[G_{mm}^{\rho\rho}\cos\left(\theta_m^{\rho}-\delta_{cR}^{\rho}\right) + B_{mm}^{\rho\rho}\sin\left(\theta_m^{\rho}-\delta_{cR}^{\rho}\right)\right] \end{aligned} \tag{3.80}$$

$$\begin{aligned} Q_m^{\rho} =& -\left(V_m^{\rho}\right)^2 B_{mm}^{\rho\rho} + V_m^{\rho} V_k^{\rho}\left[G_{mk}^{\rho\rho}\sin\left(\theta_m^{\rho}-\theta_k^{\rho}\right) - B_{mk}^{\rho\rho}\cos\left(\theta_m^{\rho}-\theta_k^{\rho}\right)\right] \\ &+ V_m^{\rho} V_{cR}^{\rho}\left[G_{mm}^{\rho\rho}\sin\left(\theta_m^{\rho}-\delta_{cR}^{\rho}\right) - B_{mm}^{\rho\rho}\cos\left(\theta_m^{\rho}-\delta_{cR}^{\rho}\right)\right] \end{aligned} \tag{3.81}$$

For the series converter:

$$P_{cR}^{\rho} = \left(V_{cR}^{\rho}\right)^2 G_{mm}^{\rho\rho} + V_{cR}^{\rho} V_k^{\rho} \left[G_{km}^{\rho\rho} \cos\left(\delta_{cR}^{\rho} - \theta_k^{\rho}\right) + B_{km}^{\rho\rho} \sin\left(\delta_{cR}^{\rho} - \theta_k^{\rho}\right) \right] + V_{cR}^{\rho} V_m^{\rho} \left[G_{mm}^{\rho\rho} \cos\left(\delta_{cR}^{\rho} - \theta_m^{\rho}\right) + B_{mm}^{\rho\rho} \sin\left(\delta_{cR}^{\rho} - \theta_m^{\rho}\right) \right] \quad (3.82)$$

$$Q_{cR}^{\rho} = -\left(V_{cR}^{\rho}\right)^2 B_{mm}^{\rho\rho} + V_{cR}^{\rho} V_k^{\rho} \left[G_{km}^{\rho\rho} \sin\left(\delta_{cR}^{\rho} - \theta_k^{\rho}\right) - B_{km}^{\rho\rho} \cos\left(\delta_{cR}^{\rho} - \theta_k^{\rho}\right) \right] + V_{cR}^{\rho} V_m^{\rho} \left[G_{mm}^{\rho\rho} \sin\left(\delta_{cR}^{\rho} - \theta_m^{\rho}\right) - B_{mm}^{\rho\rho} \cos\left(\delta_{cR}^{\rho} - \theta_m^{\rho}\right) \right] \quad (3.83)$$

For the shunt converter:

$$P_{vR}^{\rho} = -\left(V_{vR}^{\rho}\right)^2 G_{vR}^{\rho\rho} + V_{vR}^{\rho} V_k^{\rho} \left[G_{vR}^{\rho\rho} \cos\left(\delta_{vR}^{\rho} - \theta_k^{\rho}\right) + B_{vR}^{\rho} \sin\left(\delta_{vR}^{\rho} - \theta_k^{\rho}\right) \right] \quad (3.84)$$

$$Q_{vR}^{\rho} = \left(V_{vR}^{\rho}\right)^2 B_{vR}^{\rho} + V_{vR}^{\rho} V_k^{\rho} \left[G_{vR}^{\rho\rho} \sin\left(\delta_{vR}^{\rho\rho} - \theta_k^{\rho}\right) - B_{vR}^{\rho\rho} \cos\left(\delta_{vR}^{\rho} - \theta_k^{\rho}\right) \right] \quad (3.85)$$

Assuming lossless converter valves, the active power supplied to the shunt converter, P_{vR}, equals the active power demanded by the series converter, P_{cR}, i.e.

$$P_{vR} + P_{cR} = 0 \quad (3.86)$$

Furthermore, if the coupling transformers are assumed to contain no resistance then the active power at bus k matches the active power at bus m. Accordingly,

$$P_{vR} + P_{cR} = P_k + P_m = 0 \quad (3.87)$$

The UPFC power equations, in linearised form, are combined with those of the AC network. For the case when the UPFC controls the voltage magnitude at the shunt converter terminals (bus k), the active power flowing from bus m to bus k and reactive power injected at bus m (assuming that bus m is a PQ-type bus), is described by a linearised system of equations,

$$\begin{bmatrix} \Delta P_k^\rho \\ \Delta P_m^\rho \\ \Delta Q_k^\rho \\ \Delta Q_m^\rho \\ \Delta P_{mk}^\rho \\ \Delta Q_{mk}^\rho \\ \Delta P_{bb}^\rho \end{bmatrix} = \begin{bmatrix} \frac{\partial P_k^\rho}{\partial \theta_k^\rho} & \frac{\partial P_k^\rho}{\partial \theta_m^\rho} & \frac{\partial P_k^\rho}{\partial V_{vR}^\rho} V_{vR}^\rho & \frac{\partial P_k^\rho}{\partial V_m^\rho} V_m^\rho & \frac{\partial P_k^\rho}{\partial \delta_{cR}^\rho} & \frac{\partial P_k^\rho}{\partial V_{cR}^\rho} V_{cR}^\rho & \frac{\partial P_k^\rho}{\partial \delta_{vR}^\rho} \\ \frac{\partial P_m^\rho}{\partial \theta_k^\rho} & \frac{\partial P_m^\rho}{\partial \theta_m^\rho} & 0 & \frac{\partial P_m^\rho}{\partial V_m^\rho} V_m^\rho & \frac{\partial P_m^\rho}{\partial \delta_{cR}^\rho} & \frac{\partial P_m^\rho}{\partial V_{cR}^\rho} V_{cR}^\rho & 0 \\ \frac{\partial Q_k^\rho}{\partial \theta_k^\rho} & \frac{\partial Q_k^\rho}{\partial \theta_m^\rho} & \frac{\partial Q_k^\rho}{\partial V_{vR}^\rho} V_{vR}^\rho & \frac{\partial Q_k^\rho}{\partial V_m^\rho} V_m^\rho & \frac{\partial Q_k^\rho}{\partial \delta_{cR}^\rho} & \frac{\partial Q_k^\rho}{\partial V_{cR}^\rho} V_{cR}^\rho & \frac{\partial Q_k^\rho}{\partial \delta_{vR}^\rho} \\ \frac{\partial Q_m^\rho}{\partial \theta_k^\rho} & \frac{\partial Q_m^\rho}{\partial \theta_m^\rho} & 0 & \frac{\partial Q_m^\rho}{\partial V_m^\rho} V_m^\rho & \frac{\partial Q_m^\rho}{\partial \delta_{cR}^\rho} & \frac{\partial Q_m^\rho}{\partial V_{cR}^\rho} V_{cR}^\rho & 0 \\ \frac{\partial P_{mk}^\rho}{\partial \theta_k^\rho} & \frac{\partial P_{mk}^\rho}{\partial \theta_m^\rho} & 0 & \frac{\partial P_{mk}^\rho}{\partial V_m^\rho} V_m^\rho & \frac{\partial P_{mk}^\rho}{\partial \delta_{cR}^\rho} & \frac{\partial P_{mk}^\rho}{\partial V_{cR}^\rho} V_{cR}^\rho & 0 \\ \frac{\partial Q_{mk}^\rho}{\partial \theta_k^\rho} & \frac{\partial Q_{mk}^\rho}{\partial \theta_m^\rho} & 0 & \frac{\partial Q_{mk}^\rho}{\partial V_m^\rho} V_m^\rho & \frac{\partial Q_{mk}^\rho}{\partial \delta_{cR}^\rho} & \frac{\partial Q_{mk}^\rho}{\partial V_{cR}^\rho} V_{cR}^\rho & 0 \\ \frac{\partial P_{bb}^\rho}{\partial \theta_k^\rho} & \frac{\partial P_{bb}^\rho}{\partial \theta_m^\rho} & \frac{\partial P_{bb}^\rho}{\partial V_{vR}^\rho} V_{vR}^\rho & \frac{\partial P_{bb}^\rho}{\partial V_m^\rho} V_m^\rho & \frac{\partial P_{bb}^\rho}{\partial \delta_{cR}^\rho} & \frac{\partial P_{bb}^\rho}{\partial V_{cR}^\rho} V_{cR}^\rho & \frac{\partial P_{bb}^\rho}{\partial \delta_{vR}^\rho} \end{bmatrix} \begin{bmatrix} \Delta \theta_k^\rho \\ \Delta \theta_m \\ \frac{\Delta V_{vR}^\rho}{V_{vR}^\rho} \\ \frac{\Delta V_m^\rho}{V_m^\rho} \\ \Delta \delta_{cR}^\rho \\ \frac{\Delta V_{cR}^\rho}{V_{cR}^\rho} \\ \Delta \delta_{vR}^\rho \end{bmatrix} \quad (3.88)$$

where ΔP_{bb}^ρ is the power mismatch given by equation (3.86).

If voltage control at bus *k* is deactivated, the third column of (3.88) is replaced by partial derivatives of the bus and UPFC mismatch powers with respect to the bus voltage magnitude V_k^ρ. Moreover, the voltage magnitude increment of the shunt source $\Delta V_{vR}^\rho / V_{vR}^\rho$ is replaced by the voltage magnitude increment at bus *k*, $\Delta V_k^\rho / V_k^\rho$.

If both buses, *k* and *m*, are PQ-type then the linearised system of equations is

$$\begin{bmatrix} \Delta P_k^\rho \\ \Delta P_m^\rho \\ \Delta Q_k^\rho \\ \Delta Q_m^\rho \\ \Delta P_{mk}^\rho \\ \Delta Q_{mk}^\rho \\ \Delta P_{bb}^\rho \end{bmatrix} = \begin{bmatrix} \frac{\partial P_k^\rho}{\partial \theta_k^\rho} & \frac{\partial P_k^\rho}{\partial \theta_m^\rho} & \frac{\partial P_k^\rho}{\partial V_k^\rho} V_k^\rho & \frac{\partial P_k^\rho}{\partial V_m^\rho} V_m^\rho & \frac{\partial P_k^\rho}{\partial \delta_{cR}^\rho} & \frac{\partial P_k^\rho}{\partial V_{cR}^\rho} V_{cR}^\rho & \frac{\partial P_k^\rho}{\partial \delta_{vR}^\rho} \\ \frac{\partial P_m^\rho}{\partial \theta_k^\rho} & \frac{\partial P_m^\rho}{\partial \theta_m^\rho} & \frac{\partial P_m^\rho}{\partial V_k^\rho} V_k^\rho & \frac{\partial P_m^\rho}{\partial V_m^\rho} V_m^\rho & \frac{\partial P_m^\rho}{\partial \delta_{cR}^\rho} & \frac{\partial P_m^\rho}{\partial V_{cR}^\rho} V_{cR}^\rho & 0 \\ \frac{\partial Q_k^\rho}{\partial \theta_k^\rho} & \frac{\partial Q_k^\rho}{\partial \theta_m^\rho} & \frac{\partial Q_k^\rho}{\partial V_k^\rho} V_k^\rho & \frac{\partial Q_k^\rho}{\partial V_m^\rho} V_m^\rho & \frac{\partial Q_k^\rho}{\partial \delta_{cR}^\rho} & \frac{\partial Q_k^\rho}{\partial V_{cR}^\rho} V_{cR}^\rho & \frac{\partial Q_k^\rho}{\partial \delta_{vR}^\rho} \\ \frac{\partial Q_m^\rho}{\partial \theta_k^\rho} & \frac{\partial Q_m^\rho}{\partial \theta_m^\rho} & \frac{\partial Q_m^\rho}{\partial V_k^\rho} V_k^\rho & \frac{\partial Q_m^\rho}{\partial V_m^\rho} V_m^\rho & \frac{\partial Q_m^\rho}{\partial \delta_{cR}^\rho} & \frac{\partial Q_m^\rho}{\partial V_{cR}^\rho} V_{cR}^\rho & 0 \\ \frac{\partial P_{mk}^\rho}{\partial \theta_k^\rho} & \frac{\partial P_{mk}^\rho}{\partial \theta_m^\rho} & \frac{\partial P_{km}^\rho}{\partial V_k^\rho} V_k^\rho & \frac{\partial P_{mk}^\rho}{\partial V_m^\rho} V_m^\rho & \frac{\partial P_{mk}^\rho}{\partial \delta_{cR}^\rho} & \frac{\partial P_{mk}^\rho}{\partial V_{cR}^\rho} V_{cR}^\rho & 0 \\ \frac{\partial Q_{mk}^\rho}{\partial \theta_k^\rho} & \frac{\partial Q_{mk}^\rho}{\partial \theta_m^\rho} & \frac{\partial Q_{km}^\rho}{\partial V_k^\rho} V_k^\rho & \frac{\partial Q_{mk}^\rho}{\partial V_m^\rho} V_m^\rho & \frac{\partial Q_{mk}^\rho}{\partial \delta_{cR}^\rho} & \frac{\partial Q_{mk}^\rho}{\partial V_{cR}^\rho} V_{cR}^\rho & 0 \\ \frac{\partial P_{bb}^\rho}{\partial \theta_k^\rho} & \frac{\partial P_{bb}^\rho}{\partial \theta_m^\rho} & \frac{\partial P_{bb}^\rho}{\partial V_k^\rho} V_k^\rho & \frac{\partial P_{bb}^\rho}{\partial V_m^\rho} V_m^\rho & \frac{\partial P_{bb}^\rho}{\partial \delta_{cR}^\rho} & \frac{\partial P_{bb}^\rho}{\partial V_{cR}^\rho} V_{cR}^\rho & \frac{\partial P_{bb}^\rho}{\partial \delta_{vR}^\rho} \end{bmatrix} \begin{bmatrix} \Delta \theta_k^\rho \\ \Delta \theta_m \\ \frac{\Delta V_k^\rho}{V_k^\rho} \\ \frac{\Delta V_m^\rho}{V_m^\rho} \\ \Delta \delta_{cR}^\rho \\ \frac{\Delta V_{cR}^\rho}{V_{cR}^\rho} \\ \Delta \delta_{vR}^\rho \end{bmatrix} \quad (3.89)$$

In this case, V_{vR}^ρ is maintained at a fixed value within the prescribed limits

$V_{vR\ \min}^\rho \le V_{vR}^\rho \le V_{vR\ \max}^\rho$

The Jacobian terms in equations (3.88) and (3.89) are given in Appendix III.

Upon solution of the Jacobian matrix, a new set of state variables increments is obtained. The increments are used to update the series VSC voltage magnitude and phase angle for each iteration using equation (3.45):

$$\begin{aligned} \left(V_{cR}^\rho\right)^{it+1} &= \left(\frac{\Delta V_{cR}^\rho}{V_{cR}^\rho}\right)^{it} \left(V_{cR}^\rho\right)^{it} + \left(V_{cR}^\rho\right)^{it} \\ \left(\delta_{cR}^\rho\right)^{it+1} &= \left(\Delta \delta_{cR}^\rho\right)^{it} + \left(\delta_{cR}^\rho\right)^{it} \end{aligned} \quad (3.90)$$

and equation (3.46) for shunt VSC:

$$\begin{aligned} \left(V_{vR}^\rho\right)^{it+1} &= \left(\frac{\Delta V_{vR}^\rho}{V_{vR}^\rho}\right)^{it} \left(V_{vR}^\rho\right)^{it} + \left(V_{vR}^\rho\right)^{it} \\ \left(\delta_{vR}^\rho\right)^{it+1} &= \left(\Delta \delta_{vR}^\rho\right)^{it} + \left(\delta_{vR}^\rho\right)^{it} \end{aligned} \quad (3.91)$$

Voltage magnitude limits are checked at the end of each iterative step, and if one or more limits are violated, the voltage magnitude is fixed at the violated limit.

3.5.2 Numerical example of power flow control using a UPFC

In order to assess the effectiveness of the UPFC controllers to regulate active and reactive power flow and to control voltage magnitude in one of the UPFC connecting buses, the five-bus network is modified to include a three-phase UPFC model to compensate and to balance the transmission line linking buses Lake and Main. The modified network is shown in Figure 3.9. The UPFC is used to maintain the active power leaving the UPFC, towards Main, at 30 MW in each phase. The reactive power flowing towards Main is controlled in such a manner that balanced voltage magnitudes of 0.98 p.u. are obtained at the bus connecting the UPFC and compensated transmission line. The reactive power injections are set to inject 7.13 MVAR, 2.47 MVAR and 6.05 MVAR for phases *a*, *b* and *c*, respectively; voltage magnitudes at Lake bus are fixed at 1 p.u. The three-phase nodal voltage magnitudes and phase angles are given in Table 3.6, where it is shown that the UPFC is effective in regulating voltage magnitude in both of their connecting buses. Figure 3.9 shows the power flow results when the UPFC regulates reactive powers at the above values. It is clear that the UPFC is an effective device for restoring power balance. Table 3.6 shows the nodal voltage magnitudes in the phase and sequence domain.

Table 3.6 Nodal voltages in the three-phase unbalanced network with a UPFC – phase voltages

		Network buses					
Voltage	Phase	North	South	Lake	Main	Elm	LakeUPFC
(a) Phase voltages							
Magnitude (p.u.)	*a*	1.06	1.00	1.00	0.980	0.979	0.98
	b	1.06	1.00	1.00	0.977	0.973	0.98
	c	1.06	1.00	1.00	0.978	0.957	0.98
Phase Angle (deg)	*a*	0.00	-1.74	-6.05	-3.04	-5.19	-2.49
	b	240.00	238.27	234.80	235.90	235.67	236.41
	c	120.00	117.65	114.83	115.36	113.39	115.98
(b) Sequence voltages							
Magnitude (p.u.)	Zero	0.00	0.0036	0.0050	0.0087	0.0161	0.0077
	Positive	1.06	1.0000	1.0000	0.9782	0.9695	0.9799
	Negative	0.00	0.0036	0.0050	0.0073	0.0090	0.0078

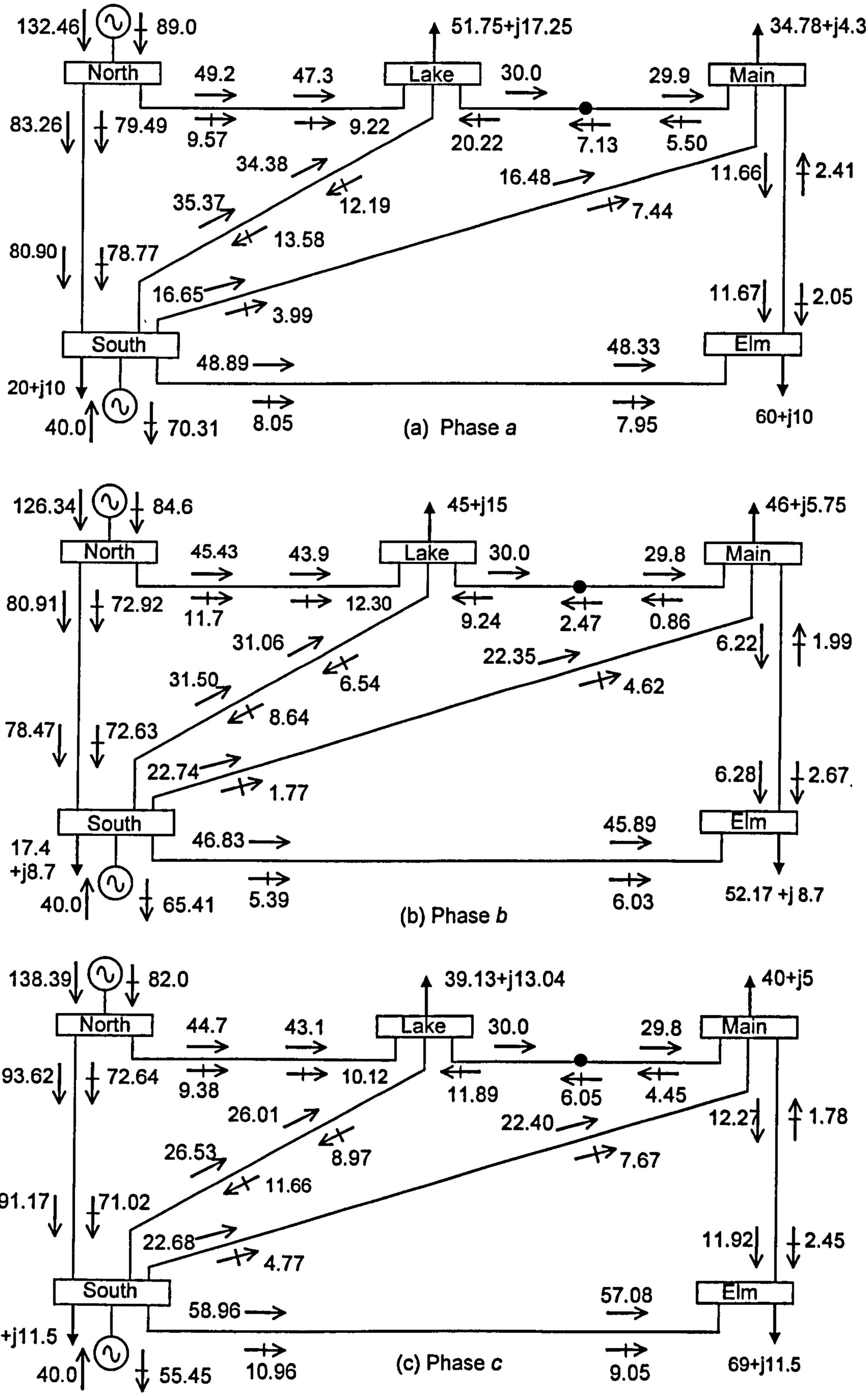

Figure 3.9 UPFC upgraded test network and power flow

3.6 High-Voltage Direct Current VSC-based

The HVDC-VSC consists of two VSC stations, one operating as a rectifier and the other as an inverter. The two converters are connected either back-to-back or joined together by a DC cable, depending on the application [38-40].

From the principles of HVDC-VSC operation outlined in Chapter 2, it may be argued that for the purpose of fundamental frequency analysis each converter station may be adequately represented by a complex voltage source V_{vR} behind the transformer reactance X_{vR} (impedance Z_{vR}). In a similar manner to the STATCOM, SSSC and UPFC, the synchronous voltage sources represent the fundamental Fourier series component of the switched voltage waveforms at the AC converter terminals of the HVDC-VSC [38- 44].

The two voltage sources work in a co-ordinated fashion and this fact is taken into account by the mismatch power equation in the equivalent circuit shown in Figure 3.10. This circuit is used to derive the mathematical model of the HVDC-VSC for inclusion in the power flow Newton-Raphson algorithm.

In polar co-ordinates the complex voltage sources representing the two VSC stations in the HVDC-VSC are:

$$\boldsymbol{E}_{vR1}^{\rho} = V_{vR1}^{\rho}\angle\delta_{vR1}^{\rho} \tag{3.92}$$

$$\boldsymbol{E}_{vR2}^{\rho} = V_{vR2}^{\rho}\angle\delta_{vR2}^{\rho} \tag{3.93}$$

In this application the two shunt voltage sources used to represent the rectifier and inverter stations have the following voltage magnitude and phase angle limits: $V_{vR1\ \min}^{\rho} < V_{vR1}^{\rho} < V_{vR\ \max}^{\rho}$; $0 < \delta_{vR1}^{\rho} < 2\pi$; $V_{vR\ \min}^{\rho} < V_{vR2}^{\rho} < V_{vR\ \max}^{\rho}$ and $0 < \delta_{vR2}^{\rho} < 2\pi$. Where ρ refer to the three-phases, *a*, *b* and *c*.

The constraining power equation for the back-to-back HVDC-VSC, i.e. R_{DC}=0, is:

$$\mathrm{Re}\left\{ \boldsymbol{E}_{vR1}^{\rho}\left(\boldsymbol{I}_{vR1}^{\rho}\right)^{*} + \boldsymbol{E}_{vR2}^{\rho}\left(\boldsymbol{I}_{vR2}^{\rho}\right)^{*} \right\} = 0 \tag{3.94}$$

and for the case when both VSC stations are linked by a DC cable, i.e. R_{DC}>0, is:

$$\mathrm{Re}\left\{ \boldsymbol{E}_{vR1}^{\rho}\left(\boldsymbol{I}_{vR1}^{\rho}\right)^{*} + \boldsymbol{E}_{vR2}^{\rho}\left(\boldsymbol{I}_{vR2}^{\rho}\right)^{*} + P_{\mathrm{DC,loss}} \right\} = 0 \tag{3.95}$$

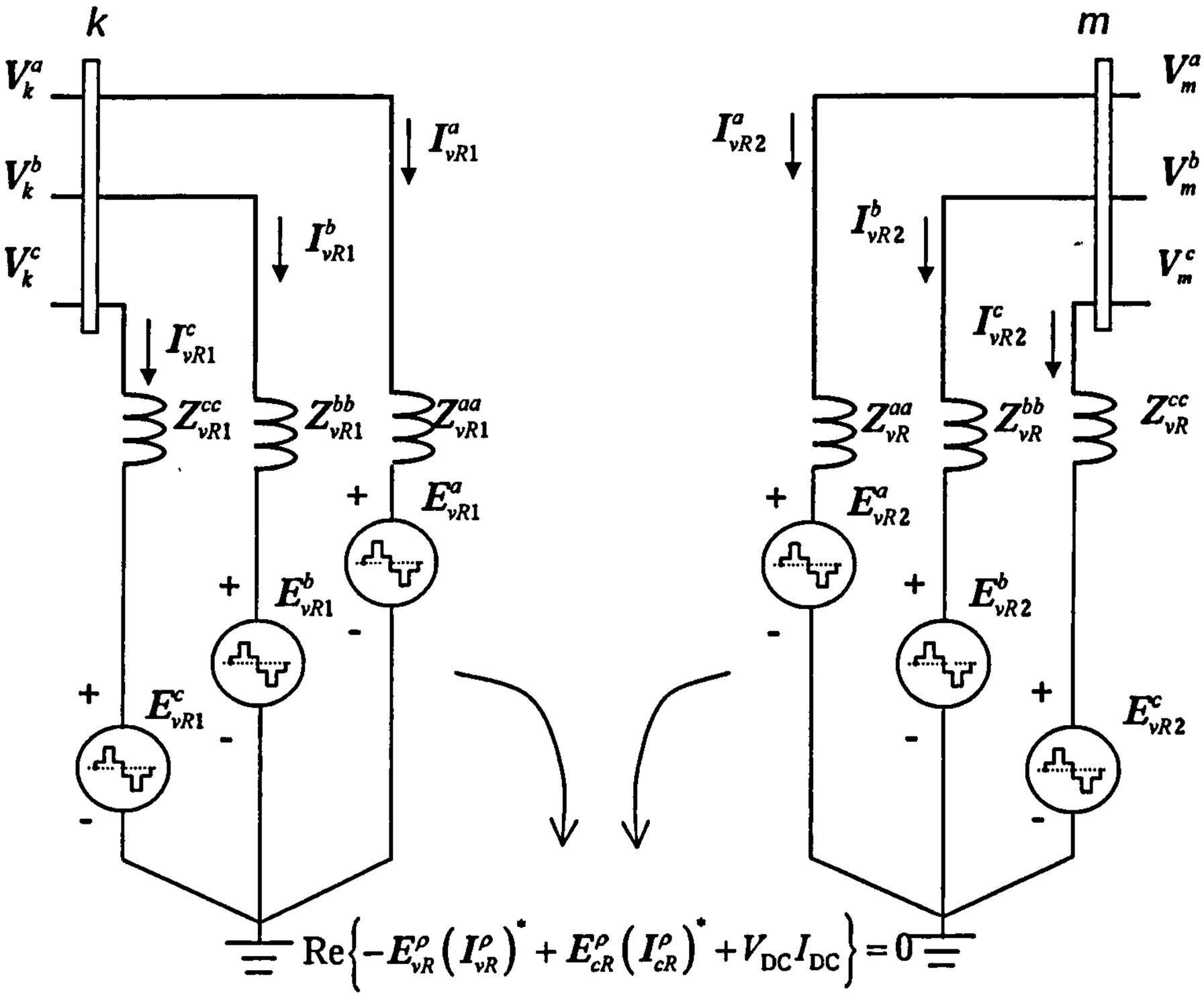

Figure 3.10 Three-phase HVDC VSC-based equivalent

3.6.1 Power flow model

Based on the equivalent circuit shown in Figure 3.10 and the transfer admittance Equation (2.21). If it is assumed that the power flows from the station connected at bus *k* (rectifier) to the station connected at bus *m* (inverter), the following power flow equations injected at bus may be written as,

$$S_k^{\rho}=V_k^{\rho}I_k^{\rho}=V_k^{\rho}\left(Y_{kk}^{\rho}\right)^{*}\left[\left(V_k^{\rho}\right)^{*}-\left(E_{vR1}^{\rho}\right)^{*}\right] \tag{3.96}$$

After performing some complex operations, the following active and reactive power equations are obtained at node *k*,

$$P_k^p=\left(V_k^p\right)^2G_{vR}^p-V_k^pV_{vR}^p\left[G_{vR}^{pp}\cos\left(\theta_k^p-\delta_{vR}^p\right)+B_{vR}^{pp}\sin\left(\theta_k^p-\delta_{vR}^p\right)\right] \tag{3.97}$$

$$Q_k^p=-\left(V_k^p\right)^2B_{vR}^{pp}-V_k^pV_{vR}^p\left[G_{vR}^{pp}\sin\left(\theta_k^p-\delta_{vR}^p\right)-B_{vR}^{pp}\cos\left(\theta_k^p-\delta_{vR}^p\right)\right] \tag{3.98}$$

The powers flowing into the rectifier are described by the following equations:

$$P_{vR}^{p} = \left(V_{vR}^{p}\right)^{2} G_{vR}^{PP} - V_{vR}^{p} V_{k}^{p} \left[G_{vR}^{pp} \cos\left(\delta_{vR}^{p} - \theta_{k}^{p}\right) + B_{vR}^{PP} \sin\left(\delta_{vR}^{P} - \theta_{k}^{P}\right) \right] \tag{3.99}$$

$$Q_{vR}^{p} = -\left(V_{vR}^{p}\right)^{2} B_{vR}^{pp} - V_{vR}^{p} V_{k}^{p} \left[G_{vR}^{pp} \sin\left(\delta_{vR}^{p} - \theta_{k}^{p}\right) - B_{vR}^{pp} \cos\left(\delta_{vR}^{p} - \theta_{k}^{p}\right) \right] \tag{3.100}$$

The power equations for bus *m* and for the inverter are obtained by exchanging the subscripts *k* and *vR*1 for *m* and *vR*2, respectively.

Moreover, one further equation is required to represent the power constraint given in the form of either equations (3.94) or (3.95), depending on the application. For the case of the full HVDC-VSC, the relevant power equation is:

$$P_{vR1} + P_{vR2} + P_{DC} = 0 \tag{3.101}$$

As described in Section 3.1, an *n*-bus power network with no voltage and power flow regulation provisions is described by a 2×(nb-1) non-linear system of equations. For each HVDC-VSC that exists in the power network the 2×(nb-1) system of equations is augmented by up to three equations to take account of the two converter stations and the power constraint equation that exists on the DC side of the converters. The solution of the combined system of non-linear equations is carried out by iteration using the Newton-Raphson method, enabling quadratic convergent solutions.

Both converter stations are capable of controlling the amount of active power injected at their respective AC buses. In a given power flow solution, one of the converters is designated to be the master station, and with the other converter being the slave station. Both stations have control over either voltage magnitude or reactive power injected at their connecting buses.

For the HVDC-VSC, when active power is regulated at the rectifier end and voltage magnitude is regulated at the inverter end, the linearised system of equations has the following structure:

$$\begin{bmatrix} \Delta P_k^{\rho} \\ \Delta Q_k^{\rho} \\ \Delta P_{vR1}^{\rho} \\ \Delta Q_{vR1}^{\rho} \\ \Delta P_{\mathrm{HVDC}}^{\rho} \end{bmatrix} = \begin{bmatrix} \frac{\partial P_k^{\rho}}{\partial \theta_k^{\rho}} & \frac{\partial P_k^{\rho}}{\partial V_k^{\rho}} V_k^{\rho} & \frac{\partial P_k^{\rho}}{\partial \delta_{vR1}^{\rho}} & \frac{\partial P_k^{\rho}}{\partial V_{vR1}^{\rho}} V_{vR1}^{\rho} & 0 \\ \frac{\partial Q_k^{\rho}}{\partial \theta_k^{\rho}} & \frac{\partial Q_k^{\rho}}{\partial V_k^{\rho}} V_k^{\rho} & \frac{\partial Q_k^{\rho}}{\partial \delta_{vR1}^{\rho}} & \frac{\partial Q_k^{\rho}}{\partial V_{vR1}^{\rho}} V_{vR1}^{\rho} & 0 \\ \frac{\partial P_{vR1}^{\rho}}{\partial \theta_k^{\rho}} & \frac{\partial P_{vR1}^{\rho}}{\partial V_k^{\rho}} V_k^{\rho} & \frac{\partial P_{vR1}^{\rho}}{\partial \delta_{vR1}^{\rho}} & \frac{\partial P_{vR1}^{\rho}}{\partial V_{vR1}^{\rho}} V_{vR1}^{\rho} & 0 \\ \frac{\partial Q_{vR1}^{\rho}}{\partial \theta_k^{\rho}} & \frac{\partial Q_{vR1}^{\rho}}{\partial V_k^{\rho}} V_k^{\rho} & \frac{\partial Q_{vR1}^{\rho}}{\partial \delta_{vR1}^{\rho}} & \frac{\partial Q_{vR1}^{\rho}}{\partial V_{vR1}^{\rho}} V_{vR1}^{\rho} & 0 \\ \frac{\partial P_{\mathrm{HVDC}}^{\rho}}{\partial \theta_k^{\rho}} & \frac{\partial P_{\mathrm{HVDC}}^{\rho}}{\partial V_k^{\rho}} V_k^{\rho} & \frac{\partial P_{\mathrm{HVDC}}^{\rho}}{\partial \delta_{vR1}^{\rho}} & \frac{\partial P_{\mathrm{HVDC}}^{\rho}}{\partial V_{vR1}^{\rho}} V_{vR1}^{\rho} & \frac{\partial P_{\mathrm{HVDC}}^{\rho}}{\partial \delta_{vR2}^{\rho}} \end{bmatrix} \begin{bmatrix} \Delta \theta_k^{\rho} \\ \frac{\Delta V_k^{\rho}}{V_k^{\rho}} \\ \Delta \delta_{vR1}^{\rho} \\ \frac{\Delta V_{vR1}^{\rho}}{P_{vR1}^{\rho}} \\ \Delta \delta_{vR2}^{\rho} \end{bmatrix} \tag{3.102}$$

where $\Delta P_{\mathrm{HVDC}}^{\rho}$ is given by

$$\Delta P^{\rho}_{\text{HVDC}} = \Delta P^{\rho}_{vR1} - \Delta P^{\rho}_{vR2} \tag{3.103}$$

is the active power flow mismatch for the DC link. Notice that since active power is regulated at the rectifier end, i.e. $\Delta P_{vR1} = P^{\text{spec}}_{vR1} - P^{\text{calc}}_{vR1}$, the corresponding active power equations for the inverter become redundant, i.e. ΔP_{vR2} and ΔP_m, and are not used in equation (3.102). However, since the voltage magnitude at bus *m* is kept constant the reactive power equations of the inverter also become redundant, i.e. ΔQ_{vR2}. The relevant Jacobian elements are given in Appendix III.

It should be remarked that for the purpose of power flow studies the equivalent circuit of one leg of the HVDC-VSC shown in Figure 3.5 is closely related to the equivalent circuit of the STATCOM (see Section 3.3), and they both share the same power flow equations, i.e. Equations (3.28) - (3.31).

3.6.2 Numerical example of power flow control using a HVDC VSC-based

In order to assess the effectiveness of HVDC-VSC controllers to regulate active and reactive power flow or to control voltage magnitude in one of the HVDC-VSC connecting buses, the five-bus network is modified a three-phase back-to-back HVDC-VSC model replaces the UPFC used in Section 3.5.2 test case, i.e. the controller is used to compensate and to balance the transmission line linking buses Lake and Main. As expected, the power flow results for both simulations coincide in this case. The HVDC station parameters associated with this conditions are V_{vR1}=1.0206, 1.0097, 1.0123 p.u. for *a*, *b* and *c* phase at inverter station (Lake) and V_{vR2}=0.9707, 0.9726 and 0.9705 p.u for *a*, *b* and *c* phase at rectifier station (Main), respectively.

However, a different situation will arise if a full HVDC-VSC model replaces the UPFC and transmission line Lake-Main since the DC cable will contain neither the inductance nor the capacitance of transmission line. In this example, the cable resistance in the DC system is taken to have the same value as the transmission line resistance in the AC system. In the case of study, both source impedances are taken to have a value of X_{vR}=0.1p.u. and have the following, per unit limits 0.9 and 1.1 p.u. The Newton-Raphson algorithm maintained its quadratic convergence characteristics. Figure 3.11 shows the power flow results. It is clear that the HVDC-VSC is an effective device for restoring power balance. Table 3.6 shows the nodal voltage magnitudes and angle in the phase and sequence domain.

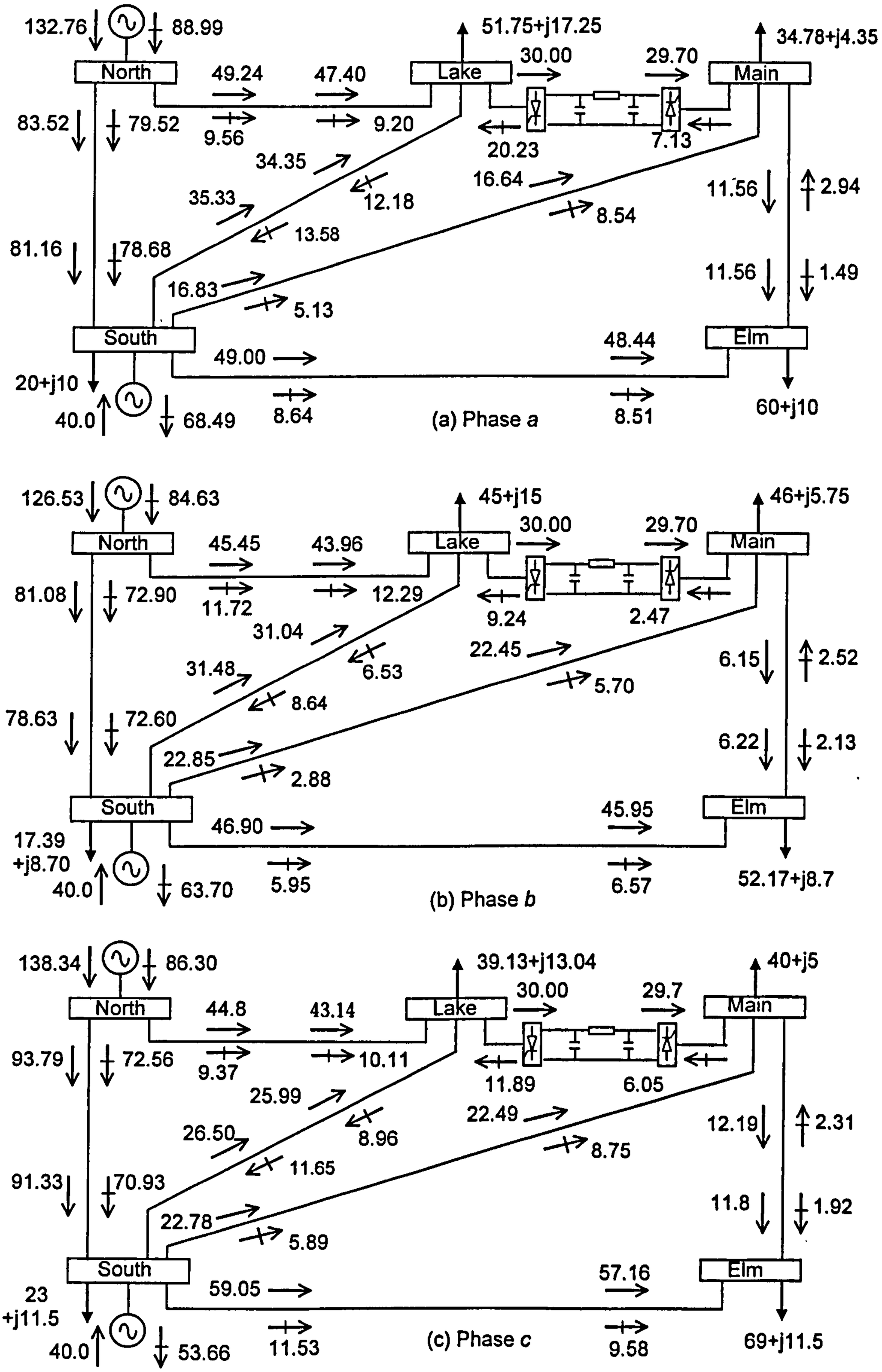

Figure 3.11 HVDC upgrade test network and power flows

3.7 Effective Initialisation of VSC-based FACTS Controllers

Owing to its quadratic rate of convergence, the Newton-Raphson method has become the preferred choice of power systems engineers for solving the non-linear system of equations that describe a power network during steady-state operation [45]. However, the effectiveness of the Newton-Raphson method in achieving feasible iterative solutions is dependent upon the selection of suitable initial values for all the state variables involved in the study. For cases of power networks that contain only conventional plant components this is not an issue, for this problem was solved in the early seventies [46].

The modelling of FACTS controllers for application in power flow analysis results in highly non-linear equations which should be suitably initialised to ensure quadratic convergence when using the Newton-Raphson method. Satisfactory solutions for FACTS controller initialization have been available for quite some time for most FACTS components. However, research experiences over many years and the large number of enquiries received from users of their models indicated that further research work in this direction was required [34-35]. It has since found that initialization of the series components, as the UPFC and SSSC may be an even more critical issue.

As part of this investigation, it was found that voltage-type, shunt elements such as the STATCOM and the two shunt sources representing the HVDC-VSC were suitably initialised by selecting per unit voltage magnitudes and phase angles of 1 and 0, respectively [30].

The approach taken to remedy the situation concerning the vulnerability of the UPFC and SSSC to unsympathetic initial conditions consists of simple analytical equations which have been shown to be very effective in aiding the Newton-Raphson method in retaining quadratic convergence.

3.7.1 UPFC modelling

A standard way of representing the UPFC, for the purpose of fundamental frequency network-wide studies, is shown in Figure 3.6. Equations (3.78) and (3.79) for active and reactive powers injected by the source were derived using the complex power equation, $S = VI^*$ and are used to obtain adequate magnitude and phase angle initial conditions. For the case when active and reactive powers are specified at node *m*, and assuming $V_k = V_m = 1$ p.u. and $\theta_k = \theta_m = 0°$ in equations (3.78) and (3.79), leads to the following simple expressions:

$$V_{cR} = X_{cR}\sqrt{\left(P_m^{sp}\right)^2 + \left(Q_m^{sp}\right)^2} \tag{3.104}$$

$$\theta_{cR} = \arctan\left(\frac{P_m^{sp}}{Q_m^{sp}}\right) \tag{3.105}$$

These equations are used to initialise the parameters of the UPFC series voltage source within the Newton-Raphson power flow solution. These parameters are referred to as $V_{vR}^{(0)}$ and $\theta_{vR}^{(0)}$.

Similar expressions may be derived to provide initial values for the parameters of the shunt voltage source. However, extensive testing has indicated that the parameters of the UPFC shunt voltage source are suitably initialised using the following per phase values: $V_{vR}^{(0)} = 1$ p.u. and $\theta_{vR}^{(0)} = 0$.

3.7.2 SSSC modelling

Similarly to the case of the UPFC model, the active and reactive powers injected by the source were derived using the complex power equation, $\boldsymbol{S} = \boldsymbol{V}\boldsymbol{I}^*$; based on the equivalent circuit shown in Figure 3.6 and equations (3.48) and (3.49). If active and reactive powers are specified at node *k*, and assuming $V_k = V_m = 1$ p.u. and $\theta_k = \theta_m = 0°$ in equations (3.48) and (3.49), equations similar to (3.104) and (3.105) are arrived at which may be used to initialise the SSSC series voltage source within the Newton-Raphson power flow solution.

3.8 Summary

Most of the analysis techniques for the steady-state operation of multiphase conventional power systems are based upon the assumption that the network is operating under balanced conditions. The advantages of this assumption is that only one phase of a three phase system need to be modelled and analysed, resulting in a reduced size of the modelling and analysing problem. However, the phase frame of reference offers a more general representation for the solution of power system problems than the frame of reference provided by the sequences. The former can accommodate networks containing any degree of imbalance whilst the latter is only applicable to power networks exhibiting perfect or near-perfect impedance balance between phases. Bearing this in mind, the work in this chapter has been concentrated on tackling the steady-state, phase domain of the latter generation of FACTS devices based up on the Synchronous Voltage Source Controller.

An existing Newton-Raphson based poly-phase power flow program has been upgraded to include the described FACTS models. The power flow equations pertaining to the FACTS controllers and the power network are solved in a single frame of reference which exhibit quadratic or near-quadratic convergence characteristics, regardless of the size of the network and the number of controllable devices. Guidelines and methods for implementing the FACTS controllers as well as their adjustments within the Newton-Raphson algorithm have also been described. The new models have been amply tested for reliability towards the convergence and accuracy of results using a wide range of power systems with different levels of complexity and different control requirements. It should be mentioned that the VSC-based models performed satisfactorily over all the control options mentioned in the open literature, e.g. constant power, constant current. The power flow results indicate that VSC-based devices are very versatile in power systems transmission control. Using the developed program, an extensive number of simulations using real-life and standard networks have been presented in order to

demonstrate the interaction between the VSC-based controllers and the transmission network.

A comprehensive research study into the initialisation procedures of VSC-based models within the context of Newton-Raphson power flows has been undertaken and the main findings have been reported in the chapter. These studies have shown that analytical equations are required for the effective initialisation of the controllers and the associated equations were presented in full.

3.9 References

[1] Laughton M.A.: "Analysis of unbalanced polyphase networks by the method of phase co-ordinates", *Proc. of* IEE, Vol. 115, No. 8, Aug. 1968, pp. 1163-1172.

[2] Shlash, M.A.: "Three phase analysis of unbalanced power system networks", PhD Thesis, University of Manchester, England, UK, May 1974.

[3] Wasley R.G. and Shlash M.A.: "Newton-Raphson algorithm for 3-phase load flow", *Proc. of* IEE, Vol. 121, No. 7, July 1974, pp. 630-638.

[4] Birt K.A., Graffy J.J. and McDonald J.D.: "Three phase load flow program", IEEE *Trans. Power App. and Syst.* Vol. PAS-95, No.1, Jan./Feb. 1976, pp. 59-65.

[5] Arrillaga J. and Harker B.J.: "Fast decoupled three-phase load flow", *Proc. of* IEE, Vol. 125, No. 8, Aug. 1978, pp. 734-740.

[6] Harker B.J. and Arrillaga J.: "3-Phase a.c./d.c. load flow", *Proc. of* IEE, Vol. 126, No. 12, Dec. 1979, pp. 1275-1281.

[7] Laughton M.A., and Saleh A.O.M.: "Unified phase coordinate load-flow and fault analysis of polyphase networks", Electrical Power & Energy Systems, Vol 2, No. 4, Oct. 1985, pp. 2805-2814.

[8] Wortman M.A., Allen D.L. and Grigsby L.L.: "Techniques for the steady-state representation of unbalanced power systems: part I. a systematic building block approach to network modelling", IEEE *Trans. Power App. Syst.*, Vol. PAS-104, No.10, Oct. 1985, pp. 2805-2814.

[9] HUMPAGE W.D., and NGUYEN T.T.: "Developments in phase-variable modelling for thyristor-controlled reactive-power compensators", IEE *Proc. Gen. Trans. Dist.-Part C*, Vol. 133, No. 5, July 1986, pp. 277-286.

[10] Chen B.K., Chen M.S. Shoults R.R. and Liang C.C.: "Hybrid three-phase load flow", IEE *Proc. Gen. Trans. Dist.-Part C*, Vol. 137, No. 3, May 1990, pp. 177-185.

[11] Xu W., Marti J.R. and Dommel H.W.: "A multiphase harmonic load flow solution technique", IEEE *Trans. Power Syst.*, Vol. 6, No. 2, Feb. 1991, pp. 174-182.

[12] Allemong J.J., Bennon R.J. and Selent P.W.: "Multiphase power flow solutions using EMTP and newtons method", IEEE *Trans. Power Syst.*, Vol. 8, No. 4, Nov. 1993, pp. 1455-1462.

[13] Zhang X.P. and Chen H.: "Asymmetrical Three-Phase Load-Flow Study based on Symmetrical Component Theory", IEE *Proc. Gen. Trans. Dist.-Part C*, Vol. 141, No. 3, May 1994, pp. 248-252.

[14] Smith B.C. and Arrillaga J.: "Improved three phase load flow using phase and sequence components", IEE *Proc. on Gen. Trans. Dist.-Part C*, Vol. 145, No. 3, May 1998, pp. 245-250.

[15] Garcia P.A.N., Pereira J.L.R, Carneriro S., Da Costa V.M. and Martins N.: "Three-phase power flow calculations using the current injection method", IEEE *Trans. Power Syst.*, Vol. 15, No. 2, May 2000, pp. 508-514.

[16] Angeles-Camacho, C.: "Steady-state modelling of the unified power flow controller for three phase power flow analysis of electric systems" M.Sc. Thesis (in Spanish), Instituto Tecnológico de Morelia, México, July 2000.

[17] Venegas T., and Fuerte-Esquivel C.R.: "Steady-state modelling of an advanced series compensator for power flow analysis of electric networks in phase co-ordinates", IEEE *Trans. Power Syst.*, Vol. 16, No. 4, Oct. 2001, pp. 758-765.

[18] *Zhang, X.-P.; Xue, C.-F.; Godfrey, K.R.;* "Modelling of the static synchronous series compensator (SSSC) in three-phase Newton power flow", IEE *Proc. Gen. Trans. and Dist.* Vol. 151, Issue: 4, July 2004, pp.486-494.

[19] Wasley, R.G. and Shlash, M.A., " Newton-Raphson algorithm for 3-phase load flow", *Proc. of* IEE, Vol. 121, No. 7, 1974, pp. 630-638.

[20] Stagg G.W. and El-Abiad A.H.: "*Computer methods in power system analysis*", McGraw-Hill, 1968. ISNB 67-129963-07-060658-7.

[21] Tinney W.F and Powell W.L.: "Notes on Newton-Raphson method for solution of AC power flow problem", Bonneville Power Administration, Portland Oregon, April 1971.

[22] Tinney W.F. and Hart C.E.: "Power flow solution by Newton's method", IEEE *Trans. on Power App. Syst.*, Vol. PAS-96, No. 11, Nov. 1967, pp. 1449-1460.

[23] Acha E.: "A quasi-Newton algorithm for the load flow solution of large networks with FACTS-controlled branches", *Proc. of the 28th UPEC Conference*, Stafford UK, 21-23, pp. 153-156, Sep. 1993.

[24] Fuerte-Esquivel, C. R.: "Modelling and analysis of FACTS devices", PhD Thesis, University of Glasgow, Scotland, UK, 1997.

[25] Fuerte-Esquivel, C.R., Acha, E., Tan, S.G. and Rico, J.J.: "Efficient object oriented power systems software for the analysis of large-scale networks containing FACTS-controlled branches", IEEE *Trans. on Power Systems*, Vol. 13, No. 2, May 1998, pp. 464-472.

[26] Capper, M.D.: "*C++ for scientist, engineers and mathematicians*", Spring-Verlag, London, UK 1994, ISBN 3-540-19847-4.

[27] Hingorani, N.G., and Gyugyi, L.: "*Understanding FACTS: concepts and technology of flexible AC transmission systems*", the Institute of Electrical and Electronics Engineers, Inc., New York, 2000. ISNB 0-780334558

[28] Song, Y. H. and Johns, A. T.: "*Flexible AC Transmission Systems (FACTS)* ", The Institutional of Electric Engineers, London United Kingdom. ISNB 0852967713

[29] Sen, K. K., "STATCOM-Static synchronous compensator: Theory, modelling, and applications", IEEE *Power Eng. Soc. Winter Meeting*, 1999, pp. 1177-1183

[30] Acha, E., Agelidis, V.G., Anaya-Lara, O. Miller, T.J.E.: "*Power electronic control in electric systems*", Butterworth-Heinemann, 2001, ISBN 0-750-65126-1.

[31] Zhang L, Crow M.L., Yang Z. and Chen S.: "The Steady-state characteristics of an SSSC integrated with energy store", IEEE *Power Eng. Society Winter Meeting*, Vol. 3, Jun.-Feb. 2001 Columbus Oh, USA, pp 1311-1336.

[32] Sen, K. K., "SSSC-Static synchronous series compensator: Theory, modelling, and applications", IEEE *Trans. Power Delivery.*, vol. 3, Jan. 1998 pp. 241-246

[33] Noroozian M. and Andersson G.: "Power flow control by use of controllable series components", IEEE *Trans. on Power Delivery*, Vol. 8, No. 3, July 1993, pp. 1420-1429.

[34] Fuerte-Esquivel, C.R.; Acha, E. and Ambriz-Perez, H.: "A comprehensive UPFC model for the quadratic load flow solution of power networks", IEEE *Trans. on Power Syst.*, Vol. 15, No. 1, Feb. 2000. pp. 102-109.

[35] Fuerte-Esquivel, C.R. and Acha, E.: "The unified power flow controller: A critical comparison of Newton-Raphson UPFC algorithms in power flow studies", IEE *Proc. Gen. Trans. and Dist*, Vol. 144, No. 5, Sep. 1997, pp. 437-444.

[36] Mehraban, A.S.; Edris, A.; Schauder, C.D.; Provanzana, J.H.; "Installation, commissioning, and operation of the world's first UPFC on the AEP system", *International Conference on Power System Technology*, Vol. 1, Aug. 1998, pp. 323-327.

[37] Nabavi, A. and Irvani, M.R.: "Steady-state and dynamic models of unified power flow controllers for power system studies", IEEE *Trans. on Power Systems*, Vol. 11, No. 4, Nov. 1996, pp. 1937-1943.

[38] Ärnlöv, B.: "HVDC 2000 - a new generation of high-voltage DC converter", ABB Power system, ABB Review 3/1996.

[39] Lescale, V. F.: "Modern HVDC: State of the art and development trends", IEEE *International conference on power system technology*, POWERCON '98, Vol. 1, 1998, pp. 446-450.

[40] Asplund, G., Eriksson, K. and Svensson, K.: "DC transmission based on voltage source converters", CIGRE SC14 Colloquium, Johannesburg, South Africa, 1997.

[41] Larsson, T., Peterson, Å., Edris, A., Kidd, D., Haley, R. and Aboytes, F.: " Eagle Pass back-to-back tie: a dual purpose application of Voltage Source Converter Technology", IEEE *PES Summer Meeting*, Vol. 3, July 2001.

[43] Asplund, G., Eriksson, K. and Svensson, K.: "HVDC light-DC transmission based on voltage source converters", ABB Power system, ABB Review 1/1998.

[44] Andersen, B. and Baker, C.: "A new era of HVDC?", IEE *Review*, March 2000, pp. 33-39.

[45] Tinney, W.F. and Hart, C.E.: "Power flow solution by Newton's method", IEEE *Trans. on Power Apparatus and Syst*, Vol. PAS-86, No. 11, Nov. 1967 pp. 1449-1460.

[46] Stott, B.: "Effective starting process for Newton-Raphson load flows", IEE *Proc.-Power*, Vol. 118, No. 8, Aug. 1971, pp. 983-987.

Chapter 4

PHASE-DOMAIN POWER FLOWS RECTANGULAR CO-ORDINATES FRAME OF REFERENCE INCLUDING VSC-BASED FACTS CONTROLLERS

4.1 Introduction

The basic formulation of the three-phase power flow problem is well known. Nodal analysis is almost universally preferred in this application, using the nodal admittance matrix. The Newton-Raphson method in polar co-ordinates is the most widely used of all formulations to solve power flows; this method has been adopted in Chapter 3 for the implementation of VSC-based FACTS controllers in power system networks. Alternatively, using rectangular co-ordinates a more efficient version of the power flow method can be developed [1-3].

The rectangular co-ordinate version uses the real and imaginary parts of the nodal complex voltages as state variables rather than the magnitudes and phase angles. In polar co-ordinate analysis, the calculated real and reactive powers are expressed as a function of voltage magnitude and phase angle, whereas in rectangular or Cartesian co-ordinates these are expressed as a function of real and imaginary voltage components. Despite the fact that the number of equations and variables are greater in the rectangular method by the number of PV-type buses, when sparsity programming is used, such an increase in size is of little significance. Indeed, each iteration in the rectangular method is marginally faster than in the polar co-ordinates method because there are no trigonometric operations to carry out [2-5].

An exhaustive literature search indicates that no works seem to be have been reported so far on power flows in rectangular co-ordinates taking into account power electronics based controllers, in particular in the phase frame of reference. Hence, this chapter presents a method to solve three-phase power flows using the Newton-Raphson technique based in rectangular co-ordinates with provision to include models of VSC-based FACTS controllers.

4.2 Power Flows using Rectangular Co-ordinates

Power flow analysis in polar co-ordinates is carried out using nodal complex voltages suitably accommodated in the polar frame of reference, and the calculated active and reactive powers are expressed as a function of voltage magnitudes and phase angles,

whereas in power flow analysis using rectangular co-ordinates, the nodal voltages are expressed as a function of their real and imaginary parts.

4.2.1 Power flow equations

With reference to Figure 3.1 and Equation 3.1, the power balance equation for a three-phase transmission line component can be written as,

$$\boldsymbol{S}^{a,b,c} = P^{a,b,c} + \mathrm{j}Q^{a,b,c} = \boldsymbol{V}^{a,b,c}\left(\boldsymbol{I}^{a,b,c}\right)^{*} \tag{4.1}$$

where

$\boldsymbol{S}^{a,b,c}$ is the complex power injected into the three-phase bus

$P^{a,b,c}$ is the active power injected into the three-phase bus

$Q_k^{a,b,c}$ is the reactive power injected into the three-phase bus

$\boldsymbol{V}^{a,b,c}$ is the complex voltage at the three-phase bus

$\boldsymbol{I}^{a,b,c}$ is the complex current injected into the three-phase bus

and *a*, *b* and *c* refer to the three phases.

In rectangular co-ordinates analysis the bus voltages and admittances are expressed as

$$\boldsymbol{V}_k^{\rho} = \begin{bmatrix} e_k^a + \mathrm{j}f_k^a \\ e_k^b + \mathrm{j}f_k^b \\ e_k^c + \mathrm{j}f_k^c \end{bmatrix} \tag{4.2}$$

and

$$\boldsymbol{Y}_{km}^{\rho\rho} = \begin{bmatrix} \boldsymbol{Y}_{km}^{aa} & \boldsymbol{Y}_{km}^{ab} & \boldsymbol{Y}_{km}^{ac} \\ \boldsymbol{Y}_{km}^{ba} & \boldsymbol{Y}_{km}^{bb} & \boldsymbol{Y}_{km}^{bc} \\ \boldsymbol{Y}_{km}^{ca} & \boldsymbol{Y}_{km}^{cb} & \boldsymbol{Y}_{km}^{cc} \end{bmatrix} = \begin{bmatrix} G_{km}^{aa} + \mathrm{j}B_{km}^{aa} & G_{km}^{ab} + \mathrm{j}B_{km}^{ab} & G_{km}^{ac} + \mathrm{j}B_{km}^{ac} \\ G_{km}^{ba} + \mathrm{j}B_{km}^{ba} & G_{km}^{bb} + \mathrm{j}B_{km}^{bb} & G_{km}^{bc} + \mathrm{j}B_{km}^{bc} \\ G_{km}^{ca} + \mathrm{j}B_{km}^{ca} & G_{km}^{cb} + \mathrm{j}B_{km}^{cb} & G_{km}^{cc} + \mathrm{j}B_{km}^{cc} \end{bmatrix} \tag{4.3}$$

Separating the real and imaginary parts of equation (4.1), in expanded form, leads to the nodal active and reactive power expressions for phase "ρ":

$$P_k^{\rho} = e_k^{\rho} \sum_{i=k,m} \sum_{j=a,b,c} \left(G_{ki}^{\rho j} e_i^j - B_{ki}^{\rho j} f_i^j\right) + f_k^{\rho} \sum_{i=k,m} \sum_{j=a,b,c} \left(G_{ki}^{\rho j} f_i^j + B_{ki}^{\rho j} e_i^j\right) \tag{4.4}$$

$$Q_k^{\rho} = f_k^{\rho} \sum_{i=k,m} \sum_{j=a,b,c} \left(G_{ki}^{\rho j} e_i^j - B_{ki}^{\rho j} f_i^j\right) - e_k^{\rho} \sum_{i=k,m} \sum_{j=a,b,c} \left(G_{ki}^{\rho j} f_i^j + B_{ki}^{\rho j} e_i^j\right) \tag{4.5}$$

where ρ is used to denote phases *a, b* and *c*. Expressions for the active and reactive powers injected at node *m* are similar in form, with subscript *m* replacing *k* and *vice versa*.

4.2.2 Form the Jacobian matrix

The linearised power flow problem using rectangular co-ordinates is constructed similarly to equation (3.10). Using the real and imaginary parts of voltages to form the Jacobian matrix and the mismatch voltages vector, equation (3.10) becomes

$$\begin{bmatrix} \Delta P_1^a \\ \vdots \\ \Delta P_{nbus}^c \\ \Delta Q_1^a \\ \vdots \\ \Delta Q_{nbus}^c \end{bmatrix} = \begin{bmatrix} \frac{\partial P_1^a}{\partial e_1^a} & \cdots & \frac{\partial P_1^a}{\partial e_{nbus}^c} & \frac{\partial P_1^a}{\partial f_1^a} & \cdots & \frac{\partial P_1^a}{\partial f_{nbus}^c} \\ \vdots & \ddots & \vdots & \vdots & \ddots & \vdots \\ \frac{\partial P_{nbus}^c}{\partial e_1^a} & \cdots & \frac{\partial P_{nbus}^c}{\partial e_{nbus}^c} & \frac{\partial P_{nbus}^c}{\partial f_1^a} & \cdots & \frac{\partial P_{nbus}^c}{\partial f_{nbus}^c} \\ \frac{\partial Q_1^a}{\partial e_1^a} & \cdots & \frac{\partial Q_1^a}{\partial e_{nbus}^a} & \frac{\partial Q_1^a}{\partial f_1^a} & \cdots & \frac{\partial Q_1^a}{\partial f_{nbus}^c} \\ \vdots & \ddots & \vdots & \vdots & \ddots & \vdots \\ \frac{\partial Q_{nbus}^c}{\partial e_1^a} & \cdots & \frac{\partial Q_{nbus}^c}{\partial e_{nbus}^c} & \frac{\partial Q_{nbus}^c}{\partial f_1^a} & \cdots & \frac{\partial Q_{nbus}^c}{\partial f_{nbus}^c} \end{bmatrix} \begin{bmatrix} \Delta e_1^a \\ \vdots \\ \Delta e_{nbus}^c \\ \Delta f_1^a \\ \vdots \\ \Delta f_{nbus}^c \end{bmatrix} \tag{4.6}$$

Each element of the Jacobian matrix in rectangular co-ordinates may take one of the following forms:

$$\frac{\partial P_{k,m}^{\rho 1}}{\partial e_{k,m}^{\rho 2}} \qquad \frac{\partial P_{k,m}^{\rho 1}}{\partial f_{k,m}^{\rho 2}}$$

$$\frac{\partial Q_{k,m}^{\rho 1}}{\partial e_{k,m}^{\rho 2}} \qquad \frac{\partial Q_{k,m}^{\rho 1}}{\partial f_{k,m}^{\rho 2}} \tag{4.7}$$

where $\rho 1$ and $\rho 1$ refer to the *a*, *b* and *c* phases. Each one of the above elements is a 3x3 matrix; with the matrix being symmetric if it represents a geometrically balanced network element, otherwise it is an asymmetric matrix.

Consider the l^{th} transmission element connected between buses *k* and *m* in (4.6), for which self and mutual Jacobian terms are given below.

For $k \neq m$

$$\frac{\partial P_{k,i}^{\rho 1}}{\partial e_{m,i}^{\rho 2}} = \left(G_{km}^{\rho 1 \rho 2} e_k^{\rho 1} + B_{km}^{\rho 1 \rho 2} f_k^{\rho 1}\right) \tag{4.8}$$

$$\frac{\partial P_{k,i}^{\rho 1}}{\partial f_{m,i}^{\rho 2}} = \left(G_{km}^{\rho 1 \rho 2} f_k^{\rho 1} - B_{km}^{\rho 1 \rho 2} e_k^{\rho 1}\right) \tag{4.9}$$

$$\frac{\partial Q_{k,i}^{\rho 1}}{\partial e_{m,i}^{\rho 2}} = \left(G_{km}^{\rho 1 \rho 2} f_k^{\rho 1} - B_{km}^{\rho 1 \rho 2} e_k^{\rho 1}\right) \tag{4.10}$$

$$\frac{\partial Q_{k,i}^{\rho 1}}{\partial f_{m,i}^{\rho 2}} = -\left(G_{km}^{\rho 1 \rho 2} e_k^{\rho 1} + B_{km}^{\rho 1 \rho 2} f_k^{\rho 1}\right) \tag{4.11}$$

For $k = m$, with $\rho 1 = \rho 2$

$$\frac{\partial P_{k,i}^{\rho 1}}{\partial e_{k,i}^{\rho 2}} = \left(G_{kk}^{\rho 1 \rho 2} e_k^{\rho 1} + B_{kk}^{\rho 1 \rho 2} f_k^{\rho 1}\right) + \mathrm{Re}\left(I_k^{\rho 1}\right) \tag{4.12}$$

$$\frac{\partial P_{k,i}^{\rho 1}}{\partial f_{k,i}^{\rho 2}} = \left(G_{kk}^{\rho 1 \rho 2} f_k^{\rho 1} - B_{kk}^{\rho 1 \rho 2} e_k^{\rho 1}\right) + \mathrm{Im}\left(I_k^{\rho 1}\right) \tag{4.13}$$

$$\frac{\partial Q_{k,i}^{\rho 1}}{\partial e_{k,i}^{\rho 2}} = \left(G_{kk}^{\rho 1 \rho 2} f_k^{\rho 1} - B_{kk}^{\rho 1 \rho 2} e_k^{\rho 1}\right) - \mathrm{Im}\left(I_k^{\rho 1}\right) \tag{4.14}$$

$$\frac{\partial Q_{k,i}^{\rho 1}}{\partial f_{k,i}^{\rho 2}} = -\left(G_{kk}^{\rho 1 \rho 2} e_k^{\rho 1} + B_{kk}^{\rho 1 \rho 2} f_k^{\rho 1}\right) + \mathrm{Re}\left(I_k^{\rho 1}\right) \tag{4.15}$$

For $\rho 1 \neq \rho 2$

$$\frac{\partial P_{k,i}^{\rho 1}}{\partial e_{k,i}^{\rho 2}} = \left(G_{kk}^{\rho 1 \rho 2} e_k^{\rho 1} + B_{kk}^{\rho 1 \rho 2} f_k^{\rho 1}\right) \tag{4.16}$$

$$\frac{\partial P_{k,i}^{\rho 1}}{\partial f_{k,i}^{\rho 2}} = \left(G_{kk}^{\rho 1 \rho 2} f_k^{\rho 1} - B_{kk}^{\rho 1 \rho 2} e_k^{\rho 1}\right) \tag{4.17}$$

$$\frac{\partial Q_{k,i}^{\rho 1}}{\partial e_{k,i}^{\rho 2}} = \left(G_{kk}^{\rho 1 \rho 2} f_k^{\rho 1} - B_{kk}^{\rho 1 \rho 2} e_k^{\rho 1}\right) \tag{4.18}$$

$$\frac{\partial Q_{k,i}^{\rho 1}}{\partial f_{k,i}^{\rho 2}} = -\left(G_{kk}^{\rho 1 \rho 2} e_k^{\rho 1} + B_{kk}^{\rho 1 \rho 2} f_k^{\rho 1}\right) \tag{4.19}$$

where the current $\left(I_{k,i}^{\rho 1}\right)$ is:

$$I_{k,J}^{\rho 1} = \sum_{l=k,m} \sum_{\rho 2=a,b,c} \left[\left(G_{kl}^{\rho 1 \rho 2} e_l^{\rho 2} - B_{kl}^{\rho 1 \rho 2} f_l^{\rho 2} \right) + \mathrm{j} \left(B_{kl}^{\rho 1 \rho 2} e_l^{\rho 2} + G_{kl}^{\rho 1 \rho 2} f_l^{\rho 1} \right) \right] \tag{4.20}$$

The Jacobian matrix and mismatch vector are evaluated at each iteration. The generic power mismatch equations at bus *k* are:

$$\Delta P_{k,m}^{\rho} = \left(P_{k,m}^{\rho} \right)^{\mathrm{sp}} - \left(P_{k,m}^{\rho} \right)^{\mathrm{cal},\, it} \tag{4.21}$$

$$\Delta Q_{k,m}^{\rho} = \left(Q_{k,m}^{\rho} \right)^{\mathrm{sp}} - \left(Q_{k,m}^{\rho} \right)^{\mathrm{cal},\, it} \tag{4.22}$$

where $\left(P_{k,m}^{\rho} \right)^{\mathrm{sp}}$ and $\left(Q_{k,m}^{\rho} \right)^{\mathrm{sp}}$ are the specified active and reactive power injections determined by the net amount of power generation and load connected to the bus and $\left(P_{k,m}^{\rho} \right)^{\mathrm{cal},\, it}$ and $\left(Q_{k,m}^{\rho} \right)^{\mathrm{cal},\, it}$ are the calculated active and reactive power injections at the bus using the corresponding nodal voltages $\left(V^{\rho} \right)^{it}$. Likewise in polar co-ordinates, the nodal voltages in phase *a* may be initialised at one and zero for the real part and the imaginary part, respectively, while phases *b*, and *c* are initialised at, $-1/2 - \mathrm{j}\sqrt{3}/2$ and $-1/2 + \mathrm{j}\sqrt{3}/2$ respectively. At each iteration the nodal voltages are updated using

$$\left(V_k^{\rho} \right)^{(it+1)} = \left[\left(e_k^{\rho} \right)^{(it)} + \left(\Delta e_k^{\rho} \right)^{(it)} \right] + \mathrm{j} \left[\left(f_k^{\rho} \right)^{(it)} + \left(\Delta f_k^{\rho} \right)^{(it)} \right] \tag{4.23}$$

The process is repeated until complex power mismatches are within a specified tolerance, e.g. $1e^{-12}$.

4.2.3 Voltage controlled bus

In the Newton-Raphson method using polar co-ordinates, for the PV-type buses, where the voltage magnitudes and the active powers are specified, ΔV^{ρ} is set equal to zero. However, in the Newton-Raphson method using rectangular co-ordinates, a nodal voltage magnitude mismatch equation is needed for each PV-type bus [3]. The equations for a voltage-controlled bus become

$$P_k^{\rho 1} = \sum_{m=1}^{\mathrm{nb}} \left\{ e_k^{\rho 1} \left(G_{km}^{\rho 1 \rho 2} e_m^{\rho 2} - B_{km}^{\rho 1 \rho 2} f_m^{\rho 2} \right) + f_{km}^{\rho 1} \left(G_{km}^{\rho 1 \rho 2} f_m^{\rho 2} + B_{km}^{\rho 1 \rho 2} e_m^{\rho 2} \right) \right\} \tag{4.24}$$

$$\left(V_k^{\rho 1} \right)^2 = \left(e_k^{\rho 1} \right)^2 + \left(f_k^{\rho 1} \right)^2 \tag{4.25}$$

Accordingly, new types of Jacobian elements are needed for the Jacobian matrix in rectangular co-ordinates where :

$$\frac{\partial\left(V_{k,m}^{\rho 1}\right)^2}{\partial e_{k,m}^{\rho 2}} \quad \text{and} \quad \frac{\partial\left(V_{k,m}^{\rho 1}\right)^2}{\partial f_{k,m}^{\rho 2}} \tag{4.26}$$

For the i^{th} element connected to a PV-type bus, say k, the Jacobian elements are

$$\frac{\partial\left(V_{k,i}^{\rho}\right)^2}{\partial e_{k,i}^{\rho}} = 2e_{k,i}^{\rho} \tag{4.27}$$

$$\frac{\partial\left(V_{k,i}^{\rho}\right)^2}{\partial f_{k,i}^{\rho}} = 2f_{k,i}^{\rho} \tag{4.28}$$

$$\frac{\partial\left(V_{k,i}^{\rho}\right)^2}{\partial e_{m,i}^{\rho}} = 0 \tag{4.29}$$

$$\frac{\partial\left(V_{k,i}^{\rho}\right)^2}{\partial f_{m,i}^{\rho}} = 0 \tag{4.30}$$

Changes in voltage magnitude for the PV-type buses at iteration *it* are calculated as follows:

$$\Delta\left[\left(V_k^{\rho}\right)^2\right]^{it} = \left[\left(V_{k(\text{Scheduled})}^{\rho}\right)^2\right]^{it} - \left[\left(V_k^{\rho}\right)^2\right]^{it} \tag{4.31}$$

At iteration *it* the reactive power at each voltage controlled bus is reviewed using equation (4.5) to calculate reactive power and to check its limits. If the source of reactive power exceeds the limits the bus changes to a load bus with fixed reactive power, equal to the violated limit.

The process is repeated until complex power mismatches are within a specified tolerance, e.g. $1e^{-12}$.

4.3 Static Synchronous Compensator

The Static Synchronous compensator (STATCOM or SSC) is represented as a voltage source. The STATCOM enables a robust voltage support at the bus where it is connected to. The STATCOM equivalent circuit is shown in Figure 3.4. A mathematical model of the STATCOM for inclusion in the power flow algorithm in rectangular co-ordinates is carried out, assuming that the three Thévenin equivalents representing the three-phase STATCOM are decoupled.

The three-phase complex voltage sources representing the VSC element of the STATCOM, in rectangular co-ordinates, are expressed as:

$$E_{vR}^{\rho} = V_{vR}^{\rho}\left(\cos\delta_{vR}^{\rho} + \mathrm{j}\sin\delta_{vR}^{\rho}\right) = e_{vR}^{\rho} + \mathrm{j}f_{vR}^{\rho} \tag{4.32}$$

where ρ refers to the phases *a*, *b* and *c*.

4.3.1 Reactive power flow model

Based on the shunt connection shown in Figure 3.4, nodal power equations where derived in Section 3.3 for the STATCOM and at its connecting bus, say *k*,

$$S_{\mathrm{vR}}^{\rho} = E_{\mathrm{vR}}^{\rho} I_{vR}^{*} = E_{\mathrm{vR}}^{\rho} Y_{vR}^{*}\left[\left(E_{vR}^{\rho}\right)^{*} - \left(V_{k}^{\rho}\right)^{*}\right] \tag{4.33}$$

$$S_{k}^{\rho} = E_{k}^{\rho} I_{k}^{*} = E_{k}^{\rho} Y_{vR}^{*}\left[\left(V_{k}^{\rho}\right)^{*} - \left(E_{vR}^{\rho}\right)^{*}\right] \tag{4.34}$$

After performing some arduous operations, the following active and reactive power equations are obtained for the converter:

$$\begin{aligned} P_{vR}^{\rho} = {} & e_{vR}^{\rho}\left[\left(G_{vR}^{\rho\rho} e_{vR}^{\rho} - B_{vR}^{\rho\rho} f_{vR}^{\rho}\right) - \left(G_{vR}^{\rho\rho} e_{k}^{\rho} - B_{vR}^{\rho\rho} f_{k}^{\rho}\right)\right] \\ & + f_{vR}^{\rho}\left[\left(G_{vR}^{\rho\rho} f_{vR}^{\rho} + B_{vR}^{\rho\rho} e_{vR}^{\rho}\right) - \left(G_{vR}^{\rho\rho} f_{k}^{\rho} + B_{vR}^{\rho\rho} e_{k}^{\rho}\right)\right] \end{aligned} \tag{4.35}$$

$$\begin{aligned} Q_{vR}^{\rho} = {} & f_{vR}^{\rho}\left[\left(G_{vR}^{\rho\rho} e_{vR}^{\rho} - B_{vR}^{\rho\rho} f_{vR}^{\rho}\right) - \left(G_{vR}^{\rho\rho} e_{k}^{\rho} - B_{vR}^{\rho\rho} f_{k}^{\rho}\right)\right] \\ & + e_{vR}^{\rho}\left[-\left(G_{vR}^{\rho\rho} f_{vR}^{\rho} + B_{vR}^{\rho\rho} e_{vR}^{\rho}\right) + \left(G_{vR}^{\rho\rho} f_{k}^{\rho} + B_{vR}^{\rho\rho} e_{k}^{\rho}\right)\right] \end{aligned} \tag{4.36}$$

To obtain the power flow equations at the bus, the subscripts in equations (4.35) and (4.36) are swapped, i.e. *vR* for *k* and *vice versa* so that:

$$\begin{aligned} P_{k}^{\rho} = {} & e_{k}^{\rho}\left[\left(G_{vR}^{\rho\rho} e_{k}^{\rho} - B_{vR}^{\rho\rho} f_{k}^{\rho}\right) - \left(G_{vR}^{\rho\rho} e_{vR}^{\rho} - B_{vR}^{\rho\rho} f_{vR}^{\rho}\right)\right] \\ & + f_{k}^{\rho}\left[\left(G_{vR}^{\rho\rho} f_{k}^{\rho} + B_{vR}^{\rho\rho} e_{k}^{\rho}\right) - \left(G_{vR}^{\rho\rho} f_{vR}^{\rho} + B_{vR}^{\rho\rho} e_{vR}^{\rho}\right)\right] \end{aligned} \tag{4.37}$$

$$\begin{aligned} Q_{k}^{\rho} = {} & f_{k}^{\rho}\left[\left(G_{vR}^{\rho\rho} e_{k}^{\rho} - B_{vR}^{\rho\rho} f_{k}^{\rho}\right) - \left(G_{vR}^{\rho\rho} e_{vR}^{\rho} - B_{vR}^{\rho\rho} f_{vR}^{\rho}\right)\right] \\ & + e_{k}^{\rho}\left[-\left(G_{vR}^{\rho\rho} f_{k}^{\rho} + B_{vR}^{\rho\rho} e_{k}^{\rho}\right) + \left(G_{vR}^{\rho\rho} f_{vR}^{\rho} + B_{vR}^{\rho\rho} e_{vR}^{\rho}\right)\right] \end{aligned} \tag{4.38}$$

Using these power equations, and assuming that a power source is available on the DC side of the converter, the linearised STATCOM model is given below, where the real and imaginary components of the nodal voltages are taken to be the state variables.

$$\begin{bmatrix} \Delta P_k^\rho \\ \Delta Q_k^\rho \\ \Delta P_{vR}^\rho \\ \Delta Q_{vR}^\rho \end{bmatrix} = \begin{bmatrix} \frac{\partial P_k^\rho}{\partial e_k^\rho} & \frac{\partial P_k^\rho}{\partial f_k^\rho} & \frac{\partial P_k^\rho}{\partial e_{vR}^\rho} & \frac{\partial P_k^\rho}{\partial f_{vR}^\rho} \\ \frac{\partial Q_k^\rho}{\partial e_k^\rho} & \frac{\partial Q_k^\rho}{\partial f_k^\rho} & \frac{\partial Q_k^\rho}{\partial e_{vR}^\rho} & \frac{\partial Q_k^\rho}{\partial f_{vR}^\rho} \\ \frac{\partial P_{vR}^\rho}{\partial e_k^\rho} & \frac{\partial P_{vR}^\rho}{\partial f_k^\rho} & \frac{\partial P_{vR}^\rho}{\partial e_{vR}^\rho} & \frac{\partial P_{vR}^\rho}{\partial f_{vR}^\rho} \\ \frac{\partial Q_{vR}^\rho}{\partial e_k^\rho} & \frac{\partial Q_{vR}^\rho}{\partial f_k^\rho} & \frac{\partial Q_{vR}^\rho}{\partial e_{vR}^\rho} & \frac{\partial Q_{vR}^\rho}{\partial f_{vR}^\rho} \end{bmatrix} \begin{bmatrix} \Delta e_k^\rho \\ \Delta f_k^\rho \\ \Delta e_{vR}^\rho \\ \Delta f_{vR}^\rho \end{bmatrix} \tag{4.39}$$

The linearised set of equations of the STATCOM model, for the case when the controller regulates voltage magnitude at bus *k* are:

$$\begin{bmatrix} \Delta P_k^\rho \\ \Delta \left(E_k^\rho\right)^2 \\ \Delta P_{vR}^\rho \\ \Delta Q_{vR}^\rho \end{bmatrix} = \begin{bmatrix} \frac{\partial P_k^\rho}{\partial e_k^\rho} & \frac{\partial P_k^\rho}{\partial f_k^\rho} & \frac{\partial P_k^\rho}{\partial e_{vR}^\rho} & \frac{\partial P_k^\rho}{\partial f_{vR}^\rho} \\ \frac{\partial \left(E_k^\rho\right)^2}{\partial e_k^\rho} & \frac{\partial \left(E_k^\rho\right)^2}{\partial f_k^\rho} & 0 & 0 \\ \frac{\partial P_{vR}^\rho}{\partial e_k^\rho} & \frac{\partial P_{vR}^\rho}{\partial f_k^\rho} & \frac{\partial P_{vR}^\rho}{\partial e_{vR}^\rho} & \frac{\partial P_{vR}^\rho}{\partial f_{vR}^\rho} \\ \frac{\partial Q_{vR}^\rho}{\partial e_k^\rho} & \frac{\partial Q_{vR}^\rho}{\partial f_k^\rho} & \frac{\partial Q_{vR}^\rho}{\partial e_{vR}^\rho} & \frac{\partial Q_{vR}^\rho}{\partial f_{vR}^\rho} \end{bmatrix} \begin{bmatrix} \Delta e_k^\rho \\ \Delta f_k^\rho \\ \Delta e_{vR}^\rho \\ \Delta f_{vR}^\rho \end{bmatrix} \tag{4.40}$$

The Jacobian elements are,

$$\frac{\partial P_k^\rho}{\partial e_k^\rho} = 2G_{vR}^{\rho\rho} e_k^\rho - \left(G_{vR}^\rho e_{vR}^\rho - B_{vR}^{\rho\rho} f_{vR}^\rho\right) \tag{4.41}$$

$$\frac{\partial P_k^\rho}{\partial f_k^\rho} = 2G_{vR}^{\rho\rho} f_k^\rho - \left(G_{vR}^{\rho\rho} f_{vR}^\rho + B_{vR}^{\rho\rho} e_{vR}^\rho\right) \tag{4.42}$$

$$\frac{\partial P_k^\rho}{\partial e_{vR}^\rho} = -\left(G_{vR}^{\rho\rho} e_k^\rho + B_{vR}^{\rho\rho} f_k^\rho\right) \tag{4.43}$$

$$\frac{\partial P_k^\rho}{\partial f_{vR}^\rho} = -\left(G_{vR}^{\rho\rho} f_k^\rho - B_{vR}^{\rho\rho} e_k^\rho\right) \tag{4.44}$$

$$\frac{\partial Q_k^\rho}{\partial e_k^\rho} = -2B_{vR}^{\rho\rho} e_k^\rho + \left(G_{vR}^{\rho\rho} f_{vR}^\rho + B_{vR}^{\rho\rho} e_{vR}^a\right) \tag{4.45}$$

$$\frac{\partial Q_k^\rho}{\partial f_k^\rho} = -2B_{vR}^{\rho\rho} f_k^\rho - \left(G_{vR}^{\rho\rho} e_{vR}^\rho - B_{vR}^{\rho\rho} f_{vR}^\rho\right) \tag{4.46}$$

$$\frac{\partial Q_k^\rho}{\partial e_{vR}^\rho} = -\left(G_{vR}^{\rho\rho} f_k^\rho - B_{vR}^{\rho\rho} e_k^\rho\right) \tag{4.47}$$

$$\frac{\partial Q_k^\rho}{\partial f_{vR}^\rho} = \left(G_{vR}^{\rho\rho} e_k^\rho + B_{vR}^{\rho\rho} f_k^\rho\right) \tag{4.48}$$

$$\frac{\partial P_{vR}^\rho}{\partial e_k^\rho} = -\left(G_{vR}^{\rho\rho} e_{vR}^\rho + B_{vR}^{\rho\rho} f_{vR}^\rho\right) \tag{4.49}$$

$$\frac{\partial P_{vR}^\rho}{\partial f_k^\rho} = -\left(G_{vR}^{\rho\rho} f_{vR}^\rho - B_{vR}^{\rho\rho} e_{vR}^\rho\right) \tag{4.50}$$

$$\frac{\partial P_{vR}^\rho}{\partial e_{vR}^\rho} = 2G_{vR}^{\rho\rho} e_{vR}^\rho - \left(G_{vR}^{\rho\rho} e_k^\rho - B_{vR}^{\rho\rho} f_k^\rho\right) \tag{4.51}$$

$$\frac{\partial P_{vR}^\rho}{\partial f_{vR}^\rho} = 2G_{vR}^{\rho\rho} f_{vR}^\rho - \left(G_{vR}^{\rho\rho} f_k^\rho + B_{vR}^{\rho\rho} e_k^\rho\right) \tag{4.52}$$

$$\frac{\partial Q_{vR}^\rho}{\partial e_k^\rho} = -\left(G_{vR}^{\rho\rho} f_{vR}^\rho - B_{vR}^{\rho\rho} e_{vR}^\rho\right) \tag{4.53}$$

$$\frac{\partial Q_{vR}^\rho}{\partial f_k^\rho} = \left(G_{vR}^{\rho\rho} e_{vR}^\rho + B_{vR}^{\rho\rho} f_{vR}^\rho\right) \tag{4.54}$$

$$\frac{\partial Q_{vR}^\rho}{\partial e_{vR}^\rho} = -2B_{vR}^{\rho\rho} e_{vR}^\rho + \left(G_{vR}^{\rho\rho} f_k^\rho + B_{vR}^{\rho\rho} e_k^\rho\right) \tag{4.55}$$

$$\frac{\partial Q_{cR}^\rho}{\partial f_{vR}^\rho} = -2B_{vR}^{\rho\rho} f_{vR}^\rho - \left(G_{vR}^{\rho\rho} e_k^\rho - B_{vR}^{\rho\rho} f_k^\rho\right) \tag{4.56}$$

For voltage magnitude control,

$$\frac{\partial \left(V_k^\rho\right)^2}{\partial e_k^\rho} = 2e_k^\rho \tag{4.57}$$

$$\frac{\partial \left(V_k^\rho\right)^2}{\partial f_k^\rho} = 2f_k^\rho \tag{4.58}$$

At each iteration, the complex voltage source is updated using

$$\left(\Delta \boldsymbol{E}_{vR}^\rho\right)^{it} = \left(\Delta e_{vR}^\rho\right)^{it} + \mathrm{j}\left(\Delta f_{vR}^\rho\right)^{it} \tag{4.59}$$

$$\left(\boldsymbol{E}_{vR}^\rho\right)^{it+1} = \left(\boldsymbol{E}_{vR}^\rho\right)^{it} + \left(\Delta \boldsymbol{E}_{vR}^\rho\right)^{it} \tag{4.60}$$

Voltage magnitude limits are checked at the end of each iterative step, and if one or more limits are violated, the voltage magnitude is fixed at the violated limit. Notice that if the STATCOM is controlling reactive power then the STATCOM generation of reactive power at each iteration is calculated and its limits checked. In case of limit violations, the reactive power is fixed at the limit violated.

4.4 Static Synchronous Series Compensation

The SSSC model in rectangular co-ordinates is based on the principles of operation outlined in Section 2.6. and the equivalent circuit shown in Figure 3.6, where it is argued that the SSSC is adequately represented by a complex voltage source in series with the transformer impedance [11-15].

The three-phase complex voltage sources representing the VSC element of the SSSC, in rectangular co-ordinates, is expressed as

$$\boldsymbol{E}_{cR}^{\rho} = V_{cR}^{\rho}\left(\cos\delta_{cR}^{\rho} + \mathrm{j}\sin\delta_{cR}^{\rho}\right) = e_{cR}^{\rho} + \mathrm{j}f_{cR}^{\rho} \tag{4.61}$$

In the current application the voltage source is modelled with the following voltage magnitude and phase angle limits per phase: $V_{cR\ \min}^{\rho} \le V_{cR}^{\rho} \le V_{cR\ \max}^{\rho}$ and $0 \le \delta_{cR}^{\rho} \le 2\pi$. Equation (4.61) is used along with transfer admittance equation (2.9) to derive the mathematical model of the SSSC and its inclusion in the three-phase power flow Newton-Raphson method using rectangular co-ordinates.

4.4.1 Power flow model

Substituting Equation (3.46) into (3.47) and expanding leads to the following active and reactive power equations for node *k* and for phases *ρ*= *a*, *b* and *c*

$$\begin{aligned} P_k^{\rho} = {} & e_k^{\rho}\left[\left(G_{cR}^{\rho\rho}e_k^{\rho} - B_{cR}^{\rho\rho}f_k^{\rho}\right) - \left(G_{cR}^{\rho\rho}e_m^{\rho} - B_{cR}^{\rho\rho}f_m^{\rho}\right) - \left(G_{cR}^{\rho\rho}e_{cR}^{\rho} - B_{cR}^{\rho\rho}f_{cR}^{\rho}\right)\right] \\ & + f_k^{\rho}\left[\left(G_{cR}^{\rho\rho}f_k^{\rho} + B_{cR}^{\rho\rho}e_k^{\rho}\right) - \left(G_{cR}^{\rho\rho}f_m^{\rho} + B_{cR}^{\rho\rho}e_m^{\rho}\right) - \left(G_{cR}^{\rho\rho}f_{cR}^{\rho} + B_{cR}^{\rho\rho}e_{cR}^{\rho}\right)\right] \end{aligned} \tag{4.62}$$

$$\begin{aligned} Q_k^{\rho} = {} & e_k^{\rho}\left[-\left(G_{cR}^{\rho\rho}f_k^{\rho} + B_{cR}^{\rho\rho}e_k^{\rho}\right) + \left(G_{cR}^{\rho\rho}f_m^{\rho} + B_{cR}^{\rho\rho}e_m^{\rho}\right) + \left(G_{cR}^{\rho\rho}f_{cR}^{\rho} + B_{cR}^{\rho\rho}e_{cR}^{\rho}\right)\right] \\ & + f_k^{a}\left[\left(G_{cR}^{\rho\rho}e_k^{\rho} - B_{cR}^{\rho\rho}f_k^{\rho}\right) - \left(G_{cR}^{\rho\rho}e_m^{a} - B_{cR}^{\rho\rho}f_m^{\rho}\right) - \left(G_{cR}^{\rho\rho}e_{cR}^{\rho} - B_{cR}^{\rho\rho}f_{cR}^{\rho}\right)\right] \end{aligned} \tag{4.63}$$

A similar set of power equations is obtained for node *m*, by interchanging the sub-scripts *k* and *m*.

4.4.2 Linearised system of equations

For the SSSC when both active and reactive powers are regulated, the linearised system of equations in rectangular co-ordinates has the following structure:

$$\begin{bmatrix} \Delta P_k^\rho \\ \Delta P_m^\rho \\ \Delta Q_k^\rho \\ \Delta Q_m^\rho \\ \Delta P_{km}^\rho \\ \Delta Q_{km}^\rho \end{bmatrix} = \begin{bmatrix} \frac{\partial P_k^\rho}{\partial e_k^\rho} & \frac{\partial P_k^\rho}{\partial e_m^\rho} & \frac{\partial P_k^\rho}{\partial f_k^\rho} & \frac{\partial P_k^\rho}{\partial f_m^\rho} & \frac{\partial P_k^\rho}{\partial e_{cR}^\rho} & \frac{\partial P_k^\rho}{\partial f_{cR}^\rho} \\ \frac{\partial P_m^\rho}{\partial e_k^\rho} & \frac{\partial P_m^\rho}{\partial e_m^\rho} & \frac{\partial P_m^\rho}{\partial f_k^\rho} & \frac{\partial P_m^\rho}{\partial f_m^\rho} & \frac{\partial P_m^\rho}{\partial e_{cR}^\rho} & \frac{\partial P_m^\rho}{\partial f_{cR}^\rho} \\ \frac{\partial Q_k^\rho}{\partial e_k^\rho} & \frac{\partial Q_k^\rho}{\partial e_m^\rho} & \frac{\partial Q_k^\rho}{\partial f_k^\rho} & \frac{\partial Q_k^\rho}{\partial f_m^\rho} & \frac{\partial Q_k^\rho}{\partial e_{cR}^\rho} & \frac{\partial Q_k^\rho}{\partial f_{cR}^\rho} \\ \frac{\partial Q_m^\rho}{\partial e_k^\rho} & \frac{\partial Q_m^\rho}{\partial e_m^\rho} & \frac{\partial Q_m^\rho}{\partial f_k^\rho} & \frac{\partial Q_m^\rho}{\partial f_m^\rho} & \frac{\partial Q_m^\rho}{\partial e_{cR}^\rho} & \frac{\partial Q_m^\rho}{\partial f_{cR}^\rho} \\ \frac{\partial P_{km}^\rho}{\partial e_k^\rho} & \frac{\partial P_{km}^\rho}{\partial e_m^\rho} & \frac{\partial P_{km}^\rho}{\partial f_k^\rho} & \frac{\partial P_{km}^\rho}{\partial f_m^\rho} & \frac{\partial P_{km}^\rho}{\partial e_{cR}^\rho} & \frac{\partial P_{km}^\rho}{\partial f_{cR}^\rho} \\ \frac{\partial Q_{km}^\rho}{\partial e_k^\rho} & \frac{\partial Q_{km}^\rho}{\partial e_m^\rho} & \frac{\partial Q_{km}^\rho}{\partial f_k^\rho} & \frac{\partial Q_{km}^\rho}{\partial f_m^\rho} & \frac{\partial Q_{km}^\rho}{\partial e_{cR}^\rho} & \frac{\partial Q_{km}^\rho}{\partial f_{cR}^\rho} \end{bmatrix} \begin{bmatrix} \Delta e_k^\rho \\ \Delta e_m^\rho \\ \Delta f_k^\rho \\ \Delta f_m^\rho \\ \Delta e_{cR}^\rho \\ \Delta f_{cR}^\rho \end{bmatrix} \tag{4.64}$$

The Jacobian elements for this application are detailed below.

For $k \neq m$:

$$\frac{\partial P_k^\rho}{\partial e_m^\rho} = -\frac{\partial Q_k^\rho}{\partial f_m^\rho} = \frac{\partial P_k^\rho}{\partial e_{cR}^\rho} = -\frac{\partial Q_k^\rho}{\partial f_{cR}^\rho} - \left(G_{cR}^{\rho\rho} e_k^\rho + B_{cR}^{\rho\rho} f_k^\rho\right) \tag{4.65}$$

$$\frac{\partial P_k^\rho}{\partial f_m^\rho} = \frac{\partial Q_k^\rho}{\partial e_m^\rho} = \frac{\partial P_k^\rho}{\partial f_{cR}^\rho} = \frac{\partial Q_k^\rho}{\partial e_{cR}^\rho} = \left(-G_{km}^{\rho\rho} f_k^\rho + B_{km}^{\rho\rho} e_k^\rho\right) \tag{4.66}$$

For $k = m$:

$$\frac{\partial P_k^\rho}{\partial e_k^\rho} = \left(G_{cR}^{\rho\rho} e_k^\rho + B_{cR}^{\rho\rho} f_k^\rho\right) + \mathrm{Re}\left(I_k^\rho\right) \tag{4.67}$$

$$\frac{\partial P_k^\rho}{\partial f_k^\rho} = \left(G_{cR}^{\rho\rho} f_k^\rho - B_{cR}^{\rho\rho} e_k^\rho\right) + \mathrm{Im}\left(I_k^\rho\right) \tag{4.68}$$

$$\frac{\partial Q_k^\rho}{\partial e_k^\rho} = \left(G_{cR}^{\rho\rho} f_k^\rho - B_{cR}^{\rho\rho} e_k^\rho\right) - \mathrm{Im}\left(I_k^\rho\right) \tag{4.69}$$

$$\frac{\partial Q_k^\rho}{\partial f_k^\rho} = -\left(G_{cR}^{\rho\rho} e_k^\rho + B_{cR}^{\rho\rho} f_k^\rho\right) + \mathrm{Re}\left(I_k^\rho\right) \tag{4.70}$$

Where the real and imaginary parts of the current $\left(I_{k,1}^{\rho 1}\right)$ are

$$\begin{aligned}\mathrm{Re}\left(\boldsymbol{I}_k^{\rho}\right) &= \left(G_{cR}^{\rho\rho} e_k^{\rho} - B_{cR}^{\rho\rho} f_k^{\rho}\right) - \sum_{l=m,cR}\left[\left(G_{cR}^{\rho\rho} e_l^{\rho} - B_{cR}^{\rho\rho} f_l^{\rho}\right)\right] \\ \mathrm{Im}\left(\boldsymbol{I}_k^{\rho}\right) &= \left(G_{cR}^{\rho\rho} f_k^{\rho} + B_{cR}^{\rho\rho} e_k^{\rho}\right) - \sum_{l=m,cR}\left[\left(B_{cR}^{\rho\rho} e_l^{\rho} + G_{cR}^{\rho\rho} f_l^{\rho}\right)\right]\end{aligned} \tag{4.71}$$

The Jacobian matrix and mismatch vectors are evaluated at each iteration.

The power mismatch equations at a generic bus *k* are

$$\begin{aligned}\Delta P_{k,m}^{\rho} &= \left(P_{k,m}^{\rho}\right)^{\mathrm{sp}} - \left(P_{k,m}^{\rho}\right)^{\mathrm{cal}} \\ \Delta Q_{k,m}^{\rho} &= \left(Q_{k,m}^{\rho}\right)^{\mathrm{sp}} - \left(Q_{k,m}^{\rho}\right)^{\mathrm{cal}}\end{aligned} \tag{4.72}$$

where $\left(P_k^{\rho}\right)^{\mathrm{sp}}$ and $\left(Q_k^{\rho}\right)^{\mathrm{sp}}$ are the net specified active and reactive powers to be controlled and $\left(P_k^{\rho}\right)^{\mathrm{cal},it}$ and $\left(Q_k^{\rho}\right)^{\mathrm{cal},it}$ are the calculated active and reactive power injections at node *k* for iteration *it*, using $\left(\boldsymbol{V}^{\rho}\right)^{it}$. In polar co-ordinates, the nodal voltages of phase *a* may be initialised at one and zero for the real part and the imaginary part, respectively and phases *b*, and *c* are initialised at, $-\frac{1}{2} - \mathrm{j}\frac{\sqrt{3}}{2}$ and $-\frac{1}{2} + \mathrm{j}\frac{\sqrt{3}}{2}$ respectively. Nodal voltages are updated during each iteration using equation (4.23), and the complex source voltages are updated using:

$$\begin{aligned}\Delta \boldsymbol{E}_{cR}^{\rho} &= \Delta e_{cR}^{\rho} + \mathrm{j}\Delta f_{cR}^{\rho} \\ \left(\boldsymbol{E}_{cR}^{\rho}\right)^{it+1} &= \left(\Delta \boldsymbol{E}_{cR}^{\rho}\right)^{it} + \left(\boldsymbol{E}_{cR}^{\rho}\right)^{it}\end{aligned} \tag{4.73}$$

If the SSSC is connected to the slack node, $\Delta \boldsymbol{V}^{\rho}$ and Q^{ρ} are set to zero, whereas if connected to a PV-type node, a voltage magnitude squared mismatch equation is needed for each PV-type bus. It should be noticed that the magnitude and phase angle of the voltage source converter are checked for limit violations, and if limit violations do occur, the VSC voltage is kept at the exceeded limit.

4.5 Unified Power Flow Controller

Assuming that the equivalent circuit of a three-phase UPFC consists of three single-phase UPFC equivalent circuits, with no couplings between them, as shown in Figure 3.8, the complex voltage sources in rectangular co-ordinates are expressed as

$$\boldsymbol{E}_{vR}^{\rho} = V_{vR}^{\rho}\left(\cos\delta_{vR}^{\rho} + \mathrm{j}\sin\delta_{vR}^{\rho}\right) = e_{vR}^{\rho} + \mathrm{j}f_{vR}^{\rho} \tag{4.74}$$

$$\boldsymbol{E}_{cR}^{\rho} = V_{cR}^{\rho}\left(\cos\delta_{cR}^{\rho} + \mathrm{j}\sin\delta_{cR}^{\rho}\right) = e_{cR}^{\rho} + \mathrm{j}f_{cR}^{\rho} \tag{4.75}$$

The magnitudes and phase angles of the voltage sources representing the series and shunt converters are controlled between limits $V^{\rho}_{vR\ \min} \le V^{\rho}_{vR} \le V^{\rho}_{vR\ \max}$ and $0 \le \delta^{\rho}_{vR} \le 2\pi$, and $V^{\rho}_{cR\ \min} \le V^{\rho}_{cR} \le V^{\rho}_{cR\ \max}$ and $0 \le \delta^{\rho}_{cR} \le 2\pi$, respectively. The magnitude of the injected series voltage determines the amount of power flow to be controlled.

4.5.1 Power flow model

From Figure 3.8 and using the rectangular voltages given by putting equations (3.74) and (3.75) into (3.76) and (3.77), the nodal active and reactive power equations for the UPFC for phases ρ= *a, b* and *c* at bus *k* for the series and shunt converters can be obtained.

At bus *k*:

$$\begin{aligned} P^{\rho}_{k} = {} & e^{\rho}_{k}\left\{\left[\left(G^{\rho\rho}_{cR}+G^{\rho\rho}_{vR}\right)e^{\rho}_{k}-\left(B^{\rho\rho}_{cR}+B^{\rho\rho}_{vR}\right)f^{\rho}_{k}\right]\right. \\ & \left.-\left(G^{\rho\rho}_{cR}e^{\rho}_{m}-B^{\rho\rho}_{cR}f^{\rho}_{m}\right)-\left(G^{\rho\rho}_{cR}e^{\rho}_{cR}-B^{\rho\rho}_{cR}f^{\rho}_{cR}\right)-\left(G^{\rho\rho}_{vR}e^{\rho}_{vR}-B^{\rho\rho}_{vR}f^{\rho}_{vR}\right)\right\} \\ & + f^{\rho}_{k}\left\{\left[\left(G^{\rho\rho}_{cR}+G^{\rho\rho}_{vR}\right)f^{\rho}_{k}+\left(B^{\rho\rho}_{cR}+B^{\rho\rho}_{vR}\right)e^{\rho}_{k}\right]\right. \\ & \left.-\left(G^{\rho\rho}_{cR}f^{\rho}_{m}+B^{\rho\rho}_{cR}e^{\rho}_{m}\right)-\left(G^{\rho\rho}_{cR}f^{\rho}_{cR}+B^{\rho\rho}_{cR}e^{\rho}_{cR}\right)-\left(G^{\rho\rho}_{vR}f^{\rho}_{vR}+B^{\rho\rho}_{vR}e^{\rho}_{vR}\right)\right\} \end{aligned} \tag{4.76}$$

$$\begin{aligned} Q^{\rho}_{k} = {} & e^{\rho}_{k}\left\{-\left[\left(G^{\rho\rho}_{cR}+G^{\rho\rho}_{vR}\right)f^{\rho}_{k}-\left(B^{\rho\rho}_{cR}+B^{\rho\rho}_{vR}\right)e^{\rho}_{k}\right]\right. \\ & \left.+\left(G^{\rho\rho}_{cR}f^{\rho}_{m}+B^{\rho\rho}_{cR}e^{\rho}_{m}\right)+\left(G^{\rho\rho}_{cR}f^{\rho}_{cR}+B^{\rho\rho}_{cR}e^{\rho}_{cR}\right)+\left(G^{\rho\rho}_{vR}f^{\rho}_{vR}+B^{\rho\rho}_{vR}e^{\rho}_{vR}\right)\right\} \\ & + f^{\rho}_{k}\left\{\left[\left(G^{\rho\rho}_{cR}+G^{\rho\rho}_{vR}\right)e^{\rho}_{k}-\left(B^{\rho\rho}_{cR}+B^{\rho\rho}_{vR}\right)f^{\rho}_{k}\right]\right. \\ & \left.-\left(G^{\rho\rho}_{cR}e^{\rho}_{m}-B^{\rho\rho}_{cR}f^{\rho}_{m}\right)-\left(G^{\rho\rho}_{cR}e^{\rho}_{cR}-B^{\rho\rho}_{cR}f^{\rho}_{cR}\right)-\left(G^{\rho\rho}_{vR}e^{\rho}_{vR}-B^{\rho\rho}_{vR}f^{\rho}_{vR}\right)\right\} \end{aligned} \tag{4.77}$$

At bus *m*:

$$\begin{aligned} P^{\rho}_{m} = {} & e^{\rho}_{m}\left[\left(G^{\rho\rho}_{cR}e^{\rho}_{m}-B^{\rho\rho}_{cR}f^{\rho}_{m}\right)-\left(G^{\rho\rho}_{cR}e^{\rho}_{k}-B^{\rho\rho}_{cR}f^{\rho}_{k}\right)-\left(G^{\rho\rho}_{cR}e^{\rho}_{cR}-B^{\rho\rho}_{cR}f^{\rho}_{cR}\right)\right] \\ & + f^{\rho}_{m}\left[\left(G^{\rho\rho}_{cR}f^{\rho}_{m}+B^{\rho\rho}_{cR}e^{\rho}_{m}\right)-\left(G^{\rho\rho}_{cR}f^{\rho}_{k}+B^{\rho\rho}_{cR}e^{\rho}_{k}\right)-\left(G^{\rho\rho}_{cR}f^{k}_{cR}+B^{\rho\rho}_{cR}e^{\rho}_{cR}\right)\right] \end{aligned} \tag{4.78}$$

$$\begin{aligned} Q^{\rho}_{m} = {} & e^{\rho}_{m}\left[-\left(G^{\rho\rho}_{cR}f^{\rho}_{m}+B^{\rho\rho}_{cR}e^{\rho}_{m}\right)+\left(G^{\rho\rho}_{cR}f^{\rho}_{k}+B^{\rho\rho}_{cR}e^{\rho}_{k}\right)+\left(G^{\rho\rho}_{cR}f^{\rho}_{cR}+B^{\rho\rho}_{cR}e^{\rho}_{cR}\right)\right] \\ & + f^{\rho}_{m}\left[\left(G^{\rho\rho}_{cR}e^{\rho}_{m}-B^{\rho\rho}_{cR}f^{\rho}_{m}\right)-\left(G^{\rho\rho}_{cR}e^{\rho}_{k}-B^{\rho\rho}_{cR}f^{\rho}_{k}\right)-\left(G^{\rho\rho}_{cR}e^{\rho}_{cR}-B^{\rho\rho}_{cR}f^{\rho}_{cR}\right)\right] \end{aligned} \tag{4.79}$$

For the series converter:

$$\begin{aligned} P^{\rho}_{cR} = {} & e^{\rho}_{cR}\left[\left(G^{\rho\rho}_{cR}e^{\rho}_{k}-B^{\rho\rho}_{cR}f^{\rho}_{k}\right)-\left(G^{\rho\rho}_{cR}e^{\rho}_{m}-B^{\rho\rho}_{cR}f^{\rho}_{m}\right)-\left(G^{\rho\rho}_{cR}e^{\rho}_{cR}-B^{\rho\rho}_{cR}f^{\rho}_{cR}\right)\right] \\ & + f^{\rho}_{cR}\left[\left(G^{\rho\rho}_{cR}f^{\rho}_{k}+B^{\rho\rho}_{cR}e^{\rho}_{k}\right)-\left(G^{\rho\rho}_{cR}f^{\rho}_{m}+B^{\rho\rho}_{cR}e^{\rho}_{m}\right)-\left(G^{\rho\rho}_{cR}f^{\rho}_{cR}+B^{\rho\rho}_{cR}e^{\rho}_{cR}\right)\right] \end{aligned} \tag{4.80}$$

$$\begin{aligned} Q_{cR}^{\rho} = e_{cR}^{\rho}\left[-\left(G_{cR}^{\rho\rho} f_k^{\rho} + B_{cR}^{\rho\rho} e_k^{\rho}\right) + \left(G_{cR}^{\rho\rho} f_m^{\rho} + B_{cR}^{\rho\rho} e_m^{\rho}\right) + \left(G_{cR}^{\rho\rho} f_{cR}^{\rho} + B_{cR}^{\rho\rho} e_{cR}^{\rho}\right)\right] \\ + f_{cR}^{\rho}\left[\left(G_{cR}^{\rho\rho} e_k^{\rho} - B_{cR}^{\rho\rho} f_k^{\rho}\right) - \left(G_{cR}^{\rho\rho} e_m^{\rho} - B_{cR}^{\rho\rho} f_m^{\rho}\right) - \left(G_{cR}^{\rho\rho} e_{cR}^{\rho} - B_{cR}^{\rho\rho} f_{cR}^{\rho}\right)\right] \end{aligned} \tag{4.81}$$

For the shunt converter:

$$\begin{aligned} P_{vR}^{\rho} = e_{vR}^{\rho}\left[\left(G_{vR}^{\rho\rho} e_k^{\rho} - B_{vR}^{\rho\rho} f_k^{\rho}\right) - \left(G_{vR}^{\rho\rho} e_{vR}^{\rho} - B_{vR}^{\rho\rho} f_{vR}^{\rho}\right)\right] \\ + f_{vR}^{\rho}\left[\left(G_{vR}^{\rho\rho} f_k^{\rho} + B_{vR}^{\rho\rho} e_k^{\rho}\right) - \left(G_{vR}^{\rho\rho} f_{vR}^{\rho} + B_{vR}^{\rho\rho} e_{vR}^{\rho}\right)\right] \end{aligned} \tag{4.82}$$

$$\begin{aligned} Q_{vR}^{\rho} = e_{vR}^{\rho}\left[-\left(G_{vR}^{\rho\rho} f_k^{\rho} + B_{vR}^{\rho\rho} e_k^{\rho}\right) + \left(G_{vR}^{\rho\rho} f_{vR}^{\rho} + B_{vR}^{\rho\rho} e_{vR}^{\rho}\right)\right] \\ + f_{vR}^{\rho}\left[\left(G_{vR}^{\rho\rho} e_k^{\rho} - B_{vR}^{\rho\rho} f_k^{\rho}\right) - \left(G_{vR}^{\rho\rho} e_{vR}^{\rho} - B_{vR}^{\rho\rho} f_{vR}^{\rho}\right)\right] \end{aligned} \tag{4.83}$$

Assuming a loss-less converter, the active power supplied to the shunt converter, P_{vR}^{ρ}, equals the active power demanded by the series converter, P_{cR}^{ρ}, i.e.

$$P_{vR}^{\rho} + P_{cR}^{\rho} = 0 \tag{4.84}$$

Furthermore, if the coupling transformers are assumed to have no resistance then the active power at bus *k* matches the active power at bus *m*. Accordingly

$$P_{vR}^{\rho} + P_{cR}^{\rho} = P_k^{\rho} + P_m^{\rho} = 0 \tag{4.85}$$

The UPFC power equations, in linearised form, are combined with those of the AC network. If both buses *k* and *m* are PQ-type, the linearised system of equations in rectangular co-ordinates is

$$\begin{bmatrix} \Delta P_k^\rho \\ \Delta P_m^\rho \\ \Delta Q_k^\rho \\ \Delta Q_m^\rho \\ \Delta P_{mk}^\rho \\ \Delta Q_{mk}^\rho \\ \Delta P_{bb}^\rho \\ \Delta Q_{vR}^\rho \end{bmatrix} = \begin{bmatrix} \frac{\partial P_k^\rho}{\partial e_k^\rho} & \frac{\partial P_k^\rho}{\partial e_m^\rho} & \frac{\partial P_k^\rho}{\partial f_k^\rho} & \frac{\partial P_k^\rho}{\partial f_m^\rho} & \frac{\partial P_k^\rho}{\partial e_{cR}^\rho} & \frac{\partial P_k^\rho}{\partial f_{cR}^\rho} & \frac{\partial P_k^\rho}{\partial e_{vR}^\rho} & \frac{\partial P_k^\rho}{\partial f_{vR}^\rho} \\ \frac{\partial P_m^\rho}{\partial e_k^\rho} & \frac{\partial P_m^\rho}{\partial e_m^\rho} & \frac{\partial P_m^\rho}{\partial f_k^\rho} & \frac{\partial P_m^\rho}{\partial f_m^\rho} & \frac{\partial P_m^\rho}{\partial e_{cR}^\rho} & \frac{\partial P_m^\rho}{\partial f_{cR}^\rho} & 0 & 0 \\ \frac{\partial Q_k^\rho}{\partial e_k^\rho} & \frac{\partial Q_k^\rho}{\partial e_m^\rho} & \frac{\partial Q_k^\rho}{\partial f_k^\rho} & \frac{\partial Q_k^\rho}{\partial f_m^\rho} & \frac{\partial Q_k^\rho}{\partial e_{cR}^\rho} & \frac{\partial Q_k^\rho}{\partial f_{cR}^\rho} & \frac{\partial Q_k^\rho}{\partial e_{vR}^\rho} & \frac{\partial Q_k^\rho}{\partial f_{vR}^\rho} \\ \frac{\partial Q_m^\rho}{\partial e_k^\rho} & \frac{\partial Q_m^\rho}{\partial e_m^\rho} & \frac{\partial Q_m^\rho}{\partial f_k^\rho} & \frac{\partial Q_m^\rho}{\partial f_m^\rho} & \frac{\partial Q_m^\rho}{\partial e_{cR}^\rho} & \frac{\partial Q_m^\rho}{\partial f_{cR}^\rho} & 0 & 0 \\ \frac{\partial P_{mk}^\rho}{\partial e_k^\rho} & \frac{\partial P_{mk}^\rho}{\partial e_m^\rho} & \frac{\partial P_{km}^\rho}{\partial f_k^\rho} & \frac{\partial P_{mk}^\rho}{\partial f_m^\rho} & \frac{\partial P_{mk}^\rho}{\partial e_{cR}^\rho} & \frac{\partial P_{mk}^\rho}{\partial f_{cR}^\rho} & 0 & 0 \\ \frac{\partial Q_{mk}^\rho}{\partial e_k^\rho} & \frac{\partial Q_{mk}^\rho}{\partial e_m^\rho} & \frac{\partial Q_{km}^\rho}{\partial f_k^\rho} & \frac{\partial Q_{mk}^\rho}{\partial f_m^\rho} & \frac{\partial Q_{mk}^\rho}{\partial e_{cR}^\rho} & \frac{\partial Q_{mk}^\rho}{\partial f_{cR}^\rho} & 0 & 0 \\ \frac{\partial P_{bb}^\rho}{\partial e_k^\rho} & \frac{\partial P_{bb}^\rho}{\partial e_m^\rho} & \frac{\partial P_{bb}^\rho}{\partial f_k^\rho} & \frac{\partial P_{bb}^\rho}{\partial f_m^\rho} & \frac{\partial P_{bb}^\rho}{\partial e_{cR}^\rho} & \frac{\partial P_{bb}^\rho}{\partial f_{cR}^\rho} & \frac{\partial P_{bb}^\rho}{\partial e_{vR}^\rho} & \frac{\partial P_{bb}^\rho}{\partial f_{vR}^\rho} \\ \frac{\partial Q_{vR}^\rho}{\partial e_k^\rho} & 0 & \frac{\partial Q_{vR}^\rho}{\partial f_k^\rho} & 0 & 0 & 0 & \frac{\partial Q_{vR}^\rho}{\partial e_{vR}^\rho} & \frac{\partial Q_{vR}^\rho}{\partial f_{vR}^\rho} \end{bmatrix} \begin{bmatrix} \Delta e_k^\rho \\ \Delta e_m^\rho \\ \Delta f_k^\rho \\ \Delta f_m^\rho \\ \Delta e_{cR}^\rho \\ \Delta f_{cR}^\rho \\ \Delta e_{vR}^\rho \\ \Delta f_{vR}^\rho \end{bmatrix} \tag{4.86}$$

The Jacobian terms in equations (4.86) are given in Appendix III.

Upon solution of the Jacobian matrix, a new set of state variable increments is obtained. The increments are used to update the real and imaginary parts of the voltage sources at each iteration where:

$$\begin{aligned} \left(\Delta E_{cR}^\rho\right)^{it+1} &= \left(\Delta e_{cR}^\rho\right)^{it} + \mathrm{j}\left(\Delta f_{cR}^\rho\right)^{it} \\ \left(\Delta E_{vR}^\rho\right)^{it+1} &= \left(\Delta e_{vR}^\rho\right)^{it} + \mathrm{j}\left(\Delta f_{vR}^\rho\right)^{it} \end{aligned} \tag{4.87}$$

$$\begin{aligned} \left(E_{cR}^\rho\right)^{it+1} &= \left(\Delta E_{cR}^\rho\right)^{it} + \left(E_{cR}^\rho\right)^{it} \\ \left(E_{vR}^\rho\right)^{it+1} &= \left(\Delta E_{vR}^\rho\right)^{it} + \left(E_{vR}^\rho\right)^{it} \end{aligned} \tag{4.88}$$

Voltage magnitude limits are checked at the end of each iterative step, and if one or more limits are exceeded, the voltage magnitude is fixed at the violated limit.

4.6 High-Voltage Direct Current VSC-based

Assuming that the equivalent circuit of a three-phase HVDC VSC-based consists of three single-phase equivalent circuits, with no couplings between them, as shown in Figure 3.10, the complex voltage sources in rectangular co-ordinates representing the

two converters in the HVDC VSC-based controller are expressed as

$$\boldsymbol{E}_{vR1}^{\rho} = V_{vR1}^{\rho}\left(\cos\delta_{vR1}^{\rho} + \mathrm{j}\sin\delta_{vR1}^{\rho}\right) = e_{vR1}^{\rho} + \mathrm{j}f_{vR1}^{\rho} \tag{4.89}$$

$$\boldsymbol{E}_{vR2}^{\rho} = V_{vR2}^{\rho}\left(\cos\delta_{vR2}^{\rho} + \mathrm{j}\sin\delta_{vR2}^{\rho}\right) = e_{vR2}^{\rho} + \mathrm{j}f_{vR2}^{\rho} \tag{4.90}$$

Both sources have voltage magnitudes and phase angles limits of the form: $V_{vR\ \min}^{\rho} \le V_{vR}^{\rho} \le V_{vR\ \max}^{\rho}; 0 \le \delta_{vR}^{\rho} \le 2\pi$; where ρ refers to the three-phases, *a*, *b* and *c*.

The constraining power equation for the back-to-back HVDC-VSC, i.e. R_{DC}=0, is:

$$\mathrm{Re}\left\{ \boldsymbol{E}_{vR1}^{\rho}\left(\boldsymbol{I}_{vR1}^{\rho}\right)^{*} + \boldsymbol{E}_{vR2}^{\rho}\left(\boldsymbol{I}_{vR2}^{\rho}\right)^{*} \right\} = 0 \tag{4.91}$$

and for the case when both VSC stations are linked by a DC cable, i.e. $R_{DC} > 0$, is:

$$\mathrm{Re}\left\{ \boldsymbol{E}_{vR1}^{\rho}\left(\boldsymbol{I}_{vR1}^{\rho}\right)^{*} + \boldsymbol{E}_{vR2}^{\rho}\left(\boldsymbol{I}_{vR2}^{\rho}\right)^{*} + P_{\mathrm{DC,loss}} \right\} = 0 \tag{4.92}$$

4.6.1 Power flow model

Based on the equivalent circuit shown in Figure 3.10, and the transfer admittance equation (2.21), the following nodal power equation was derived in Chapter 3 (equation (3.96)).

$$\boldsymbol{S}_{k}^{\rho} = \boldsymbol{V}_{k}^{\rho}\,\boldsymbol{I}_{k}^{\rho} = \boldsymbol{V}_{k}^{\rho}\left(\boldsymbol{Y}_{kk}^{\rho}\right)^{*}\left[\left(\boldsymbol{V}_{k}^{\rho}\right)^{*} - \left(\boldsymbol{E}_{vR1}^{\rho}\right)^{*}\right] \tag{4.93}$$

This expression assumes that a three-phase complex power is injected at node *k*. Moreover, if it is assumed that the power flows from the station connected at bus *k* (rectifier) to the station connected at bus *m* (inverter), using rectangular co-ordinates to represent the voltages sources and after performing some complex operations, the following active and reactive power equations are obtained at node *k*:

$$\begin{aligned} P_{k}^{\rho} = {} & e_{k}^{\rho}\left[\left(G_{vR1}^{\rho\rho}e_{k}^{\rho} - B_{vR1}^{\rho\rho}f_{k}^{\rho}\right) - \left(G_{vR1}^{\rho\rho}e_{vR1}^{\rho} - B_{vR1}^{\rho\rho}f_{vR1}^{\rho}\right)\right] \\ & + f_{k}^{\rho}\left[\left(G_{vR1}^{\rho\rho}f_{k}^{\rho} + B_{vR1}^{\rho\rho}e_{k}^{\rho}\right) - \left(G_{vR1}^{\rho\rho}f_{v1R}^{\rho} + B_{vR1}^{\rho\rho}e_{vR1}^{\rho}\right)\right] \end{aligned} \tag{4.94}$$

$$\begin{aligned} Q_{k}^{\rho} = {} & e_{k}^{\rho}\left[\left(G_{vR1}^{\rho\rho}f_{k}^{\rho} - B_{vR1}^{\rho\rho}e_{k}^{\rho}\right) + \left(G_{vR1}^{\rho\rho}f_{vR1}^{\rho} + B_{vR1}^{\rho\rho}e_{vR1}^{\rho}\right)\right] \\ & + f_{k}^{\rho}\left[\left(G_{vR1}^{\rho\rho}e_{k}^{\rho} - B_{vR1}^{\rho\rho}f_{k}^{\rho}\right) - \left(G_{vR1}^{\rho\rho}e_{vR1}^{\rho} - B_{vR1}^{\rho\rho}f_{vR1}^{\rho}\right)\right] \end{aligned} \tag{4.95}$$

The powers in the rectifier are:

$$P_{vR1}^{\rho} = e_{vR1}^{\rho}\left[\left(G_{vR1}^{\rho\rho}e_{vR1}^{\rho} - B_{vR1}^{\rho\rho}f_{vR1}^{\rho}\right) - \left(G_{vR1}^{\rho\rho}e_{k}^{\rho} - B_{vR1}^{\rho\rho}f_{k}^{\rho}\right)\right] + f_{vR1}^{\rho}\left[\left(G_{vR1}^{\rho\rho}f_{vR1}^{\rho} + B_{vR1}^{\rho\rho}e_{vR1}^{\rho}\right) - \left(G_{vR1}^{\rho\rho}f_{k}^{\rho} + B_{vR1}^{\rho\rho}e_{k}^{\rho}\right)\right] \quad (4.96)$$

$$Q_{vR1}^{\rho} = e_{vR1}^{\rho}\left[-\left(G_{vR1}^{\rho\rho}f_{vR1}^{\rho} + B_{vR1}^{\rho\rho}e_{vR1}^{\rho}\right) + \left(G_{vR1}^{\rho\rho}f_{k}^{\rho} + B_{vR1}^{\rho\rho}e_{k}^{\rho}\right)\right] + f_{vR1}^{\rho}\left[\left(G_{vR1}^{\rho\rho}e_{vR1}^{\rho} - B_{vR1}^{\rho\rho}f_{vR1}^{\rho}\right) - \left(G_{vR1}^{\rho\rho}e_{k}^{\rho} - B_{vR1}^{\rho\rho}f_{k}^{\rho}\right)\right] \quad (4.97)$$

The power equations for bus *m* and for the inverter are obtained by exchanging the subscripts *k* and *vR*1 for *m* and *vR*2, respectively.

One further equation is required to represent the power constraint given in the form of either equations (3.94) or (3.95), depending on the application. For the case of the full HVDC-VSC, the relevant power equation is:

$$P_{vR1} + P_{vR2} + P_{DC} = 0 \quad (4.98)$$

It should be remarked that for the purpose of power flow studies the equivalent circuit of one leg of the HVDC-VSC shown in Figure 3.10 is closely related to the equivalent circuit of the STATCOM.

Likewise the polar method for each HVDC-VSC that exists in the power network the 2×(nb-1) system of equations is augmented by up to three equations to take account of the two converter stations and the power constraint equation that exists on the DC side of the converters.

For the HVDC-VSC, when active power is regulated at the rectifier end and voltage magnitude is regulated at the inverter end, the linearised system of equations in rectangular co-ordinates has the following structure:

$$\begin{bmatrix} \Delta P_k^{\rho} \\ \Delta Q_k^{\rho} \\ \Delta P_{vR1}^{\rho} \\ \Delta Q_{vR1}^{\rho} \\ \Delta P_{\mathrm{HVDC}}^{\rho} \\ \Delta Q_{vR2}^{\rho} \end{bmatrix} = \begin{bmatrix} \frac{\partial P_k^{\rho}}{\partial e_k^{\rho}} & \frac{\partial P_k^{\rho}}{\partial f_k^{\rho}} & \frac{\partial P_k^{\rho}}{\partial e_{vR}^{\rho}} & \frac{\partial P_k^{\rho}}{\partial f_{vR}^{\rho}} & 0 & 0 \\ \frac{\partial Q_k^{\rho}}{\partial e_k^{\rho}} & \frac{\partial Q_k^{\rho}}{\partial f_k^{\rho}} & \frac{\partial Q_k^{\rho}}{\partial e_{vR}^{\rho}} & \frac{\partial Q_k^{\rho}}{\partial f_{vR}^{\rho}} & 0 & 0 \\ \frac{\partial P_{vR1}^{\rho}}{\partial e_k^{\rho}} & \frac{\partial P_{vR1}^{\rho}}{\partial f_k^{\rho}} & \frac{\partial P_{vR1}^{\rho}}{\partial e_{vR1}^{\rho}} & \frac{\partial P_{vR1}^{\rho}}{\partial f_{vR1}^{\rho}} & 0 & 0 \\ \frac{\partial Q_{vR1}^{\rho}}{\partial e_k^{\rho}} & \frac{\partial Q_{vR1}^{\rho}}{\partial f_k^{\rho}} & \frac{\partial Q_{vR1}^{\rho}}{\partial e_{vR1}^{\rho}} & \frac{\partial Q_{vR1}^{\rho}}{\partial f_{vR1}^{\rho}} & 0 & 0 \\ \frac{\partial P_{\mathrm{HVDC}}^{\rho}}{\partial e_k^{\rho}} & \frac{\partial P_{\mathrm{HVDC}}^{\rho}}{\partial f_k^{\rho}} & \frac{\partial P_{\mathrm{HVDC}}^{\rho}}{\partial e_{vR}^{\rho}} & \frac{\partial P_{\mathrm{HVDC}}^{\rho}}{\partial f_{vR}^{\rho}} & \frac{\partial P_{\mathrm{HVDC}}^{\rho}}{\partial e_{vR2}^{\rho}} & 0 \\ \frac{\partial Q_{vR2}^{\rho}}{\partial e_k^{\rho}} & \frac{\partial Q_{vR2}^{\rho}}{\partial f_k^{\rho}} & 0 & 0 & \frac{\partial Q_{vR2}^{\rho}}{\partial e_{vR2}^{\rho}} & \frac{\partial Q_{vR2}^{\rho}}{\partial f_{vR2}^{\rho}} \end{bmatrix} \begin{bmatrix} \Delta e_k^{\rho} \\ \Delta f_k^{\rho} \\ \Delta e_{vR1}^{\rho} \\ \Delta f_{vR1}^{\rho} \\ \Delta e_{vR2}^{\rho} \\ \Delta f_{vR2}^{\rho} \end{bmatrix} \quad (4.99)$$

Notice that since active power is regulated at the rectifier end, i.e. $\Delta P_{vR1} = P_{vR1}^{spec} - P_{vR1}^{calc}$, the corresponding active power equations of the inverter become redundant, i.e. ΔP_{vR2} and ΔP_m. $\Delta P_{\text{HVDC}}^{\rho} = \Delta P_{vR1}^{\rho} - \Delta P_{vR2}^{\rho}$ is the active power flow mismatch for the DC link. The relevant Jacobian elements are given in Appendix III.

At the end of each iteration, both voltage sources are updated using

$$\left(\Delta E_{vR1}^{\rho}\right)^{it} = \left(\Delta e_{vR1}^{\rho}\right)^{it} + \mathrm{j}\left(\Delta f_{vR1}^{\rho}\right)^{it} \tag{4.100}$$

$$\left(\Delta E_{vR1}^{\rho}\right)^{it} = \left(\Delta e_{vR1}^{\rho}\right)^{it} + \mathrm{j}\left(\Delta f_{vR1}^{\rho}\right)^{it} \tag{4.101}$$

and

$$\left(E_{vR1}^{\rho}\right)^{it+1} = \left(E_{vR1}^{\rho}\right)^{it} + \Delta\left(E_{vR1}^{\rho}\right)^{it} \tag{4.102}$$

$$\left(E_{vR2}^{\rho}\right)^{it+1} = \left(E_{vR2}^{\rho}\right)^{it} + \Delta\left(E_{vR2}^{\rho}\right)^{it} \tag{4.103}$$

4.7 Evaluation of Power Flow Algorithms in Polar and Rectangular Co-ordinates Including FACTS VSC-based Controllers

To show the effectiveness of the power flow models developed for VSC-based FACTS equipment, new software has been written in C++ using the Oriented Object Programming (OOP) philosophy. The software has been tested for robustness and full functionality. Similarly to the Newton-Raphson polar-based algorithm, the newly written Newton-Raphson algorithm using rectangular co-ordinates retains the efficiency and quadratic convergence characteristics of the Newton-Raphson method.

After testing the proposed algorithm with several power systems, meaningful comparisons can be drawn between the two formulations; as expected both programs arrive to the same power flow results. The systems used to compare the performance of both algorithms are the IEEE 118 buses, the 1080 buses and the Mexican system comprising 2172 buses [29].

Their respective CPU time requirements recorded on a desktop computer are shown in Table 4.1. The PC system used in this study has an Intel® Pentium® 4 processor (1.5GHz) with 256MB RAM Memory. Generally speaking, the CPU time depends on the programming techniques used as well as the power system under study. The CPU times shown exclude input/output and the admittance matrix set-up time requirements. The CPU time for constructing the Jacobian matrix and solving of sparse equations using LU decomposition and forward/backward substitutions are shown.

Ordering of the sparse Jacobian using second the Tinney scheme [31] is carried out only at the first iteration; after that the elimination order remains the same throughout

the solution process. It is verified that the ordering process is the time consuming part of the solution. Table 4.1 shows the CPU times for all relevant stages of the solution.

Table 4.1 CPU times in seconds

		Test system					
		IEEE 118 buses		IEEE 1080 buses		Mexican 2172 buses	
Process		Polar	Rect.	Polar	Rect.	Polar	Rect.
Jacobian ordering		0.08	0.07	0.90	0.90	4.58	4.30
At each iteration	Power calculations	0.01	0.01	0.06	0.02	0.12	0.04
	Jacobian construction	0.03	0.01	0.24	0.03	0.57	0.11
	LU and Solution	0.02	0.02	0.14	0.14	0.85	0.82
Overall time		0.98	0.96	6.58	6.13	24.43	23.32

From the CPU times reported in Table 4.1, it can be seen that overall times for the polar method are longer than for the rectangular method. Notice that the differences are basically in the parts of the process where calculations involve trigonometric operations, i.e. power calculation and Jacobian build up. Jacobian ordering, LU factorisation and solution process show little difference between the two methods. In both algorithms these functions are implemented using sparsity techniques with pointers pointing to structures [30]. As expected, CPU time differences increase with increasing sizes of networks.

The total number of iterations needed for both algorithms to converge is the same: 6, 5 and 7 respectively. For all three systems the convergence rates of active and reactive powers show a similar profile, as seen in Figure 4.1(a) and (b)

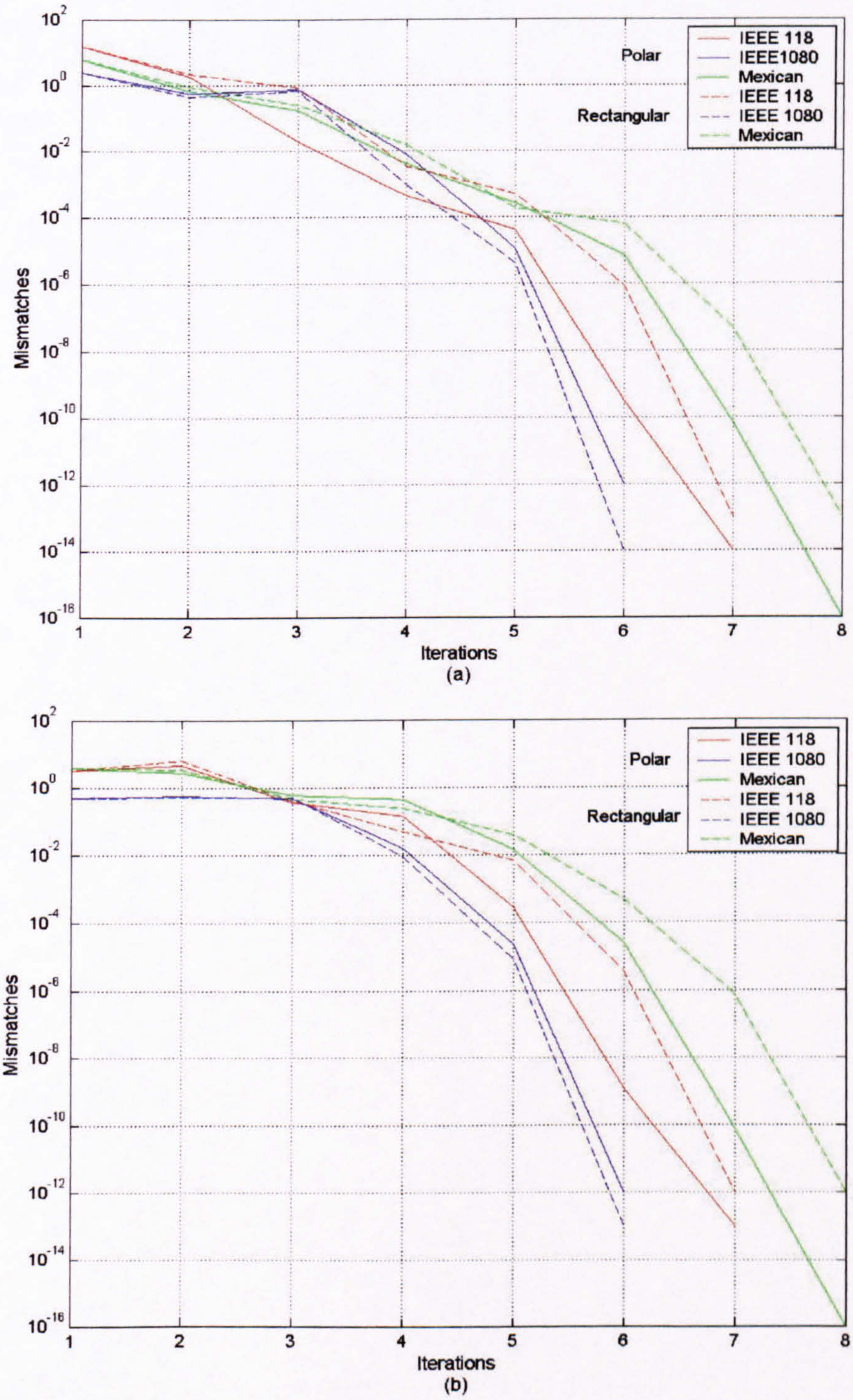

Figure 4.1 Convergence rate for (a) active and (b) reactive power absolute mismatches in both polar and rectangular co-ordinates

4.8 Solution of Large-scale Multiphase Power Network with Embedded VSC-based FACTS Controllers

4.8.1 IEEE 118-node system

The three-phase power flow program written in C++, with the VSC-based FACTS models incorporated, has been used to solve a wide range of test systems, giving in each case very robust solutions. To illustrate this point, the IEEE 118-node system was modified to incorporate three different kinds of VSC-based FACTS controllers.

Four STATCOMs, two back-to-back HVDC-VSCs and two full HVDC-VSC links were embedded in different parts of the network. The STATCOMs were connected at nodes 28, 53, 58 and 75 in order to control voltage magnitude at 1 p.u. at those nodes. One back-to-back HVDC-VSC was added at the sending end of transmission line connecting nodes 20 and 21 to increase the active power flow from 28.7 MW to 32 MW at node 21. The voltage magnitude at node 20 was kept at 1 p.u. The second back-to-back HVDC-VSC was connected in series with transmission line 37-33 to increase active power flow by 25% at node 33. Also, voltage magnitude was kept at 1 p.u. at node 33. Transmission lines 96-97 and 114-115 were replaced by full HVDC-VSC links. Both DC links are used to control voltage magnitude at 1 p.u. at nodes 96 and 114, respectively. The first DC link is used to keep unchanged the active power flow, as in the base case, in node 96. The second DC link is used to double the active power flowing from nodes 114 to 115. The Newton-Raphson method algorithm maintaing its quadratic convergence characteristic and the solution is achieved in six iterations for a power mismactch tolerance of 1e-12.

The DC cable resistance in both links is taken to be 1%. Figure 4.2 shows the nodal voltage profile for both cases: the base case and the modified case, when eight VSC-based FACTS controllers are incorporated in the network. Table 4.2 shows the final values of the voltage sources representing the eight FACTS controllers.

Table 4.2 Source voltages in the IEEE118-node system

Devices	Converter station	V_{cR} (p.u.)	δ_{cR} (deg)
STATCOM	28	1.07447	13.39
	53	1.05323	13.73
	58	1.05298	14.80
	75	1.09606	22.46
Back-to-back HVDC	20	1.02248	13.90
	20'	1.01707	9.40
	33	1.02787	12.19
	33'	1.01175	8.82
Full HVDC Link	96	1.03945	28.04
	97	0.97025	27.36
	114	1.04284	13.95
	115	1.05375	14.45

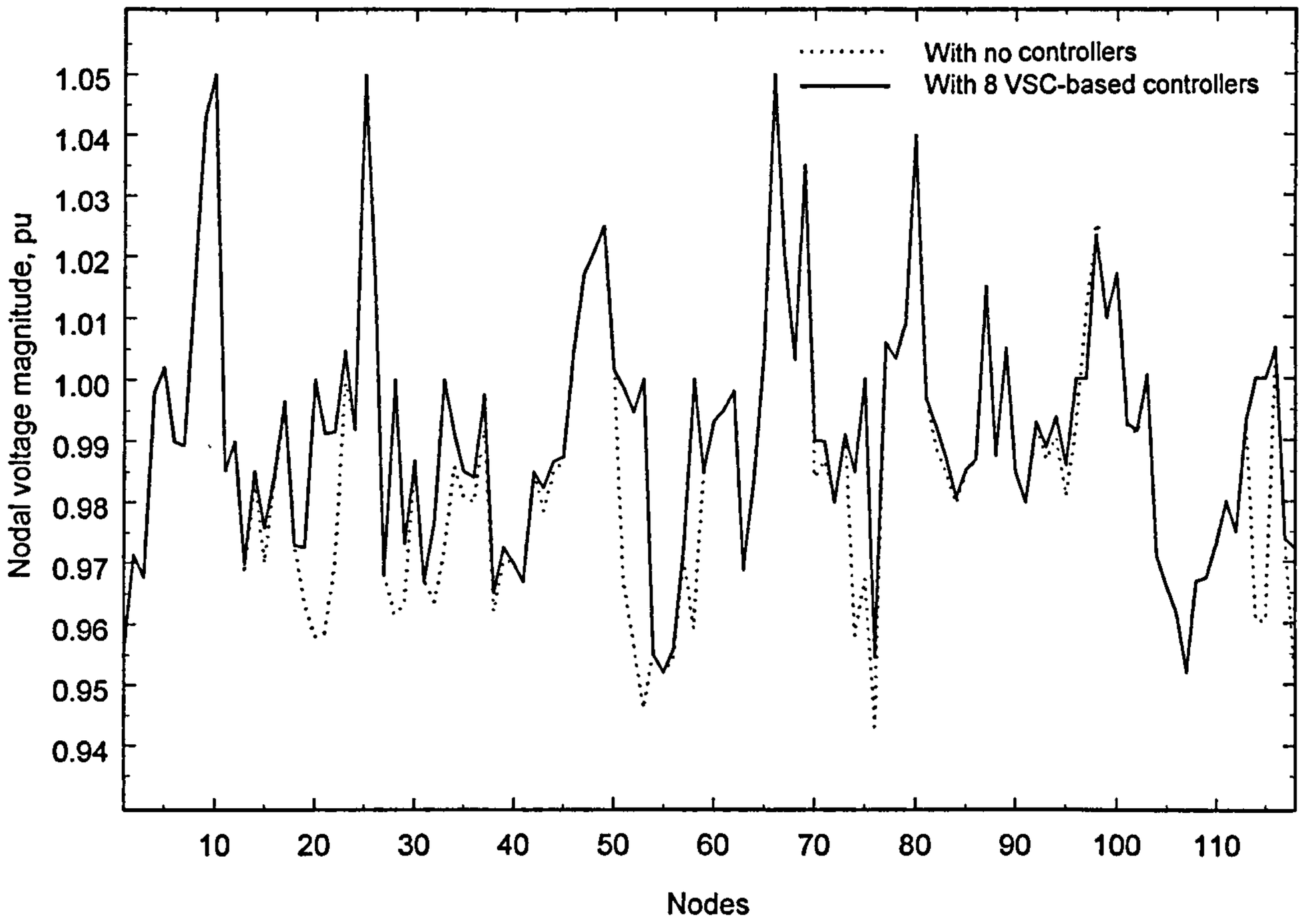

Figure 4.2 Nodal voltage profile in the 118-node IEEE test system

4.8.2 New England test system

The IEEE New England test system is used to assess further the FACTS models in rectangular co-ordinates developed in this chapter. The test network shown in Figure 4.3 consists of 10 generators, 12 transformers and 34 transmission lines connecting 39 buses. In addition to the solution of the network with no controllers, three other cases are assessed:

- One STATCOM is placed at bus 17 in order to increase the nodal voltage magnitude from 0. 9836 p.u. to 1.0 p.u.
- A Static Synchronous Series Controller is installed at bus 17 and an additional node, to reverse the active power flowing from bus 17 to bus 16, and to keep it at 100 MW instead of 94 MW. Also, reactive power flowing from bus 17 to bus 16 is set to be controlled at 20 MVAR.
- A Back-to-Back HVDC-VSC is installed between buses 16 and 17 to invert the active power flowing from bus 17 to bus 16 and to keep it at 100 MW arriving to bus 16, and with a nodal voltage magnitude in bus 16 of 1 p.u.

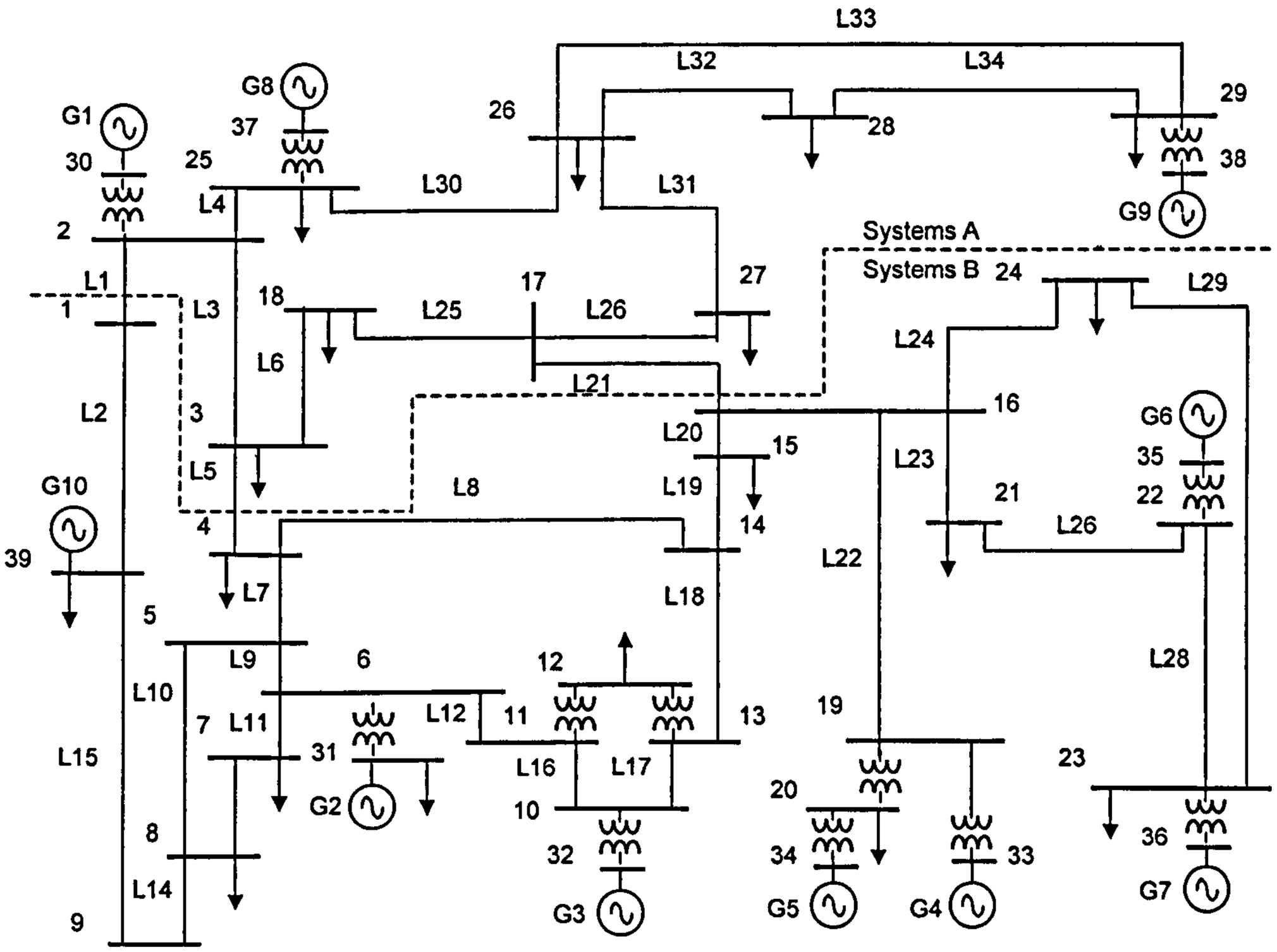

Figure 4.3 New England test network

The proposed FACTS VSC-based models achieve their intended control functions. The power flow results indicate that in order to keep the nodal voltage magnitude at 1 p.u. at the bus where the STATCOM is connected to, it injects 67.81 MVAR of reactive power, with the following STATCOM parameters: voltage source $V_{vR} = 1.05$ p.u. at each phase and $\delta_{vR} = 2.85, 242.85$ and 122.85 degrees for phase *a* *b* and *c*, respectively. Use of the STATCOM results in an improved network voltage profile, especially at buses electrically close to the controller. Figure 4.4 shows the network voltage profile for the three cases and for the system with no controllers. The HVDC-BTB is used to keep a unitary voltage magnitude at bus 16, having an effect on voltage similar to that of the STATCOM, however, at bus 17 where the other unit is connected to, whose function is to regulate active power flow, the voltage drops slightly. In general, an improvement can be seen in the network's voltage profile. The SSSC, which has no direct control over voltage regulation, has a small impact on the network voltage profile, as can be seen from Figure 4.4 the main impact of the SSSC is on power flow regulation.

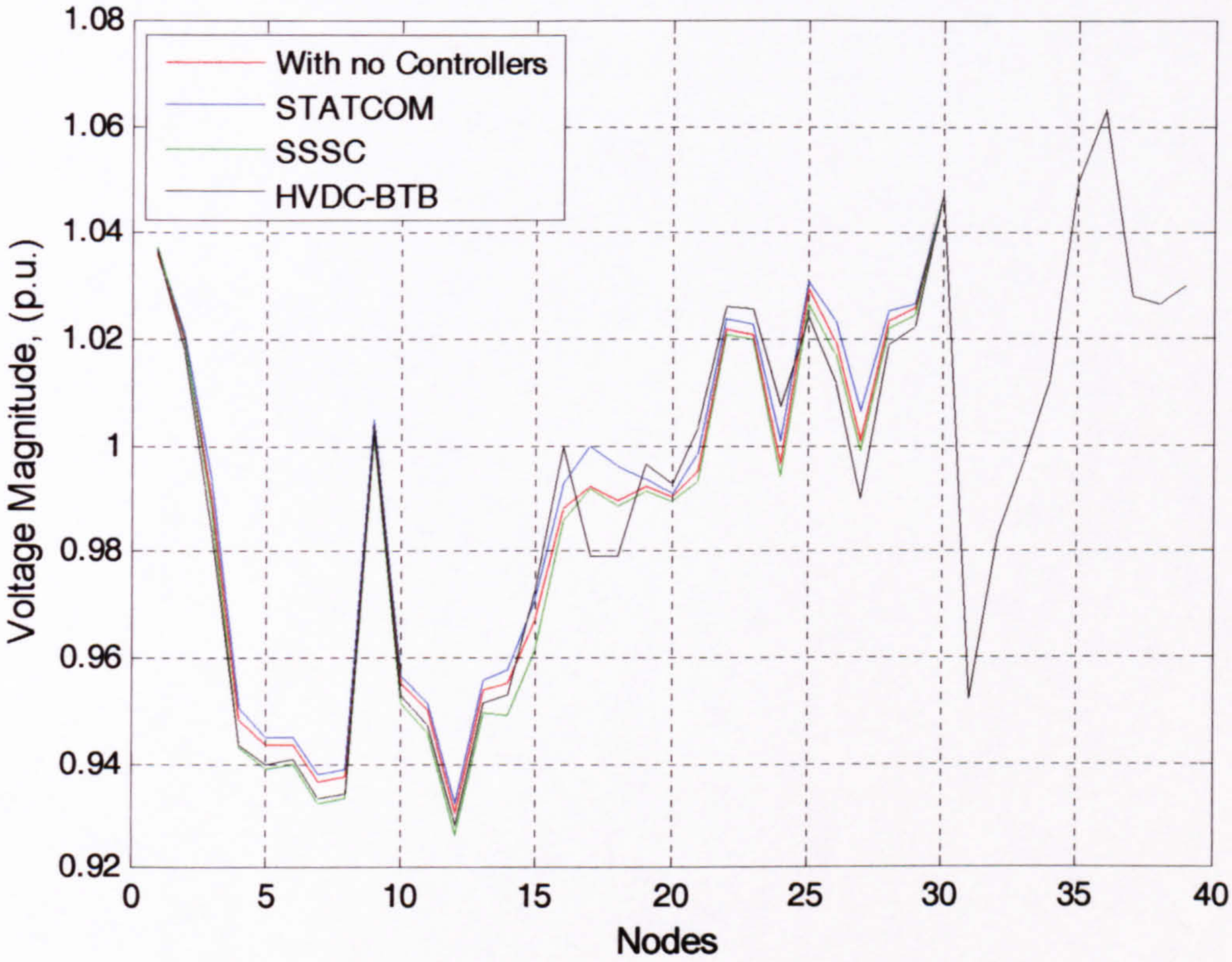

Figure 4.4 Network voltage profile

Active power flows are only marginally affected by STATCOM equipment; and it is no surprise to see that the STATCOM placed at node 17 has little impact on the power flow in transmission lines connected to bus 17. A different situation arises at points where the SSSC and the HVDC are connected, since both controllers are used not only to control a specified active power flow, but to even reverse the flow of active power, now flowing from 17 to 16. From Figure 4.5, it can be seen the drastic changes in power flow caused by both controllers. Due to the power flow reversal, transmission lines electrically close to the controller are also affected and their power flow is also reversed or increased. Transmission line 20 experiences the biggest increase with almost a 100% increment. Figure 4.5(a-b) show the active and reactive power flows at the sending end of all transmission lines.

As can seen from Figure 4.3, the test system being studied can be seen to consist of two grids joined together by three transmission lines, L1, L5 and L21. FACTS controllers were selected to be installed in transmission line L21 connecting bus 16 to 17. The power exchanged between both systems, for the four previous cases is shown in Table 4.3. For completeness, Table 4.4 shows the internal voltages of the controllers.

Table 4.3 Power flow exchange between the two subsystems in p.u.

Network	Flowing from: System A		Flowing to: System B	
	Active	Reactive	Active	Reactive
Without	0.0756	-2.3368	0.0608	1.1467
STATCOM	0.0748	-2.8007	0.0589	1.9342
SSSC	0.1567	-2.5965	0.0518	1.4759
BTB HVDC	0.0678	-2.6233	0.0541	1.7616

Table 4.4 Internal voltage sources parameters

System		Voltage	
		Magnitude (p.u)	Angle (deg)
STATCOM	a	1.067	2.855
	b	1.067	242.85
	c	1.067	122.85
SSSC	a	0.2681	-84.18
	b	0.2681	-204.18
	c	0.2681	35.82
BTB HVDC	a_1	1.1962	17.99
	b_1	1.1962	257.99
	c_1	1.1962	137.99
	a_2	0.88	-9.09
	b_2	0.88	230.01
	c_2	0.88	110.91

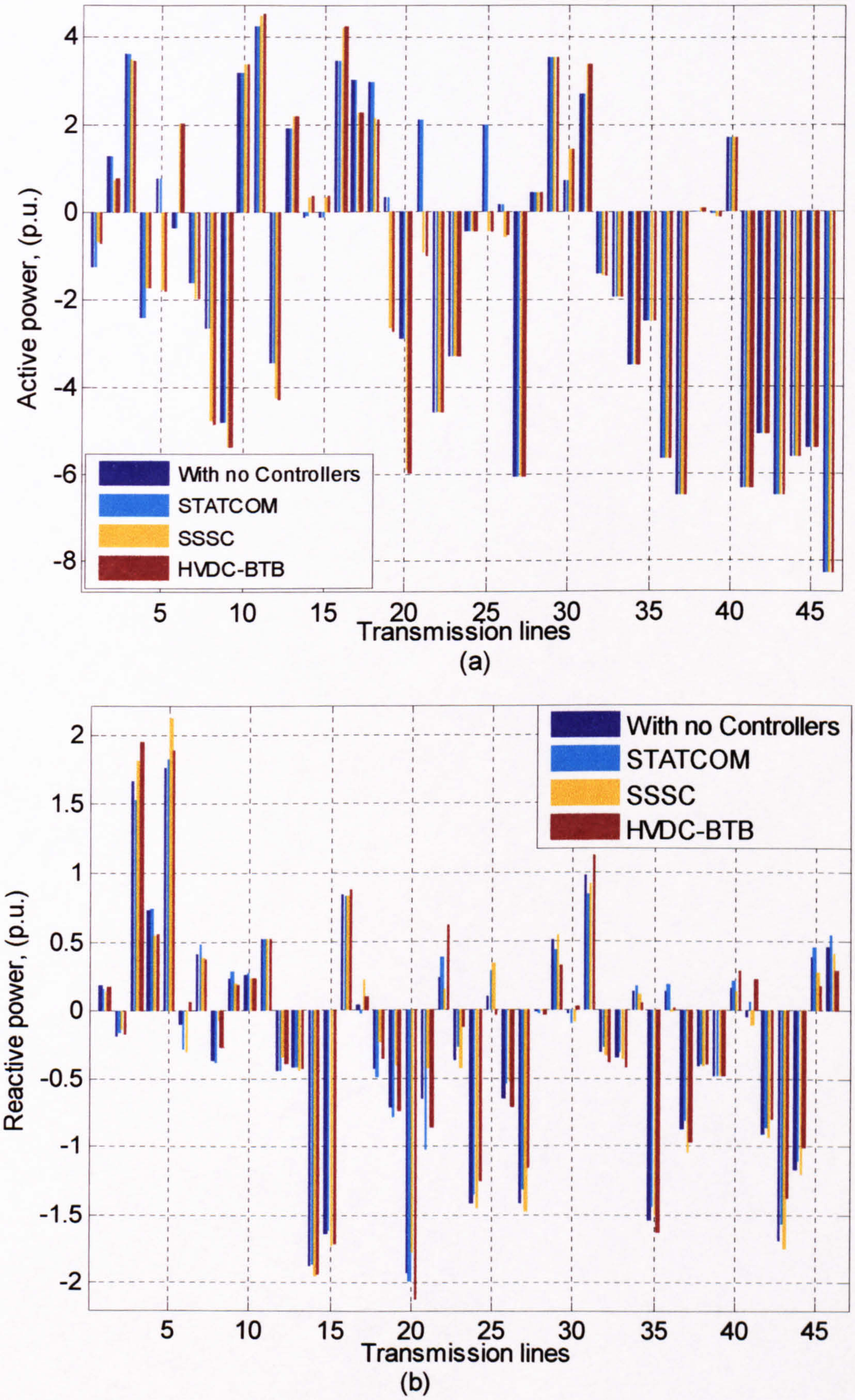

Figure 4.5 Transmission lines power flows, sending end

FACTS controllers may be used to change the power flow distribution in a power system, and depending on specific conditions, changes can either increase or decrease active power losses. For the above three cases only the STATCOM is used to boost the voltage magnitude, resulting in reduced total active power losses. On the other hand, the BTB HVDC-VSC is used to force drastic increases in power flow in addition to voltage magnitude boost at one of the buses. It should be borne in mind that optimal placement of the controllers may reduce losses by improving the system voltage profile, beyond the research reported in this chapter.

4.9 Summary

This chapter presents an alternative modelling approach to the way FACTS controllers are currently modelled in Newton-Raphson algorithms. Instead of using polar co-ordinates to obtain the mathematical model of conventional power networks components and VSC-based controllers, the models are realised using only rectangular co-ordinates. The VSC-based models have been incorporated along with the network components in a three-phase power flow algorithm in rectangular co-ordinates in which the real and imaginary parts of the nodal voltages are used as state variables.

Models of VSC-based FACTS controllers in rectangular co-ordinates have been tested using several power systems of different sizes and degrees of operational complexity. The results obtained showed that the rectangular models have strong convergence capabilities, equal to their polar counterparts, and can be used to simulate with accuracy large-scale power networks.

Rectangular power network modelling avoids using trigonometric expressions in key functions of the algorithm. It should be remarked that extensive testing has been conducted over a period of time, using a large number of test networks and the polar version seems to be slightly more time-consuming than the rectangular version, and the results presented in this chapter form a basis for comparison.

Many power system applications involve the repeated solution of power flows solutions, with modifications to the network and/or nodal constrains in each case. Dynamic power flows, optimal power flows and outage assessments are some examples where repetitive power flows solutions are used. The rectangular co-ordinates formulation has been applied very successfully in dynamic power flows analysis, as presented in the next two chapters.

4.10 References

[1] Stott, B.: "Review of load-flow calculation methods", *Proc. of* IEEE, Vol. 62, No. 7, July 1974, pp. 916-929.

[2] Keyhani, A.; Abur, A. and Hao, S.: "Evaluation of power techniques for personal computers", IEEE *Trans. on Power System*, Vol. 4, No. 2, May 1989. pp. 817-826.

[3] Stagg, G.W. and El-Abiad, A.H.: "*Computer methods in power system analysis*", McGraw-Hill, 1968. ISNB 67-1296307-060658-7

[4] Arrillaga J. and Watson, N.R.: "*Computer Modelling of Electrical Power Systems*", Second Ed. John Wiley & Sons, Chichester, UK. 2001. ISBN 0-471-87249-0

[5] Fuerte-Esquivel, C.R., Venegas, T., Angeles-Camacho, C., Garcia, A.N., Pereira, J.L.R., Carneiro, S., Jr., da Costa, V.M., and Martins, N.: Discussion of "Three-phase power flow calculations using the current injection method" [and reply], IEEE *Trans. on Power Syst.*, Vol. 15, No. 4, Nov. 2000. pp. 1451-1453

[6] An, T., Powell, M.T., Thanawala, H.L. and Jenkins, N.: "Assessment of two different STATCOM configurations for FACTS application in power systems", *International Conference on Power System Technology. Proc.* POWERCON '98, Vol. 1, Aug. 1998. pp. 307 – 312.

[7] Hanson, D.J.: "A transmission SVC for national grid company plc incorporating a ±75 MVAr STATCOM", IEE *colloquium, flexible AC trans. system. - The FACTS* (Ref. No. 1998/500), Nov. 1998. pp. 5/1 - 5/8.

[8] Cavaliere, C.A.C., Watanabe, E.H., and Aredes, M.: "Multi-pulse STATCOM operation under unbalanced voltages", IEEE/PES *Winter Meeting 2002*, Vol. 1, Jan. 2002. pp. 567 – 572.

[9] Schauder, C., Stacey, E., Lund, M., Gyugyi, L., Kovalsky, L., Keri, A., Mehraban, A. and Edris, A.: "AEP UPFC project: installation, commissioning and operation of the ±160 MVA STATCOM (phase I)", IEEE *Trans. on Power Delivery*, Vol. 13, No. 4, Oct. 1998. pp. 1530-1535.

[10] Sen, K.K.: "STATCOM-Static synchronous compensator: theory, modelling, and applications", IEEE/PES *Winter Meeting 1999*, Vol. 2, Jan-Feb 1999. pp. 1177-1183.

[11] Noroozian, M. and Andersson, G.: "Power flow control by use of controllable series components", IEEE *Trans. on Power Delivery*, Vol. 8, No. 3, July 1993. pp. 1420-1429.

[12] Sunil Kumar, L., and Ghosh, A.: "Modelling and control design of a static synchronous series compensator", IEEE *Trans. on Power Delivery*, Vol. 14, No. 4, Oct. 1999. pp.1448-1453.

[13] Sen, K.K.: "SSSC-Static synchronous series compensator: theory, modelling, and applications", IEEE *Trans. on Power Delivery*, Vol. 13, No. 1, Jan. 1998, pp. 241-246.

[14] Zhang, X-P.: "Advanced modelling of the multicontrol functional static synchronous series compensator (SSSC) in Newton power flow", IEEE *Trans. on Power System*, Vol. 18, Issue: 4, Nov. 2003 pp. 1410-1416.

[15] Zhang, I.; Crow, M.L.; Yang, Z.; and Chen, S.: "The steady-state characteristics of an SSSC integrated with energy storage". IEEE/PES *Winter Meeting, 2001*, Vol. 3, Jan.-Feb. 2001. pp. 1311-1316

[16] Gyugyi L., Schauder C.D., Williams S.L. Rietman T.R., Torgerson D.R. and Edris A.: "The unified power flow controller: a new approach to power transmission control", IEEE *Trans. on Power Delivery*, Vol. 10, No 2, April 1995, pp. 1085-1097.

[17] Fuerte-Esquivel, C.R., Acha, E. and Ambriz-Perez, H.: "A cComprehensive UPFC model for the quadratic load flow solution of power networks", IEEE *Trans. on Power System*, Vol. 15, No. 1, Feb. 2000. pp. 102-109.

[18] Fuerte-Esquivel, C.R and Acha, E.: "The unified power flow controller: a critical comparison of Newton-Raphson UPFC algorithms in power flow studies", IEE *Proc – Gen., Trans. and Dist.*, Vol. 144, No. 5, Sep. 1997. pp. 437-444.

[19] Nabavi-Niaki A. and Iravani M.R.: "Steady-state and dynamic models of unified power flow controller (UPFC) for power system studies", Presented at 1996 IEEE/PES *Winter Meeting*, 257-6 PWRS, Jan. 21-25, 1996, Baltimore, MD.

[20] Schauder, C.: "The unified power flow controller-a concept becomes reality" IEE *Colloquium Flexible AC Transmission Systems - The FACTS* (Ref. No. 1998/500), Nov. 1998. pp. 7/1 - 7/6

[21] Angeles-Camacho, C.: "Steady-state modelling of the unified power flow controller for three phase power flow analysis of electric systems", *M.Sc. Thesis* (in Spanish), Department of Electrical and Electronics Engineering, Instituto Tecnológico de Morelia, Aug. 2000.

[22] Hingorani, N.G.: "High Voltage DC Transmission: A power electronics work-horse", IEEE *Spectrum*, Vol. 33, No.4, April 1996, pp. 63-72.

[23] Asplund, G.: "Application of HVDC Light to Power System Enhancement", IEEE/PES *Winter Meeting 2000*, Session: Development and Application of Self-Commutated Converters in Power Systems, Singapore, Jan. 2000.

[24] Asplund, G., Eriksson, K. and Svensson, K.: "DC transmission based on voltage source converters", CIGRE *SC14 Colloquium*, Johannesburg, South Africa, 1997.

[25] Asplund, G., Eriksson, K. and Svensson, K.: "HVDC Light-DC transmission based on voltage source converters", ABB *Power system*, ABB Review 1/1998.

[26] Andersen, B. and Baker, C.: "A New Era of HVDC?", *IEE Review*, March 2000, pp. 33-39.

[27] Larsson, T., Peterson, Å., Edris, A., Kidd, D., Haley, R. and Aboytes, F.: " Eagle Pass back-to-back tie: a dual-purpose application of Voltage Source Converter Technology", IEEE PES *Summer Meeting*, Vol. 3, July 2001.

[28] Angeles-Camacho, C., Tortelli, O. L., Acha, E. Fuerte-Esquivel, C. R., "Inclusion of a high voltage DC-voltage source converter model in a Newton-Raphson power flow algorithm", IEE *Proc.-Gener. Transm. & Distrib.*, Vol. 150, No. 6, Nov. 2003. pp. 691-695.

[29] Fuerte-Esquivel, C. R.: "Modelling and analysis of FACTS devices", *PhD Thesis*, University of Glasgow, Scotland, UK, 1997

[30] Fuerte-Esquivel C.R., Acha, E., Tan S.G. and Rico J.J.: "Efficient object oriented power system software for the analysis of large-scale networks containing FACTS-controlled branches", IEEE *Trans. on Power System*, Vol. 3, No. 2, May 1998. pp. 464-472.

[31] Tinney, W.F. and Walker, W.J.: "Direct solutions of sparse network equations by optimally ordered triangular factorisation", *Proc. of* IEEE, Vol. 55, Nov. 1967. pp. 1801-1809.

Chapter 5

DYNAMIC PHASE-DOMAIN MODELLING OF POWER PLANT COMPONENTS

5.1 Introduction

The location of energy resources in many countries is remote from population centres and industrial development, and large blocks of electrical energy are transmitted over long distances. Moreover, load growth has increased to an all-time high during the past decades. Thus, significant increases in network generation and transmission capacity has been required to accommodate the load growth and maintain systems reliability. Another happening affecting power networks is deregulation of the industry and the creation of energy markets. This has promoted the expansion of large interconnected electricity highways, which are no longer constrained by national and political boundaries. Because of the coupling between power systems, disturbances that occur in one part of the system may affect the operation of the interconnected systems. Increasing demands on generation and transmission systems and interconnectivity have created the need for a better understanding of system stability margins. In order to study the behaviour of today's and future's power systems it is necessary to continue developing dynamic simulation models, methods and software to enable more realistic analysis of large-scale power systems. The three-phase transient stability approach adopted in this research project is a step forward in this direction.

Many power systems are experiencing increased loadings at localised points of the transmission system, which may lead to lightly damped, low frequency (0.2-0.8 Hz) inter-area oscillations. Such oscillations can severely restrict system operation by requiring the curtailment of electric power transfers. These oscillations can also lead to widespread system disturbances if cascading outages of transmission lines occur due to oscillatory power swings. It is also common for many generators throughout the interconnected system to participate to some degree in inter-area oscillations since every generator connected to the system operates in synchronism with every other generator in the interconnected system [1-4].

5.2 Power System Stability

Power System Stability may be defined as the ability that an electric power system has, for a given initial operating condition, to regain a state of operating equilibrium after being subjected to a physical disturbance, with system variables bounded so that system integrity is preserved. Integrity of the system is preserved when practically the entire power system remains intact with no tripping of generators or loads, except for those disconnected by the isolation of the faulted elements or intentionally tripped to

preserve the continuity of operation of the rest of the system. A key issue in the control of large-scale power network operation is to maintain stability.

If following a transient disturbance the power system is stable, it will reach a new equilibrium state with practically the entire system remaining intact, i.e., with all generators and loads connected through a single contiguous transmission system. The actions of automatic controls and possibly human operators will eventually restore the system to normal state. On the other hand, if the system is unstable, it will result in a run-away or run-down situation; for example, a progressive increase in angular separation of generator rotors, or a progressive decrease in bus voltages. An unstable system condition could lead to cascading outages and a shutdown of a major portion of the power system [4-11]. Power systems are continually experiencing fluctuations of small magnitudes. However, for assessing stability when subjected to a specified disturbance, it is usually valid to assume that the system is initially in a true steady-state operating condition.

An IEEE/CIGRÉ joint task force has recently published a classification of power system stability and definitions, classification is based in identifying causes of instability, applying suitable analysis tools and developing corrective measures [1]. Figure 5.1 show the proposed classification of power systems stability, using it and accord with the proposed terminology the present work can be situated in the shadow of the graphic, where the study period of interest may extend from few seconds to tens of minutes and with appropriated assumptions, systems and power plant equations are linearised. Frequency stability and voltage stability are concern with loss of loads or generation.

As far as this author is aware, stability analysis of large-scale power system with embedded FACTS controllers has not received much research attention, certainly, the phase domain dynamic aspects of the topic have not yet been tackled anywhere.

The main objective of this part of the research work is the realization of simple mathematical models of conventional power system components to assess the three-phase dynamic operation of electrical power networks. These models should be easily coupled with the dynamic models of FACTS equipment to be developed in the next chapter to perform a simultaneous solution of the network and dynamics equations using the implicit trapezoidal method and the Newton-Raphson method [12-14].

The first step in the project concerning transient stability is the development of conventional power plant component models in the phase domain. The novelty of the task in hand being the suitability of the transmission network models for large-scale, three-phase dynamic power flows analysis.

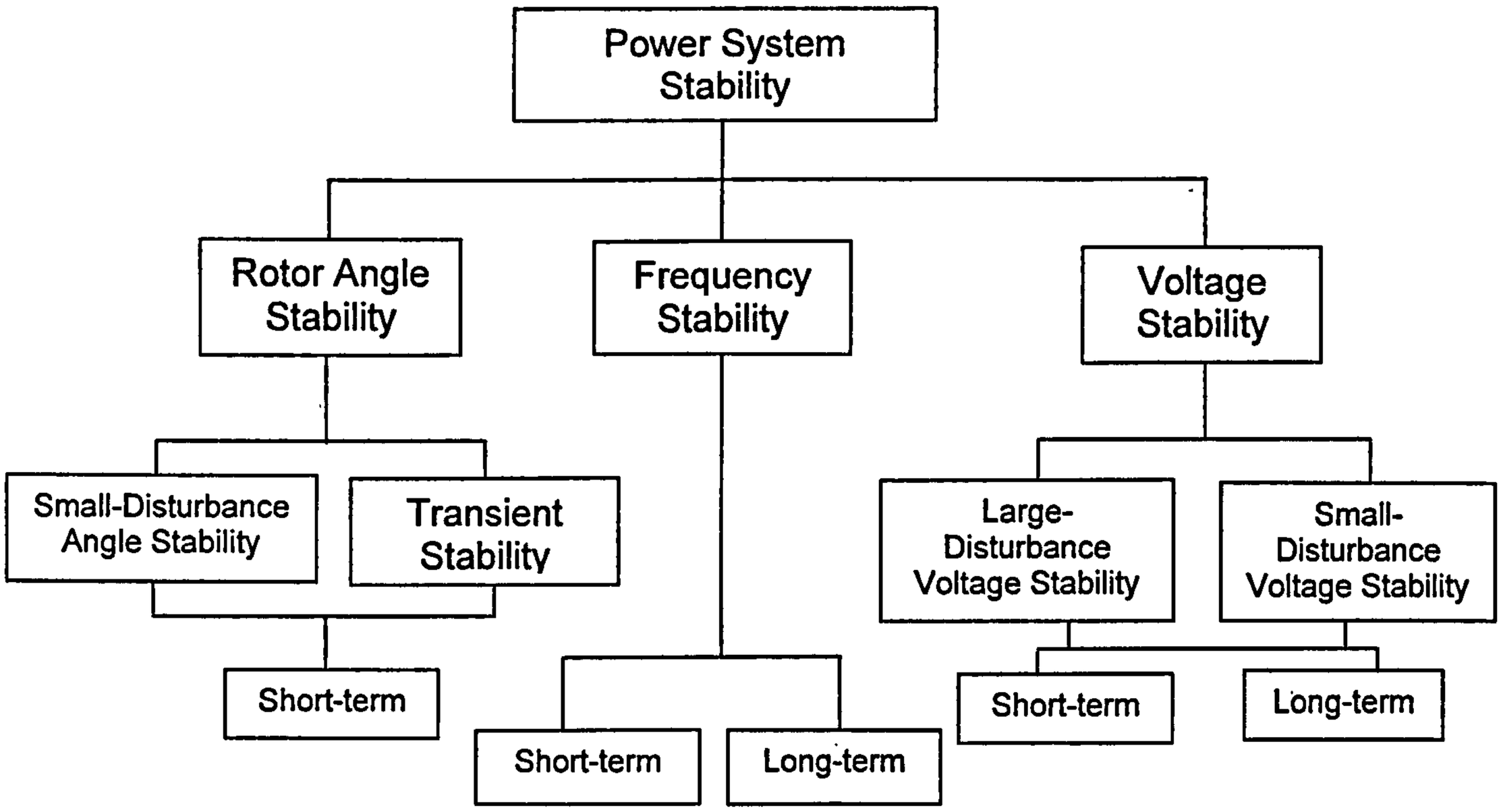

Figure 5.1 Classification of power system stability

5.3 Dynamic Modelling Philosophy

As discussed in previous chapters, power networks can be modelled as a set of non-linear equations corresponding to active and reactive nodal power injections, these are linearised around a base operating point determined by generation and load powers, and nodal voltages. On the other hand, models of active power plant components, such as generators, are described by a set of first order differential equations. By suitable combination of both sets of equations the complete power system model, aimed at time response calculations of large-scale power networks, can be reduced to an algebraic-differential initial value problem of the form,

$$\frac{dy}{dt} = F(y,x) \tag{5.1}$$

$$0 = G(x,y) \tag{5.2}$$

where y and x are vectors of integrable and non-integrable algebraic variables. In general, F and G are non-linear vector functions and thus the non-integrable network variables cannot be eliminated algebraically. The initial conditions for a stability study are determined by a steady-state power flow solution. Thereafter equations (5.1) and (5.2) must be solved simultaneously as a function of time [12-13].

Consequently the objective of the dynamic power analysis is to solve y and x as a function of time. Set (5.1) comprises the differential equations of all synchronous generators, since each generator is coupled to the other power plants only through the network, set (5.1) is a collection of separate subsets. Set (5.2) comprises network equations and the stator equations of each machine, transformed into the network reference frame. This set of equations is interdependent and therefore the solution technique must provide a simultaneous solution. The open literature offers a wide range of numerical methods to solve them. B. Stott [12] reviews the basic requirements of numerical methods used to compute the system dynamic response, and concludes that they should be as fast as possible within the boundaries of accuracy, reliability, economy of computer storage, flexibility, and ease of maintenance. Furthermore, Stott reviews the advantages and disadvantages of the most popular integration methods. In his work the integrations methods are classified into two main techniques, partitioned and simultaneous. A partitioned solution is one where the differential and algebraic portions of the equations are not solved at the same time. Whereas, the simultaneous approach is where the differential equations are transformed into algebraic equations and combined with the network algebraic equations for all variables to be solved simultaneously. The partitioned solution is the traditional method, used in nearly all-present day industrial programs.

5.4 Power Plant Components Dynamic Modelling

Power-generating plants or generating stations comprise the various devices involved in energy transformation from mechanical to electrical; generators, voltages regulators, governors, turbines and auxiliary equipment. The main components of the generation system are shown in Figure 5.2. In terms of water turbine the unit governor receives information on the system frequency and power, which together with pre-defined set values, is used to control the turbine guide vanes to regulate the water flows through the penstock in order to match the system power requirements and regulate the grid frequency. The governor also receives a power reference signal, which is used to provide a feed-forward estimate of the gate opening needed for a given change in generated power. This signal gives a rapid initial response after which the final gate position is determined by governor action [15].

Dynamic models of the power-generation plant components are normally described by ordinary differential equations. This section illustrates the procedures used to create typical models, suitable for dynamic power flows and steady-state stability in time frame of reference. IEEE task forces have periodically issued recommendations for the modelling of the various power plant components [16].

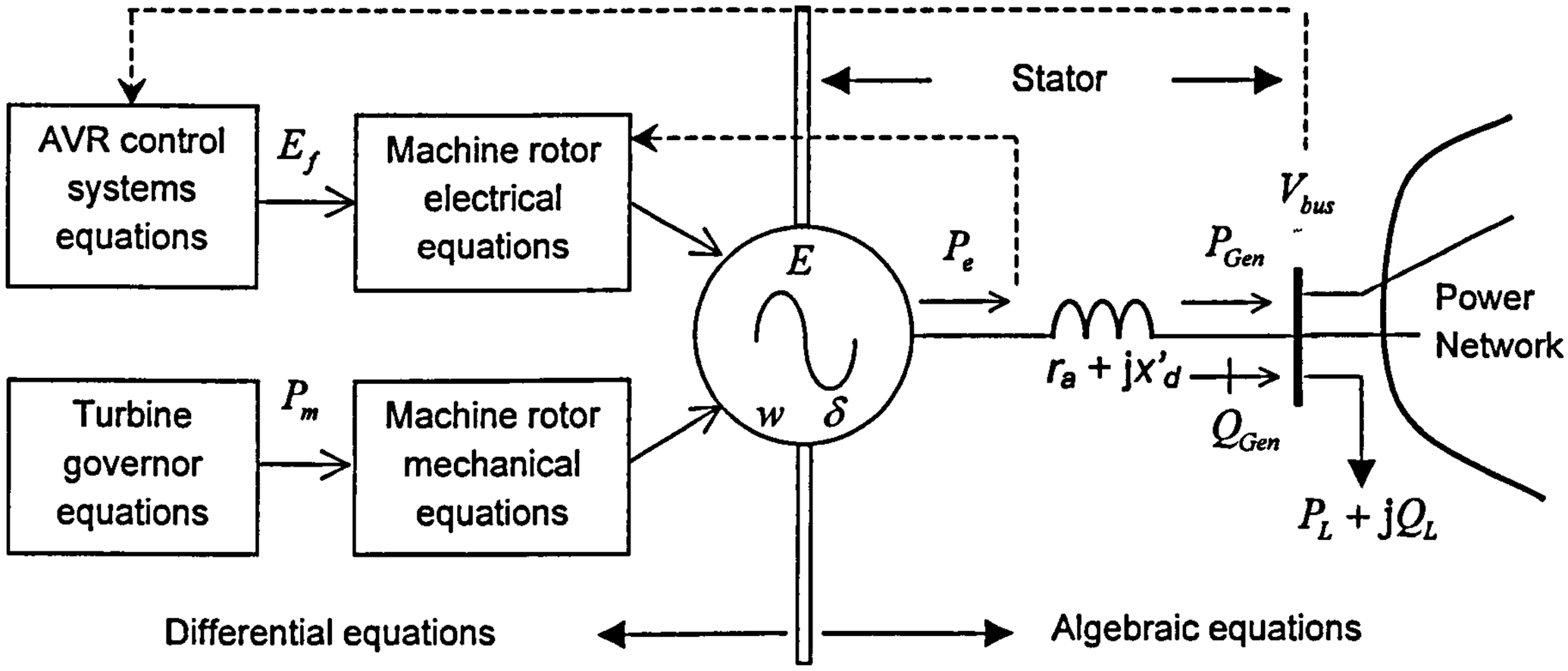

Figure 5.2 Power plant block diagram [12]

5.4.1 Synchronous generator model

Generators are devices that convert mechanical energy to electrical energy. Every generator or synchronous machine connected to the system operates in synchronism with every other generator in the system. The characteristics of generators have a considerable influence on the stability limits of a system. Synchronous generators undergo electrical and mechanical phenomena when seen from a dynamic perspective, resulting in components which are not straightforward to model. Its dynamic behaviour can be described by a set of non-linear differential equations [16-17].

In general, when a power system is in steady-state, the electrical power output of each generator is equal to the power applied to the rotor. However, and because the operation of the power system is quite susceptible to disturbances (load changes, short circuits and equipment outages), such power balance could be lost resulting in a power mismatches between the input and output power of generators, and therefore the rotors depart form steady-state operation. To study this phenomena and the impact on the whole system, dynamic models of generators are required. Complexity of the model depends on a number of factors such as the kind of disturbance being studied, location of the disturbance and time duration of the even [16-21].

Electromechanical equations: the starting point for developing comprehensive electromechanical models of the power system is the schematic representation of the basic power balance of the generator, shown in Figure 5.3. The equation of motion of the turbine is derived using Figure 5.2 along with Newton law's for rational motions.

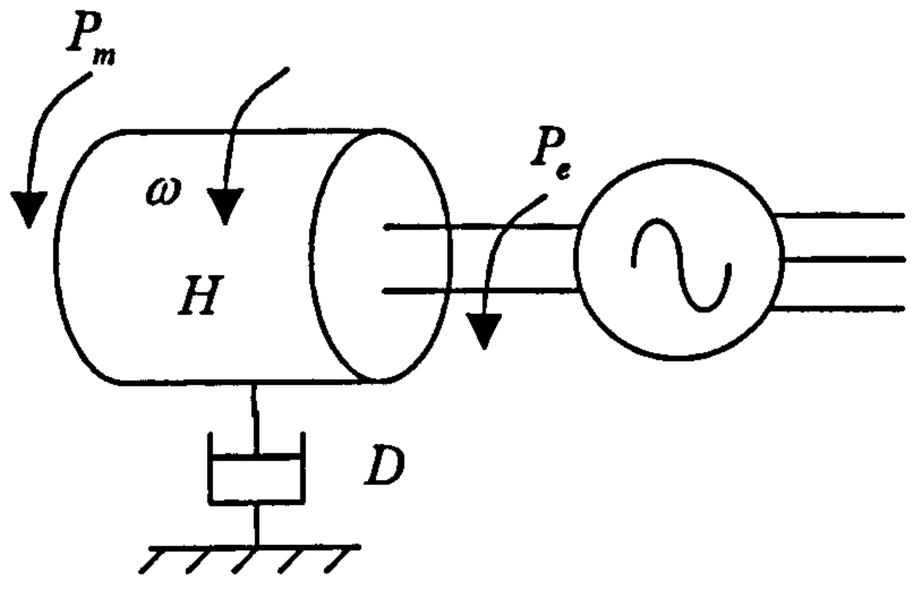

Figure 5.3 Diagram of the power balance of a generator

The power balance equation for each generator node is given by the following expression

$$M\frac{d^2\delta}{dt^2}+D\frac{d\delta}{dt}=P_m-P_e \tag{5.3}$$

where δ denotes the rotor position relative to a certain rotating frame. The term $d\delta/dt$ represents the angular velocity and $d^2\delta/dt^2$ is the angular acceleration of the rotor. In this expression P_m is the mechanical input power which counters the electrical power P_e. This second order differential equation known as the *swing equation*, can be decomposed into two first order differential equations by a change of variable (i.e. setting $\frac{d\delta}{dt}=(\omega-\omega_0)$)

$$\frac{d\omega}{dt}=\frac{\pi f_0}{H}\left[P_m-P_e-D(\omega-\omega_0)\right] \tag{5.4}$$

$$\frac{d\delta}{dt}=\omega-\omega_0 \tag{5.5}$$

where

M is the inertia moment, $2H/\omega_0$
H is the inertia constant, kW/KVA
P_m is the mechanical power of the generator, p.u.
P_e is the electrical power of the generator, p.u.
D is the damping coefficient, s/rad
ω_0 is the synchronous speed, $2\pi f_0$, rad/s
f_0 is the synchronous frequency, Hz
δ is the load angle, rad

Electromagnetic equations: virtually all synchronous machine models used for routine large-scale studies are based on Park's transformation [22-23] of the machine three-phase quantities relating the flux linkages into components along direct (*d*) and quadrature (*q*) axes. A generator model with three stator windings and in the rotor one field winding and two hypothetical short-circuited winding (Figure 5.4(b)). This level of representation normally is adequate to represent most transient effects.

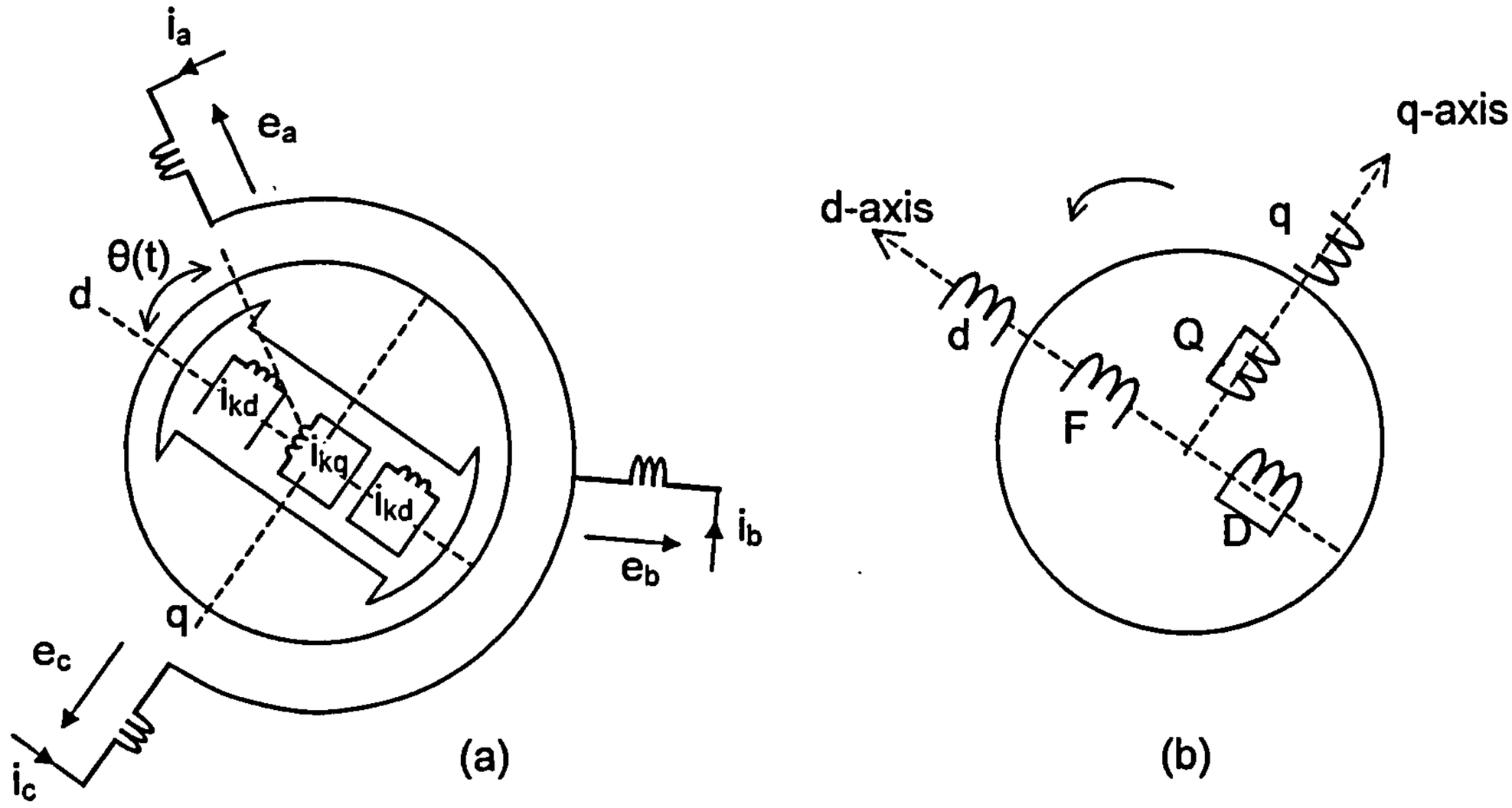

Figure 5.4 Synchronous machine: (a) Schematic representation and (b) equivalent five winding model

With reference to Figure 5.4, assuming a balanced design of the machine and operation at near synchronous speed, the algebraic equations that describe generator voltage relations can be written by a set of equations based on direct and quadrature parameters,

$$V_t = E_a - r_a I_a - \mathrm{j}x_d I_d - \mathrm{j}x_q I_q \tag{5.6}$$

$$I_a = I_d + \mathrm{j}I_q \tag{5.7}$$

where

V_t is the terminal voltage of phase a

E_a is the excitation voltage or voltage behind the generator's impedance at phase a

r_a is the armature resistance for phase a

x_d is the direct reactance

x_q is the quadrature axis reactance

I_d is the direct axis current

I_q is the quadrature axis current

I_a is the phase a current

It should be noticed that the following simplifying assumptions are made in this model:

a. saturation is neglected
b. permeance harmonics do not exist
c. frequency conversion effects are disregarded

Differential Equations (5.4)-(5.5), representing mechanical motión, together with Equation (5.6) for voltage behind the generator's impedance are the minimum required to study synchronous generator dynamics [18-19].

5.4.2 Automatic voltage regulator model

In the control of synchronous generators, automatic voltage regulators (AVRs) have been used over many years. AVRs have evolved from the early electromechanical types to the solid state AVRs controlled with analogue circuits found most commonly in service today. With recent advances in microprocessors technology making faster and more powerful processors readily available it is now possible to implement more complex forms of adaptive and fixed parameters based controllers [24]. A variable-voltage exciter whose output is controlled by the voltage regulator supplies field current to a synchronous generator. Modern excitation systems are very fast and reliable. The exciter and its voltage regulator are collectively referred as the excitation system. Several general-purpose models for excitation systems have been published [25-27]. AVRs have a local voltage control system in a feedback loop that aims to keep the voltage at the machine terminals at a set level. The exciter produces the field voltage, E_{fd} based on the reference voltage, V_{ref} and the machine terminal voltage, V_t. When a disturbance occurs in the system, and as a result, V_t drops, the AVR boots up the field voltage; this action increases the terminal voltage.

The present work uses a simplified AVR model, similar to the one used by other researchers [28-30]. The excitation system is the IEEE type 1 [28], but with no saturation representation. Figure 5.5 shows the block diagram of the AVR.

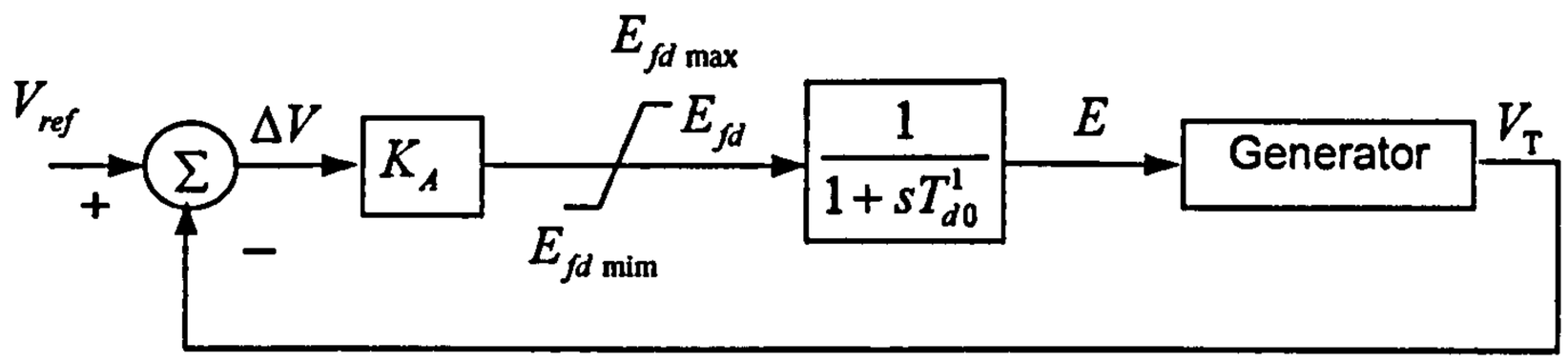

Figure 5.5 Automatic Voltage Regulator block diagram

The differential equation for the AVR is linear, and its state variables and control input quantities can be arranged as follows:

$$\Delta V = V_{ref} - V_T \tag{5.8}$$

$$E_{fd} = K_A \Delta V \qquad E_{fd\,\min} \le E_{fd} \le E_{fd\,\max} \tag{5.9}$$

$$\frac{dE}{dt} = \frac{K_A\left(V_{ref} - V_T\right) - E}{T_{do}} \tag{5.10}$$

where

E is the open-circuit terminal voltage magnitude or excitation voltage
E_{fd} is the applied voltage
T_{d0} is the open-circuit field transient time constant
V_{ref} is the pre-specified reference voltage (magnitude)
K_A is the excitation gain

The voltage reference, V_{ref}, may be calculated as

$$V_{ref} = \frac{E^0}{K_A} + V_T^0$$

where E^0 and V^0 are the initial excitation and terminal voltages of the generator.

5.4.3 Governor model

The turbine speed governor is one of the most important piece equipment in a power station. The governor system should be capable of controlling the speed of the turbine at all power outputs and operation modes. Its performance plays an important role in power systems operation [29]. The governor system receives information on the system's frequency and power demand, and acts to correct any frequency deviation from the base operating frequency by mean of valves adjustments. This is done by varying the amount of steam flow in the case of a steam turbine, water in the case of a hydro unit, and fuel in the case of a combustion turbine or diesel engine. Depending on the governor control parameters, the turbine may either add or subtract damping from the natural damping [32-34].

Two governor models are used in the present work. Both models are simplified representations of those given in the IEEE report in reference 35 and 36. The block diagram in Figure 5.6 gives the model for the speed governor system used in steam turbines.

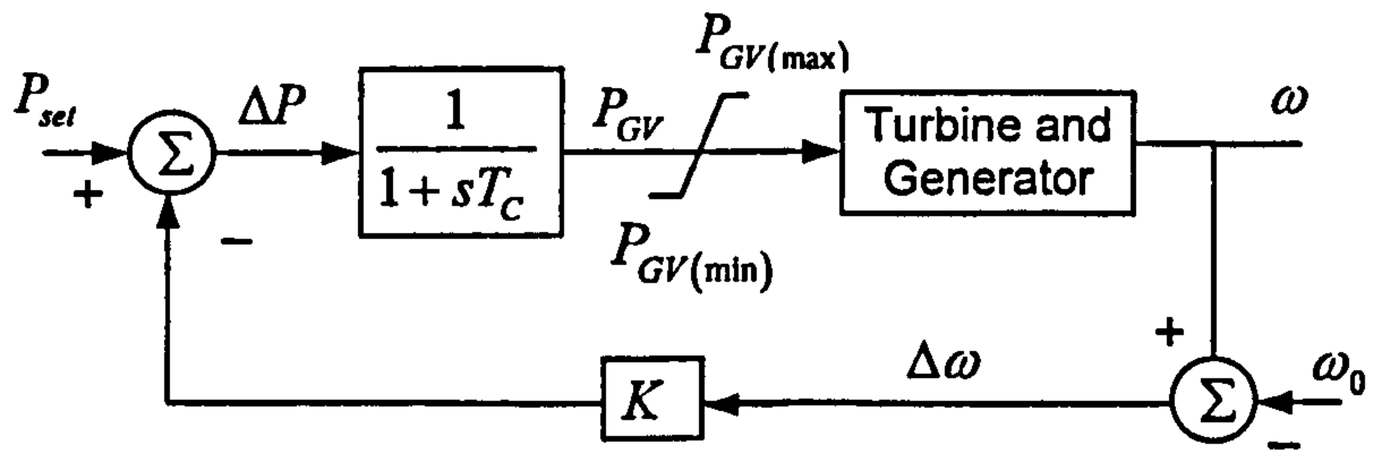

Figure 5.6 Steam turbine block diagram

The mathematical equations for the adopted steam turbine model are.

$$\Delta\omega = \omega - \omega_0 \tag{5.11}$$

$$\Delta P = P_{\text{set}} - K\Delta\omega \tag{5.12}$$

$$\frac{dP_{\text{GV}}}{dt} = \frac{\Delta P - P_{GV}}{T_c} \tag{5.13}$$

where

K is the governor gain
T_c is the governor time constant
P_{set} is the power set point

A typical hydraulic speed governor system produces a position that is assumed to be linear. It gives an instantaneous indication of speed, and is represented by a gain *K* which is the reciprocal of droop. The present work uses the model recommended in references [28,35] for hydro speed governors undergoing slow transients, and it is shown in Figure 5.7.

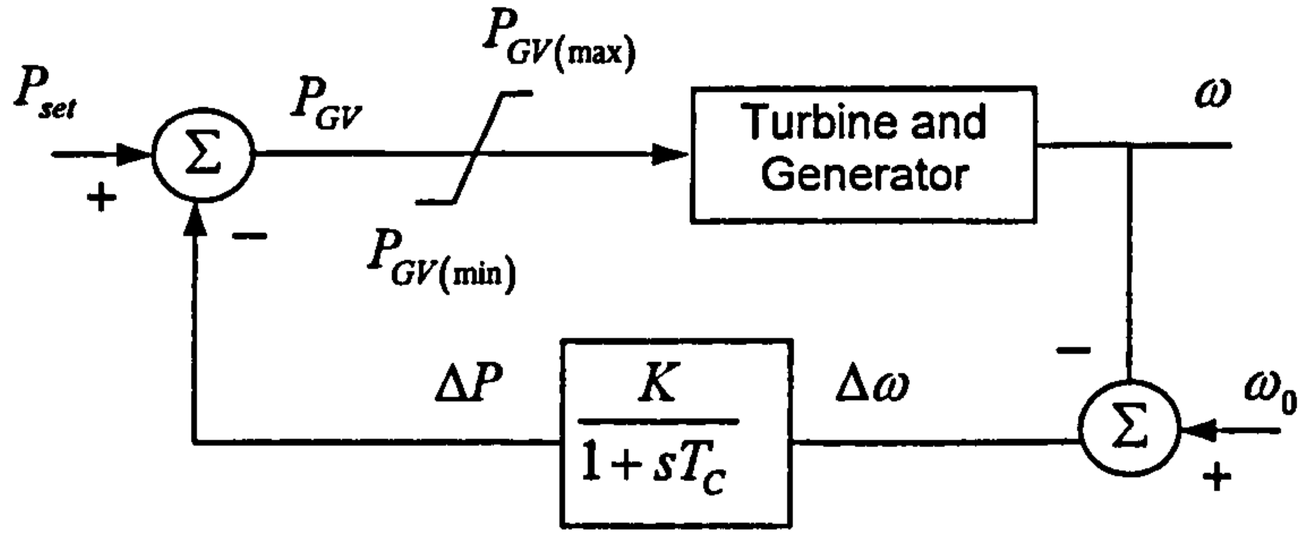

Figure 5.7 Hydro governor block diagram

Based on Figure 5.7, the mathematical equations for the adopted hydro speed governor model are

$$\Delta\omega = \omega_0 - \omega \tag{5.14}$$

$$\frac{d\Delta P}{dt} = \frac{K\Delta\omega - \Delta P}{T_c} \tag{5.15}$$

$$P_{\text{GV}} = P_{set} - \Delta P \tag{5.16}$$

where:

K is the governor gain
T_c is the governor time constant
P_{set} is the power set point

5.4.4 Turbine model

The element of a generating unit, spun by the force of water or steam to drive the electric generator, is the turbine. A turbine usually consists of a series of curved vanes or blades on a central spindle. For dynamic power flow studies or dynamic stability studies, the turbine model need to be represented in some detailed.

Steam turbines, the model adopted in the present work is the so-called tandem compound, double reheat type as defined by the IEEE [35-36]. The tandem compound type has only one shaft driving the generator, on which three turbines, high pressure (HP), intermediate pressure (IP) and low pressure (LP) turbines are mounted. The simple model adopted in the present work is based on the block diagram shown in Figure 5.8.

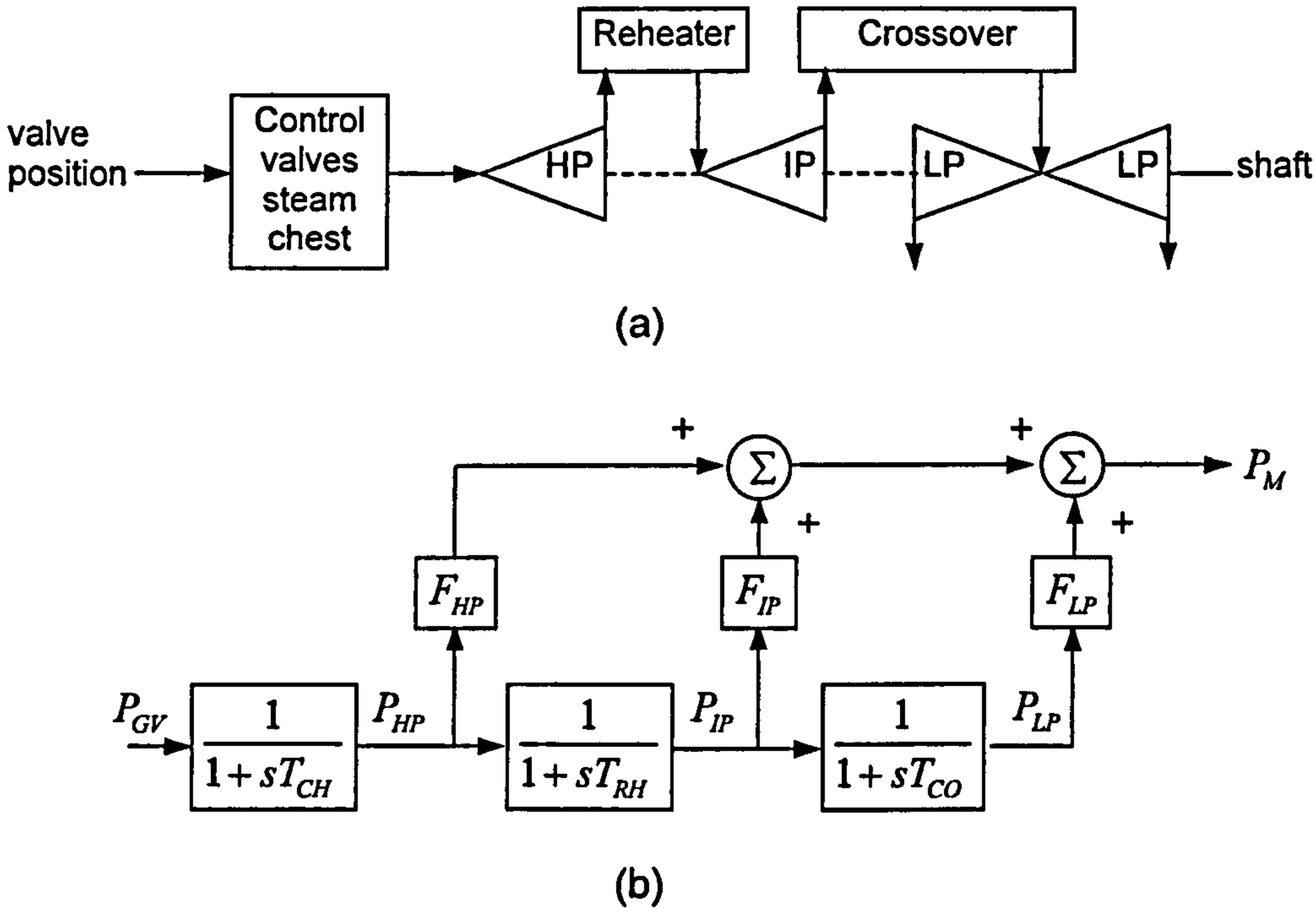

Figure 5.8 Steam turbine; (a) System configuration, (b) approximate linear model

The mathematical equations that represent the steam turbine are given as follows:

$$\frac{dP_{HP}}{dt} = \frac{P_{GV} - P_{HP}}{T_{CH}} \tag{5.17}$$

$$\frac{dP_{IP}}{dt} = \frac{P_{HP} - P_{IP}}{T_{RH}} \tag{5.18}$$

$$\frac{dP_{LP}}{dt} = \frac{P_{IP} - P_{LP}}{T_{CO}} \tag{5.19}$$

$$P_m = P_{HP}F_{HP} + P_{IP}F_{IP} + P_{LP}F_{LP} \tag{5.20}$$

where

P_{GV} is the output power from control valve
T_{CH} is the steam chest time constant (including the high pressure (HP) stage of the turbine time constant)
T_{RH} is the re-heater time constant (including the intermediate-pressure (IP) stage of the turbine time constant)
T_{CO} is the steam storage of the cross-over time constant (including the low-pressure (LP) stage of the turbine time constant)
F_{HP} is the HP turbine power fraction
F_{IP} is the IP turbine power fraction
F_{LP} is the LP turbine power fraction
P_m is the equivalent generator input mechanical power

Hydraulic turbines, transient characteristics of hydro turbines are determined by the dynamics of the water flow in the penstock. Appropriates hydraulic turbine models have been proposed by the IEEE task forces [35-36] for dynamic studies. The simple model adopted in the present work is based on the block diagram shown in Figure 5.9 and its corresponding mathematical equation is:

$$\frac{dP_m}{dt} = \frac{P_{GV} - T_W P_{GV} - P_m}{T_W/2} \tag{5.21}$$

where

T_W is the water time constant
P_{GV} is the equivalent input power to turbine
P_m is the equivalent input power to generator

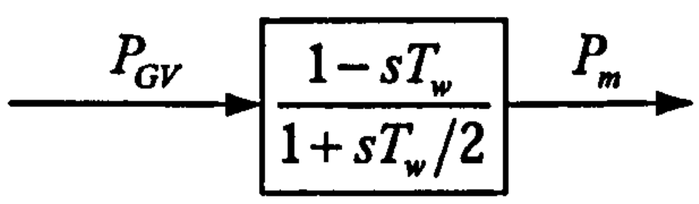

Figure 5.9 Simple linear model for hydro turbines

5.5 Power System Components Dynamic Models

For dynamic power flow assessment, conventional models of the power system components are modelled with algebraic equations that are essentially the same as those used in steady-state operation, i.e. the fast dynamics associated with the synchronous machine stator, transmission lines, and loads are neglected. Algebraic

equations of the network derived from the power plant component models developed in previous chapters are coupled to the ordinary differentials equations. Three-phase transmission lines are modelled by standard nominal π-models. Mutual couplings between phases are considered. Loads are typically modelled as passive components, which are functions of voltage and frequency. In this work, a constant load power representation is used. Conventional shunt compensation is modelled as constant shunt admittances.

5.6 Dynamic Power Flow Algorithm

A general three-phase dynamic power flow algorithm using the implicit trapezoidal rule and the Newton-Raphson iterative method has been developed. The numerical method is shown in Appendix IV [12, 14, 28]. The algorithm takes advantage of the three-phase power flow algorithm in rectangular coordinates presented in the previous chapter. Figure 5.10 shows the overall structure of the dynamic power flow algorithm.

5.7 Differential Equations Discretization

The ordinary differential equations developed in previous sections for the power plant components need to be transformed into algebraic equations, something that can be achieved by applying the trapezoidal method given in Appendix IV. The ensuing algebraic equations are solved, simultaneously, with the algebraic equations representing the network.

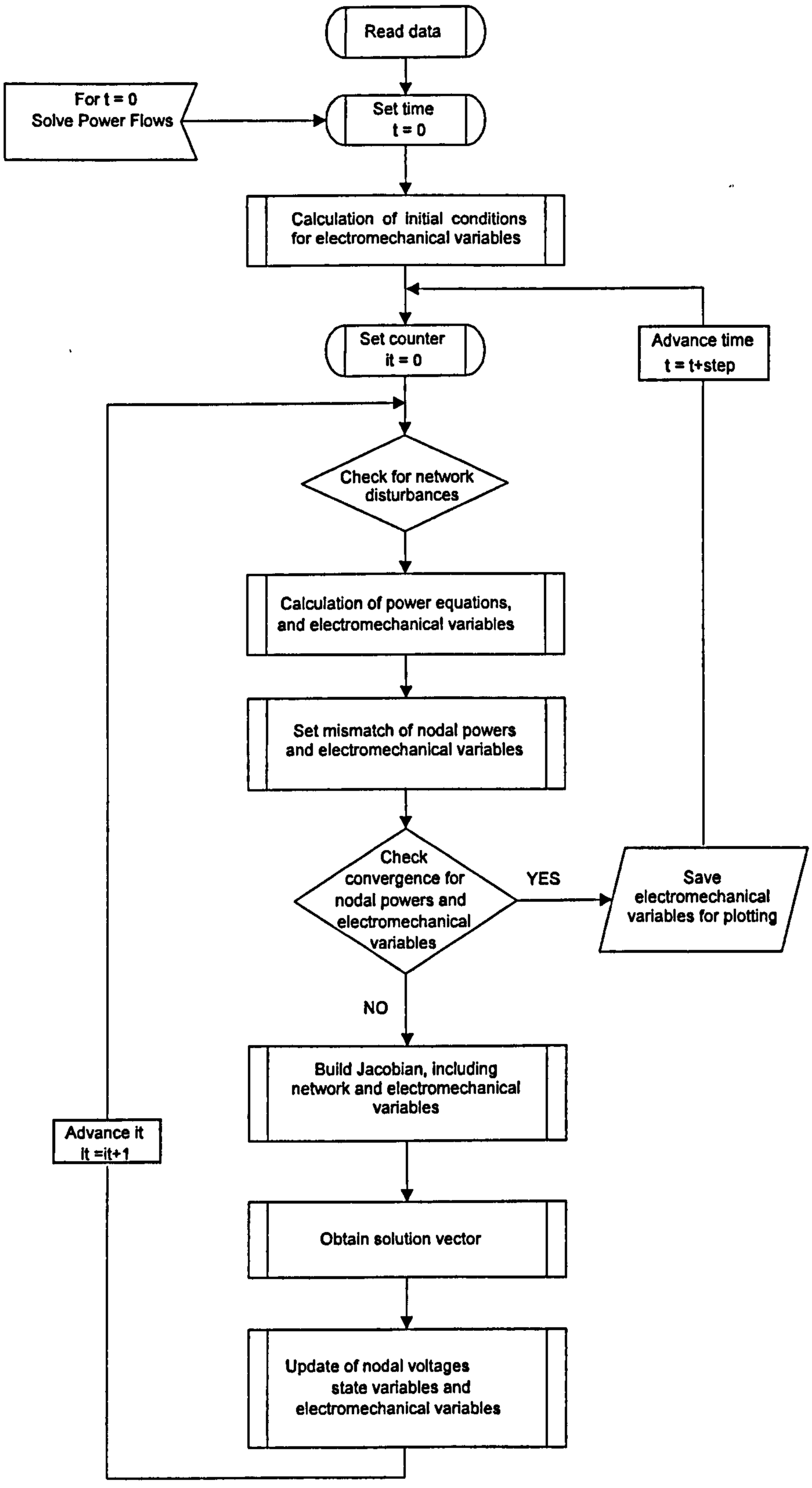

Figure 5.10 Dynamic power flow algorithm

5.7.1 Synchronous generator

Section 5.4.1 provides the dynamic model of the generator. The swing equation, represented by Equations (5.4) and (5.5), is the differential equations to be algebraisized, and used in the simultaneous-solution method. The electrical power supplied by the generator to the network can be obtained using the generator equivalent circuit in the frame of reference, as shown in Figure 5.11.

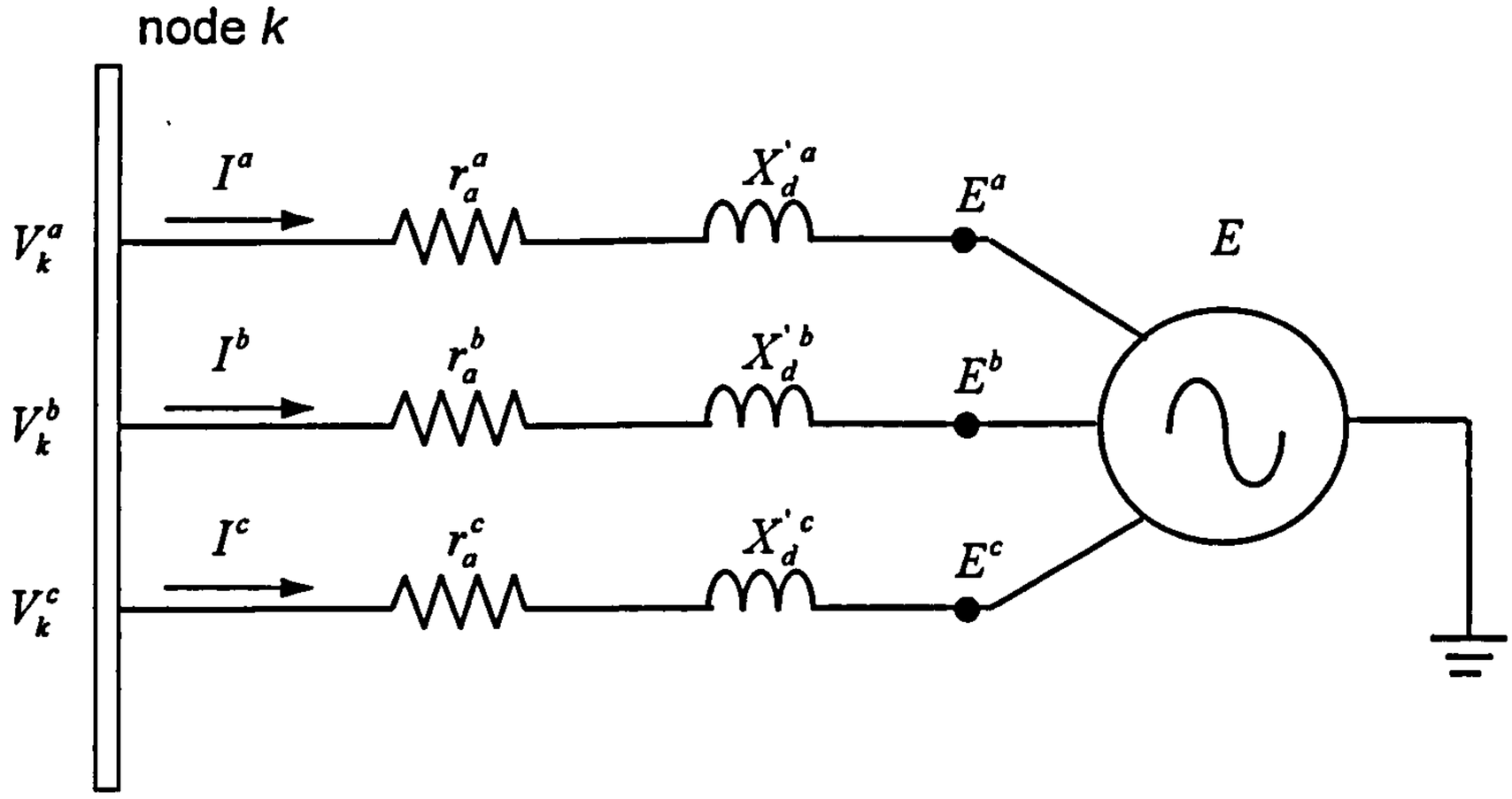

Figure 5.11 Generator equivalent circuit

Some modelling assumptions are made; first we assume that the phase angle (δ) of the voltage behind the transient reactance coincides with the mechanical angle relative to the synchronous rotating reference. Moreover, saliency is neglected, i.e. $\left(x_d^{'} = x_q^{'}\right)$. The three complex voltages behind the transient reactances are assumed to be displaced from each other by 120°,

$$E = |E| \begin{bmatrix} \cos\delta + \mathrm{j}\sin\delta \\ \cos\left(\delta - \frac{2\pi}{3}\right) + \mathrm{j}\sin\left(\delta - \frac{2\pi}{3}\right) \\ \cos\left(\delta + \frac{2\pi}{3}\right) + \mathrm{j}\sin\left(\delta + \frac{2\pi}{3}\right) \end{bmatrix} = |E| \begin{bmatrix} \cos\delta^a + \mathrm{j}\sin\delta^a \\ \cos\delta^b + \mathrm{j}\sin\delta^b \\ \cos\delta^c + \mathrm{j}\sin\delta^c \end{bmatrix} \tag{5.22}$$

In rectangular co-ordinates nodal voltage at bus *k* becomes:

$$V_k = \begin{bmatrix} e_k^a + \mathrm{j}f_k^a \\ e_k^b + \mathrm{j}f_k^b \\ e_k^c + \mathrm{j}f_k^c \end{bmatrix} \tag{5.23}$$

With these assumptions, and using Figure 5.11 along with Equations (5.22) and (5.23), the expressions for the three-phase complex electrical power may be written as

$$S_k^\rho = V_k^\rho I_a^{\rho^*} = V_k^\rho Y^{\rho^*} \left(V_k^\rho - E\right)^* \tag{5.24}$$

$$S_e^\rho = E^\rho I_k^{\rho^*} = E^\rho Y^{\rho^*} \left(E^\rho - V_k^\rho\right)^* \tag{5.25}$$

After performing some complex algebraic operations and collecting real and imaginary parts, the three-phase active and reactive powers at bus k supplied by the generator become:

$$\begin{aligned} P_k = {} & \frac{|E|}{r_a^{a2} + X_d^{'a2}}\left[-r_a^a\left(e_k^a \cos\delta^a + f_k^a \sin\delta^a\right) + X_d^{'a}\left(f_k^a \cos\delta^a - e_k^a \sin\delta^a\right)\right] + \frac{\left(V_k^a\right)^2 r_a^a}{r_a^{a2} + X_d^{'a2}} \\ & + \frac{|E|}{r_a^{b2} + X_d^{'b2}}\left[-r_a^b\left(e_k^b \cos\delta^b + f_k^b \sin\delta^b\right) + X_d^{'b}\left(f_k^b \cos\delta^b - e_k^b \sin\delta^b\right)\right] + \frac{\left(V_k^b\right)^2 r_a^b}{r_a^{b2} + X_d^{'b2}} \\ & + \frac{|E|}{r_a^{c2} + X_d^{'c2}}\left[-r_a^c\left(e_k^c \cos\delta^c + f_k^c \sin\delta^c\right) + X_d^{'c}\left(f_k^c \cos\delta^c - e_k^c \sin\delta^c\right)\right] + \frac{\left(V_k^c\right)^2 r_a^c}{r_a^{c2} + X_d^{'c2}} \end{aligned} \tag{5.26}$$

$$\begin{aligned} Q_k = {} & \frac{|E|}{r_a^{a2} + X_d^{'a2}}\left[r_a^a\left(e_k^a \sin\delta^a - f_k^a \cos\delta\right) - X_d^{'a}\left(e_k^a \cos\delta^a + f_k^a \sin\delta^a\right)\right] + \frac{\left(V_k^a\right)^2 r_a^a}{r_a^{a2} + X_d^{'a2}} \\ & + \frac{|E|}{r_a^{b2} + X_d^{'b2}}\left[r_a^b\left(e_k^b \sin\delta^b - f_k^b \cos\delta^b\right) - X_d^{'b}\left(e_k^b \cos\delta^b + f_k^b \sin\delta^b\right)\right] + \frac{\left(V_k^b\right)^2 r_a^b}{r_a^{b2} + X_d^{'b2}} \\ & + \frac{|E|}{r_a^{c2} + X_d^{'c2}}\left[r_a^c\left(e_k^c \sin\delta^c - f_k^c \cos\delta^c\right) - X_d^{'c}\left(e_k^c \cos\delta^c - f_k^c \sin\delta^c\right)\right] + \frac{\left(V_k^c\right)^2 r_a^c}{r_a^{c2} + X_d^{'c2}} \end{aligned} \tag{5.27}$$

Whereas the powers at the terminal of the synchronous generator become,

$$\begin{aligned} P_e = {} & \frac{|E|}{r_a^{a2} + X_d^{'a2}}\left[-r_a^a\left(e_k^a \cos\delta^a + f_k^a \sin\delta^a\right) + X_d^{'a}\left(e_k^a \sin\delta^a - f_k^a \cos\delta^a\right)\right] + \frac{|E|^2 r_a^a}{r_a^{a2} + X_d^{'a2}} \\ & + \frac{|E|}{r_a^{b2} + X_d^{'b2}}\left[-r_a^b\left(e_k^b \cos\delta^b + f_k^b \sin\delta^b\right) + X_d^{'b}\left(e_k^b \sin\delta^b - f_k^b \cos\delta^b\right)\right] + \frac{|E|^2 r_a^b}{r_a^{b2} + X_d^{'b2}} \\ & + \frac{|E|}{r_a^{c2} + X_d^{'c2}}\left[-r_a^c\left(e_k^c \cos\delta^c + f_k^c \sin\delta^c\right) + X_d^{'c}\left(e_k^c \sin\delta^c - f_k^c \cos\delta^c\right)\right] + \frac{|E|^2 r_a^c}{r_a^{c2} + X_d^{'c2}} \end{aligned} \tag{5.28}$$

$$Q_e = -\frac{|E|}{r_a^{a2} + X_d^{'a2}}\left[r_a^a\left(e_k^a \sin\delta^a - f_k^a \cos\delta^a\right) + X_d^{'a}\left(e_k^a \cos\delta^a + f_k^a \sin\delta^a\right)\right] + \frac{|E|^2 X_d^{'a}}{r_a^{a2} + X_d^{'a2}}$$
$$-\frac{|E|}{r_a^{b2} + X_d^{'b2}}\left[r_a^b\left(e_k^b \sin\delta^b - f_k^b \cos\delta^b\right) + X_d^{'b}\left(e_k^b \cos\delta^b + f_k^b \sin\delta^b\right)\right] + \frac{|E|^2 X_d^{'b}}{r_a^{b2} + X_d^{'b2}}$$
$$-\frac{|E|}{r_a^{c2} + X_d^{'c2}}\left[r_a^c\left(e_k^c \sin\delta^c - f_k^c \cos\delta^c\right) + X_d^{'c}\left(e_k^c \cos\delta^c - f_k^c \sin\delta^c\right)\right] + \frac{|E|^2 X_d^{'c}}{r_a^{c2} + X_d^{'c2}} \quad (5.29)$$

Substituting the active power equation (5.28) and the mechanical power equation ((5.20) in the case of a steam turbine) into the speed differential equation (5.4) of the generator, it becomes:

$$\frac{d\omega}{dt} = \frac{\pi f_0}{H}\{P_{HP}F_{HP} + P_{IP}F_{IP} + P_{LP}F_{LP}$$
$$-\frac{|E|}{r_a^{a2} + X_d^{'a2}}\left[-r_a^a\left(e_k^a \cos\delta^a + f_k^a \sin\delta^a\right) + X_d^{'a}\left(e_k^a \sin\delta^a - f_k^a \cos\delta^a\right)\right]$$
$$-\frac{|E|}{r_a^{b2} + X_d^{'b2}}\left[-r_a^b\left(e_k^b \cos\delta^b + f_k^b \sin\delta^b\right) + X_d^{'b}\left(e_k^b \sin\delta^b - f_k^b \cos\delta^b\right)\right] \quad (5.30)$$
$$-\frac{|E|}{r_a^{c2} + X_d^{'c2}}\left[-r_a^c\left(e_k^c \cos\delta^c + f_k^c \sin\delta^c\right) + X_d^{'c}\left(e_k^c \sin\delta^c - f_k^c \cos\delta^c\right)\right]$$
$$+\frac{3|E|^2 r_a^a}{r_a^{a2} + X_d^{'a2}} - D(\omega - \omega_0)\Big\}$$

Based on practical designs, equal armature resistance and admittances can be selected for all three phases so that equation (5.30) can be reduced to:

$$\frac{d\omega}{dt} = \frac{\pi f_0}{H}\Big\{P_{HP}F_{HP} + P_{IP}F_{IP} + P_{LP}F_{LP} - \frac{|E|}{r_a^2 + X_d^{'2}}$$
$$\Big\{-r_a\left[\left(e_k^a \cos\delta^a + f_k^a \sin\delta^a\right) + \left(e_k^b \cos\delta^b + f_k^b \sin\delta^b\right) + \left(e_k^c \cos\delta^c + f_k^c \sin\delta^c\right)\right]$$
$$+X_d^{'}\left[\left(e_k^a \sin\delta^a - f_k^a \cos\delta^a\right) + \left(e_k^b \sin\delta^b - f_k^b \cos\delta^b\right) + \left(e_k^c \sin\delta^c - f_k^c \cos\delta^c\right)\right]\Big\} \quad (5.31)$$
$$+\frac{3|E|^2 r_a}{r_a^{\,2} + X_d^{'2}} - D(\omega - \omega_0)\Big\}$$

Application of the trapezoidal rule to differential equations (5.31) and (5.5), yields explicit expressions for the synchronous speed and rotor angle. These are derived as follows:

$$\omega_{(t)} = \omega_{(t-\Delta t)} + \frac{\Delta t}{2}\left(\left.\frac{d\omega}{dt}\right|_{(t)} + \left.\frac{d\omega}{dt}\right|_{(t-\Delta t)} \right) \tag{5.32}$$

$$\delta_{(t)} = \delta_{(t-\Delta t)} + \frac{\Delta t}{2}\left(\left.\frac{d\delta}{dt}\right|_{(t)} + \left.\frac{d\delta}{dt}\right|_{(t-\Delta t)} \right) \tag{5.33}$$

Substitution of equations (5.30) and (5.6) into equations (5.32) and (5.33) and grouping term together gives

$$F_{(t)}(\omega) + F_{(t-\Delta t)}(\omega) + k_{(\omega)} = 0 \tag{5.34}$$

$$F_{(t)}(\delta) + F_{(t-\Delta t)}(\delta) + k_{(\delta)} = 0 \tag{5.35}$$

where

$$\begin{aligned} F_{(t)}(\omega) = \omega_{(t)} + \frac{\Delta t}{2}\frac{\pi f_0}{H}\Bigg\{ & \frac{|E|_{(t)}}{r_a^2 + X_d^{'2}} \\ & \Big\{ -r_a \Big[\left(e^a_{k(t)}\cos\delta^a_{(t)} + f^a_{k(t)}\sin\delta^a_{(t)}\right) + \left(e^b_{k(t)}\cos\delta^b_{(t)} + f^b_{k(t)}\sin\delta^b_{(t)}\right) \\ & \quad + \left(e^c_{k(t)}\cos\delta^c_{(t)} + f^c_{k(t)}\sin\delta^c_{(t)}\right) \Big] \\ & + X_d^{'} \Big[\left(e^a_{k(t)}\sin\delta^a_{(t)} - f^a_{k(t)}\cos\delta^a_{(t)}\right) + \left(e^b_{k(t)}\sin\delta^b_{(t)} - f^b_{k(t)}\cos\delta^b_{(t)}\right) \\ & \quad + \left(e^c_{k(t)}\sin\delta^c_{(t)} - f^c_{k(t)}\cos\delta^c_{(t)}\right) \Big] \Big\} \\ & + \frac{3|E|^2_{(t)}\, r_a}{r_a^{\,2} + X_d^{'2}} + D\omega_{(t)} - F_{\mathrm{HP}}P_{\mathrm{HP}(t)} - F_{\mathrm{IP}}P_{\mathrm{IP}(t)} - F_{\mathrm{LP}}P_{\mathrm{LP}(t)} \Bigg\} \end{aligned} \tag{5.36}$$

and

$$\begin{aligned} F_{(t-\Delta t)}(\omega) = -\omega_{(t-\Delta t)} + \frac{\Delta t}{2}\frac{\pi f_0}{H}\Bigg\{ & \frac{|E|_{(t-\Delta t)}}{r_a^2 + X_d^{'2}} \\ & \Big\{ -r_a \Big[\left(e^a_{k(t-\Delta t)}\cos\delta^a_{(t-\Delta t)} + f^a_{k(t-\Delta t)}\sin\delta^a_{(t-\Delta t)}\right) + \left(e^b_{k(t-\Delta t)}\cos\delta^b_{(t-\Delta t)} + f^b_{k(t-\Delta t)}\sin\delta^b_{(t-\Delta t)}\right) \\ & \quad + \left(e^c_{k(t-\Delta t)}\cos\delta^c_{(t-\Delta t)} + f^c_{k(t-\Delta t)}\sin\delta^c_{(t-\Delta t)}\right) \Big] \\ & + X_d^{'} \Big[\left(e^a_{k(t-\Delta t)}\sin\delta^a_{(t-\Delta t)} - f^a_{k(t-\Delta t)}\cos\delta^a_{(t-\Delta t)}\right) + \left(e^b_{k(t-\Delta t)}\sin\delta^b_{(t-\Delta t)} - f^b_{k(t-\Delta t)}\cos\delta^b_{(t-\Delta t)}\right) \\ & \quad + \left(e^c_{k(t-\Delta t)}\sin\delta^c_{(t-\Delta t)} - f^c_{k(t-\Delta t)}\cos\delta^c_{(t-\Delta t)}\right) \Big] \Big\} \\ & + \frac{3|E|^2_{(t-\Delta t)}\, r_a}{r_a^{\,2} + X_d^{'2}} + D\omega_{(t-\Delta t)} - F_{\mathrm{HP}}P_{\mathrm{HP}(t-\Delta t)} - F_{\mathrm{IP}}P_{\mathrm{IP}(t-\Delta t)} - F_{\mathrm{LP}}P_{\mathrm{LP}(t-\Delta t)} \Bigg\} \end{aligned} \tag{5.37}$$

$$k_{(\omega)} = -\frac{\Delta t \pi f_0}{H} D\omega_0 \tag{5.38}$$

For the rotor angle:

$$F_{(t)}(\delta) = \delta_{(t)} - \frac{\Delta t}{2}\omega_{(t)} \tag{5.39}$$

$$F_{(t-\Delta t)}(\delta) = -\delta_{(t-\Delta t)} - \frac{\Delta t}{2}\omega_{(t-\Delta t)} \tag{5.40}$$

$$k_{(\delta)} = 2\Delta t \pi f_0 \tag{5.41}$$

It should be noted that equations (5.38) and (5.41) are constants. Terms relating to time (t) and equations (5.36) and (5.39), are used to derive the terms in the Jacobian matrix to be evaluated in each iteration.

The Jacobian elements relating to the generator synchronous speed ω are,

$$\frac{\partial F(\omega)}{\partial e_k^a} = \frac{\Delta t \pi f_0}{2H} \frac{|E|_{(t)}}{r_a^{\,2} + x_d'^2}\left(-r_a \cos\delta + x_d' \sin\delta\right) \tag{5.42}$$

$$\frac{\partial F(\omega)}{\partial f^a} = \frac{\Delta t \pi f_0}{2H} \frac{|E|}{r_a^{\,2} + x_d'^2}\left(r_a \sin\delta + x_d' \cos\delta\right) \tag{5.43}$$

$$\frac{\partial F(\omega)}{\partial e_k^b} = \frac{\Delta t \pi f_0}{2H} \frac{|E|_{(t)}}{r_a^{\,2} + x_d'^2}\left[-r_a \cos\left(\delta - 2\pi/3\right) + x_d' \sin\left(\delta - 2\pi/3\right)\right] \tag{5.44}$$

$$\frac{\partial F(\omega)}{\partial f_k^b} = \frac{\Delta t \pi f_0}{2H} \frac{|E|}{r_a^{\,2} + x_d'^2}\left[r_a \sin\left(\delta - 2\pi/3\right) + x_d' \cos\left(\delta - 2\pi/3\right)\right] \tag{5.45}$$

$$\frac{\partial F(\omega)}{\partial e_k^c} = \frac{\Delta t \pi f_0}{2H} \frac{|E|_{(t)}}{r_a^{\,2} + x_d'^2}\left[-r_a \cos\left(\delta + 2\pi/3\right) + x_d' \sin\left(\delta + 2\pi/3\right)\right] \tag{5.46}$$

$$\frac{\partial F(\omega)}{\partial f_k^c} = \frac{\Delta t \pi f_0}{2H} \frac{|E|}{r_a^{\,2} + x_d'^2}\left[r_a \sin\left(\delta + 2\pi/3\right) + x_d' \cos\left(\delta + 2\pi/3\right)\right] \tag{5.47}$$

$$\frac{\partial F(\omega)}{\partial \omega} = 1 + \left(\frac{\Delta t \pi f_0}{2H}\right) D \tag{5.48}$$

$$\begin{aligned}\frac{\partial F(\omega)}{\partial \delta} = \frac{\Delta t \pi f_0}{2H} \frac{|E|_{(t)}}{r_a^{\,2} + X_d'^{\,2}} \Big\langle & r_a \left\{\left[e_k^a \sin\delta - f_k^a \cos\delta\right] + \left[e_k^b \sin\left(\delta - 2\pi/3\right) - f_k^b \cos\left(\delta - 2\pi/3\right)\right] + \left[e_k^c \sin\left(\delta + 2\pi/3\right) - f_k^c \cos\left(\delta + 2\pi/3\right)\right]\right\} \\ & + X_d' \left\{\left[e_k^a \cos\delta + f_k^a \sin\delta\right] + \left[e_k^b \cos\left(\delta - 2\pi/3\right) + f_k^b \sin\left(\delta - 2\pi/3\right)\right] \right. \\ & \left. + \left[e_k^c \cos\left(\delta + 2\pi/3\right) + f_k^c \sin\left(\delta + 2\pi/3\right)\right]\right\}\Big\rangle\end{aligned} \tag{5.49}$$

$$\frac{\partial F(\omega)}{\partial |E|} = \frac{\Delta t \pi f_0}{2H} \frac{1}{r_a^2 + X_d^{'2}} \Big\langle -r_a \left\{ \left[e_k \cos\delta + f_k \sin\delta \right] \right.$$
$$+ \left[e_k^b \cos(\delta - 2\pi/3) + f_k^b \sin(\delta - 2\pi/3) \right] + \left[e_k^c \cos(\delta + 2\pi/3) + f_k^c \sin(\delta + 2\pi/3) \right] \Big\}$$
$$+ X_d^{'} \left\{ \left[e_k^a \sin\delta - f_k^a \cos\delta \right] + \left[e_k^b \sin(\delta - 2\pi/3) - f_k^b \cos(\delta - 2\pi/3) \right] \right. \quad (5.50)$$
$$\left. + \left[e_k^c \sin(\delta + 2\pi/3) - f_k^c \cos(\delta + 2\pi/3) \right] \right\} + \frac{6|E| r_a}{r_a^{\ 2} + X_d^{'2}} \Big\rangle$$

$$\frac{\partial F(\omega)}{\partial P_{HP}} = -\frac{\Delta t \pi f_0}{2H} F_{HP} \quad (5.51)$$

$$\frac{\partial F(\omega)}{\partial P_{IP}} = -\frac{\Delta t \pi f_0}{2H} F_{IP} \quad (5.52)$$

$$\frac{\partial F(\omega)}{\partial P_{LP}} = -\frac{\Delta t \pi f_0}{2H} F_{LP} \quad (5.53)$$

While the Jacobian elements for the angles are

$$\frac{\partial F(\delta)}{\partial \omega} = -\frac{\Delta t}{2} \quad (5.54)$$

$$\frac{\partial F(\delta)}{\partial \delta} = 1 \quad (5.55)$$

5.7.2 Automatic voltage regulator

The algebraic form of the AVR differential equation (5.10) is

$$E_{(t)} = E_{(t-\Delta t)} + \frac{\Delta t}{2} \left(\left. \frac{dE}{dt} \right|_{(t)} + \left. \frac{dE}{dt} \right|_{(t-\Delta t)} \right) \quad (5.56)$$

Substitution of equation (5.10) into equation (5.56) and grouping terms together gives

$$F_{(t)}(E) + F_{(t-\Delta t)}(E) + k_{(E)} = 0 \quad (5.57)$$

where

$$F_t(E) = E_{(t)} - \frac{\Delta t}{2} \left[\frac{-K_A \left(e_{(t)}^2 + f_{(t)}^2 \right)^{1/2} - E_{(t)}}{T_{d0}^{'}} \right] \quad (5.58)$$

$$F_{(t-\Delta t)}(E) = -E_{(t-\Delta t)} - \frac{\Delta t}{2}\left[\frac{-K_A\left(e^2_{(t-\Delta t)} + f^2_{(t-\Delta t)}\right)^{1/2} - E_{(t-\Delta t)}}{T'_{d0}}\right] \tag{5.59}$$

$$k_{(E)} = -\Delta t\left[\frac{K_A V_{ref}}{T'_{d0}}\right] \tag{5.60}$$

The Jacobian elements for the Automatic Voltage Regulator are

$$\frac{\partial F(E)}{\partial e} = \frac{\Delta t K_A}{2T'_{d0}}\frac{e}{\left(e^2+f^2\right)^{1/2}} \tag{5.61}$$

$$\frac{\partial F(E)}{\partial f} = \frac{\Delta t K_A}{2T'_{d0}}\frac{f}{\left(e^2+f^2\right)^{1/2}} \tag{5.62}$$

$$\frac{\partial F(E)}{\partial E} = 1 + \frac{\Delta t}{2T'_{d0}} \tag{5.63}$$

5.7.3 Governor

The algebraic form of the governor equation (5.13) is

$$P_{GV(t)} = P_{GV(t-\Delta t)} + \frac{\Delta t}{2}\left(\left.\frac{dP_{GV}}{dt}\right|_{(t)} + \left.\frac{dP_{GV}}{dt}\right|_{(t-\Delta t)}\right) \tag{5.64}$$

Substitution of equation (5.13) into equation(5.64) and grouping terms together gives

$$F_{(t)}\left(P_{GV}\right) + F_{(t-\Delta t)}\left(P_{GV}\right) + k_{(P_{GV})} = 0 \tag{5.65}$$

where

$$F_{(t)}\left(P_{GV}\right) = P_{GV(t)} - \frac{\Delta t}{2}\left[\frac{-K\omega_{(t)} - P_{GV(t)}}{T_c}\right] \tag{5.66}$$

$$F_{(t-\Delta t)}\left(P_{GV}\right) = -P_{GV(t-\Delta t)} - \frac{\Delta t}{2}\left[\frac{-K\omega_{(t-\Delta t)} - P_{GV(t-\Delta t)}}{T_c}\right] \tag{5.67}$$

$$k_{(P_{GV})} = -\Delta t\left[\frac{P_{set} + K\omega_0}{T_c}\right] \tag{5.68}$$

The Jacobian elements for this governor model are:

$$\frac{\partial F(P_{GV})}{\partial \omega} = \frac{\Delta t K}{2T_c} \tag{5.69}$$

$$\frac{\partial F(P_{GV})}{\partial P_{GV}} = 1 + \frac{\Delta t}{2T_c} \tag{5.70}$$

The governor equation (5.15) for cases of slow transients, in algebraic form is:

$$\Delta P_{(t)} = \Delta P_{(t-\Delta t)} + \frac{\Delta t}{2}\left(\left.\frac{d\Delta P}{dt}\right|_{(t)} + \left.\frac{d\Delta P}{dt}\right|_{(t-\Delta t)} \right) \tag{5.71}$$

Substitution of equation (5.15) into equation (5.71) and grouping terms together gives

$$F_{(t)}(\Delta P) + F_{(t-\Delta t)}(\Delta P) + k_{(\Delta P)} = 0 \tag{5.72}$$

where

$$F_{(t)}(\Delta P) = \Delta P_{(t)} - \frac{\Delta t}{2}\left[\frac{K\omega_{(t)} - \Delta P_{(t)}}{T_c} \right] \tag{5.73}$$

$$F_{(t-\Delta t)}(\Delta P) = -\Delta P_{(t-\Delta t)} - \frac{\Delta t}{2}\left[\frac{K\omega_{(t-\Delta t)} - \Delta P_{(t-\Delta t)}}{T_c} \right] \tag{5.74}$$

$$k_{(\Delta P)} = -\Delta t \frac{K\omega_0}{T_c} \tag{5.75}$$

The Jacobian elements for the governor model, assuming slow transients, are:

$$\frac{\partial F(\Delta P)}{\partial \omega} = -\Delta t \frac{K}{2T_c} \tag{5.76}$$

$$\frac{\partial F(\Delta P)}{\partial \Delta P} = 1 + \frac{\Delta t}{2T_c} \tag{5.77}$$

5.7.4 Steam turbine

The differential equations of the steam turbine model can be written in algebraic form for the steam turbine high-pressure:

$$P_{\mathrm{HP}(t)} = P_{\mathrm{HP}(t-\Delta t)} + \frac{\Delta t}{2}\left(\left.\frac{dP_{\mathrm{HP}}}{dt}\right|_{(t)} + \left.\frac{dP_{\mathrm{HP}}}{dt}\right|_{(t-\Delta t)} \right) \tag{5.78}$$

Substitution of equation (5.17), which corresponds to the steam turbine high-pressure, into equation (5.78) and grouping terms together gives

$$F_{(t)}(P_{HP}) + F_{(t-\Delta t)}(P_{HP}) + k_{(P_{HP})} = 0 \tag{5.79}$$

where

$$F_{(t)}(P_{HP}) = P_{HP(t)} - \frac{\Delta t}{2}\left(\frac{P_{GV(t)} - P_{HP(t)}}{T_{CH}}\right) \tag{5.80}$$

$$F_{(t-\Delta t)}(P_{HP}) = -P_{HP(t-\Delta t)} - \frac{\Delta t}{2}\left(\frac{P_{GV(t-\Delta t)} - P_{HP(t-\Delta t)}}{T_{CH}}\right) \tag{5.81}$$

$$k_{(P_{HP})} = 0 \tag{5.82}$$

For the steam turbine intermediate-pressure

$$P_{IP(t)} = P_{IP(t-\Delta t)} + \frac{\Delta t}{2}\left(\left.\frac{dP_{IP}}{dt}\right|_{(t)} + \left.\frac{dP_{IP}}{dt}\right|_{(t-\Delta t)}\right) \tag{5.83}$$

Substitution of equation (5.18), which corresponds to the steam turbine intermediate-pressure, into equation (5.83) and grouping terms together gives

$$F_{(t)}(P_{IP}) + F_{(t-\Delta t)}(P_{IP}) + k_{(P_{IP})} = 0 \tag{5.84}$$

where

$$F_{(t)}(P_{IP}) = P_{IP(t)} - \frac{\Delta t}{2}\left(\frac{P_{HP(t)} - P_{IP(t)}}{T_{RH}}\right) \tag{5.85}$$

$$F_{(t-\Delta t)}(P_{IP}) = -P_{IP(t-\Delta t)} - \frac{\Delta t}{2}\left(\frac{P_{HP(t-\Delta t)} - P_{IP(t-\Delta t)}}{T_{RH}}\right) \tag{5.86}$$

$$k_{(P_{IP})} = 0 \tag{5.87}$$

Finally, for the steam turbine low-pressure:

$$P_{LP(t)} = P_{LP(t-\Delta t)} + \frac{\Delta t}{2}\left(\left.\frac{dP_{LP}}{dt}\right|_{(t)} + \left.\frac{dP_{LP}}{dt}\right|_{(t-\Delta t)}\right) \tag{5.88}$$

Substitution equation (5.19), which corresponds to the steam turbine low-pressure, into equation (5.88) and grouping terms together gives

$$F_{(t)}(P_{LP}) + F_{(t-\Delta t)}(P_{LP}) + k_{(P_{LP})} = 0 \tag{5.89}$$

where

$$F_{(t)}\left(P_{\mathrm{LP}}\right)=P_{\mathrm{LP(t)}}-\frac{\Delta t}{2}\left(\frac{P_{\mathrm{IP(t)}}-P_{\mathrm{LP(t)}}}{T_{\mathrm{CO}}}\right) \tag{5.90}$$

$$F_{(t-\Delta t)}\left(P_{\mathrm{LP}}\right)=-P_{\mathrm{LP(t-\Delta t)}}-\frac{\Delta t}{2}\left(\frac{P_{\mathrm{IP(t-\Delta t)}}-P_{\mathrm{LP(t-\Delta t)}}}{T_{\mathrm{CO}}}\right) \tag{5.91}$$

$$k_{(P_{LP})}=0 \tag{5.92}$$

The Jacobian elements for the three-stage steam turbine model are:

$$\frac{\partial F\left(P_{\mathrm{HP}}\right)}{\partial P_{\mathrm{GV}}}=-\frac{\Delta t}{2T_{\mathrm{CH}}} \tag{5.93}$$

$$\frac{\partial F\left(P_{\mathrm{HP}}\right)}{\partial P_{\mathrm{HP}}}=1+\frac{\Delta t}{2T_{\mathrm{CH}}} \tag{5.94}$$

$$\frac{\partial F\left(P_{\mathrm{IP}}\right)}{\partial P_{\mathrm{HP}}}=-\frac{\Delta t}{2T_{\mathrm{RH}}} \tag{5.95}$$

$$\frac{\partial F\left(P_{\mathrm{IP}}\right)}{\partial P_{\mathrm{IP}}}=1+\frac{\Delta t}{2T_{\mathrm{RH}}} \tag{5.96}$$

$$\frac{\partial F\left(P_{\mathrm{LP}}\right)}{\partial P_{\mathrm{IP}}}=-\frac{\Delta t}{2T_{\mathrm{CO}}} \tag{5.97}$$

$$\frac{\partial F\left(P_{\mathrm{LP}}\right)}{\partial P_{\mathrm{LP}}}=1+\frac{\Delta t}{2T_{\mathrm{CO}}} \tag{5.98}$$

5.8 Dynamic Power Flow Formulation

In order to apply the Newton-Raphson method using the simultaneous approach, to solve the system equations representing the power network and the algebraic equations of generating plants, the dynamic power flow formulation is expressed by the following relationship:

$$\begin{bmatrix}X\\Y\end{bmatrix}_t^{it}=\begin{bmatrix}X\\Y\end{bmatrix}_t^{it-1}-\begin{bmatrix}A & B\\C & D\end{bmatrix}_t^{(-1)it-1}\begin{bmatrix}F(X)\\F(Y)\end{bmatrix}_t^{it-1} \tag{5.99}$$

where X and Y are the variables to be updated at each iteration, *it*. The variables X are formed from the real and imaginary parts of the nodal voltages, i.e. $X=\left[e_k^{\rho}\ \ f_k^{\rho}\right]^T$,

whereas Y is formed from the generating plants variables, i.e. $Y=\left[w_i \;\; \delta_i \;\; E_i \;\; P_{GVi} \;\; P_{HPi} \;\; P_{IPi} \;\; P_{LPi} \;\; DP_i\right]^T$ when steam power plants are present. Alternatively, the following state vector is used $Y=\left[\omega_i \;\; \delta_i \;\; E_i \;\; \Delta P_i \;\; P_{mi}\right]^T$ for hydro plants. The matrix $\begin{bmatrix} A & B \\ C & D \end{bmatrix}$ is the Jacobian matrix, formed by sub matrices A, B, C and D.

5.8.1 Jacobian matrix formation

The Jacobian matrix may consist of up to two times the number of nodes plus eight times the number of steam plants and five times the number of hydro plants.

Sub-matrix A only contains Jacobian entries representing the transmission network, whereas D only contains Jacobian entries of generating plants. Submatrices B and C are made up of Jacobian terms corresponding to the coupling of the transmission network and generating plant components; these entries are interfacing entries between the static and dynamic elements. Jacobian submatrices for steam power plants have the following structures:

$$A=\begin{bmatrix} \frac{\partial P_k^\rho}{\partial e_k^\rho} & \frac{\partial P_k^\rho}{\partial f_k^\rho} & \cdots & \frac{\partial P_k^\rho}{\partial e_{nb}^\rho} & \frac{\partial P_k^\rho}{\partial f_{nb}^\rho} \\ \frac{dQ_k^\rho}{de_k^\rho} & \frac{dQ_k^\rho}{df_k^\rho} & \cdots & \frac{dQ_k^\rho}{de_{nb}^\rho} & \frac{dQ_k^\rho}{df_{nb}^\rho} \\ \vdots & \vdots & \ddots & \vdots & \vdots \\ \frac{\partial P_{nb}^\rho}{\partial e_k^\rho} & \frac{\partial P_{nb}^\rho}{\partial f_k^\rho} & \cdots & \frac{\partial P_{nb}^\rho}{\partial e_{nb}^\rho} & \frac{\partial P_{nb}^\rho}{\partial e_{nb}^\rho} \\ \frac{dQ_{nb}^\rho}{de_k^\rho} & \frac{dQ_{nb}^\rho}{df_k^\rho} & \cdots & \frac{dQ_{nb}^\rho}{de_{nb}^\rho} & \frac{dQ_{nb}^\rho}{de_{nb}^\rho} \end{bmatrix} \tag{5.100}$$

$$B=\begin{bmatrix} \frac{\partial P_k^\rho}{\partial \omega_i} & \frac{\partial P_k^\rho}{\partial \delta_i} & \frac{\partial P_k^\rho}{\partial E_i} & \frac{\partial P_k^\rho}{\partial P_{GVi}} & \frac{\partial P_k^\rho}{\partial P_{HPi}} & \frac{\partial P_k^\rho}{\partial P_{IPi}} & \frac{\partial P_k^\rho}{\partial P_{LPi}} & \frac{\partial P_k^\rho}{\partial DP_i} \\ \frac{\partial Q_k^\rho}{\partial \omega_i} & \frac{\partial Q_k^\rho}{\partial \delta_i} & \frac{\partial Q_k^\rho}{\partial E_i} & \frac{\partial Q_k^\rho}{\partial P_{GVi}} & \frac{\partial Q_k^\rho}{\partial P_{HPi}} & \frac{\partial Q_k^\rho}{\partial P_{IPi}} & \frac{\partial Q_k^\rho}{\partial P_{LPi}} & \frac{\partial Q_k^\rho}{\partial DP_i} \\ \vdots & \vdots & \vdots & \vdots & \vdots & \vdots & \vdots & \vdots \\ \frac{\partial P_{nb}^\rho}{\partial \omega_i} & \frac{\partial P_{nb}^\rho}{\partial \delta_i} & \frac{\partial P_{nb}^\rho}{\partial E_i} & \frac{\partial P_{nb}^\rho}{\partial P_{GVi}} & \frac{\partial P_{nb}^\rho}{\partial P_{HPi}} & \frac{\partial P_{nb}^\rho}{\partial P_{IPi}} & \frac{\partial P_{nb}^\rho}{\partial P_{LPi}} & \frac{\partial P_{nb}^\rho}{\partial DP_i} \\ \frac{\partial Q_{nb}^\rho}{\partial \omega_i} & \frac{\partial Q_{nb}^\rho}{\partial \delta_i} & \frac{\partial Q_{nb}^\rho}{\partial E_i} & \frac{\partial Q_{nb}^\rho}{\partial P_{GVi}} & \frac{\partial Q_{nb}^\rho}{\partial P_{HPi}} & \frac{\partial Q_{nb}^\rho}{\partial P_{IPi}} & \frac{\partial Q_{nb}^\rho}{\partial P_{LPi}} & \frac{\partial Q_{nb}^\rho}{\partial DP_i} \end{bmatrix} \tag{5.101}$$

$$C=\begin{bmatrix}
\frac{\partial F_i(\omega)}{\partial e_k^\rho} & \frac{\partial F_i(\omega)}{\partial e_k^\rho} & \frac{\partial F_i(E)}{\partial e_k^\rho} & \frac{\partial F_i(P_{GV})}{\partial e_k^\rho} & \frac{\partial F_i(P_{HP})}{\partial e_k^\rho} & \frac{\partial F_i(P_{IP})}{\partial e_k^\rho} & \frac{\partial F_i(P_{LP})}{\partial e_k^\rho} & \frac{\partial F_i(DP)}{\partial e_k^\rho} \\
\frac{\partial F_i(\omega)}{\partial f_k^\rho} & \frac{\partial F_i(\omega)}{\partial f_k^\rho} & \frac{\partial F_i(E)}{\partial f_k^\rho} & \frac{\partial F_i(P_{GV})}{\partial f_k^\rho} & \frac{\partial F_i(P_{HP})}{\partial f_k^\rho} & \frac{\partial F_i(P_{IP})}{\partial f_k^\rho} & \frac{\partial F_i(P_{LP})}{\partial f_k^\rho} & \frac{\partial F_i(DP)}{\partial f_k^\rho} \\
\vdots & \vdots & \vdots & \vdots & \vdots & \vdots & \vdots & \vdots \\
\frac{\partial F_i(\omega)}{\partial e_{nb}^\rho} & \frac{\partial F_i(\delta)}{\partial e_{nb}^\rho} & \frac{\partial F_i(E)}{\partial e_{nb}^\rho} & \frac{\partial F_i(P_{GV})}{\partial e_{nb}^\rho} & \frac{\partial F_i(P_{HP})}{\partial e_{nb}^\rho} & \frac{\partial F_i(P_{IP})}{\partial e_{nb}^\rho} & \frac{\partial F_i(P_{LP})}{\partial e_{nb}^\rho} & \frac{\partial F_i(DP)}{\partial e_{nb}^\rho} \\
\frac{\partial F_i(\omega)}{\partial f_{nb}^\rho} & \frac{\partial F_i(\delta)}{\partial f_{nb}^\rho} & \frac{\partial F_i(E)}{\partial f_{nb}^\rho} & \frac{\partial F_i(P_{GV})}{\partial f_{nb}^\rho} & \frac{\partial F_i(P_{HP})}{\partial f_{nb}^\rho} & \frac{\partial F_i(P_{IP})}{\partial f_{nb}^\rho} & \frac{\partial F_i(P_{LP})}{\partial f_{nb}^\rho} & \frac{\partial F_i(DP)}{\partial f_{nb}^\rho}
\end{bmatrix}^T \tag{5.102}$$

$$D=\begin{bmatrix}
\frac{\partial F_i(\omega)}{\partial \omega_i} & \frac{\partial F_i(\omega)}{\partial \delta_i} & \frac{\partial F_i(\omega)}{\partial E_i} & \frac{\partial F_i(\omega)}{\partial P_{GVi}} & \frac{\partial F_i(\omega)}{\partial P_{HPi}} & \frac{\partial F_i(\omega)}{\partial P_{IPi}} & \frac{\partial F_i(\omega)}{\partial P_{LPi}} & \frac{\partial F_i(\omega)}{\partial DP_i} \\
\frac{\partial F_i(\delta)}{\partial \omega_i} & \frac{\partial F_i(\delta)}{\partial \delta_i} & \frac{\partial F_i(\delta)}{\partial E_i} & \frac{\partial F_i(\delta)}{\partial P_{GVi}} & \frac{\partial F_i(\delta)}{\partial P_{HPi}} & \frac{\partial F_i(\delta)}{\partial P_{IPi}} & \frac{\partial F_i(\delta)}{\partial P_{LPi}} & \frac{\partial F_i(\delta)}{\partial DP_i} \\
\frac{\partial F_i(E)}{\partial \omega_i} & \frac{\partial F_i(E)}{\partial \delta_i} & \frac{\partial F_i(E)}{\partial E_i} & \frac{\partial F_i(E)}{\partial P_{GVi}} & \frac{\partial F_i(E)}{\partial P_{HPi}} & \frac{\partial F_i(E)}{\partial P_{IPi}} & \frac{\partial F_i(E)}{\partial P_{LPi}} & \frac{\partial F_i(E)}{\partial DP_i} \\
\frac{\partial F_i(P_{GV})}{\partial \omega_i} & \frac{\partial F_i(P_{GV})}{\partial \delta_i} & \frac{\partial F_i(P_{GV})}{\partial E_i} & \frac{\partial F_i(P_{GV})}{\partial P_{GVi}} & \frac{\partial F_i(P_{GV})}{\partial P_{HPi}} & \frac{\partial F_i(P_{GV})}{\partial P_{IPi}} & \frac{\partial F_i(P_{GV})}{\partial P_{LPi}} & \frac{\partial F_i(P_{GV})}{\partial DP_i} \\
\frac{\partial F_i(P_{HP})}{\partial \omega_i} & \frac{\partial F_i(P_{HP})}{\partial \delta_i} & \frac{\partial F_i(P_{HP})}{\partial E_i} & \frac{\partial F_i(P_{HP})}{\partial P_{GVi}} & \frac{\partial F_i(P_{HP})}{\partial P_{HPi}} & \frac{\partial F_i(P_{HP})}{\partial P_{IPi}} & \frac{\partial F_i(P_{HP})}{\partial P_{LPi}} & \frac{\partial F_i(P_{HP})}{\partial DP_i} \\
\frac{\partial F_i(P_{IP})}{\partial \omega_i} & \frac{\partial F_i(P_{IP})}{\partial \delta_i} & \frac{\partial F_i(P_{IP})}{\partial E_i} & \frac{\partial F_i(P_{IP})}{\partial P_{GVi}} & \frac{\partial F_i(P_{IP})}{\partial P_{HPi}} & \frac{\partial F_i(P_{IP})}{\partial P_{IPi}} & \frac{\partial F_i(P_{IP})}{\partial P_{LPi}} & \frac{\partial F_i(P_{IP})}{\partial DP_i} \\
\frac{\partial F_i(P_{LP})}{\partial \omega_i} & \frac{\partial F_i(P_{LP})}{\partial \delta_i} & \frac{\partial F_i(P_{LP})}{\partial E_i} & \frac{\partial F_i(P_{LP})}{\partial P_{GVi}} & \frac{\partial F_i(P_{LP})}{\partial P_{HPi}} & \frac{\partial F_i(P_{LP})}{\partial P_{IPi}} & \frac{\partial F_i(P_{LP})}{\partial P_{LPi}} & \frac{\partial F_i(P_{LP})}{\partial DP_i} \\
\frac{\partial F_i(DP)}{\partial \omega_i} & \frac{\partial F_i(DP)}{\partial \delta_i} & \frac{\partial F_i(DP)}{\partial E_i} & \frac{\partial F_i(DP)}{\partial P_{GVi}} & \frac{\partial F_i(DP)}{\partial P_{HPi}} & \frac{\partial F_i(DP)}{\partial P_{IPi}} & \frac{\partial F_i(DP)}{\partial P_{LPi}} & \frac{\partial F_i(DP)}{\partial DP_i}
\end{bmatrix} \tag{5.103}$$

5.8.2 Mismatch vector

The mismatch vector comprises entries of active and reactive nodal powers and algebraic functions of power plant components, i.e. $F(X)=\left[\Delta P_k^\rho \;\; \Delta Q_k^\rho\right]^T$ and $F(Y)=\left[F(w_i)\;F(\delta_i)\;F(E_i)\;F(P_{GVi})\;F(P_{HPi})\;F(P_{IPi})\;F(P_{LPi})\;F(DP_i)\right]^T$ for the steam plants or $F(Y)=\left[F(\omega_i)\;F(\delta_i)\;F(E_i)\;F(\Delta P_i)\;F(P_{mi})\right]^T$ for the hydro plants. In these vector expressions *T* denotes the transpose operation.

The vector $F(X)$ is formed by the generic network active and reactive powers injected at bus *k*, due to the contribution of all the power plant components terminating at this bus; e.g. for the generator, transmission lines, loads, etc, where:

$$F(P_k) = P_{Gk} - P_{Lk} - \sum_{i=1}^{n} P_{calk}^{i} = 0 \tag{5.104}$$

$$F(Q_k) = Q_{Gk} - Q_{Lk} - \sum_{i=1}^{n} Q_{calk}^{i} = 0 \tag{5.105}$$

The vector *F(Y)* is formed by the generic dynamic equations of a generating plant connected at a given bus so that:

$$F(\omega) = F_{(t)}(\omega) + F_{(t-\Delta t)}(\omega) + k_{(\omega)} = 0 \tag{5.106}$$

$$F(\delta) = F_{(t)}(\delta) + F_{(t-\Delta t)}(\delta) + k_{(\delta)} = 0 \tag{5.107}$$

$$F(E) = F_{(t)}(E) + F_{(t-\Delta t)}(E) + k_{(E)} = 0 \tag{5.108}$$

$$F(P_{GV}) = F_{(t)}(P_{GV}) + F_{(t-\Delta t)}(P_{GV}) + k_{(P_{GV})} = 0 \tag{5.109}$$

$$F(P_{HP}) = F_{(t)}(P_{HP}) + F_{(t-\Delta t)}(P_{HP}) + k_{(P_{HP})} = 0 \tag{5.110}$$

$$F(P_{IP}) = F_{(t)}(P_{IP}) + F_{(t-\Delta t)}(P_{IP}) + k_{(P_{IP})} = 0 \tag{5.111}$$

$$F(P_{LP}) = F_{(t)}(P_{LP}) + F_{(t-\Delta t)}(P_{LP}) + k_{(P_{LP})} = 0 \tag{5.112}$$

Terms with the subscript $(t-\Delta t)$ are calculated using initial values obtained from power flows results and remain constant for the whole of the iterative process at time (t), whereas terms with the subscript (t) are updated at the end of each iteration step (it) using:

$$(X)^{it+1} = (X)^{it} + (\Delta X)^{it} \tag{5.113}$$

$$(Y)^{it+1} = (Y)^{it} + (\Delta Y)^{it} \tag{5.114}$$

Repetitive solutions at time (t) are carried out until changes at each nodal voltage and generators' state variables are less than a prescribed small tolerance, say $1e^{-12}$. Updated values of power flows are obtained for time (t) along with a new set of values for the state variables at each generating plant. The new set of state variables is used to obtain an improved solution at time $(t+1)$. The whole process is repeated until the maximum time scheduled for simulation is completed, or up to a time when loss of system stability become apparent.

5.9 Power Disturbances and Network Topological Changes

The dynamic power flow enables the study of different kinds of disturbances, which may occur at any point in time during simulation time. Among these are load increments/decrements, switching in and out of transmission lines, short-circuits faults, and loss of generation. Simulation of each kind of disturbance is handled differently within the software. Load changes only effect the power mismatch equations; transmission line changes result in modification to the Jacobian matrix for the buses involved. Loss of generation has an effect in both Jacobian and power mismatches. Simulation of short-circuits faults require additional functions to deal with fault calculations.

The software extension has been carried out following the OOP philosophy, and new classes have been written to incorporate generating plant variables and constants. In addition, a loop for time has been inserted in the main program. For the first step time, steady-state power flow results are used to initialise generating plant variables and to set the required references values. An auxiliary file is used to read the scheduled transient events. The extended software has been tested for functionality and robustness; exhibiting quadratic convergence characteristics.

5.10 Case Studies for Dynamic Power Flows

The New England network used in Chapter 4 and shown in Figure 4.3 was used for testing the dynamic power flow algorithm. For the purpose of this test case, the generators were selected to be steam power plants. Gains and time constants were adjusted to maximize dynamic effects. Appendix II gives the parameters used for the thermal power plants. Values for the speed governing system and turbine parameters are also given at Appendix II. Generating plants were assumed to be equipped with AVR, governor and a three-stage steam turbine. The dynamic response of the network was assessed by simulating major disturbance events and less severe events causing only voltage step changes of different magnitudes. Both balanced and unbalanced events have been studied. The three-phase power flows are shown in Figure 4.5 and the nodal voltage given in Figure 4.4 for the case of balanced conditions. These values are taken as the base case for all the simulations that follow in this chapter relating to the New England reduced network in Figure 4.3.

The system used is a very robust one so, the dynamic effects exhibited by this system are somewhat exaggerated, compared to those exhibited by a more realistic system with a large number of lines and generating plants. Nevertheless, it still provides a reasonable basis for comparison of the various scenarios. The commercial software, ETAP® Power station 3.0.1 [6] was used to validate and compare balanced cases. This is done by comparing the three-phase balanced solution given by the dynamic power flow algorithm with the positive sequence of ETAP®. The results obtained with ETAP® show a slight difference due to the fact that ETAP® software uses more elaborated models than the ones used in the present work. Nevertheless, they are in good agreement. As far as the author is aware there is no commercial software available to carry out unbalanced transient or dynamic studies of large-scale power systems with embedded VSC-based FACTS equipment.

5.11 Load Related Transient Events

This case study is a sudden reduction of three-phase power system load following by a restoration to its normal level. The per phase load connected to buses 26, 27 and 28 are 139, 281 and 206 MW and 17, 75.5 and 27.6 MWAR, respectively. Active and reactive powers are disconnected at the end of the first minute and restored two minutes later. With reference to equations (5.104)-(5.105), it becomes apparent that any step load perturbation in power network loads have an effect on the outputs of all generating plants in the interconnected system. Power generation is altered by the regulatory action of the speed governor and turbine; hence, frequency and nodal voltages are deviated from schedule values. The remaining variables at each generator are also altered. Figure 5.12 and Figure 5.13 show the response of the generating plants to a step load disturbance whereas Figure 5.14(a) and (b) show the nodal voltages magnitudes and phase angles of the system, respectively.

Figure 5.12(b) shows load angle differences per phase for both synchronous generators. It should be noticed that the maximum departure now reaches 35 degrees, suggesting that the systems would return back to the steady-state, without loss of synchronism.

From the generating plant variables behaviour shown in Figure 5.13(a-d), the response of the speed governor and turbine is clearly appreciated. The control system attempts to ride through the disturbance by adjusting the various parameters in the generating plant to bring these values back to their previous steady-state values.

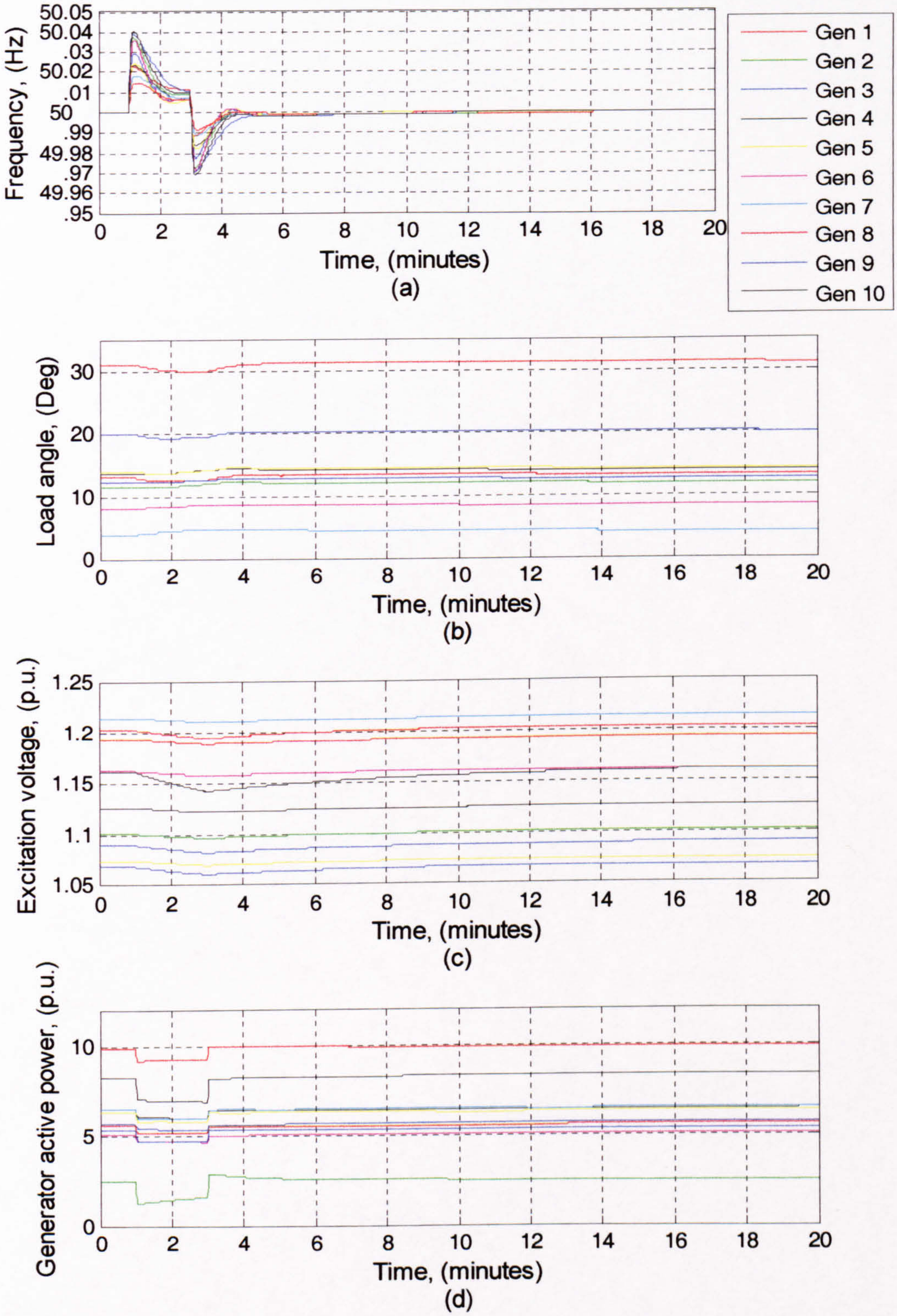

Figure 5.12. Generating plant responses to a three-phase load disturbance; (a) frequency; (b) load angle difference; (c) excitation voltage; (d) active power

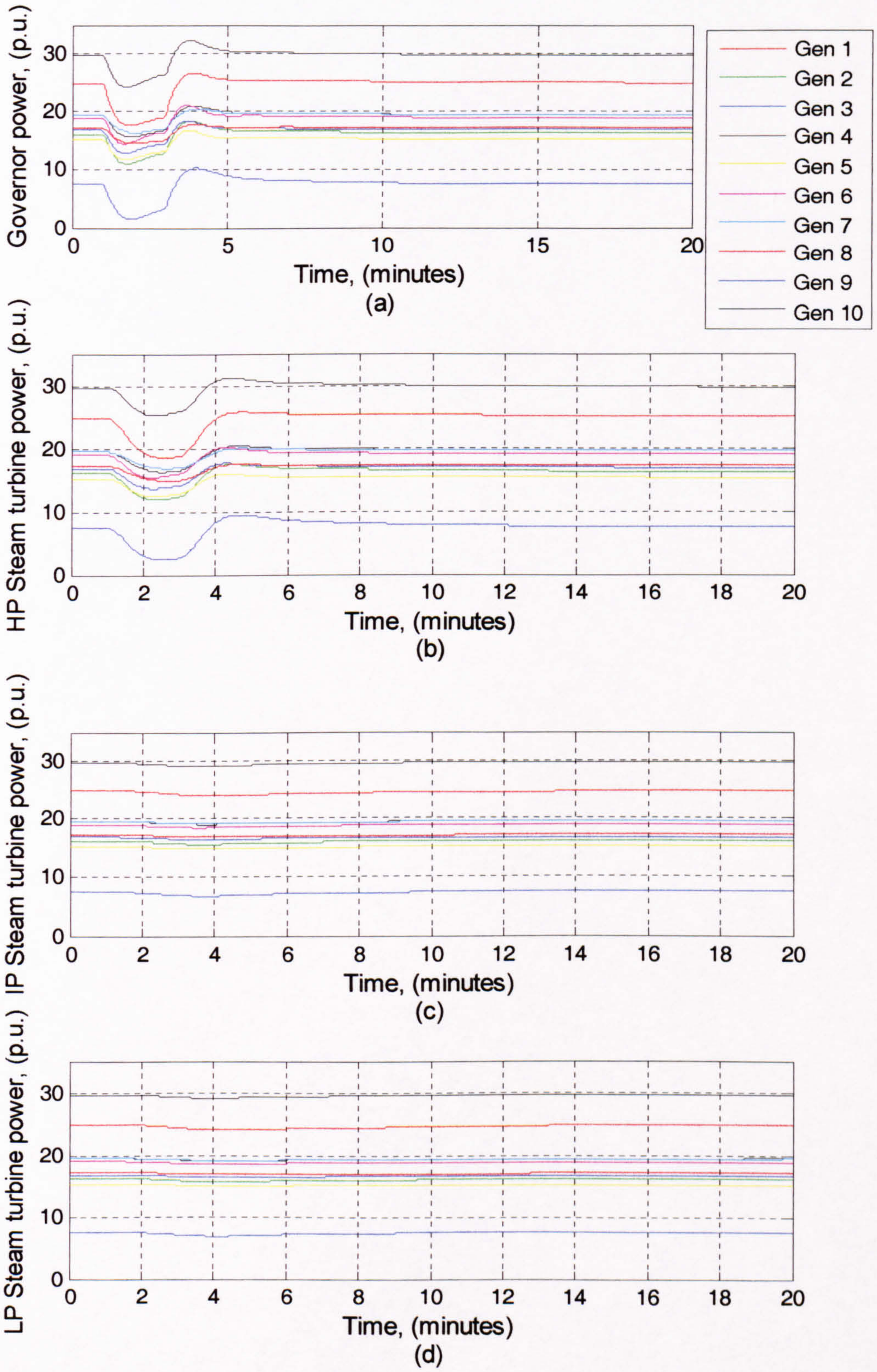

Figure 5.13 Generating plant responses to a three-phase load disturbance; (a) governor power; steam turbine (b) HP; (c) IP; (d) LP

By observing Figure 5.12(d) and Figure 5.14(a) and (b), it is noticed that a load disconnection causes a decrease in the generator power output, together with a step increase in nodal voltage magnitudes and phase angles. Conversely, a positive effect is noticed following reconnection of the load.

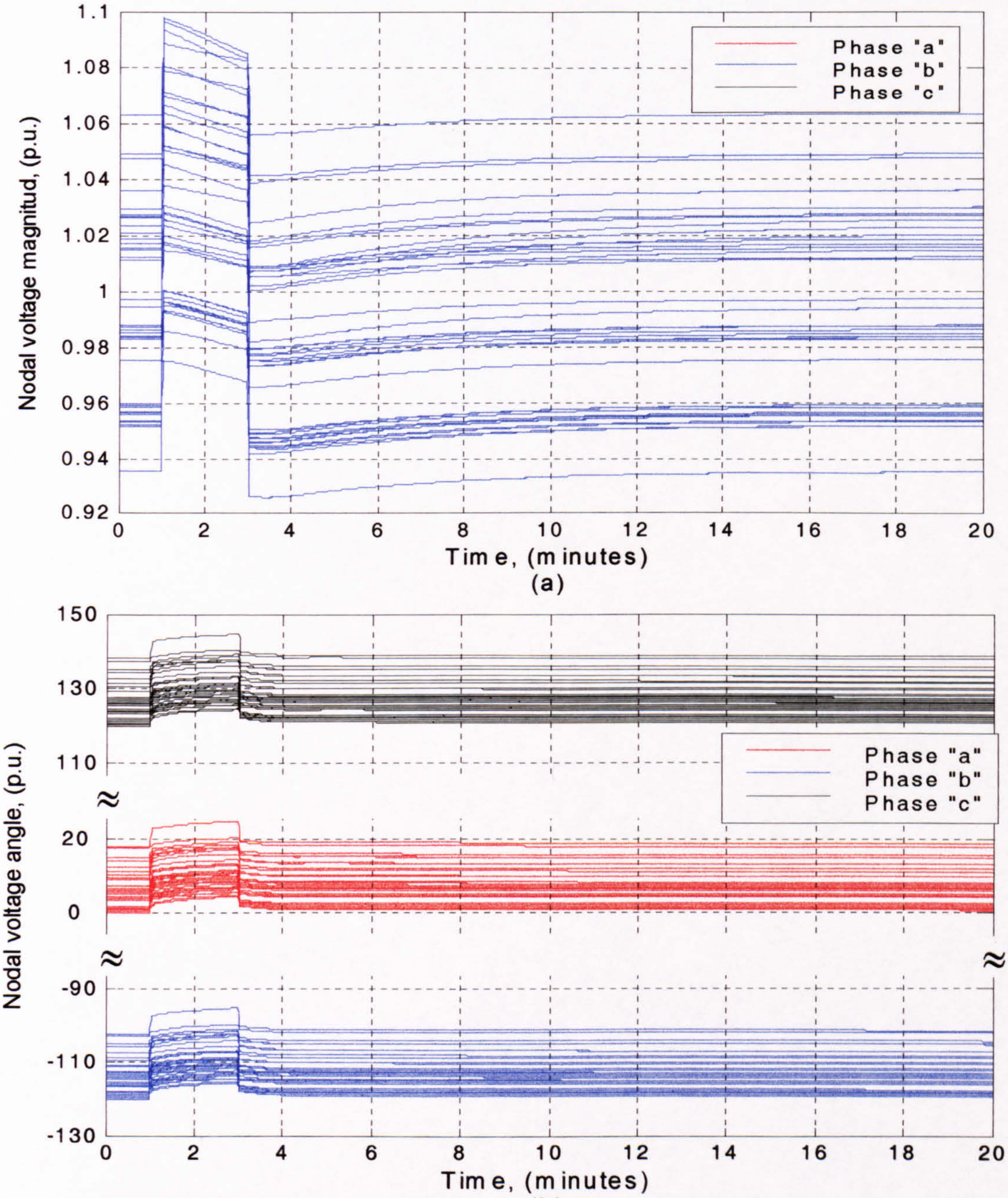

Figure 5.14 Nodal voltage responses of the system to a three-phase load disturbance; (a) magnitude; (b) phase angle

5.12 Unbalance Load Disturbance

For the purpose of studying an unbalanced disturbance phase *a* of the load at selected buses is disconnected and reconnected at equal times as in the previous section, i.e. at one and three minutes. The responses of the power plants are shown in Figure 5.15 and Figure 5.16, whereas nodal voltage magnitude and phase angles, are shown in Figure 5.17(a) and (b), respectively. As expected, since the disturbance is a single-phase event it induces imbalances in all the generating power plant parameters as well as in the three-phase nodal voltages. In this case study, the load that tripped out is one third of the total three-phase load.

Unbalanced load disturbances are more difficult cases to solve since these cause imbalances on the active and reactive power outputs of the synchronous generators connected to the system. It can be observed from Figure 5.15(d) that the greater active power fluctuation takes place in the phase which has a tripped-out load causing an opposite effect in the remaining phases, the imbalances experienced by the output powers are transmitted to the remaining parameters, excitation voltages and load angle differences. It should be noticed in Figure 5.15(a) that frequency fluctuations are slightly lower than in the balanced three-phase case. Figure 5.15(b) shows that the load angle differences are unbalanced, with the greater fluctuation occurring in phase *c*. Fluctuations in governor powers and steam turbines powers as shown in Figure 5.16(a-d), are fairly small, as expected, because the tripped-out power is less significant than in the balanced three-phase case and so is the mechanical power.

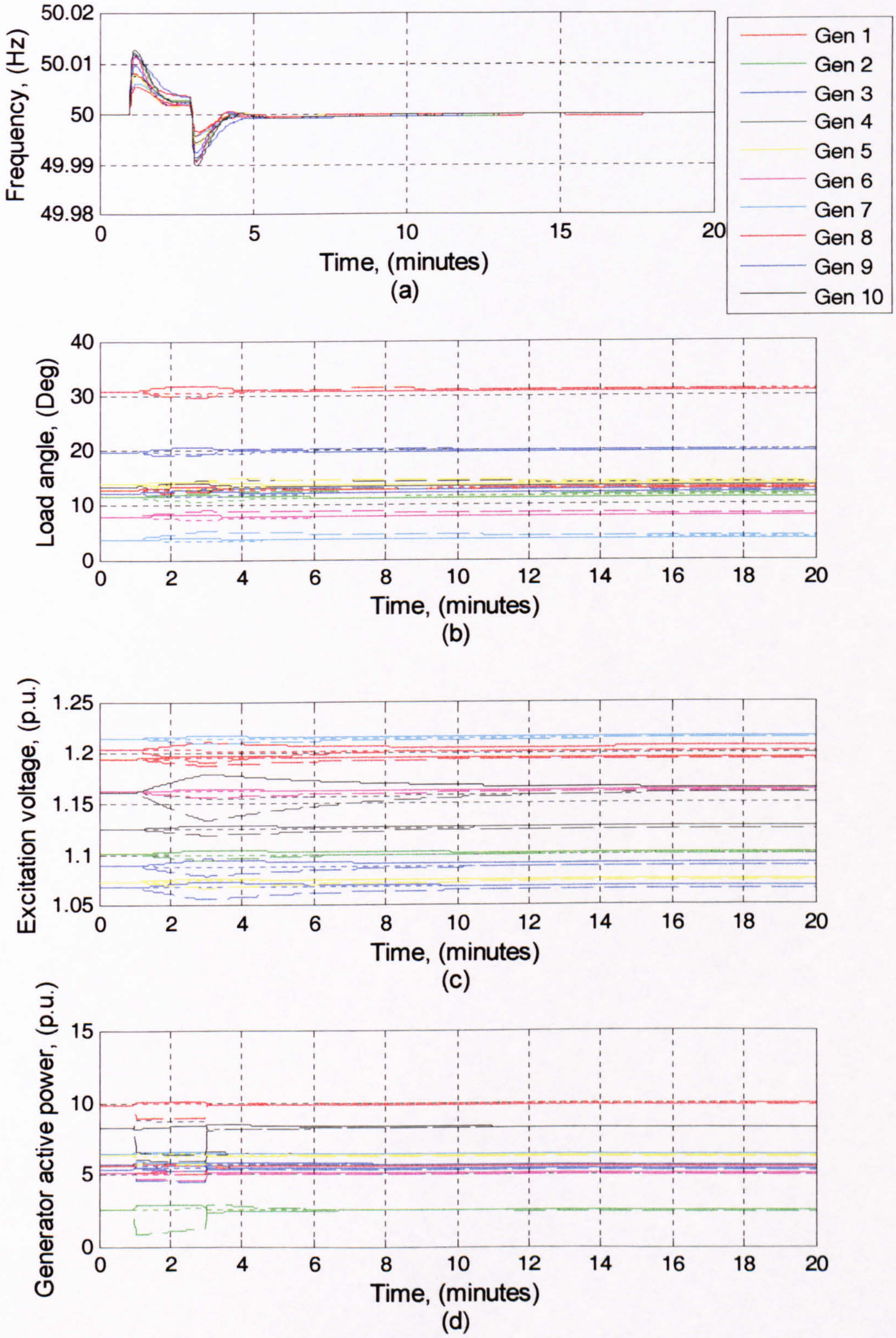

Figure 5.15 Generating plant variable responses due to an unbalanced loading condition; (a) frequency; (b) load angle; (c) excitation voltage; (d) active power

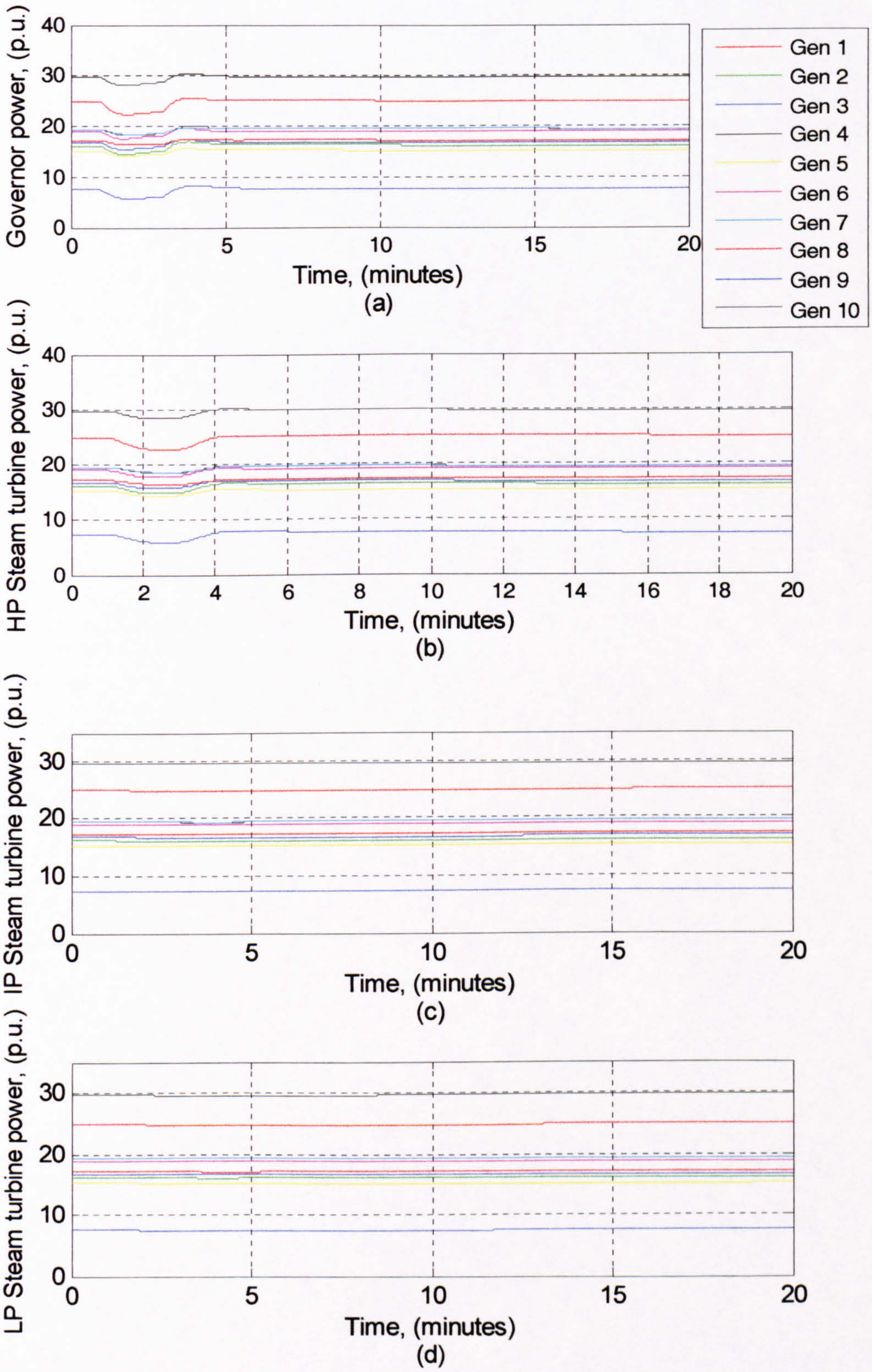

Figure 5.16 Generating plant variable responses due to an unbalanced loading condition; (a) governor power; steam turbine (b) HP; (c) IP; (d) LP

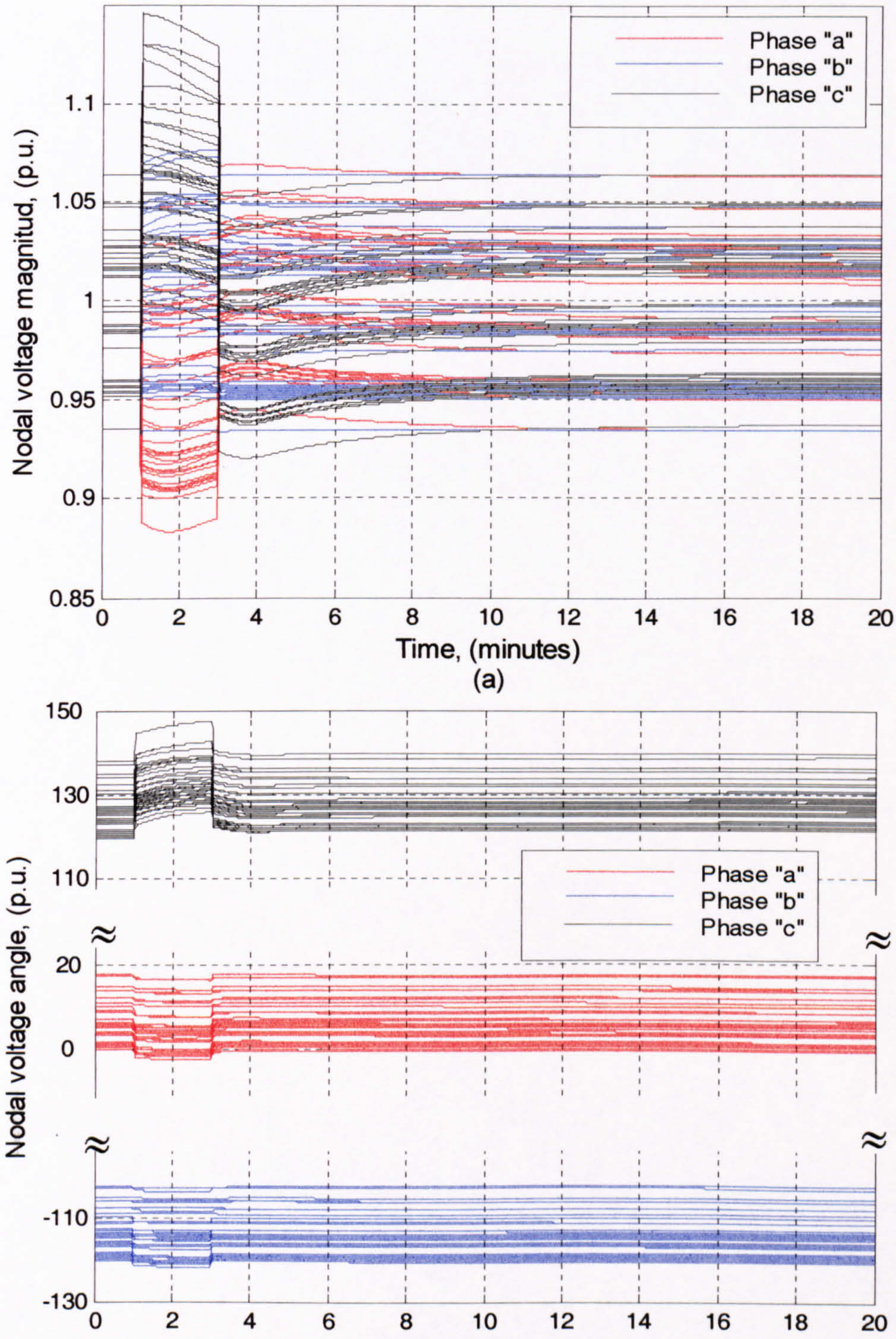

Figure 5.17 Three-phase nodal voltage in the system for the case of an unbalanced three-phase load disturbance; (a) magnitude; (b) phase angle

5.13 Transmission Line Outages

In general, disturbances in transmission lines lead to smaller voltage steps than those caused by load tripping. However, transmission line disconnections produce topological changes in the system and a new steady-state is reached. In order to assess dynamic effects due to transmission line outages, the transmission line connected between buses 16 and 17 is selected. The increase in active power generation produces voltage steps at all nodes of the network. Figure 5.18 and Figure 5.19 show the generating plants responses to a transmission line outage, whereas Figure 5.20 shows the nodal voltage magnitudes and phase angles.

From Figure 5.18(a), it can be seen that transmission lines outages have a negligible impact on frequency fluctuations. Also, the displacement between phase angles is minimum, as shown Figure 5.18(b). Excitation voltage and active power outputs are shown in Figure 5.18(c-d). Increases in generated power have an impact on the mechanical components of the generating plants. Figure 5.19(a-b) show the outputs of the various mechanical components of the generating plant, it can be seen to have a minimal effect in the speed governors and in the three steam stage turbines.

Figure 5.20 shows nodal voltage fluctuations, magnitudes in (a) and phase angles in (b).

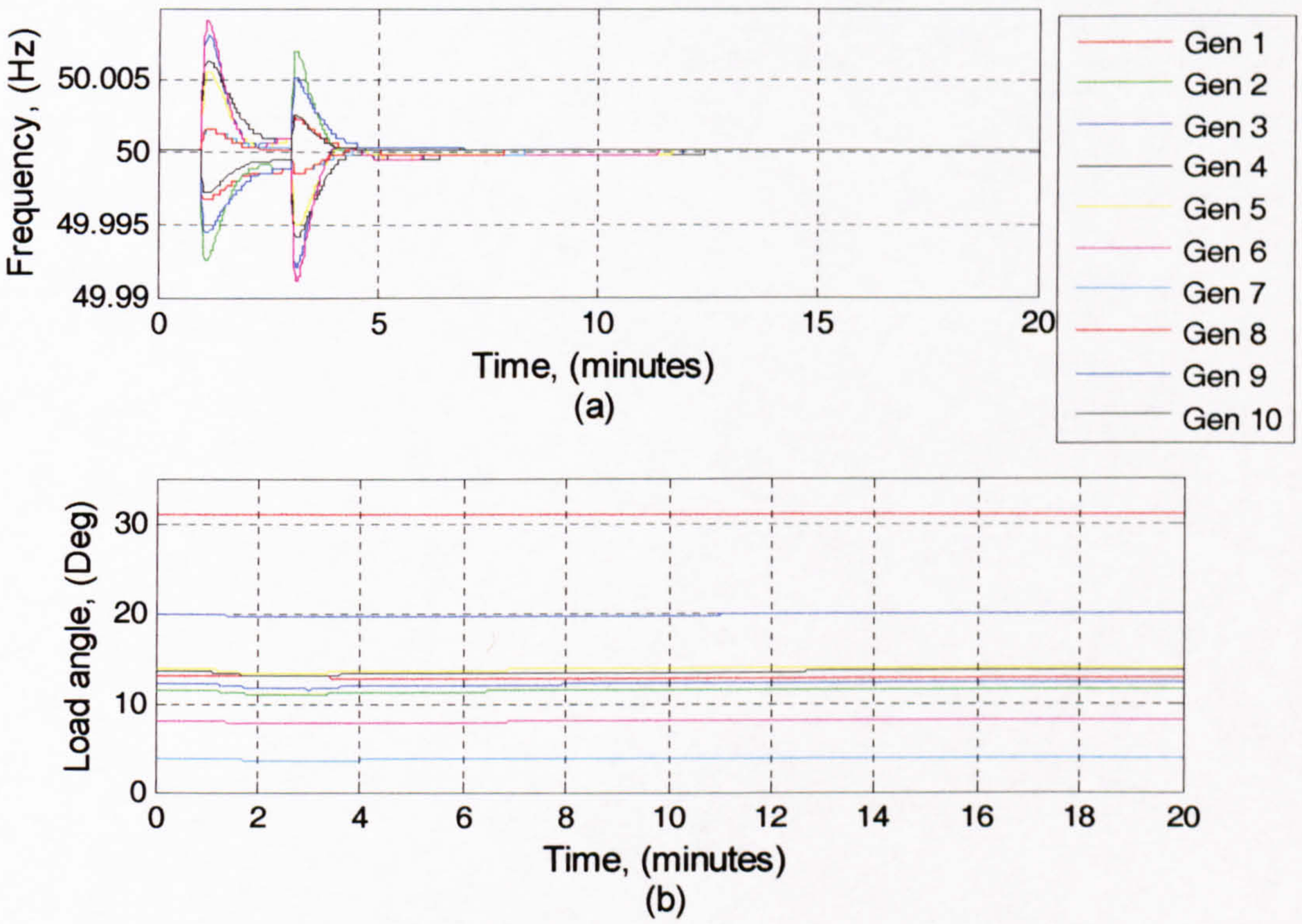

Figure 5.18 Generating plant response of the system to a line outage; (a) frequency; (b) load angle; (c) excitation voltage; (d) active power

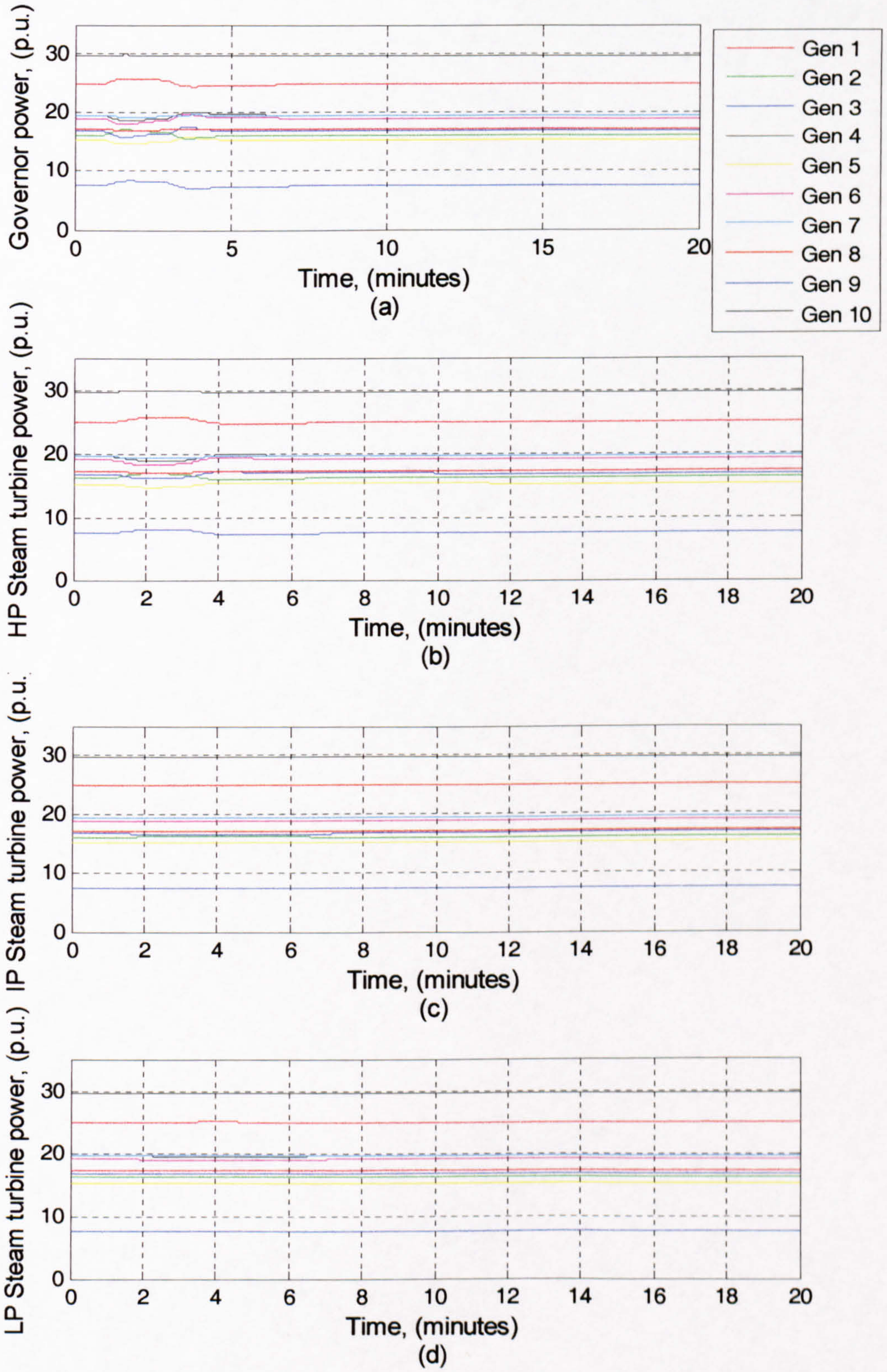

Figure 5.19 Generating plant response of the system to a line outage; (a) governor power; steam turbine (b) HP; (c) IP; (d) LP

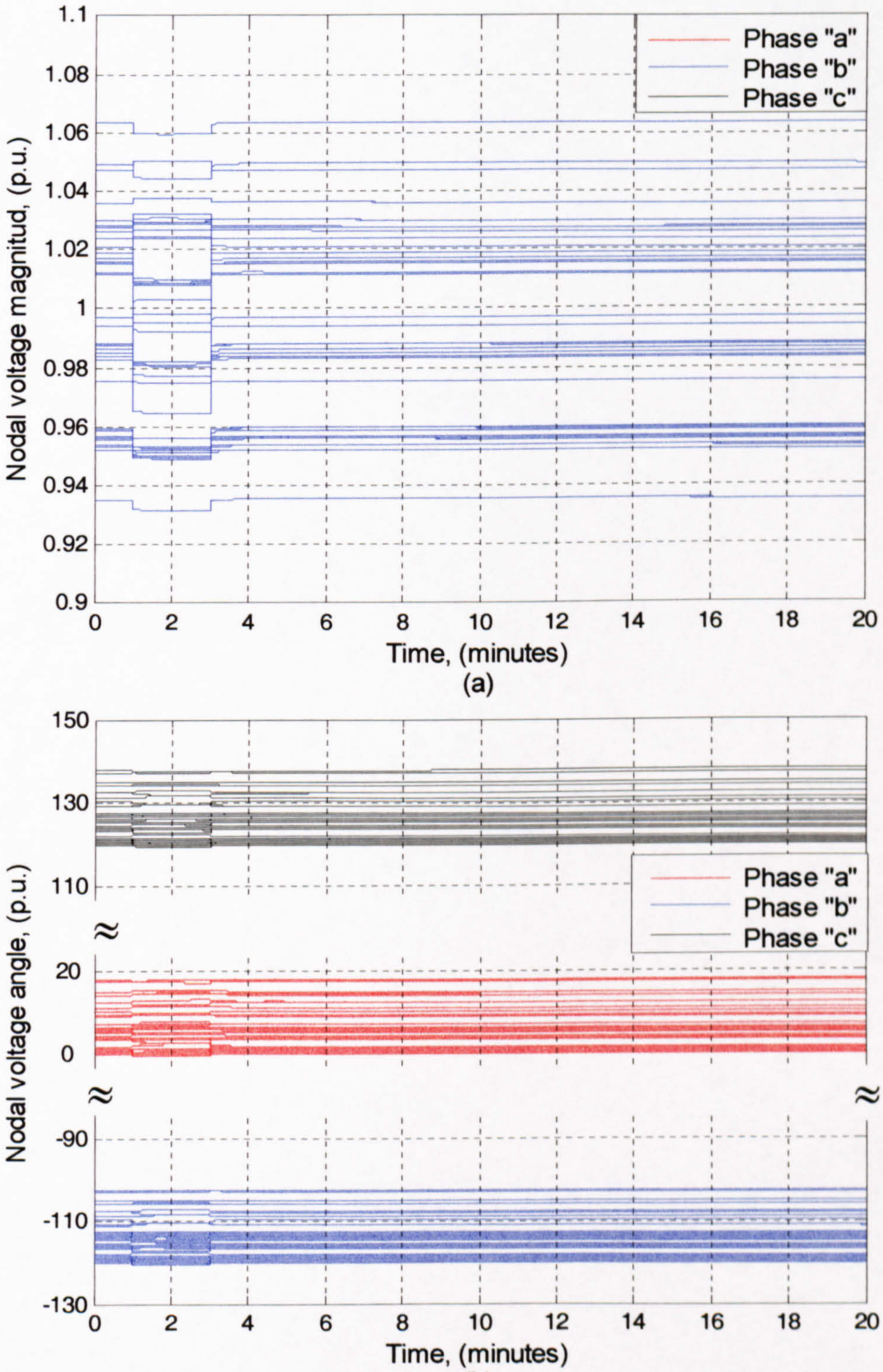

Figure 5.20 System nodal voltages for the case of a three-phase transmission line outage; (a) magnitude and (b) phase angle

5.14 Unbalanced Transmission Lines Events

To assess the effect of unbalanced transmission lines outages, phase a of the transmission line connected between buses 16 and 17 was selected. The generating plant responses are shown in Figure 5.21 and Figure 5.22, whereas Figure 5.23 shows the nodal voltages. It is noticed that apart from frequency fluctuations which do not seem to be significant, all other generating plant parameters are not only unbalanced but the fluctuations are smaller than for the balanced case. The mechanical parameters show larger fluctuations than in the balanced case, leading to a slower recovery.

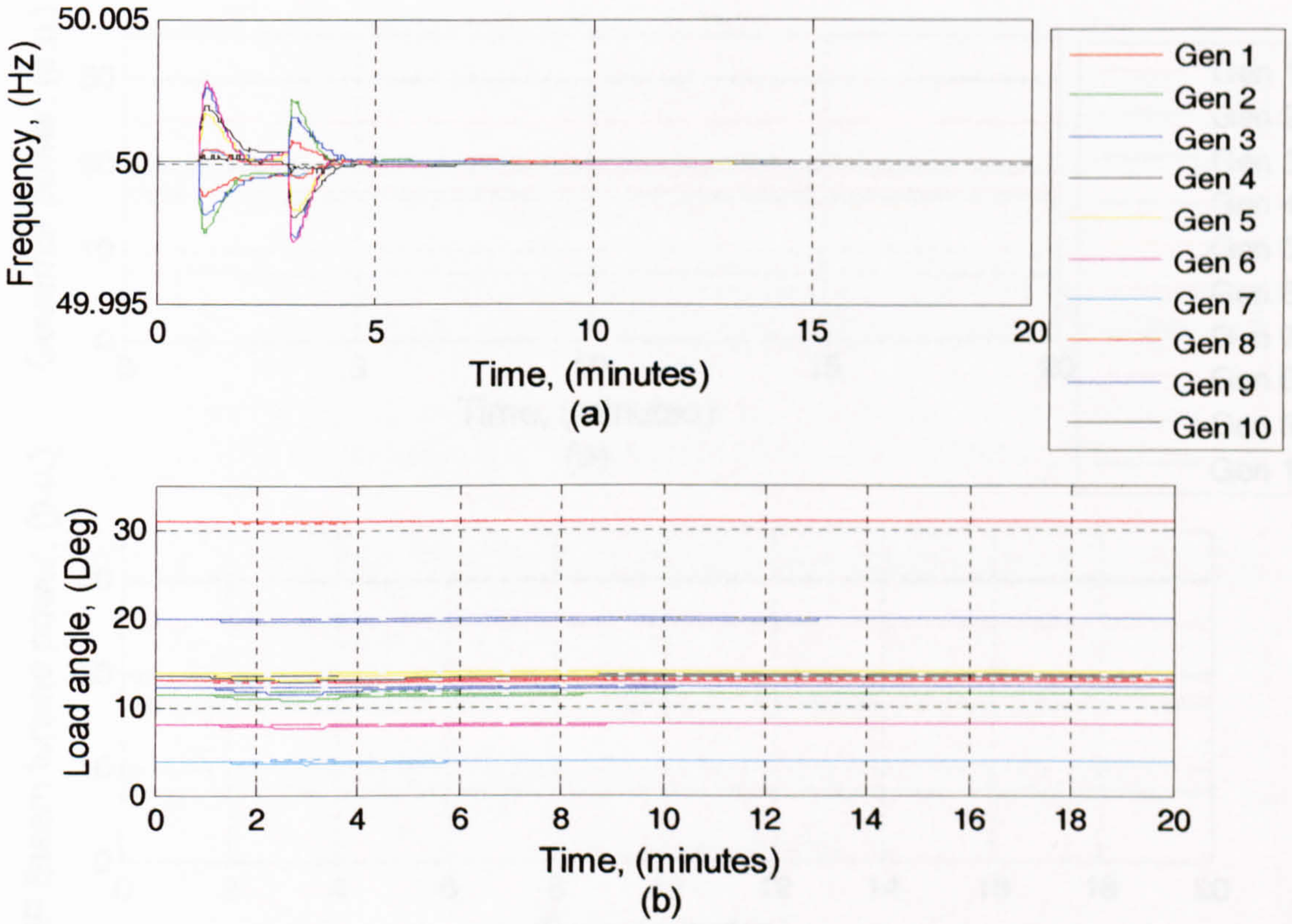

Figure 5.21 Generating plants responses due to an unbalanced transmission line disturbance; (a) frequency; (b) load angle; (c) excitation voltage; (d) active power

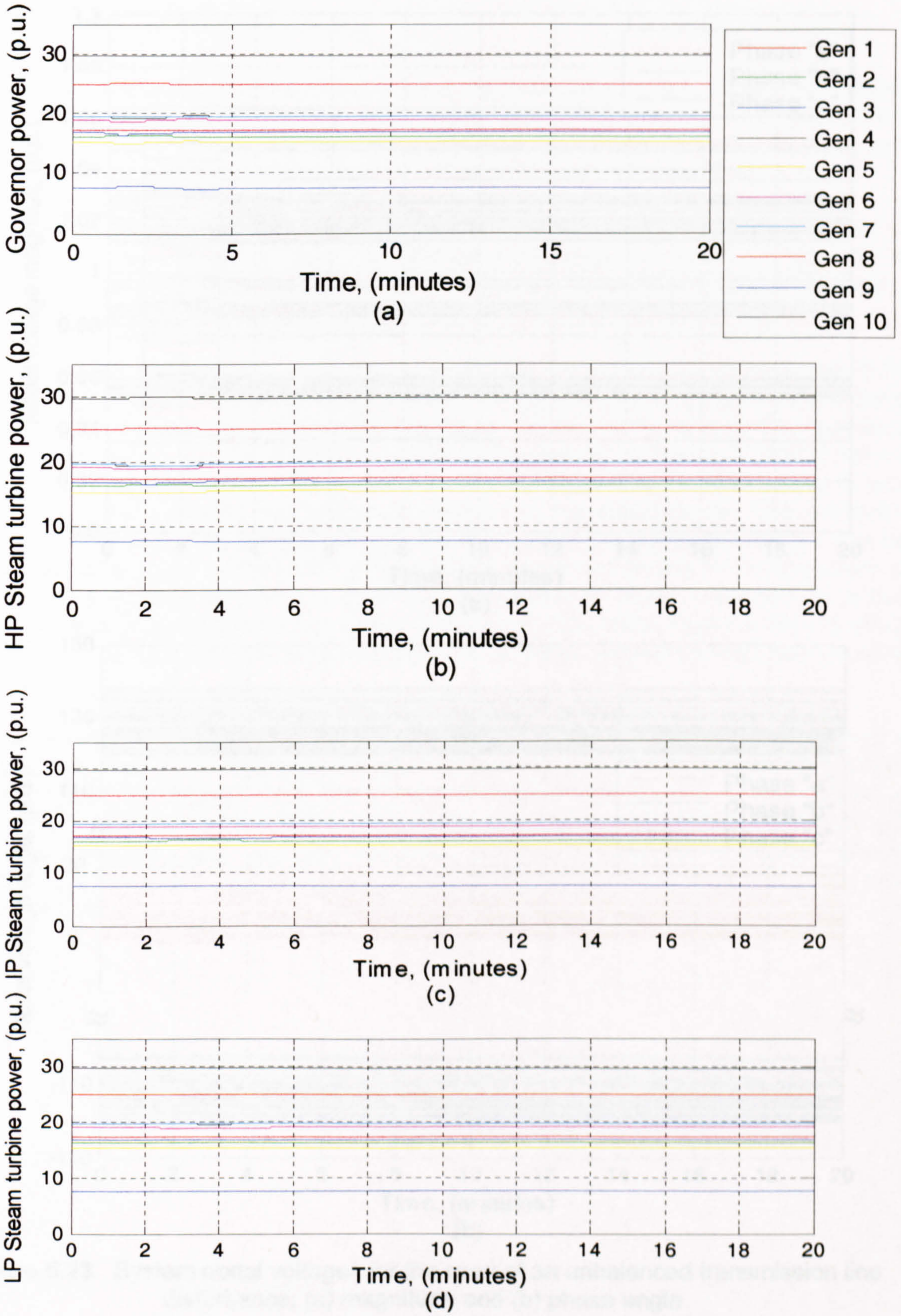

Figure 5.22 Generating plants responses due to an unbalanced transmission line disturbance; (e) governor power; steam turbine (f) HP; (g) IP; (h) LP

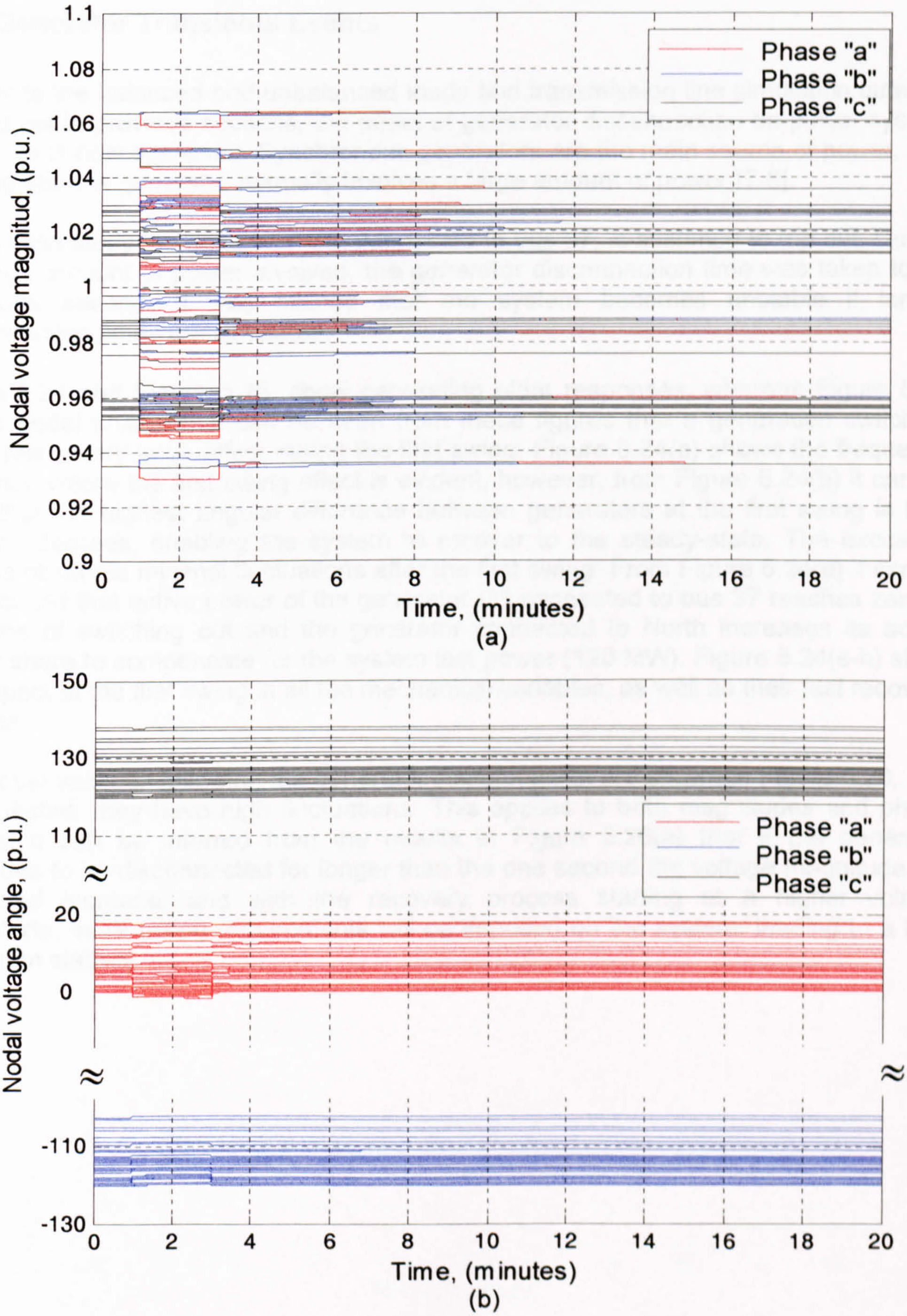

Figure 5.23 System nodal voltages for the case of an unbalanced transmission line disturbance; (a) magnitude and (b) phase angle

5.15 Generator Transients Events

Further to the balanced and unbalanced loads and transmission line simulation outages carried out in previous sections, the effect of generator disconnection on power system dynamics is now assessed. Synchronous generators are the main source of power, and tripping out one generator normally involves a large amount of power [7-8].

In this case study the generator G8, connected to bus 37, is assumed to trip out. Due to the large amount of power involved, the generator disconnection time was taken to be only one second. It was noticed that the system becomes unstable if longer disconnection times are simulated.

Figure 5.24 and Figure 5.25, show generating plant responses, whereas Figure 5.26 shows nodal voltages. It can be seen from these figures that a generation switching event has a very large effect during the first swing. Figure 5.24(a) shows the frequency response where the first swing effect is evident, however, from Figure 5.24(b) it can be seen that the highest angular difference between generators at the first swing is less than 60 degrees, enabling the system to recover to the steady-state. The excitation voltage observes minimal fluctuations after the first swing. From Figure 5.24(d) it can be appreciated that active power of the generator G8 connected to bus 37 reaches zero at the time of switching out and the generator connected to North increases its active power share to compensate for the system lost power (120 MW). Figure 5.24(e-h) show the impact of the first swing in all the mechanical variables, as well as their fast recovery process.

The nodal voltages following the generator disconnection are shown in Figure 5.26, and as expected, they have high fluctuations. This applies to both magnitudes and phase angles. It can be inferred from the results in Figure 5.26(a) that if the generator continues to be disconnected for longer than the one second the voltage magnitude will continued increase, and with the recovery process starting at a higher voltage magnitude, more taxing requirements will be imposed on the system, leading to a loss of system stability.

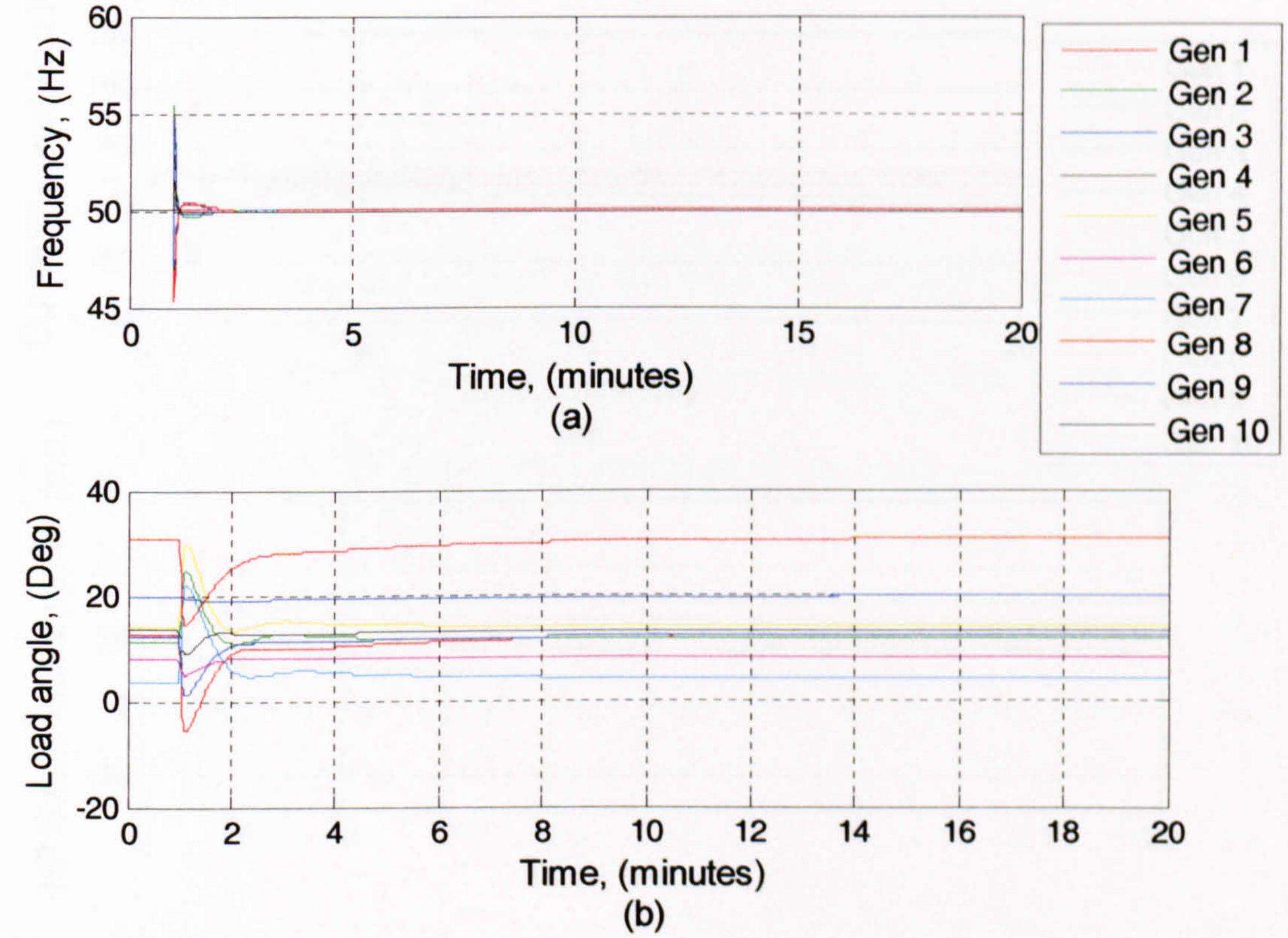

Figure 5.24 Generating plants responses to a generator disturbance; (a) frequency; (b) load angle; (c) excitation voltage; (d) active power

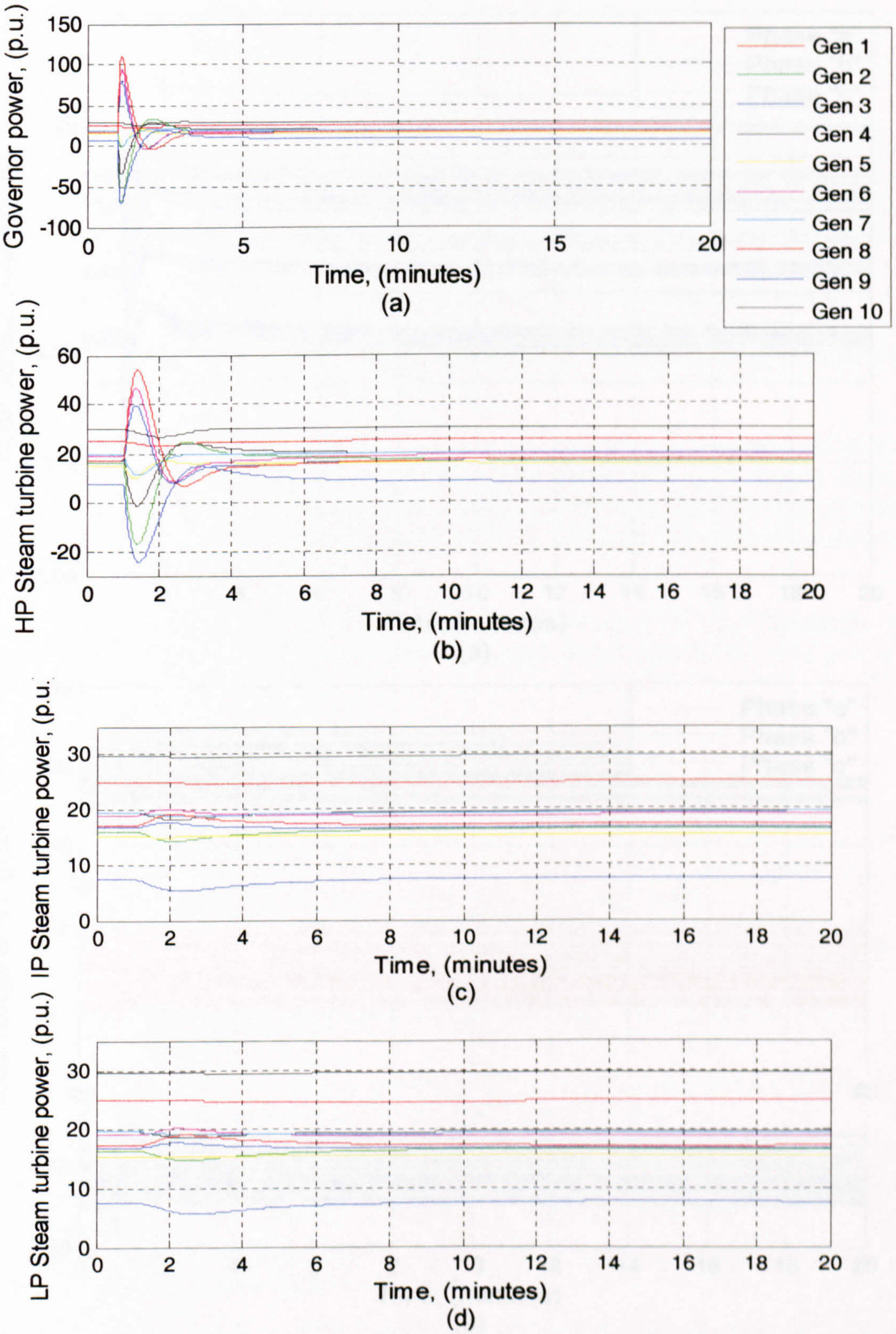

Figure 5.25 Generating plants responses to a generator disturbance; (a) governor power; steam turbine (b) HP; (c) IP; (d) LP

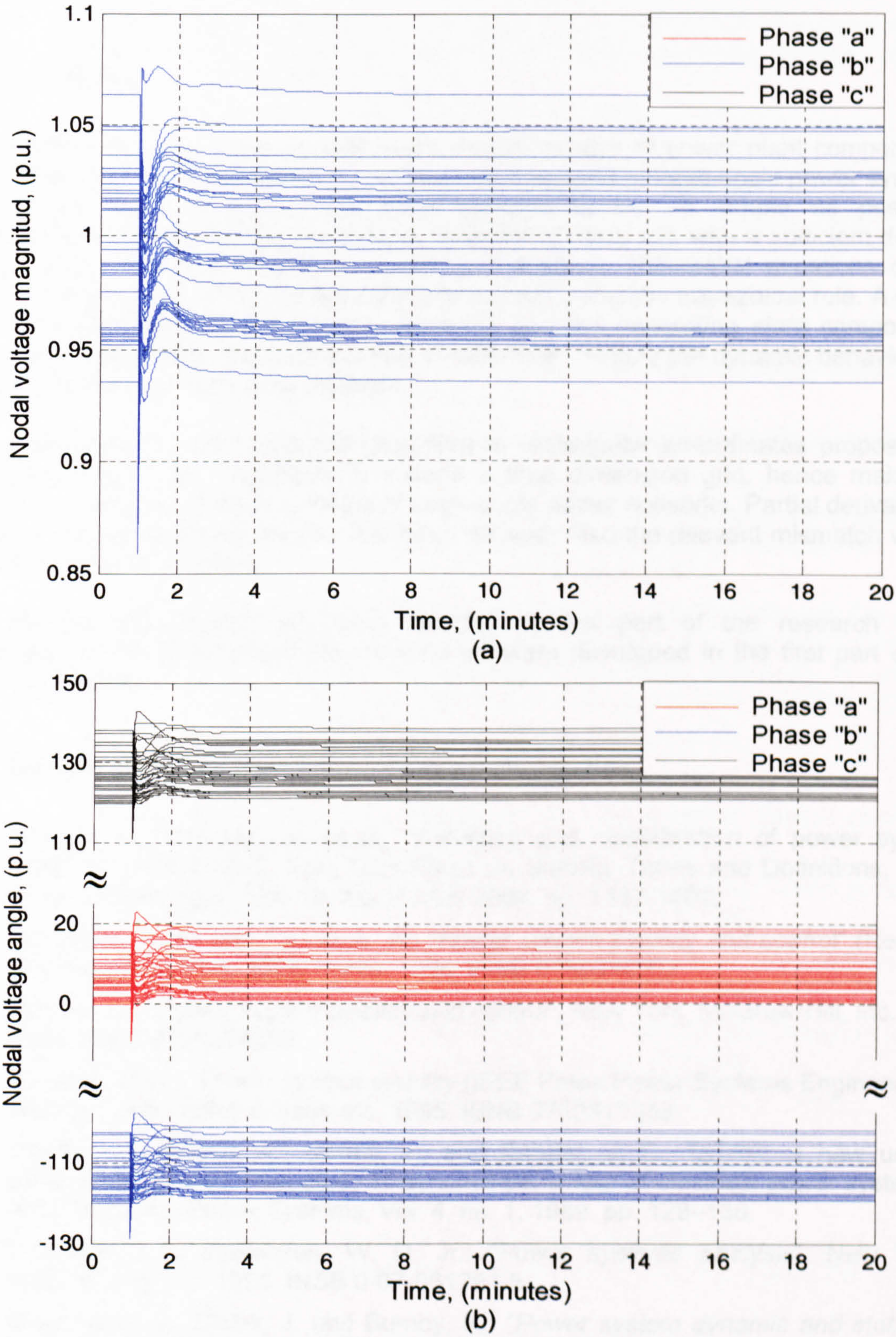

Figure 5.26 Nodal voltage of the system following a generator disturbance; (a) magnitude and (b) phase angle

5.16 Summary

This chapter has presented several mathematical models of power plant components. The dynamic power flow algorithm is aimed at the solution of large-scale power systems and hence, these models have been selected to be as simple as possible. Nevertheless, they have been judiciously selected to carry out, with a sufficient degree of accuracy, three-phase dynamic power flow analysis. Differential equations of the various models have been algebraically represented using the trapezoidal rule. A set of non-linear equations for the network elements and the generating plant components have been assembled in a unified frame of reference to study the dynamic behaviour of large-scale three-phase power systems.

The three-phase Newton-Raphson algorithm in rectangular co-ordinates proposed in Chapters 4 has been expanded to include a time dimension grid, hence making it possible to carry out dynamic studies of large-scale power networks. Partial derivates of the power plant model equations have been derived. Also the relevant mismatch vector equations have been given.

The simultaneous-solution approach adopted in this part of the research takes advantage of the three-phase steady-state software developed in the first part of the research project.

5.17 References

[1] Kundur, P., Paserba, J., *et al.*: "Definition and classification of power system stability", IEEE/CIGRE Joint Task Force on Stability Terms and Definitions, IEEE *Trans. Power Syst.*, Vol. 19, No. 2, May 2004. pp. 1387-1401.

[2] Anderson, P. M. and Fouad, A. A.: "*Power system stability and contro*l" (Revised Printing). New York: IEEE *Press*. 1994. INSB 0780310292

[3] Kundur, P.: "*Power system stability and control*'. New York, McGraw-Hill, Inc. 1994. ISNB 0780334639

[4] Kimbark, E.W.: "*Power system stability* (IEEE Press Power Systems Engineering Series)", John Wiley & Sons Inc, 1995. ISNB 0780311353.

[5] Stubbe, M., Bihain, A., Deuse, J., and Baader, J. C., "STAG, a new unified software program for the study of dynamic behaviour of electrical power systems", IEEE *trans. on Power Systems*, Vol. 4, no. 1, 1989. pp. 129–138.

[6] Grainger, J.J., Stevenson, W. D. Jr.: "*Power systems analysis*", New York, McGraw-Hill, Inc. 1994. INSB 0-07-061293-5

[7] Machowski, J., Bialek, J. and Bumby, R.: "*Power system dynamic and stability*", John Wiley and Sons Ltd, Chichester, UK. 1997. INSB 0471956430.

[8] Byerly, R.T. and Kimbark, E.W.: "Stability of large electric power systems", IEEE press, New York, USA, 1974, ISNB 0-87942-037-5

[9] Van Cutsem, T., Jacquemart, Y., Marquet, J. N., and Pruvot, P., "Comprehensive analysis of mid-Term, voltage stability", IEEE *Trans. on Power System*, Vol. 10, Aug. 1995. pp. 1173–1182.

[10] Ajjarapu, V. and Christy, C.: "The continuation power flow: A tool for steady-state voltage stability analysis", IEEE PICA *Conference Proc.* May 1991. pp. 304-311.

[11] Johnson, R.B.I., Short, M.J., and Cory, B.J.: "Improved simulation techniques for power system dynamics", IEEE *Trans., Power System*, Vol. 3, No. 4, 1988. pp. 1691-1698.

[12] Stott, B.: "Power system dynamic response calculations", IEEE *Proc.*, Vol. 67, Feb. 1979. pp. 219-241.

[13] Dommel, H. W. and Sato, N.: "Fast transient stability solutions", IEEE *Trans PAS-91*, No. 4, July/Aug. 1972. pp. 1643-1650.

[14] Burden, R. and Fires, J.: "Numerical analysis", Seventh Edition, Brooks/Cole Pub Co, 2000. INSB: 0534382169.

[15] Xu, X., Mathur, R. M., Rogers, G. J., and Kundur, P., "Modeling of generators and their controls in power system simulations using singular perturbations", IEEE *Trans. on Power Syst.*, vol. 13, no. 1, Feb. 1998. pp.109–114.

[16] Power System Engineering and Electric Machinery Committees on the IEEE power Engineering Society. *IEEE Standard* 1110-2002, (revision of 1110-1991): "IEEE guide for the synchronous generator modelling practices in stability analyses", Institute of Electrical and Electronics Engineers, New York, Inc. 2002.

[17] Crary, S.B.: "*Power system stability*", John Wiley & Sons Inc., New York USA, 1950. ISNB 0178635898

[18] Stagg G.W. and El-Abiad A.H.: "*Computer methods in power system analysis*", McGraw-Hill, 1968. ISBN 67-12963-07-060658-7

[19] Arrillaga, J. and Watson, N.R.: "*Computer modelling of electrical power systems*", John Wiley & Sons Inc. Chichester, UK. 1997. INSB 0471872490

[20] Dorf, R. C.: "*The electrical engineering handbook*", CRC Press LLC, Boca Raton, USA, 2000, ISNB 0849385741

[21] Rafian, M., and Laughton, M.A.: "Determination of synchronous machine phase co-ordinate parameters", IEE *Proc.*, Vol. 123, 1976. pp. 818–824.

[22] Park, R. H., "Two-reaction theory of synchronous machines," Part I, AIEE *Transactions*, Vol. 48, 1929. pp. 716-730.

[23] Park, R. H., "Two-reaction theory of synchronous machines," Part II, AIEE *Transactions*, Vol. 52, 1933. pp. 352-355.

[24] Kim, J., Moon, S., Kim K.: "A study on an AVR parameter tuning method using real-time simulator", IEEE *Power Eng. Soc. Summer Meeting*, 2000, Vol. 3, July 2000. pp.1936-1941.

[25] Hirayama, K.; Tone, Y., at al,: "Digital AVR application to power plants"; IEEE *Trans. Energy Conv.*, Vol. 8, No. 4, Dec. 1993. pp. 602–609.

[26] Seaman, C.E.: "Design of a novel digital automatic voltage regulator", IEE *Coll. Gen. Exc. Syst. and Stab.*, Feb 1996. pp. 5/1 - 5/4.

[27] Elsedawi, I.R., Elassal, E.H., and Azzouz, E.M.: "Effects of AVR systems on the performance of synchronous generators", IEEE *Canadian Conf. Elect. & Comp. Eng.* CCECE'97. Vol. 1. May. 1997. pp.47-50.

[28] Rafian, M., Sterling, M.J.H, and Irving, M. R.: "Real-time power systems simulation" *IEE Proc.* Vol. 134. Pt. C. No. 3, May 1987. pp. 206-1988.

[29] Berry, T., Dale, L.A., Daniels, A.R. Dunn, R.W.: "Real time modelling of multimachine power system", IEE *Proc.-C*, Vol. 140, No. 4, July 1993. pp. 241-248

[30] Do, V., Barry, A. O.; "A real-time model of the synchronous machine based on digital signal processors", IEEE *Trans. App. Supercond.*, Vol.3 No. 1,. March 1993. pp 60-66.

[31] IEEE Committee Report, "Computer representation of excitation systems", IEEE *Trans.* PAS-87, No. 6, June 1968, pp 60-66.

[32] Fasol, K.H: "A short history of hydropower control", IEEE *Control Systems Magazine*, Vol. 22, Issue 4, Aug. 2002. pp. 68–76.

[33] De Jaeger, E., Janssens, N.L:, Malfliet, B, and Van De Meulebroeke, F.: "Hydro turbine model for system dynamic studies", IEEE *Trans. Power Syst.*, Vol. 9, No. 4, Nov. 1994. pp. 1709-1715.

[34] Vournas, C.D.: "Second order hydraulic turbine models for multimachine stability studies", IEEE *Trans. Energy Conv.*, Vol. 5, Issue 2, June 1990. pp. 239–244.

[35] IEEE committee report: "Dynamic models for steam and hydro turbines in power system studies", IEEE *trans.* Vol. PAS-92 1973. pp.1904-1915.

[36] Working group on prime mover and energy supply models for system dynamic performance studies; "Hydraulic turbine and turbine control models for system dynamic studies", IEEE *Trans. Power Syst.*, Vol. 7, Issue 1, Feb. 1992. pp: 167–179.

Chapter 6

DYNAMIC PHASE-DOMAIN MODELLING OF VSC-BASED FACTS CONTROLLERS

6.1 Introduction

Recent power system "black-outs" in North America and Europe have highlighted the vulnerability of today's power networks and has given renewed encouragement to power systems researchers to develop new models and methods with much improved functionality aimed at preventing widespread outages [1-3]. The versatility of the steady-state three-phase power flow algorithm with provisions for VSC-based FACTS controllers has already been demonstrated in both polar and rectangular co-ordinates. Building on these research developments, this chapter presents dynamic models of the VSC-based FACTS controllers in the phase frame of reference suitable for direct incorporation into a dynamic power flow algorithm.

As discussed in Chapter 2, VSC-based controllers employ inverters whose operational characteristics resemble those of synchronous voltage sources [9-10]. If employed as shunt devices, they behave analogously to synchronous condensers, except that VSCs have no mechanical inertia, and are therefore capable of responding much more rapidly to changing system conditions; they do not contribute short circuit current, they have no moving parts, and they have a symmetric lead-lag capability [11-16]. Theoretically, a VSC-based controller can go from full lag to full lead in fractions of a cycle. In the present research work, relating to power system long-term dynamic assessment, VSC-based controllers are modelled as having a quasi-instantaneous response to the set voltages and powers. From this perspective the controllers may be assumed to be ideal, with an almost instantaneous speed of response. The justifications for this modelling approach are the very small time constants that VSC-based FACTS controller have, which use IGBT devices, and the very long time constants associated with long-term dynamics.

6.2 Static Synchronous Compensator

The performance of the STATCOM is analogous to that of the rotating synchronous condenser, but its response time is much faster, it can be used in a similar way to the synchronous condenser to provide dynamic compensation to a transmission system [15]. Its speed of response enables increased transient stability margins, voltage support enhancements, and damping of low frequency oscillation. The three-phase voltage generated by the STATCOM is adjusted with little delay by virtue of semiconductor device switching [9-10].

The main operational objective of the STATCOM is to increase power transmission capability by voltage control at the point of connection of the power network. The dynamic behaviour of the compensator, in the normal compensating range, is well characterized by the transfer function block diagram shown in Figure 6.1. In standard control mode, the STATCOM is operated as a voltage regulator; when a disturbance occurs, and as result V_{bus} drops (or rises), the voltage source V_{vR} is adjusted. This enables the set voltage to be kept by supplying or absorbing reactive power to the system.

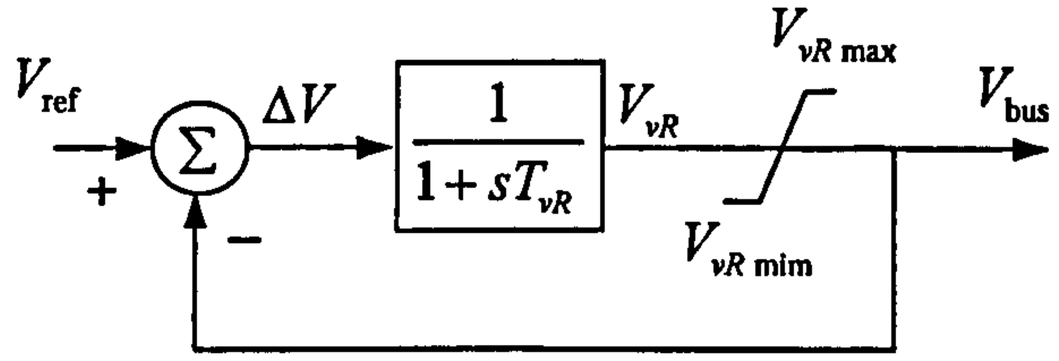

Figure 6.1 STATCOM linear model for voltage magnitude control

Due to the very fast response of the VSC, values of T_{vR} are in the order of μs. The STATCOM can be seen as a ideal voltage regulator for long-term dynamic power flows. In other words V_{bus} is maintained at the set value V_{ref} in the face of disturbances, causing voltage variation, and the STATCOM dynamic model should not be necessarily included in the algorithm. Instead, the steady-state model developed for the power flow solution is used.

The differential equations, state variables and control input parameters can be arranged as follows

$$\Delta V = V_{ref} - V_{bus} \tag{6.1}$$

$$\frac{dV_{vR}}{dt} = \frac{\Delta V - V_{vR}}{T_{vR}} \qquad V_{vR\ min} \le V_{vR} \le V_{vR\ max} \tag{6.2}$$

where

V_{bus} is the nodal voltage magnitude
V_{vR} is the voltage source converter
T_{vR} is the transient time constant
V_{ref} is the pre-specified reference voltage (magnitude)

The ordinary differential equation of the STATCOM (6.2) is transformed into an algebraic equation, to be solved simultaneously with the algebraic equations representing the network and the generating plant equations, which are already available in algebraic form. Applying trapezoidal rule, the algebraic form of the STATCOM differential equation becomes

$$V_{vR(t)} = V_{vR(t-\Delta t)} + \frac{\Delta t}{2}\left[\left.\frac{dV_{vR}}{dt}\right|_{(t)} + \left.\frac{dV_{vR}}{dt}\right|_{(t-\Delta t)}\right] \tag{6.3}$$

Substitution of equation (5.10) in (6.3) and grouping terms together gives

$$f_{(t)}\left(V_{vR}\right) + f_{(t-\Delta t)}\left(V_{vR}\right) + k_{(V_{vR})} = 0 \tag{6.4}$$

where

$$f_{(t)}\left(V_{vR}\right) = V_{vR(t)} + \frac{\Delta t}{2}\left[\frac{V_{\text{bus}(t)} + V_{vR(t)}}{T_{vR}}\right] \tag{6.5}$$

$$f_{(t-\Delta t)}\left(V_{vR}\right) = -V_{vR(t-\Delta t)} + \frac{\Delta t}{2}\left[\frac{V_{\text{bus}(t-\Delta t)} + V_{vR(t-\Delta t)}}{T_{vR}}\right] \tag{6.6}$$

$$K_{(V_{vR})} = -\frac{\Delta t}{T_{vR}} V_{\text{ref}} \tag{6.7}$$

The Jacobian elements for the STATCOM are

$$\frac{\partial f\left(V_{vR}\right)}{\partial e} = \frac{\Delta t}{2T_{vR}} \frac{e}{\left(e^2 + f^2\right)^{1/2}} \tag{6.8}$$

$$\frac{\partial f\left(V_{vR}\right)}{\partial f} = \frac{\Delta t}{2T_{vR}} \frac{f}{\left(e^2 + f^2\right)^{1/2}} \tag{6.9}$$

$$\frac{\partial f\left(V_{vR}\right)}{\partial V_{vR}} = 1 + \frac{\Delta t}{2T_{vR}} \tag{6.10}$$

In this research it is assumed that the STATCOM have a delay-free impact on the network control, hence the dynamic equations of the closed loop controls are not used. Instead, the steady-state model developed for the power flow solution is used.

6.2.1 Voltage magnitude control using STACTCOMs in dynamic power flows

The New England test system shown in Figure 4.3 and used in the previous chapter for disturbance analysis is used to investigate the effectiveness of the STATCOM model to maintain stability following a three-phase load trip. Using the software developed, a dynamic power flow analysis was carried out. The STATCOM is connected at bus 17 and set to maintain the nodal voltage magnitude at one per unit. The objective of this simulation is to assess the capability of the controller to keep a constant voltage magnitude at the connecting bus and to improve transient stability. The scenario

considered in this simulation is the same as in Section 5.10, where the power system has no STATCOM. The balanced three-phase load trips out for two minutes and then becomes reconnected.

Figure 6.2 and Figure 6.3 show the generating plant responses to the three-phase load trip. Figure 6.2(a) gives less than 0.1% frequency fluctuations during the first swing; and an even smaller frequency following load reconnection. From (b), it can be seen that angular differences are also fairly small. In (c), the excitation voltages exhibit, at first, variations and then settle to their pre-load-trip values. The active power outputs, shown in (d), exhibit very little change other than a power reduction following the load tripping, (d). The mechanical parameters are shown in Figure 6.3(a-d), where it can be observed that the most significant changes take place in the governor HP steam turbine parameters during the connection and disconnection of the load. In contrast very little changes is exhibited by the IP and the LP steam turbine parameters.

Analyses of Figure 6.4 show that significant changes occur in nodal voltage magnitudes when the STATCOM is present in the network compared with the case study where no STATCOM is included. For one the voltage magnitude in the STATCOM bus is maintained at its set value of one per unit. Keeping the voltage magnitude at the STATCOM bus at one per unit smooths out the recovery of the system after a disturbance has occurred, moving the system away from the possibility of voltage instability.

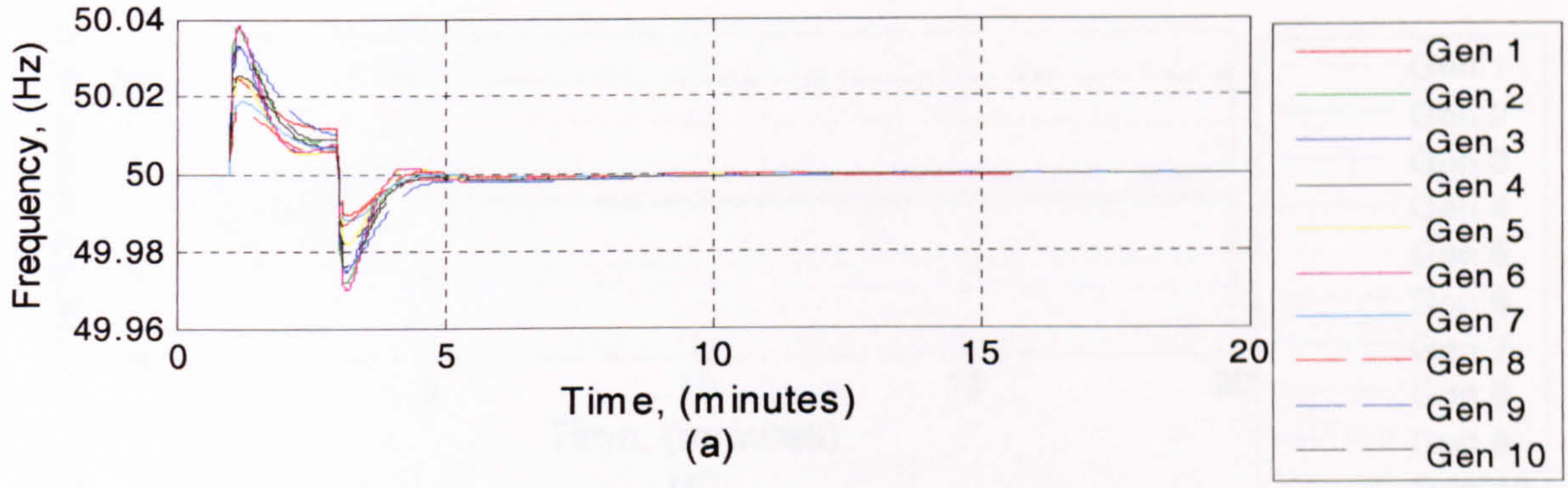

Figure 6.2 Generating plant responses of the system with one STATCOM; (a) frequency; (b) load angle; (c) excitation voltage; (d) active power

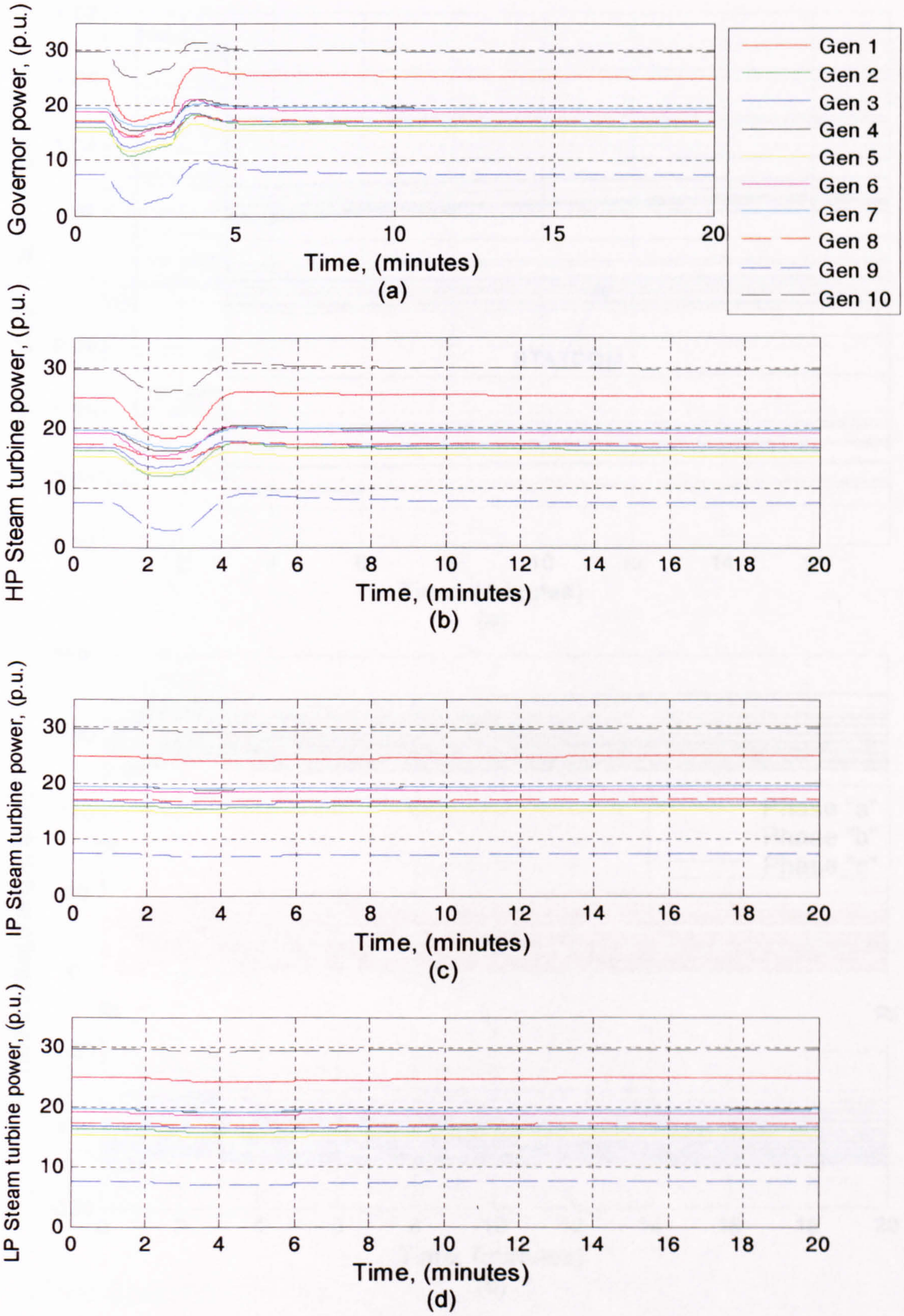

Figure 6.3 Generating plant responses of the system with one STATCOM; (a) governor power; steam turbine (b) HP; (c) IP; (d) LP

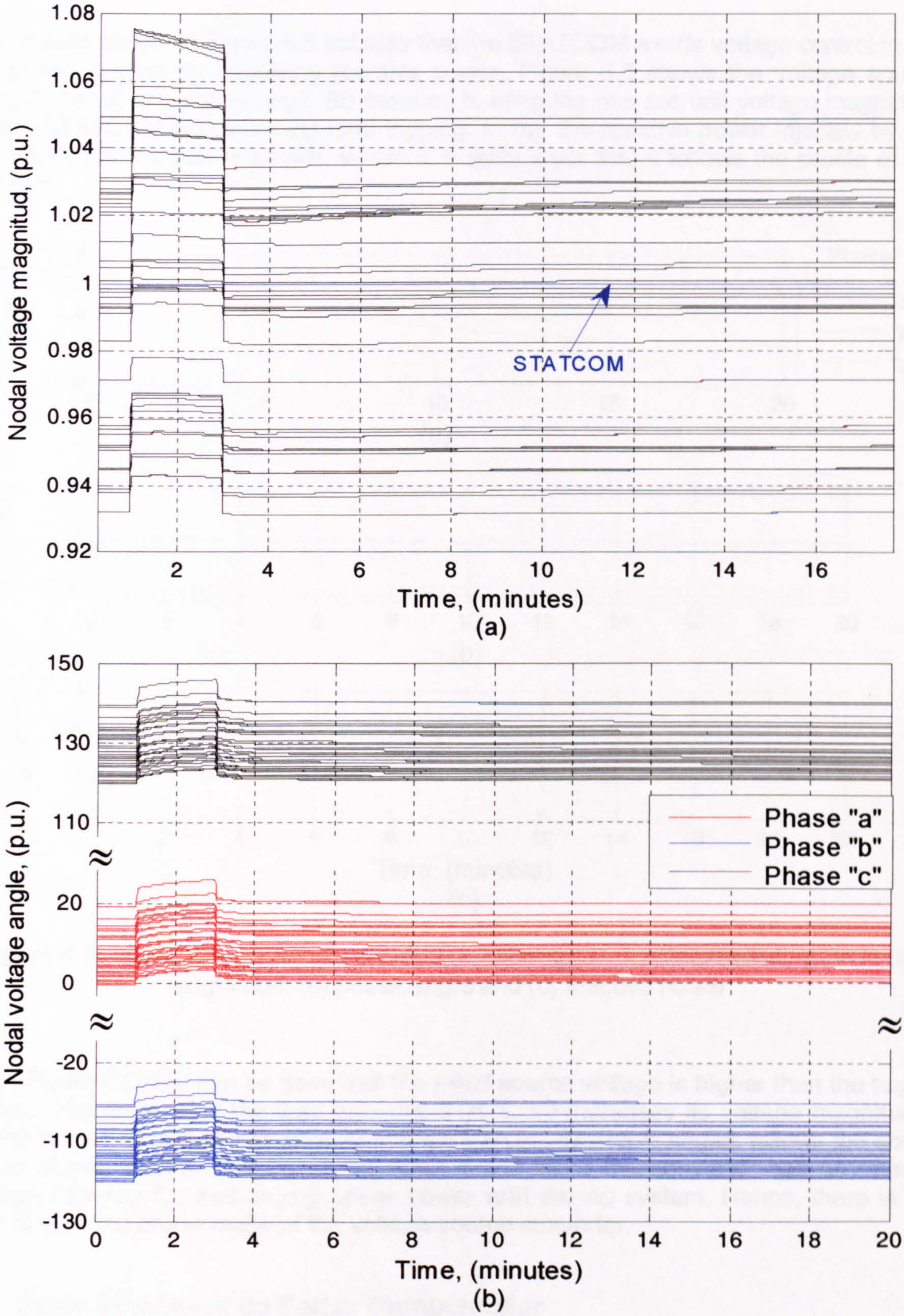

Figure 6.4 Nodal voltage responses of the system with one STATCOM; (a) magnitude and (b) phase angle

The results shown in Figure 6.5 indicate that the STATCOM exerts voltage control in the AC power system by supplying reactive power. Figure 6.5 shows the voltage source magnitude (a) and phase angle (b) required to keep the one per unit voltage magnitude at the STATCOM bus following load tripping. In (c), the reactive power injected by the STATCOM at the bus is shown, where it is quite clear that it follows the profile of the voltage.

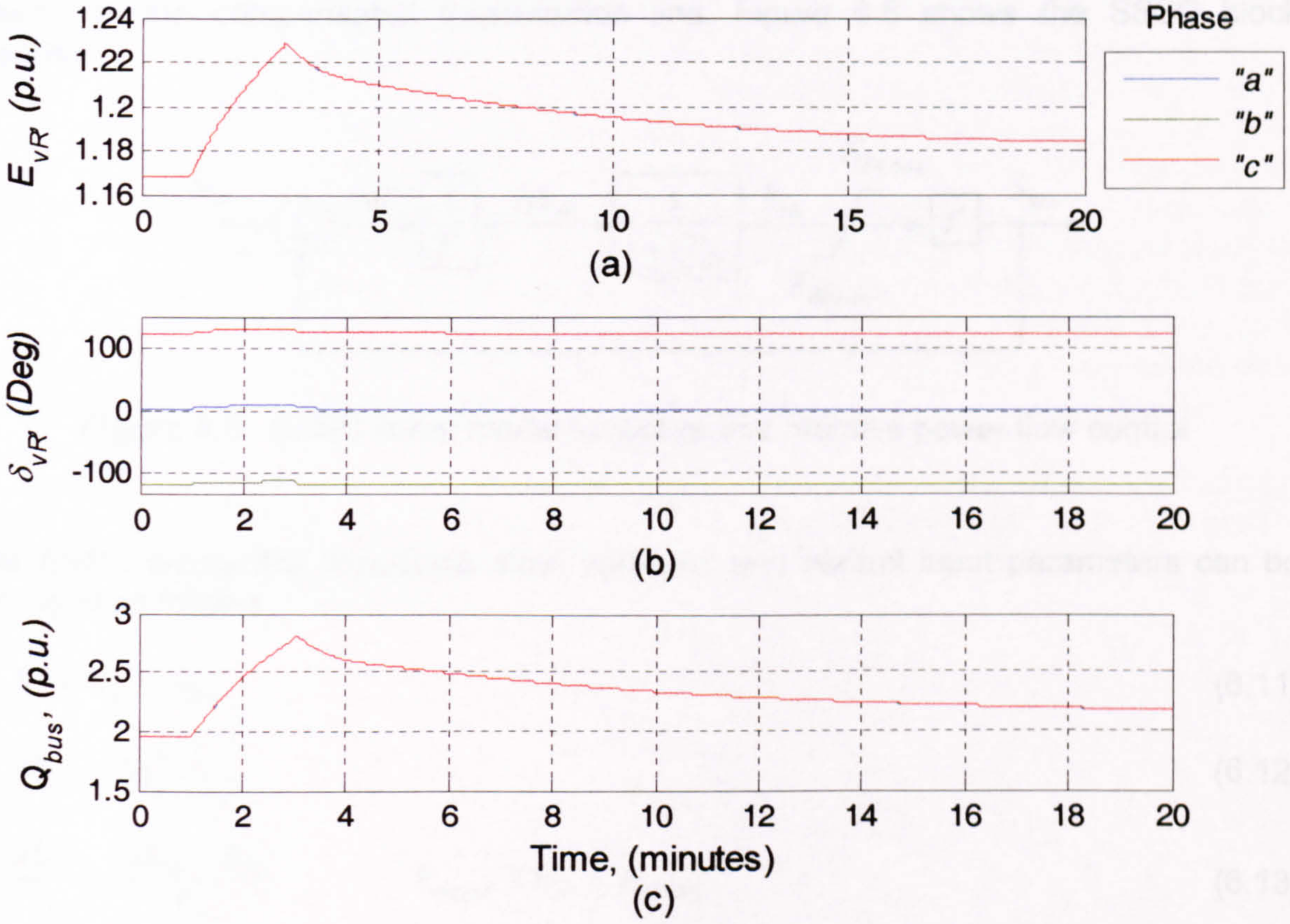

Figure 6.5 STATCOM internal parameters following a load disturbance; voltage (a) magnitude; (b) phase angle and (c) reactive power

From Figure 6.5(a) it can be seen that the initial source voltage is higher than the target voltage. However, after the load trips the STATCOM increases its voltage magnitude. From Figure 6.5(b), it can be noticed that the STATCOM phase angles follows the nodal phase angles pattern. This is an expected result since the converter has no energy storage capacity for exchanging active power with the AC system. Hence, there is no control over the phase angle of the voltage source converter.

6.3 Static Synchronous Series Compensator

The SSSC resembles a STATCOM, which generates a controllable AC voltage source, except that the SSSC is connected in series with the AC system, as opposed to being a

shunt-connected controller. As a result of this the SSSC series voltage is in quadrature with the line current and acts like an equivalent inductive or capacitive reactance to control power flow in the compensated transmission line. The SSSC, just like the STATCOM, works as a voltage regulator, which computes the converter voltage E_{cR} required to obtain the desired injected voltage; the voltage regulation is assisted by a feed-forward type regulator that measure the injected voltage. General applications of the SSSC are power flow control, and voltage and phase angle stability enhancement [16-17]. In the present research, the SSSC is used to control active and reactive power flowing in the compensated transmission line. Figure 6.6 shows the SSSC block diagram.

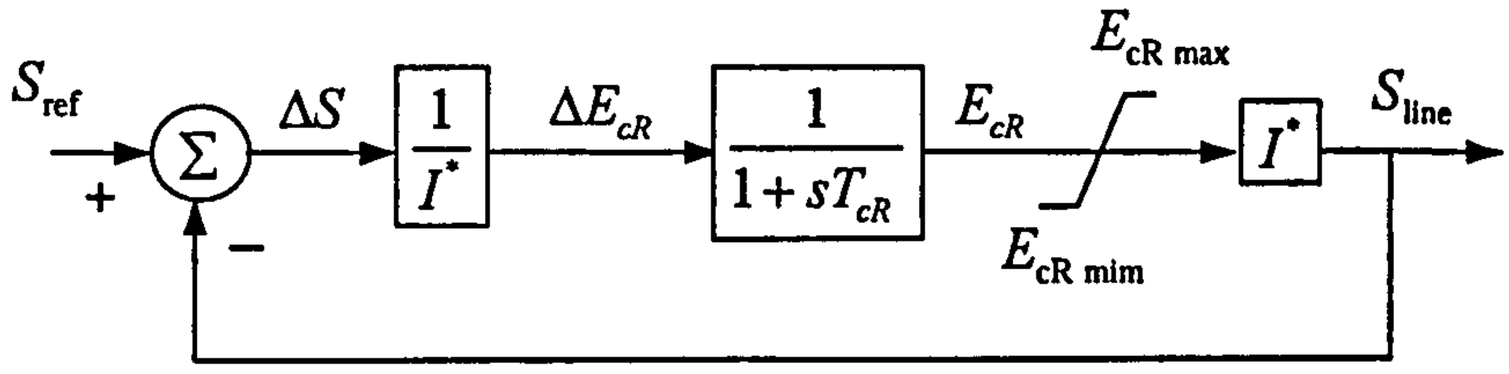

Figure 6.6 SSSC linear model for active and reactive power flow control

The SSSC differential equations, state variables and control input parameters can be arranged as follows

$$\Delta S = S_{ref} - S_{line} \tag{6.11}$$

$$\Delta E_{cR} = \Delta S\left(\frac{1}{I^*}\right) \tag{6.12}$$

$$\frac{dE_{cR}}{dt} = \frac{\Delta E_{cR} - E_{cR}}{T_{cR}} \qquad E_{cR\,min} \le E_{cR} \le E_{cR\,max} \tag{6.13}$$

where

S_{line} is the complex power flowing in the transmission line
S_{ref} is the target complex power
I^* is the complex current
T_{cR} is the transient converter time constant
E_{cR} is the voltage source converter

6.3.1 Power flow control using SSSCs in dynamic power flows

The New England test system is used to investigate the effectiveness of the SSSC model in a three-phase dynamic power flow solution. The study is carried out for the case when a SSSC is connected between bus 17 and an auxiliary bus, aiming at

controlling active and reactive power flows, leaving bus 17 towards bus 16, at 100 MW and 20 MVAR per phase, respectively.

The objective of the study is to assess the effectiveness of the SSSC in maintaining power flow control at set values during a non-steady state. The disturbance is assumed to be the same as in Section 5.10: a three-phase load tripping out for time duration of 2s.

The response of the generating plants to a three-phase load tripping out, with an SSSC embedded in the system, is shown in Figure 6.7 and Figure 6.8. From Figure 6.7(a), it can be seen that during the first swing the frequency increases by almost 0.05 Hz; in (b) some generators increase the difference load angle by a few degrees, but then they remain constant. In (c) the excitation voltage of some generators decrease during the first swing and an increase in recovering time of those generators can be appreciated. In (d), there are no significant changes in active power generation other than those done to the reduction of active power during load tripping. As shown in Figure 6.8, changes in the mechanical parameters are confined to the governors and there is gradual reduction in the values of these parameters following the load tripping and then a gradual increase once the load has been reconnected.

From Figure 6.9 (a), it can be noticed that there is a steep voltage magnitude increase during the first swing, only to be following by a voltage decrement once the load is reconnected. From then on the recovery is steady but long. The phase angles on the other hand, are rapidly stabilised.

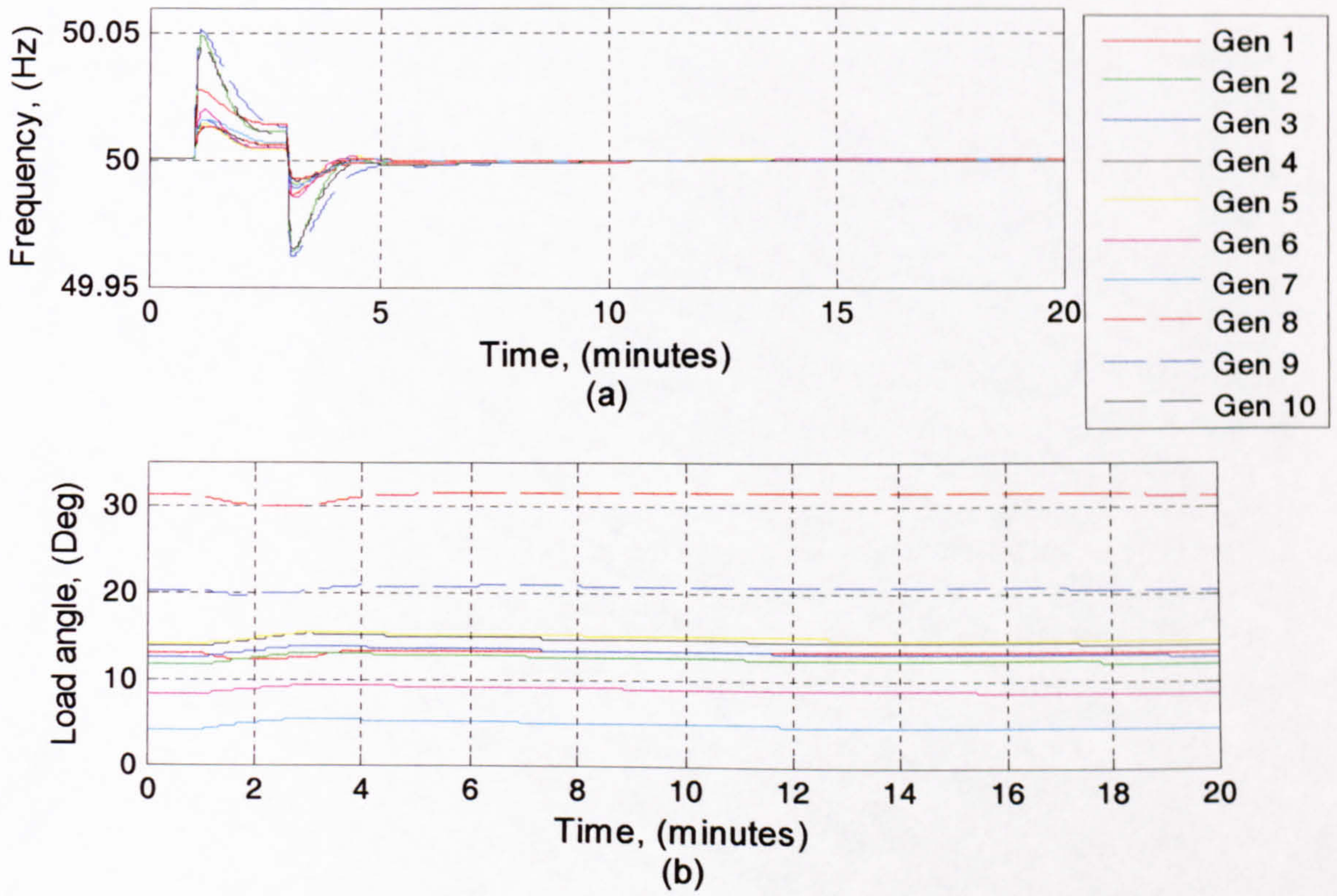

Figure 6.7 Generating plant responses of the system with a SSSC embedded; (a) frequency; (b) load angle; (c) excitation voltage; (d) active power

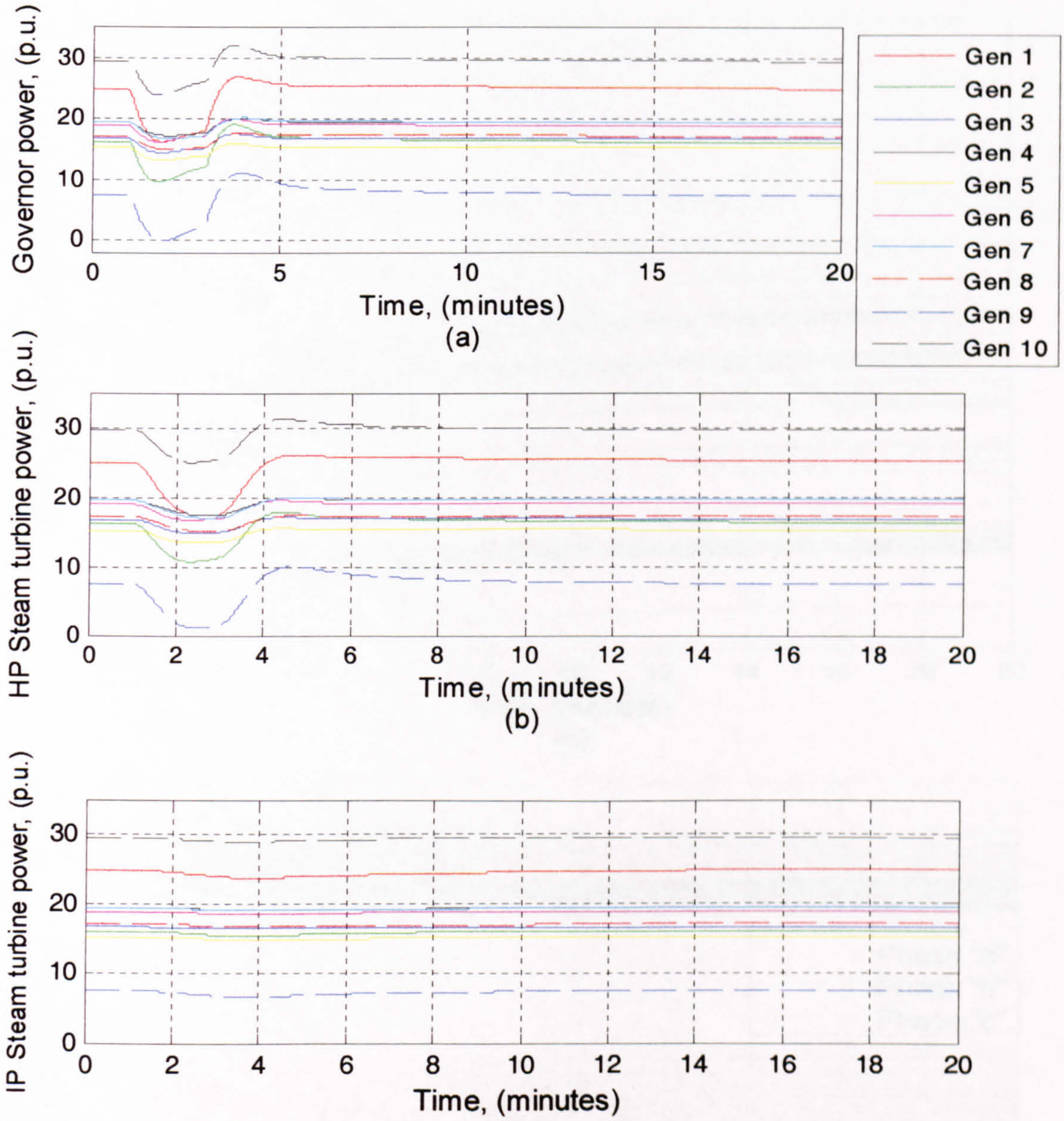

Figure 6.8 Generating plant responses of the system with a SSSC embedded; (a) governor power; steam turbine (b) HP; (c) IP; (d) LP

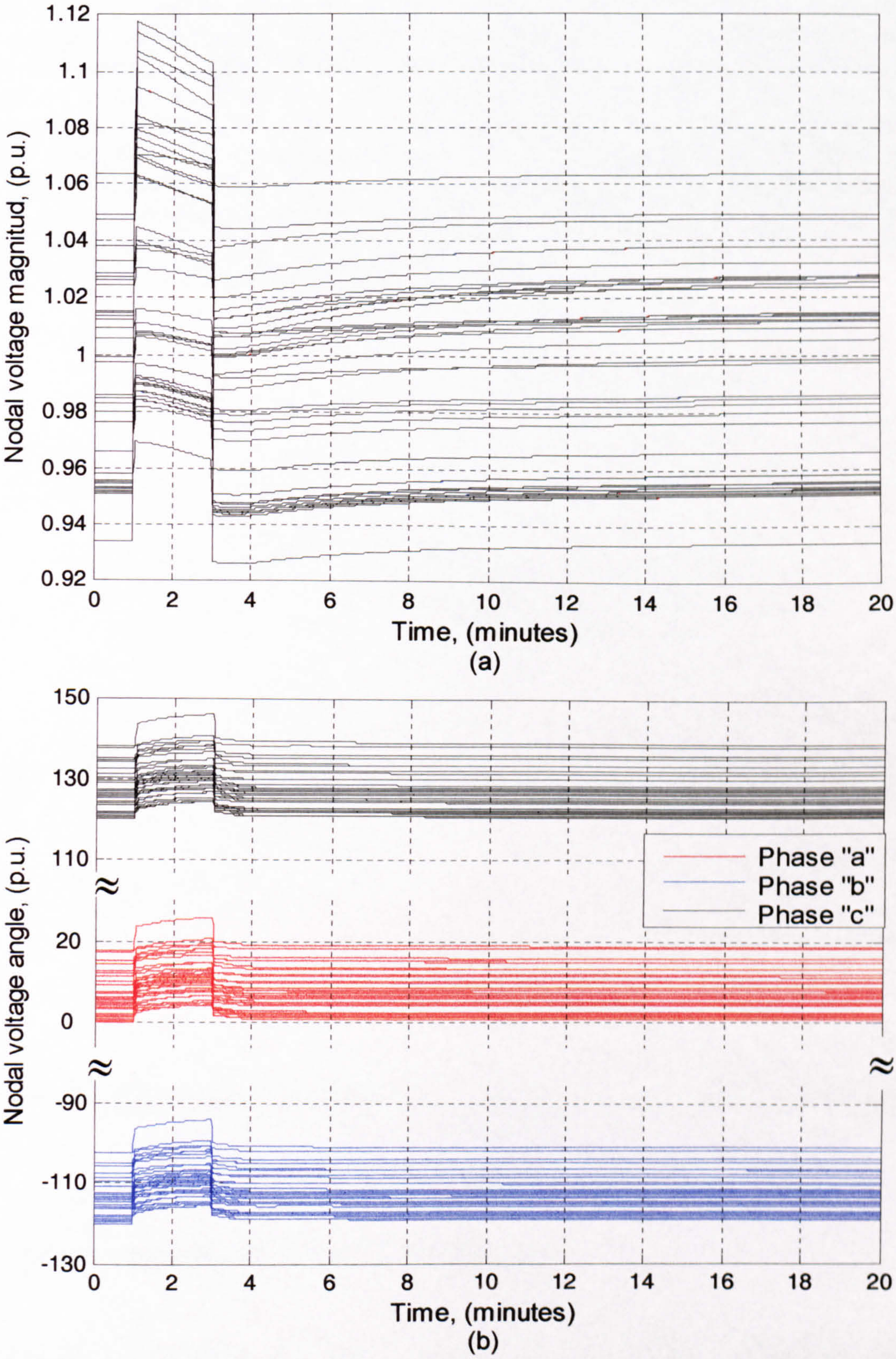

Figure 6.9 Nodal voltage responses of the system with a SSSC embedded; (a) magnitude and (b) phase angle

Figure 6.10 (a) and (b) show the series voltage source parameters, magnitude and phase angles, respectively. The SSSCs, as expected, keeps the active and reactive power flows at the specified values for the time duration of the study. To achieve control the source output is adjusted to inject the right amount of series voltage to the line. During the disturbance, the series voltage source demands a significant increase in its voltage magnitude by a significant margin, although it returns to its initial values following reconnection of the load. It can be noticed from Figure 6.10(b), that the voltage source phase angles are in quadrature with the nodal voltage phase angles; the voltage steps influence the voltage source phase angles, however, their recovery process follows that of the nodal voltage angular pattern.

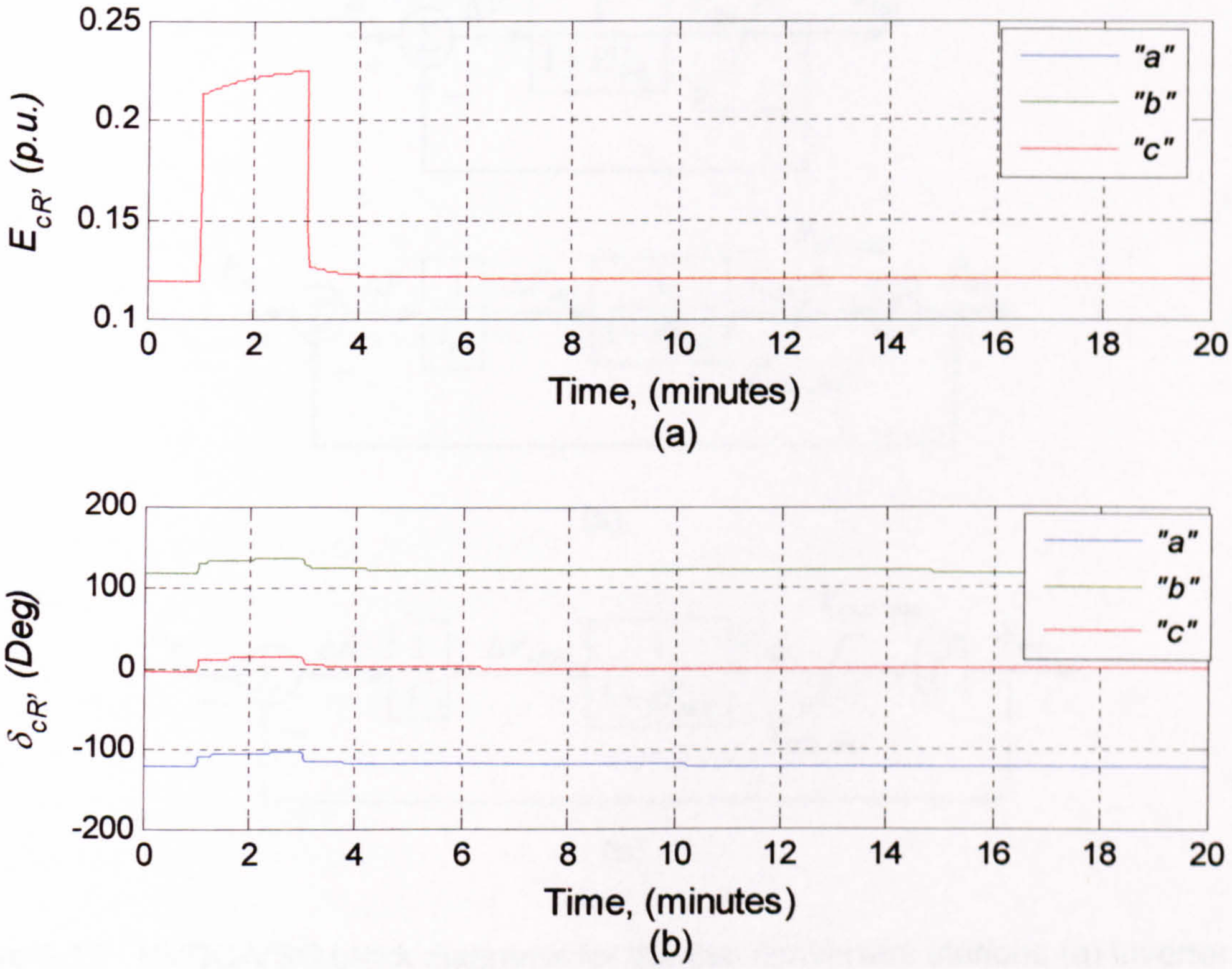

Figure 6.10 SSSC parameter responses to a load disturbance; Voltage (a) magnitude and (b) phase angle

6.4 High-Voltage Direct Current VSC-based

The HVDC VSC-based can be represented by two shunt-connected voltage sources (rectifier and inverter) and an active power constraint equation. The main characteristic of the HVDC-VSC controller is its ability to independently control active power and reactive power or voltage magnitude at their connecting AC

systems buses. In the present research both converter controllers are considered to be identical. The two controllers act independently from one other with no communication between them. They are used to control active and reactive powers at the rectifier side and nodal voltage at the inverter side. It should be remarked that voltage control at the inverter AC bus is carried out in the same way as for the STATCOM (Section 6.3) and one feedback loop for active power. The rectifier uses a feedback loop for complex power in the same way as for the SSSC.

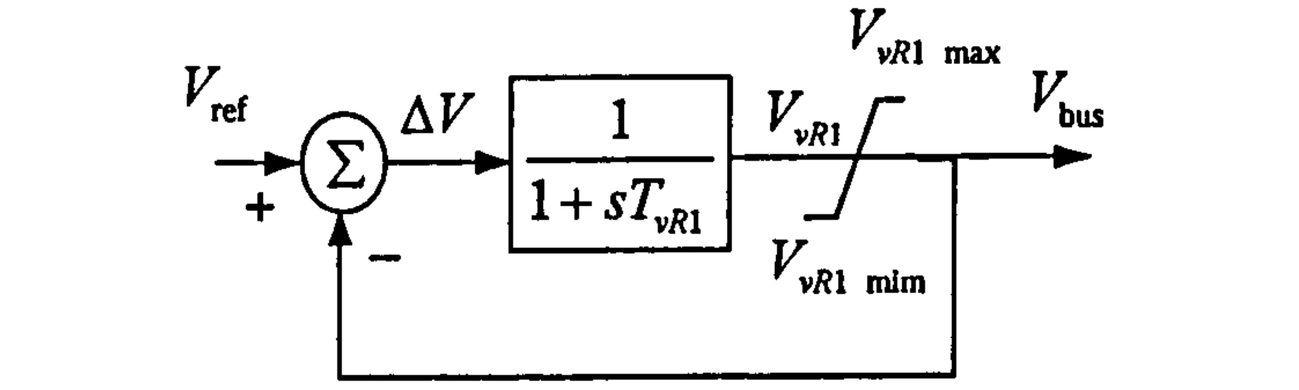

(a)

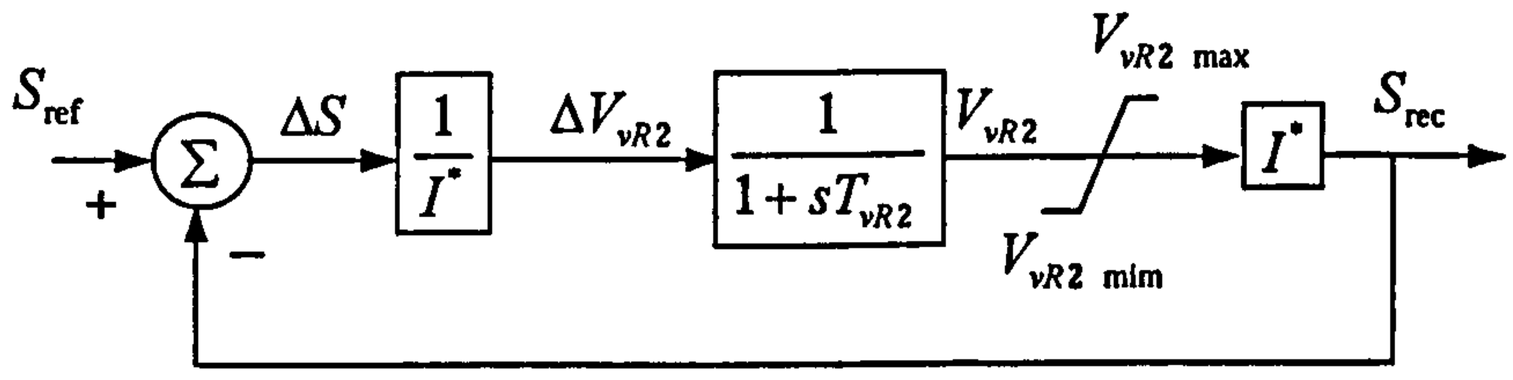

(b)

Figure 6.11 HVDC-VSC block diagrams for the two converters stations (a) inverter and (b) rectifier

The differential equations and control input parameters of the HVDC-VSC can be arranged as follows:

For inverter voltage control:

$$\Delta V = V_{ref} - V_{bus} \tag{6.14}$$

$$\frac{dV_{vR1}}{dt} = \frac{(V_{ref} - V_{bus}) - V_{vR1}}{T_{vR1}} \qquad V_{vR1\ min} \le V_{vR1} \le V_{vR1\ max} \tag{6.15}$$

For active power control:

$$\Delta P = P_{\text{ref}} - P_{\text{inv}} \tag{6.16}$$

$$\Delta V_{cR1} = \Delta P\left(\frac{1}{I^{*}_{inv}}\right) \tag{6.17}$$

$$\frac{dV_{vR1}}{dt} = \frac{\Delta V_{vR1} - V_{vR1}}{T_{vR1}} \qquad V_{vR1\ \min} \le V_{vR1} \le V_{vR1\ \max} \tag{6.18}$$

For rectifier complex power control:

$$\Delta S = S_{\text{ref}} - S_{\text{line}} \tag{6.19}$$

$$\Delta V_{vR2} = \Delta S\left(\frac{1}{I^{*}_{\text{rec}}}\right) \tag{6.20}$$

$$\frac{dV_{vR2}}{dt} = \frac{\Delta V_{vR2} - V_{vR2}}{T_{vR2}} \qquad V_{vR2\ \min} \le V_{vR2} \le V_{vR2\ \max} \tag{6.21}$$

where

V_{bus} is the nodal voltage magnitude
V_{vR1} is the voltage source converter (rectifier)
V_{vR2} is the voltage source converter (inverter)
V_{ref} is the pre-specified reference voltage (magnitude)
P_{inv} is the complex power flowing at the transmission line
P_{ref} is the complex power to be controlled
I^{*} is the complex current
T_{vR1} is the rectifier transient time constant
T_{vR2} is the inverter transient time constant

6.4.1 Power flow control using an HVDC-VSC

The HVDC-VSC test case involves a back-to-back HVDC replacing the SSSC used in Section 6.41 connected at the sending end of the transmission line linking buses 16 and 17. An auxiliary bus is used to connect the HVDC-VSC, which is used to keep the nodal voltage magnitude in bus 16 at one per unit and to maintain active power flowing from the auxiliary bus towards bus 17 to 100 MW per phase. The HVDC-VSC is set to keep the control parameters at their reference values for the whole of the simulation study.

The generating plant responses to the load tripping event, for this test case, are shown in Figure 6.12 and Figure 6.13, whereas Figure 6.14 shows the nodal voltages.

From Figure 6.12(a), it can be seen that the frequency response increases during the first swing by about 0.05 Hz; In (b), the phase angular differences are given and show little sign of perturbation. In (d), active power generations show very little change other than the power drop in response to the load trip event. In (c) the excitation voltage of some generators drop during the first swing and then recovering to their pre-disturbance values. From Figure 6.13(a-d), it can be seen that the governor and the HP steam turbine powers drop as required in the system following the load tripping. The LP and IP steam turbine parameters show little change.

By comparing the results in Figure 6.14 and Figure 5.13, it can be seen that major changes take place in nodal voltage magnitudes when the system contains an HVDC-VSC controller. The most important change, with respect to network with no HVDC-VSC controller, is that the voltage magnitude in the bus supported by the HVDC-VSC controller is maintained at the established value of 1.0 p.u. Keeping the voltage magnitudes at the HVDC bus constant smooth out the recovery process back to the steady-state thus enhancing transient stability.

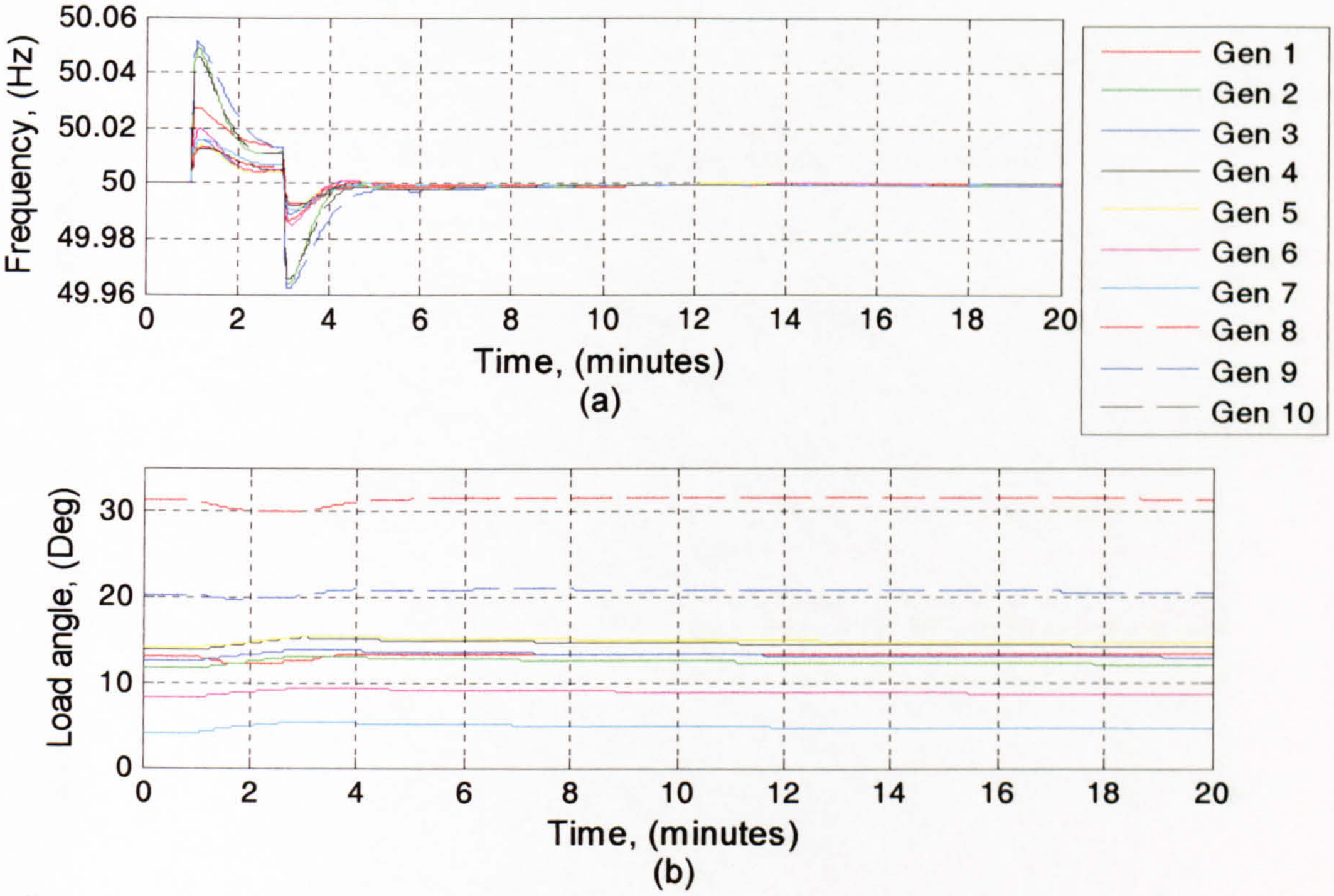

Figure 6.12 Generating plant responses of the system with a BTB HVDC embedded; (a) frequency; (b) load angle; (c) excitation voltage; (d) electrical active power

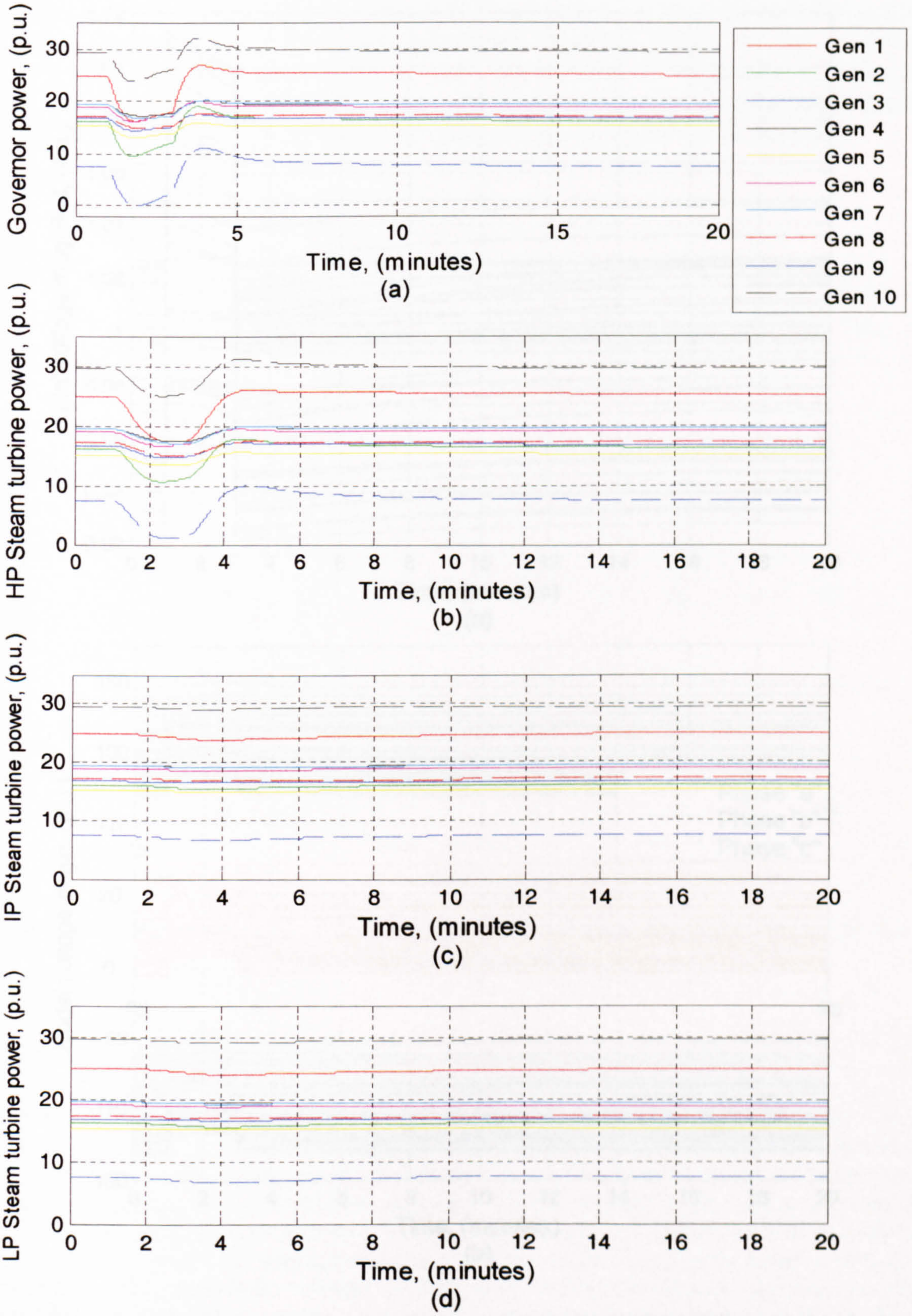

Figure 6.13 Generating plant responses of the system with a BTB HVDC embedded; (a) governor power; steam turbine (b) HP; (c) IP; (d) LP

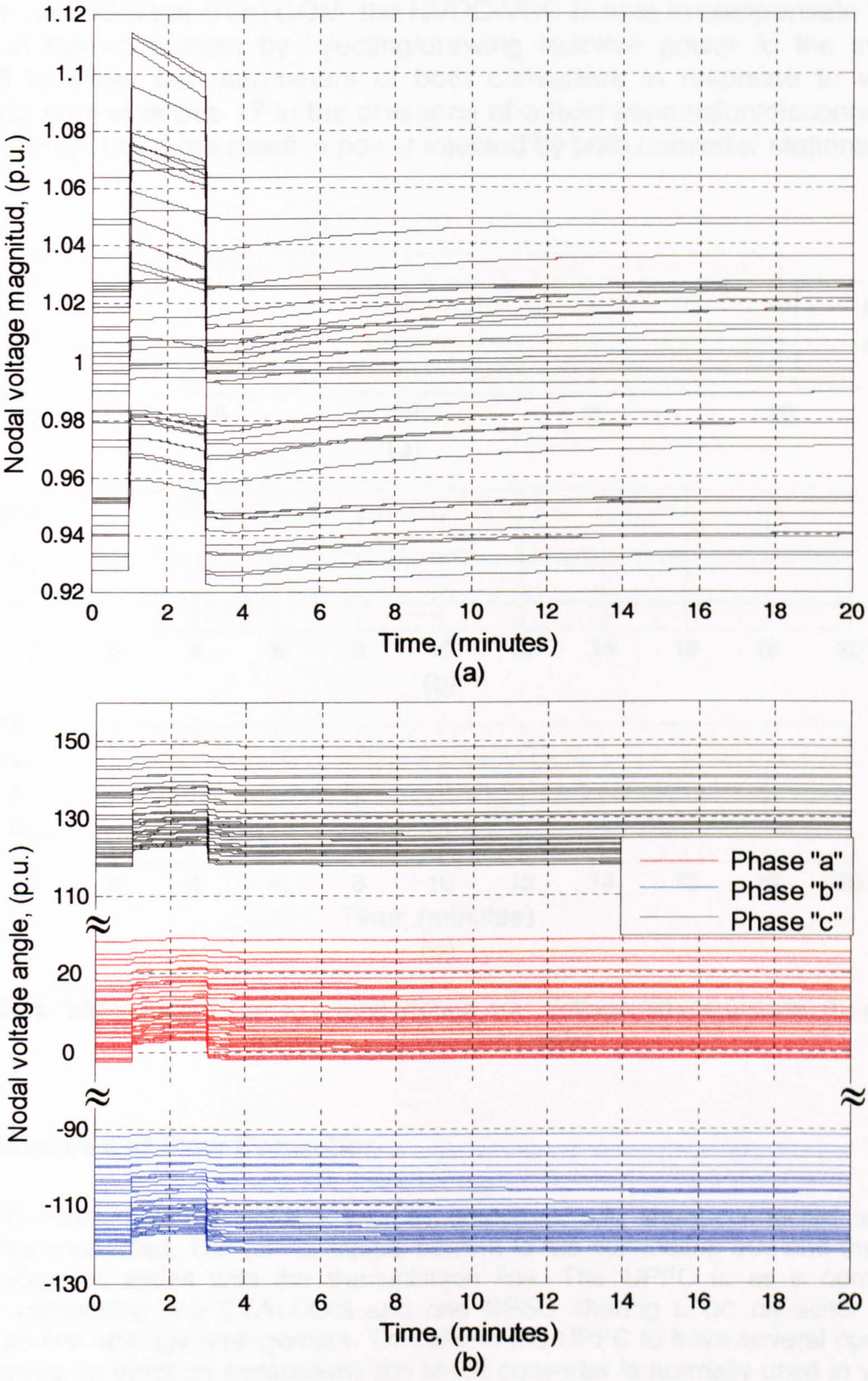

Figure 6.14 Nodal voltage responses of the system with HVDC-VSC embedded; (a) magnitude and (b) phase angle

As is the case with the STATCOM, the HVDC-VSC is able to compensate for the voltage in the AC system by injecting/drawing reactive power to the system. Figure 6.15 show the parameters of both converters in response to voltage magnitude control at bus 17 in the presence of a load connection/disconnection. Figure 6.15(c) shows the reactive power injected by both converter stations.

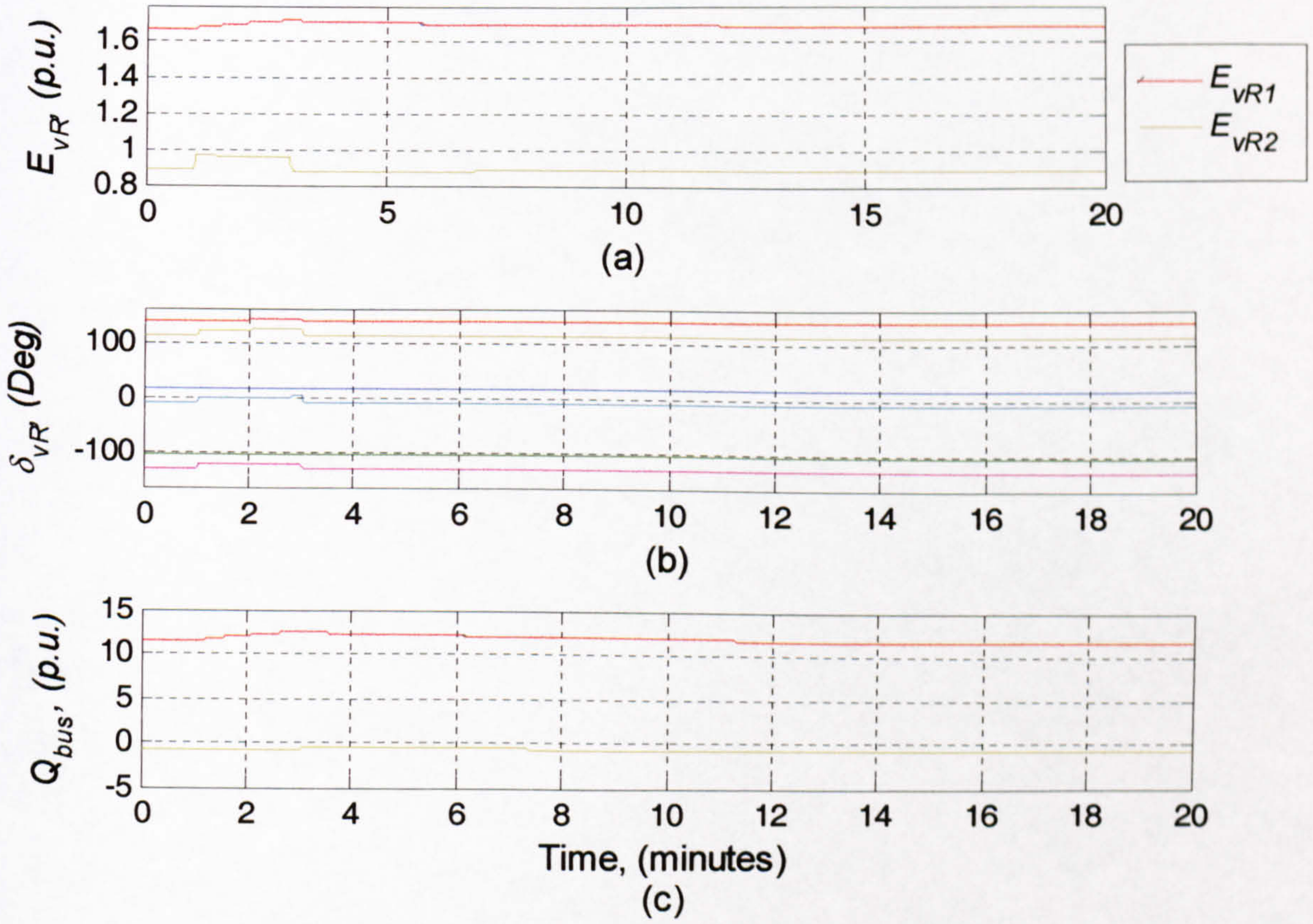

Figure 6.15 VSCs parameters to a load tripped out; voltage (a) magnitude; (b) phase angle and (c) reactive power

6.5 Unified Power Flow Controller

The UPFC consists of two voltage source converters, one shunt-connected and the other series-connected. The former injects current to the connecting bus and the latter injects voltage in series with the transmission line. The UPFC is as a compound controller comprising one STATCOM and one SSSC sharing a DC capacitor and a common control strategy arrangement. This allows the UPFC to have several operating control modes. In practical applications the shunt converter is normally used in voltage control mode. The automatic voltage control uses voltage feedback signals, usually representing the magnitude of the positive sequence component of bus voltage. The series converter controls the magnitude and angle of the voltage injected in series with the line. The series converter has many possible operating modes. Automatic power

flow control mode is used in most practical applications. Figure 6.16 shows the block diagrams of the UPFC.

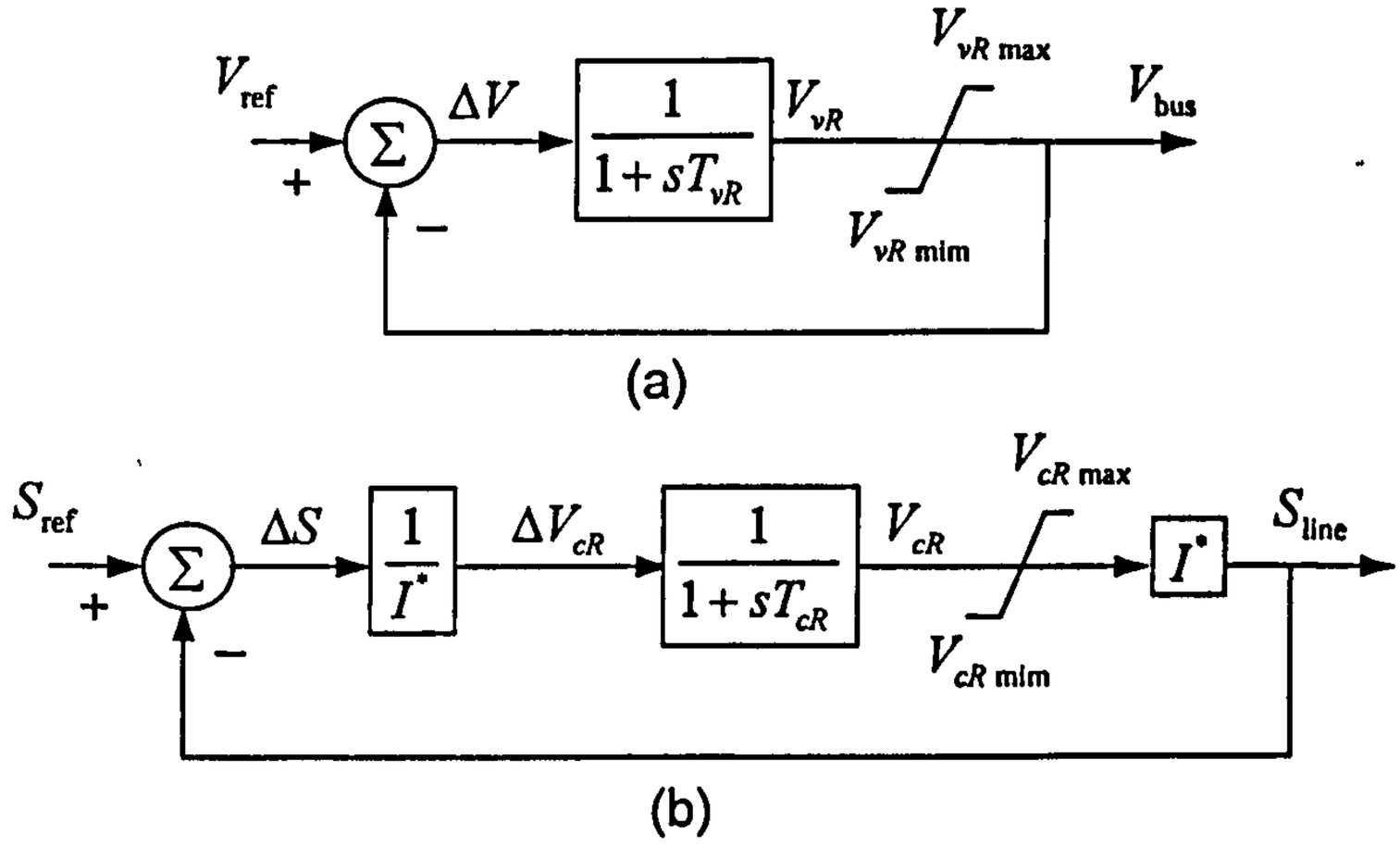

Figure 6.16 Block diagrams of (a) shunt-connected and (b) series connected converters of the UPFC

The differential equations and control input parameters of the UPFC can be arranged as follows:

For the shunt-connected converter

$$\Delta V = V_{ref} - V_{bus} \tag{6.22}$$

$$\frac{dV_{vR}}{dt} = \frac{\Delta V - V_{vR}}{T_{vR}} \qquad V_{vR\,min} \le V_{vR} \le V_{vR\,max} \tag{6.23}$$

and the series converter

$$\Delta S = S_{ref} - S_{line} \tag{6.24}$$

$$\Delta V_{cR} = \Delta S\left(\frac{1}{I^*}\right) \tag{6.25}$$

$$\frac{dV_{cR}}{dt} = \frac{\Delta V_{cR} - V_{cR}}{T_{cR}} \qquad V_{cR\,min} \le V_{cR} \le V_{cR\,max} \tag{6.26}$$

where

V_{bus} is the nodal voltage magnitude
V_{vR} is the voltage source converter (Shunt)
V_{ref} is the pre-specified reference voltage (magnitude)

S_{line} is the complex power flowing at the transmission line
S_{ref} is the complex power to be controlled
I^* is the complex current
T_{cR} is the transient time constant for shunt
T_{vR} is the transient time constant for series converters
V_{cR} is the voltage source converter (series)

6.6 Dynamic Power Flow Analysis of a Larger Multiphase Power Systems with VSC-based Controllers

To show the ability of the newly developed software to solve large-scale power networks, it has been used to solve a number of test networks of different sizes and degrees of operational complexity.

To illustrate this point, the IEEE 57-node system was modified to incorporate VSC-based FACTS controllers. Two STATCOMs were embedded in different points of the network. They were connected at buses 19 and 50, respectively; both controllers are used to control voltage magnitude at 1.01 p.u. which were originally at 0.9989 and 1.0314 p.u. respectively. Both converters are taken to have reactance values of 0.1 X_{vR} and 0 resistance values.

Two disturbances, including transmission lines and loads outages, are simulated in a total study time of 30 minutes. The first event takes place at the end of minute one, being the tripping of phase *a* of four transmission lines. The transmission lines affected are those connected between buses, 22 to 24, 22 to 23, 22 to 38 and 21 to 22. Also, a three-phase load at bus 33 is tripped out. Transmission lines and load are fully reconnected at minute four. A second disturbance takes place at minute 15, when phase *a* of the loads at buses 52, 53 and 54 becomes disconnected at the same time as the transmission line connecting buses 53 to 54, all power plants elements are fully reconnected after 3 minutes, i.e. minute 18 of the simulation. Figure 6.17 show the generating plants frequency responses and Figure 6.18 shows the nodal voltage magnitudes. Voltage variations in all nodes can be observed following disconnections/reconnections of loads and transmission lines. However, in this case study, all voltages are below 1.0 p.u. and voltage value of 0.94 is observed only for a fraction of a second.

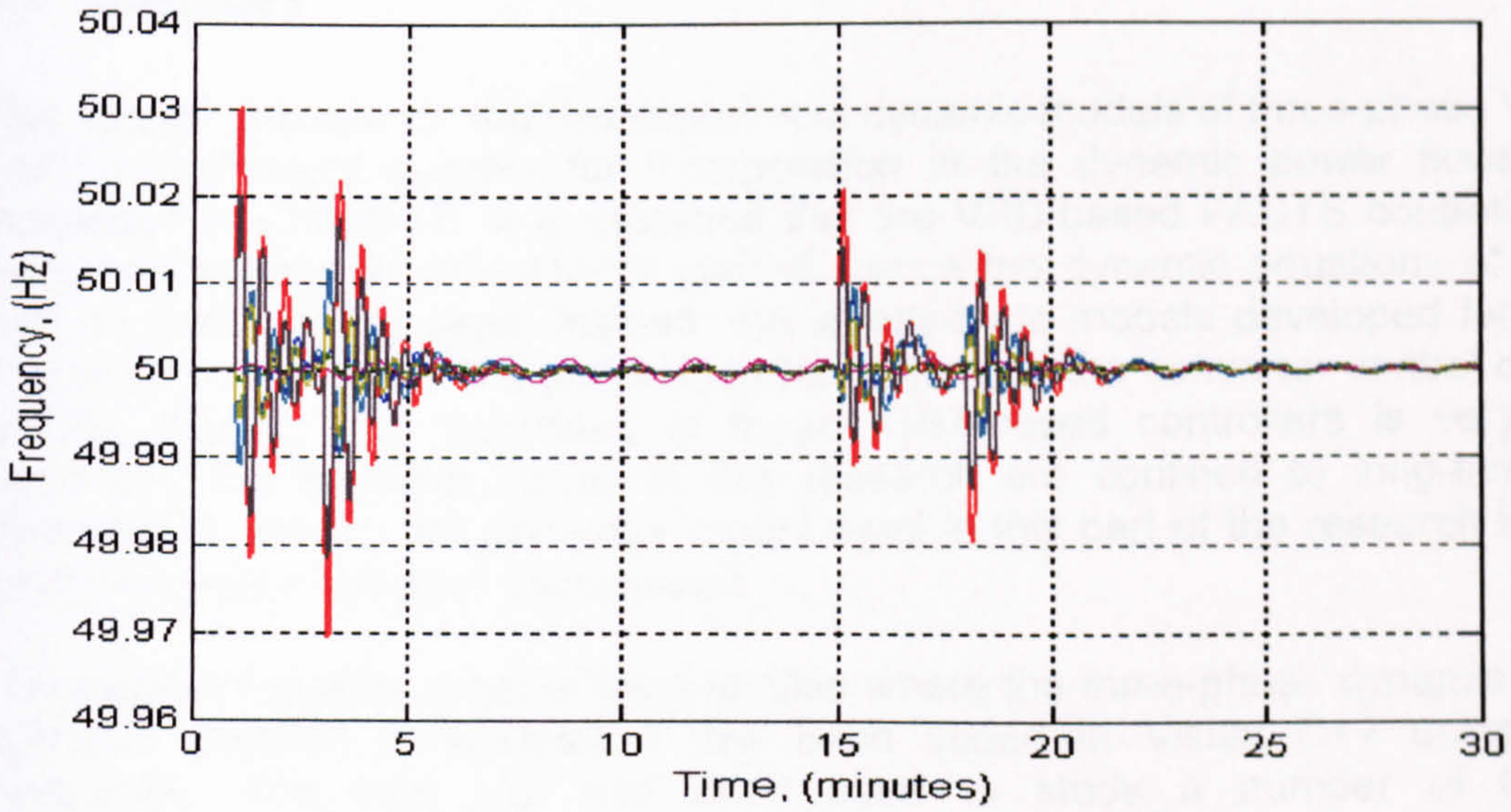

Figure 6.17 Frequency responses of generating plants in the system IEEE57-buses system

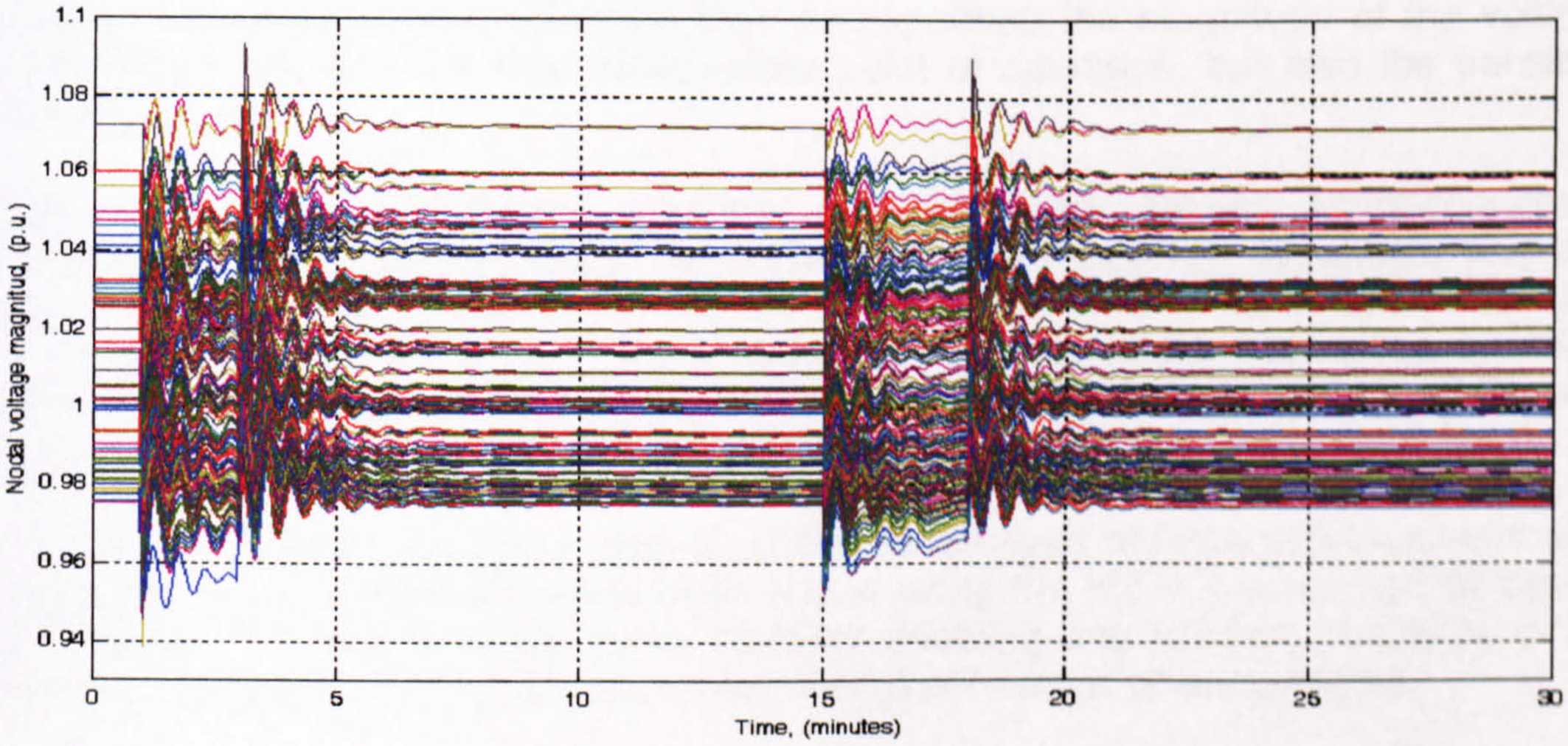

Figure 6.18 Nodal voltage magnitude in the system IEEE57-buses system

It can be concluded that the dynamic power flow models of VSC-based FACTS, as proposed, developed and incorporated into the algorithm, and used to solve for large-scale power systems is an effective tool suitable for three-phase frame of reference studies.

6.7 Summary

This chapter focuses on the development of dynamic models of three-phase VSC-based FACTS controllers suitable for incorporation in the dynamic power flows algorithm developed in Chapter 5. It is assumed that the VSC-based FACTS controllers have a delay-free impact on the network control, hence the dynamic equations of the closed loop controls are not used. Instead, the steady-state models developed for the power flow solution are used. The justification for neglecting the converter control dynamics is twofold: first by the responses of these IGBT-based controllers is very fast, and secondary the dynamic issues in this research are confined to long-term dynamic assessment. Indeed the generator model used in this part of the research is only valid for the long-term dynamic assessment.

The chapter presents a set of case studies where the three-phase dynamic power flow algorithm detailed in Chapter 5 has been coded in Visual C++ using the OOP philosophy. The new tool has been used to study a number of three-phase disturbances. The basic quality assurance tests performed have shown that the program works correctly for both balanced and unbalanced conditions.

The New England test system was used in order to illustrate the dynamic performance of FACTS models performance in power systems undergoing voltage steps in response to system changes. It was observed that, as expected, the magnitude of the voltage step affected not only the new steady-state point of operation, but also the transient recovery process.

When the various VSC-based solutions are compared, the AC shunt-connected controllers, i.e. the STATCOM and the HVDC-VSC have a certain advantage over the AC series-connected controllers, i.e. the SSSC, since the shunt converters act immediately in the right direction by boosting the voltage during first swing, enabling larger power transfers. Series compensation, however, can reduce power oscillations during the back swings, acting more effectively during this period.

The three-phase dynamic power flow algorithm for analysis of large-scale systems with VSC-based FACTS controllers has been tested using the IEEE 7-generator, 57-buses test system. The software has good flexibility enabling any number of events to be analysed. Moreover, the software has been tested with larger power systems.

6.8 References

[1] http://www.nationalgrid.com/uk/library/documents/pdfs/ExecutiveSummary.pdf

[2] US-Canada power system outage task force: "Final report on the August 14, 2003 blackout in the United States and Canada: Causes and recommendations", April 2004. http://pserc.org/Resources.htm

[3] Handschin, E.: "Real time control of electric power systems", *Proc. of the symposium on real-time control of electric power systems*, Brown, Bovery & company Limited, Baden, Switzerland, 1971.

[4] http://pserc.org/Resources.htm, Blackouts reports.

[5] Rafian, M.; Sterling, M.J. H., and Irving, M.R.: "Real-time power system simulation", IEE *proc.*, Vol. 134, Pt. C, No. 3, May 1987, pp. 206-223.

[6] ETAP Power Station® 3.0, Operation Technology, Inc. June 2000. http://www.etap.com

[7] Kundur, P.: "*Power system stability and control*", McGraw-Hill, NY, 1994. ISNB 007035958X.

[8] Stagg G.W. and El-Abiad A.H.: "*Computer methods in power system analysis*", McGraw-Hill, 1968. ISBN 67-12963-07-060658-7

[9] Hingorani, N.G. and Gyugyi, L.: "*Understanding FACTS concepts and technology of flexible AC transmission systems*", The Institute of Electrical and Electronics Engineers, NY, 2000. ISNB 0-780334558.

[10] Song, Y. H. and Johns, A. T.: "*Flexible AC transmission systems (FACTS)*", The Institution of Electrical Engineers, London, United Kingdom, 1999, INSB 0852967713.

[11] Povh, D. and Mihalic, R.: "Enhancement of transient stability on AC transmission by means of controlled series and parallel compensation", *International Conference on AC and DC Power Transmission*, Sep 1991. pp. 8 – 12.

[12] Schauder, C. and Mehta, H.: "Vector analysis and control of advanced static VAR compensators", IEE *Proc.-C* Vol. 104, No.4, July 1993, pp299-306.

[13] Natesan, R. and Radman, G.: "Effects of STATCOM, SSSC and UPFC on voltage stability", IEEE *Symposium on System Theory*, 2004, pp. 546-550.

[14] Nelson, R.J.; Bian, J. et al.: "Transient stability enhancement with FACTS controllers", IEE *AC and DC Power Trans.*, April-May 1996, pp. 269-74.

[15] Hosseini, H.S. and Ajami, A.: "Transient stability enhancement of AC transmission system using STATCOM", IEEE *TENCON '02*, Vol. 3, Oct. 2002 pp.1809 –1812.

[16] Wang, H. F.: "Design of SSSC damping controller to improve power system oscillation stability", IEEE *AFRICON*, Vol. 1, Sept.-Oct. 1999. pp. 495 - 500.

[17] Sen, K. k.: "SSSC-Static synchronous series compensator: Theory, modelling, and applications", IEEE *Trans. on Power Del*, Vol. 13, No. 1, Jan. 1998, pp. 241-6.

[18] Arrillaga, J.: "*High voltage direct current transmission*", the Institution of Electrical Engineers, 2nd Edition, London, UK, 1998. ISNB 0852969414.

[19] Padiyar, K.R.: "*HVDC power transmission systems technology and system interaction*", new age international (P) limited publishers. New Deli, 2002; ISBN 81-224-0102-3.

[20] Angeles-Camacho, C.; Tortelli, O. L.; Acha, E. and Fuerte-Esquivel, C. R.: "Inclusion of a high voltage DC-voltage source converter model in a Newton-Raphson power flow algorithm", IEE *Proc.-Gener. Transm. & Distrib.*, Vol. 150, No. 6, Nov. 2003. pp. 691-695.

Chapter 7

CONCLUSIONS AND FUTURE WORK

7.1 Conclusions

Flexible AC transmission systems which utilizes voltage source converters represent the main research concern in this dissertation. The goal has been to develop models of VSC-based FACTS controllers and to study their interaction with the electrical power network using its natural frame of reference termed the phase domain. VSC-based FACTS controllers are used to provide dynamic voltage support, power system stabilization, and enhanced power controllability and quality in transmission and distribution networks.

The research work is divided in to three main parts, namely: FACTS equipment characteristics, steady-state modelling and simulation, and dynamic modelling and simulation.

For the purposes of steady-state modelling and simulation of FACTS controllers the most relevant characteristics of the FACTS equipment were singled out. Flexible mathematical models have been derived in the form of nodal admittance matrices that use the frame of reference of the phases.

This was followed by the development of steady-state mathematical models of the most common elements found in conventional electric power systems. All power plant component models have been formulated in the frame of reference of the phases and interfaced with the models of FACTS components.

Two related but distinct power flow algorithms have been used: the Newton-Raphson method in polar co-ordinates and the Newton-Raphson method in rectangular co-ordinates. Both algorithms solve the non-linear power flow equations by iteration to a specified tight tolerance. In polar co-ordinates, the magnitudes and phase angles of nodal voltage and injected voltages of FACTS components are used as state variables; whereas in rectangular co-ordinates the real and imaginary parts of nodal voltages and injected FACTS voltages are the ones used as state variables. The results show that the Newton-Raphson power flow method retains its convergence characteristics in both cases. The object oriented programming philosophy used to implement the power flow algorithms should facilitate the inclusion of any new power systems component or FACTS controller that may became available in future.

In the second main area of research, the dynamic model of generating plants was addressed. For the purpose of this research namely, three-phase dynamic power flows, mathematical models of the synchronous generator with automatic voltage regulator, speed governor and turbine have been developed. A set of ordinary differential

equations describing the component was obtained for each generating plant component. In each case, the differential equations of each component were converted to algebraic form using the trapezoidal rule. The differential-algebraic model of the power system has been coded in software to carry out time domain studies of power systems with combined dynamic and static elements. An implicit trapezoidal integration method with Newton iteration has been selected to solve, simultaneously, the differential and static system equations. The models and the solution method have proven capable of performing adequately for the purpose of power system long-term dynamic assessment. Several network disturbances in both balanced and unbalanced conditions have been studied using the developed algorithm.

In a second phase of the research on dynamic modelling, dynamic models of VSC-FACTS controllers were developed. A set of differential equations that depict the basic control capabilities of FACTS controllers were obtained. However, due the very small time constants of the IGBT used in the VSCs, an instantaneous speed of response was assumed for all VSC-based FACTS controllers, and the steady-state models have been used to assess dynamic power flows. A balanced and an unbalanced three-phase load disturbance has been used to assess the effect of VSC-based FACTS controllers on the network.

During the course of this research, a comprehensive and integrated software environment has been developed for power flows and dynamic power flow analysis of large-scale power systems in the phase domain. The software which integrates VSC-based FACTS controllers and power plant components models allows the simulation of large-scale power systems with VSC-based FACTS controllers in the phase domain. Using the newly developed software comprehensive simulations have been carried out in order to assess both the steady-state and the dynamic behaviour of the models developed. The software developed in the present research work should find application in related applications areas such as systems planning and optimal design of power systems with provision to include VSC-based FACTS controllers.

7.2 Future Work

The operational complexity of large-scale electric power systems increase as power systems continue to expand due to interconnection of otherwise independent power systems. They have become so interdependent that unscheduled events in one area can propagate and have a significant impact on other areas that would appear, at first glance, to be relatively remote from the source of the initial event. This has been shown to be the case by the series of blackouts that occurred around the world in 2004. It has emerged that new tools are needed for the study and planning of the very large-scale systems which are now in operation. Alongside ever-expanding power systems a new generation of power electronics based controllers are emerging, which need to be studied in closer detail. The present work has made progress in modelling the power system in its natural frame of operation with VSC-based controllers. However, it is clear that a lot more work needs to be done.

Further research work relating to steady-state FACTS controllers would need to be modelled bearing in mind its power electronic topology, including PWM control and DC

voltage performance. Integration of the various current and emerging power electronic based controllers needs to be carried out. Modelling of embedded generation technologies should see incorporation into the power system analysis software produced as part of this research, including wind farm and other forms of small generating plants. A logical extension of the present research is the inclusion of algorithms to prioritise the control of nodal voltage when more than one controller is available. Algorithms to establish suitable coordination of reactive power sources to correct bus voltage violations and algorithms to enable appropriate selection of controllers and their location. One area that requires immediate attention in the present work is the implementation of a graphical interface for input/output data.

Concerning dynamic power flows, it is clear that assumptions taken to simplify the models of power generating plant would need to be relaxed to be able to apply the software tool to short-term transient stability assessment. With more complex generating plant models, short-circuit fault analysis should be implanted with ease owing to the modularity and re-usability offered by the OOP methodology. Implementation of a fault analysis module should make it possible to study different types of faults outside of the framework of intricate transformations between the sequence and the phase frames of reference. Analysis of short-circuit faults along with power flow and transient stability are three of the more widely used tools in the analysis of electrical power systems.

Because the main object of the present research is to show that the VSC-based FACTS behaviour in dynamic power flows illustrate that the FACTS steady-state models are good enough. However, full dynamic FACTS models, where the set of differential equations are included in the dynamic algorithm, need to be appled, to update the short-term transient stability assessment.

The voltage dependency of the loads has an influence on voltage stability; loads are typically modelled as constant current, constant impedance or constant active and reactive powers depending on the characteristics of the load. In this work the loads are only modelled as constant power loads. It is important to model the load characteristics more accurately in future work.

Future work is seen to be unlimited from the point of view of the power electronics and the development of new technologies to modernise the actual electric power system. With the great many advances in computing speed and storage capacity, there is no compelling reasons why FACTS and network models should not be modelled in the more flexible and comprehensive frame of reference afforded by the phases.

APPENDIX I: MATHEMATICAL DERIVATION OF ACTIVE AND REACTIVE POWER EQUATIONS

This appendix shows the mathematical process used to derivate the three-phase expressions of active and reactive power in both polar co-ordinates and rectangular co-ordinates used in the present research.

I.1 Conventional Power Plant Components

I.1.1 Polar co-ordinates

In polar co-ordinates the complex power equation written in (3.3), Section 3.2 represent the complex power injected into the bus *k* by a three-phase transmission line connected between bus *k* and *m*. It is a function of the bus voltages and the transmission line admittance matrix:

$$S_k^{\rho} = P_k^{\rho} + \mathrm{j}Q_k^{\rho} = V_k^{\rho} \sum_{i=k,m} \left(Y_{ki}^{\rho}\right)^{*} \left(V_i^{\rho}\right)^{*} \tag{I.1}$$

The bus voltages are expressed as a function of the voltage magnitude and phase angle. Hence, the voltage at node *k* is

$$V_k^{\rho} = \left[V_k^a \angle \theta_k^a \;\; V_k^b \angle \theta_k^b \;\; V_k^c \angle \theta_k^c\right]^T \tag{I.2}$$

The transmission line admittances matrix is expressed in complex form as:

$$Y_{km}^{\rho} = \begin{bmatrix} Y_{km}^{aa} & Y_{km}^{ab} & Y_{km}^{ac} \\ Y_{km}^{ba} & Y_{km}^{bb} & Y_{km}^{bc} \\ Y_{km}^{ca} & Y_{km}^{cb} & Y_{km}^{cc} \end{bmatrix} = \begin{bmatrix} G_{km}^{aa} + \mathrm{j}B_{km}^{aa} & G_{km}^{ab} + \mathrm{j}B_{km}^{ab} & G_{km}^{ac} + \mathrm{j}B_{km}^{ac} \\ G_{km}^{ba} + \mathrm{j}B_{km}^{ba} & G_{km}^{bb} + \mathrm{j}B_{km}^{bb} & G_{km}^{bc} + \mathrm{j}B_{km}^{bc} \\ G_{km}^{ca} + \mathrm{j}B_{km}^{ca} & G_{km}^{cb} + \mathrm{j}B_{km}^{cb} & G_{km}^{cc} + \mathrm{j}B_{km}^{cc} \end{bmatrix} \tag{I.3}$$

Nodal voltages (I.2) can be writen as a diagonal matrix to compute the complex power so that this diagonal matrix and equation (I.3) are substituted into (I.1). The complex power at bus *k* becomes

$$\begin{bmatrix} S_k^a \\ S_k^b \\ S_k^c \end{bmatrix} = \begin{bmatrix} V_k^a & 0 & 0 \\ 0 & V_k^b & 0 \\ 0 & 0 & V_k^c \end{bmatrix} \left\{ \begin{bmatrix} Y_{km}^{aa} & Y_{km}^{ab} & Y_{km}^{ac} \\ Y_{km}^{ba} & Y_{km}^{bb} & Y_{km}^{bc} \\ Y_{km}^{ca} & Y_{km}^{cb} & Y_{km}^{cc} \end{bmatrix}^* \begin{bmatrix} V_k^a \\ V_k^b \\ V_k^c \end{bmatrix}^* + \begin{bmatrix} Y_{km}^{aa} & Y_{km}^{ab} & Y_{km}^{ac} \\ Y_{km}^{ba} & Y_{km}^{bb} & Y_{km}^{bc} \\ Y_{km}^{ca} & Y_{km}^{cb} & Y_{km}^{cc} \end{bmatrix}^* \begin{bmatrix} V_m^a \\ V_m^b \\ V_m^c \end{bmatrix}^* \right\} \tag{I.4}$$

Then

$$\begin{bmatrix} S_k^a \\ S_k^b \\ S_k^c \end{bmatrix} = \begin{bmatrix} V_k^a Y_{km}^{aa} & V_k^a Y_{km}^{ab} & V_k^a Y_{km}^{ac} \\ V_k^b Y_{km}^{ba} & V_k^b Y_{km}^{bb} & V_k^b Y_{km}^{bc} \\ V_k^c Y_{km}^{ca} & V_k^c Y_{km}^{cb} & V_k^c Y_{km}^{cc} \end{bmatrix}^* \begin{bmatrix} V_k^a \\ V_k^b \\ V_k^c \end{bmatrix}^* + \begin{bmatrix} V_k^a Y_{km}^{aa} & V_k^a Y_{km}^{ab} & V_k^a Y_{km}^{ac} \\ V_k^b Y_{km}^{ba} & V_k^b Y_{km}^{bb} & V_k^b Y_{km}^{bc} \\ V_k^c Y_{km}^{ca} & V_k^c Y_{km}^{cb} & V_k^c Y_{km}^{cc} \end{bmatrix}^* \begin{bmatrix} V_m^a \\ V_m^b \\ V_m^c \end{bmatrix}^* \tag{I.5}$$

Finally the three-phase complex power becomes:

$$\begin{bmatrix} S_k^a \\ S_k^b \\ S_k^c \end{bmatrix} = \begin{bmatrix} V_k^a Y_{km}^{aa^*} V_k^{a^*} + V_k^a Y_{km}^{ab^*} V_k^{b^*} + V_k^a Y_{km}^{ac^*} V_k^{c^*} \\ V_k^b Y_{km}^{ba^*} V_k^{a^*} + V_k^b Y_{km}^{bb^*} V_k^{b^*} + V_k^b Y_{km}^{bc^*} V_k^{c^*} \\ V_k^c Y_{km}^{ca^*} V_k^{a^*} + V_k^c Y_{km}^{cb^*} V_k^{b^*} + V_k^c Y_{km}^{cc^*} V_k^{c^*} \end{bmatrix} + \begin{bmatrix} V_k^a Y_{km}^{aa^*} V_m^{a^*} + V_k^a Y_{km}^{ab^*} V_m^{b^*} + V_k^a Y_{km}^{ac^*} V_m^{c^*} \\ V_k^b Y_{km}^{ba^*} V_m^{a^*} + V_k^b Y_{km}^{bb^*} V_m^{b^*} + V_k^b Y_{km}^{bc^*} V_m^{c^*} \\ V_k^c Y_{km}^{ca^*} V_m^{a^*} + V_k^c Y_{km}^{cb^*} V_m^{b^*} + V_k^c Y_{km}^{cc^*} V_m^{c^*} \end{bmatrix} \tag{I.6}$$

It is clear now that the complex power for one phase, say phase *a*, can be write as:

$$S_k^a = V_k^a Y_{km}^{aa^*} V_k^{a^*} + V_k^a Y_{km}^{ab^*} V_k^{b^*} + V_k^a Y_{km}^{ac^*} V_k^{c^*} + V_k^a Y_{km}^{aa^*} V_m^{a^*} + V_k^a Y_{km}^{ab^*} V_m^{b^*} + V_k^a Y_{km}^{ac^*} V_m^{c^*} \tag{I.7}$$

Expanding equation (I.7) with the nodal voltages expressed in terms of a function of voltage magnitude and phase angle and admittances in complex form yields:

$$\begin{aligned} S_k^a = {} & V_k^a e^{j\theta_k^a} \left(G_{km}^{aa} - jB_{km}^{aa}\right) V_k^a e^{-j\theta_k^a} + V_k^a e^{j\theta_k^a} \left(G_{km}^{ab} - jB_{km}^{ab}\right) V_k^b e^{-j\theta_k^b} + V_k^a e^{j\theta_k^a} \left(G_{km}^{ac} - jB_{km}^{ac}\right) V_k^c e^{-j\theta_k^c} \\ & + V_k^a e^{j\theta_k^a} \left(G_{km}^{aa} - jB_{km}^{aa}\right) V_m^a e^{-j\theta_k^a} + V_k^a e^{j\theta_k^a} \left(G_{km}^{ab} - jB_{km}^{ab}\right) V_m^b e^{-j\theta_k^b} + V_k^a e^{j\theta_k^a} \left(G_{km}^{ac} - jB_{km}^{ac}\right) V_m^c e^{-j\theta_k^c} \end{aligned} \tag{I.8}$$

then

$$\begin{aligned} S_k^a = {} & V_k^a V_k^a e^{j\left(\theta_k^a-\theta_k^a\right)}\left(G_{km}^{aa}-jB_{km}^{aa}\right)+V_k^a V_k^b e^{j\left(\theta_k^a-\theta_k^b\right)}\left(G_{km}^{ab}-jB_{km}^{ab}\right)+V_k^a V_k^c e^{j\left(\theta_k^a-\theta_k^c\right)}\left(G_{km}^{ac}-jB_{km}^{ac}\right) \\ & +V_k^a V_m^a e^{j\left(\theta_k^a-\theta_m^a\right)}\left(G_{km}^{aa}-jB_{km}^{aa}\right)+V_k^a V_m^b e^{j\left(\theta_k^a-\theta_m^b\right)}\left(G_{km}^{ab}-jB_{km}^{ab}\right)+V_k^a V_m^c e^{j\left(\theta_k^a-\theta_m^c\right)}\left(G_{km}^{ac}-jB_{km}^{ac}\right) \end{aligned} \tag{I.9}$$

Applying the Euler identity in equation (I.9)

$$\begin{aligned} S_k^a = {} & V_k^a V_k^a\left(G_{km}^{aa}-jB_{km}^{aa}\right)\left[\cos\left(\theta_k^a-\theta_k^a\right)+j\sin\left(\theta_k^a-\theta_k^a\right)\right] \\ & +V_k^a V_k^b\left(G_{km}^{ab}-jB_{km}^{ab}\right)\left[\cos\left(\theta_k^a-\theta_k^b\right)+j\sin\left(\theta_k^a-\theta_k^b\right)\right] \\ & +V_k^a V_k^c\left(G_{km}^{ac}-jB_{km}^{ac}\right)\left[\cos\left(\theta_k^a-\theta_k^c\right)+j\sin\left(\theta_k^a-\theta_k^c\right)\right] \\ & +V_k^a V_m^a\left(G_{km}^{aa}-jB_{km}^{aa}\right)\left[\cos\left(\theta_k^a-\theta_m^a\right)+j\sin\left(\theta_k^a-\theta_m^a\right)\right] \\ & +V_k^a V_m^b\left(G_{km}^{ab}-jB_{km}^{ab}\right)\left[\cos\left(\theta_k^a-\theta_m^b\right)+j\sin\left(\theta_k^a-\theta_m^b\right)\right] \\ & +V_k^a V_m^c\left(G_{km}^{ac}-jB_{km}^{ac}\right)\left[\cos\left(\theta_k^a-\theta_m^c\right)+j\sin\left(\theta_k^a-\theta_m^c\right)\right] \end{aligned} \tag{I.10}$$

Separating real and imaginary parts, leads to the active and reactive power respectively, for the active power the expression becomes

$$\begin{aligned} P_k^a = {} & V_k^a V_k^a\left[G_{km}^{aa}\cos\left(\theta_k^a-\theta_k^a\right)+B_{km}^{aa}\sin\left(\theta_k^a-\theta_k^a\right)\right] \\ & +V_k^a V_k^b\left[G_{km}^{ab}\cos\left(\theta_k^a-\theta_k^b\right)+B_{km}^{ab}\sin\left(\theta_k^a-\theta_k^b\right)\right] \\ & +V_k^a V_k^c\left[G_{km}^{ac}\cos\left(\theta_k^a-\theta_k^c\right)+B_{km}^{ac}\sin\left(\theta_k^a-\theta_k^c\right)\right] \\ & +V_k^a V_m^a\left[G_{km}^{aa}\cos\left(\theta_k^a-\theta_m^a\right)+B_{km}^{aa}\sin\left(\theta_k^a-\theta_m^a\right)\right] \\ & +V_k^a V_m^b\left[G_{km}^{ab}\cos\left(\theta_k^a-\theta_m^b\right)+B_{km}^{ab}\sin\left(\theta_k^a-\theta_m^b\right)\right] \\ & +V_k^a V_m^c\left[G_{km}^{ac}\cos\left(\theta_k^a-\theta_m^c\right)+B_{km}^{ac}\sin\left(\theta_k^a-\theta_m^c\right)\right] \end{aligned} \tag{I.11}$$

A simplest expression for the active power at bus *k* phase *a* can be write as:

$$P_k^a = V_k^a\left\{\sum_{i=k,m}\sum_{j=a,b,c} V_i^j\left[G_{km}^{aj}\cos\left(\theta_k^a-\theta_i^j\right)+B_{km}^{aj}\sin\left(\theta_k^a-\theta_i^j\right)\right]\right\} \tag{I.12}$$

Similar expressions can be obtained for phases *b* and *c*. A generalized expression for the three-phases at bus *k* can be write as:

$$P_k^\rho = V_k^\rho\left\{\sum_{i=k,m}\sum_{j=a,b,c} V_i^j\left[G_{km}^{\rho j}\cos\left(\theta_k^\rho-\theta_i^j\right)+B_{km}^{\rho j}\sin\left(\theta_k^a-\theta_i^j\right)\right]\right\} \tag{I.13}$$

where ρ refer to the phases *a*, *b* and *c*

For the reactive power:

$$\begin{aligned}
Q_k^a = {} & V_k^a V_k^a \left[G_{km}^{aa} \sin\left(\theta_k^a - \theta_k^a\right) - B_{km}^{aa} \cos\left(\theta_k^a - \theta_k^a\right) \right] \\
& + V_k^a V_k^b \left[G_{km}^{ab} \sin\left(\theta_k^a - \theta_k^b\right) - B_{km}^{ab} \cos\left(\theta_k^a - \theta_k^b\right) \right] \\
& + V_k^a V_k^c \left[G_{km}^{ac} \sin\left(\theta_k^a - \theta_k^c\right) - B_{km}^{ac} \cos\left(\theta_k^a - \theta_k^c\right) \right] \\
& + V_k^a V_m^a \left[G_{km}^{aa} \sin\left(\theta_k^a - \theta_m^a\right) - B_{km}^{aa} \cos\left(\theta_k^a - \theta_m^a\right) \right] \\
& + V_k^a V_m^b \left[G_{km}^{ab} \sin\left(\theta_k^a - \theta_m^b\right) - B_{km}^{ab} \cos\left(\theta_k^a - \theta_m^b\right) \right] \\
& + V_k^a V_m^c \left[G_{km}^{ac} \sin\left(\theta_k^a - \theta_m^c\right) - B_{km}^{ac} \cos\left(\theta_k^a - \theta_m^c\right) \right]
\end{aligned} \tag{I.14}$$

And the generalized expressions for the reactive power injected into the phases of the bus *k* are:

$$Q_k^\rho = V_k^\rho \left\{ \sum_{i=k,m} \sum_{j=a,b,c} V_i^j \left[G_{km}^{\rho j} \sin\left(\theta_k^\rho - \theta_i^j\right) - B_{km}^{\rho j} \cos\left(\theta_k^\rho - \theta_i^j\right) \right] \right\} \tag{I.15}$$

As expected, the expressions for calculating the active and reactive powers injected into bus *m* are of the same form as (I.13) and (1.15), with the subscript *m* replacing *k* and *vice versa*:

$$P_m^\rho = V_m^\rho \left\{ \sum_{i=m,k} \sum_{j=a,b,c} V_i^j \left[G_{mi}^{\rho j} \cos\left(\theta_m^\rho - \theta_i^j\right) + B_{mi}^{\rho j} \sin\left(\theta_m^\rho - \theta_i^j\right) \right] \right\} \tag{I.16}$$

$$Q_m^\rho = V_m^\rho \left\{ \sum_{i=m,k} \sum_{j=a,b,c} V_i^j \left[G_{mi}^{\rho j} \sin\left(\theta_m^\rho - \theta_i^j\right) - B_{mi}^{\rho j} \cos\left(\theta_m^\rho - \theta_i^j\right) \right] \right\} \tag{I.17}$$

Active and reactive power expressions for all power plant components can be obtained in order to in the same manner as the above process build up the three-phase power system.

I.1.2 Rectangular co-ordinates

In order to illustrate the process to obtain the active and reactive power injected into bus *k* in the rectangular co-ordinates frame of reference equation (I.7) is used. Substituting nodal voltage and admittance elements in its rectangular from it becomes:

$$
\begin{aligned}
\boldsymbol{S}_k^a = & \left(e_k^a + \mathrm{j}f_k^a\right)\left(G_{km}^{aa} - \mathrm{j}B_{km}^{aa}\right)\left(e_k^a - \mathrm{j}f_k^a\right) \\
& + \left(e_k^a + \mathrm{j}f_k^a\right)\left(G_{km}^{ab} - \mathrm{j}B_{km}^{ab}\right)\left(e_k^b - \mathrm{j}f_k^b\right) \\
& + \left(e_k^a + \mathrm{j}f_k^a\right)\left(G_{km}^{ac} - \mathrm{j}B_{km}^{ac}\right)\left(e_k^c - \mathrm{j}f_k^c\right) \\
& + \left(e_k^a + \mathrm{j}f_k^a\right)\left(G_{km}^{aa} - \mathrm{j}B_{km}^{aa}\right)\left(e_m^a - \mathrm{j}f_m^a\right) \\
& + \left(e_k^a + \mathrm{j}f_k^a\right)\left(G_{km}^{ab} - \mathrm{j}B_{km}^{ab}\right)\left(e_m^b - \mathrm{j}f_m^b\right) \\
& + \left(e_k^a + \mathrm{j}f_k^a\right)\left(G_{km}^{ac} - \mathrm{j}B_{km}^{ac}\right)\left(e_m^c - \mathrm{j}f_m^c\right)
\end{aligned}
\tag{I.18}
$$

then

$$
\begin{aligned}
\boldsymbol{S}_k^a = & \left[e_k^a\left(G_{km}^{aa}e_k^a - B_{km}^{aa}f_k^a\right) + f_k^a\left(G_{km}^{aa}f_k^a + B_{km}^{aa}e_k^a\right)\right] + \mathrm{j}\left[f_k^a\left(G_{km}^{aa}e_k^a - B_{km}^{aa}f_k^a\right) - e_k^a\left(G_{km}^{aa}f_k^a + B_{km}^{aa}e_k^a\right)\right] \\
& + \left[e_k^a\left(G_{km}^{ab}e_k^b - B_{km}^{ab}f_k^b\right) + f_k^a\left(G_{km}^{ab}f_k^b + B_{km}^{ab}e_k^b\right)\right] + \mathrm{j}\left[f_k^a\left(G_{km}^{ab}e_k^b - B_{km}^{ab}f_k^b\right) - e_k^a\left(G_{km}^{ab}f_k^b + B_{km}^{ab}e_k^b\right)\right] \\
& + \left[e_k^a\left(G_{km}^{ac}e_k^c - B_{km}^{ac}f_k^c\right) + f_k^a\left(G_{km}^{ac}f_k^c + B_{km}^{ac}e_k^c\right)\right] + \mathrm{j}\left[f_k^a\left(G_{km}^{ac}e_k^c - B_{km}^{ac}f_k^c\right) - e_k^a\left(G_{km}^{ac}f_k^c + B_{km}^{ac}e_k^c\right)\right] \\
& + \left[e_k^a\left(G_{km}^{aa}e_m^a - B_{km}^{aa}f_m^a\right) + f_k^a\left(G_{km}^{aa}f_m^a + B_{km}^{aa}e_m^a\right)\right] + \mathrm{j}\left[f_k^a\left(G_{km}^{aa}e_m^a - B_{km}^{aa}f_m^a\right) - e_k^a\left(G_{km}^{aa}f_m^a + B_{km}^{aa}e_m^a\right)\right] \\
& + \left[e_k^a\left(G_{km}^{ab}e_m^b - B_{km}^{ab}f_m^b\right) + f_k^a\left(G_{km}^{ab}f_m^b + B_{km}^{ab}e_m^b\right)\right] + \mathrm{j}\left[f_k^a\left(G_{km}^{ab}e_m^b - B_{km}^{ab}f_m^b\right) - e_k^a\left(G_{km}^{ab}f_m^b + B_{km}^{ab}e_m^b\right)\right] \\
& + \left[e_k^a\left(G_{km}^{ac}e_m^c - B_{km}^{ac}f_m^c\right) + f_k^a\left(G_{km}^{ac}f_m^c + B_{km}^{ac}e_m^c\right)\right] + \mathrm{j}\left[f_k^a\left(G_{km}^{ac}e_m^c - B_{km}^{ac}f_m^c\right) - e_k^a\left(G_{km}^{ac}f_m^c + B_{km}^{\dot{a}c}e_m^c\right)\right]
\end{aligned}
\tag{I.19}
$$

Separating real and imaginary parts leads to expressions for active and reactive power respectively, for the active power, the expression becomes

$$
\begin{aligned}
P_k^a = & \left[e_k^a\left(G_{km}^{aa}e_k^a - B_{km}^{aa}f_k^a\right) + f_k^a\left(G_{km}^{aa}f_k^a + B_{km}^{aa}e_k^a\right)\right] \\
& + \left[e_k^a\left(G_{km}^{ab}e_k^b - B_{km}^{ab}f_k^b\right) + f_k^a\left(G_{km}^{ab}f_k^b + B_{km}^{ab}e_k^b\right)\right] \\
& + \left[e_k^a\left(G_{km}^{ac}e_k^c - B_{km}^{ac}f_k^c\right) + f_k^a\left(G_{km}^{ac}f_k^c + B_{km}^{ac}e_k^c\right)\right] \\
& + \left[e_k^a\left(G_{km}^{aa}e_m^a - B_{km}^{aa}f_m^a\right) + f_k^a\left(G_{km}^{aa}f_m^a + B_{km}^{aa}e_m^a\right)\right] \\
& + \left[e_k^a\left(G_{km}^{ab}e_m^b - B_{km}^{ab}f_m^b\right) + f_k^a\left(G_{km}^{ab}f_m^b + B_{km}^{ab}e_m^b\right)\right] \\
& + \left[e_k^a\left(G_{km}^{ac}e_m^c - B_{km}^{ac}f_m^c\right) + f_k^a\left(G_{km}^{ac}f_m^c + B_{km}^{ac}e_m^c\right)\right]
\end{aligned}
\tag{I.20}
$$

A simple expression for the active power at bus *k* phase *a* can be write as:

$$P_k^a = e_k^a \sum_{i=k,m} \sum_{j=a,b,c} \left(G_{km}^{aj} e_i^j - B_{km}^{aj} f_i^j \right) + f_k^a \sum_{i=k,m} \sum_{j=a,b,c} \left(G_{km}^{aj} f_i^j + B_{km}^{aj} e_i^j \right) \tag{I.21}$$

Similar expressions can be obtained for phases *b* and *c*. A generalized expression for the three-phases at bus *k* can be write as,

$$P_k^\rho = e_k^\rho \sum_{i=k,m} \sum_{j=a,b,c} \left(G_{km}^{\rho j} e_i^j - B_{km}^{\rho j} f_i^j \right) + f_k^\rho \sum_{i=k,m} \sum_{j=a,b,c} \left(G_{km}^{\rho j} f_i^j + B_{km}^{\rho j} e_i^j \right) \tag{I.22}$$

where ρ refer to the phases *a*, *b* and *c*

For the reactive power the below expression is obtained,

$$\begin{aligned} Q_k^a = & \left[f_k^a \left(G_{km}^{aa} e_k^a - B_{km}^{aa} f_k^a \right) - e_k^a \left(G_{km}^{aa} f_k^a + B_{km}^{aa} e_k^a \right) \right] \\ & + \left[f_k^a \left(G_{km}^{ab} e_k^b - B_{km}^{ab} f_k^b \right) - e_k^a \left(G_{km}^{ab} f_k^b + B_{km}^{ab} e_k^b \right) \right] \\ & + \left[f_k^a \left(G_{km}^{ac} e_k^c - B_{km}^{ac} f_k^c \right) - e_k^a \left(G_{km}^{ac} f_k^c + B_{km}^{ac} e_k^c \right) \right] \\ & + \left[f_k^a \left(G_{km}^{aa} e_m^a - B_{km}^{aa} f_m^a \right) - e_k^a \left(G_{km}^{aa} f_m^a + B_{km}^{aa} e_m^a \right) \right] \\ & + \left[f_k^a \left(G_{km}^{ab} e_m^b - B_{km}^{ab} f_m^b \right) - e_k^a \left(G_{km}^{ab} f_m^b + B_{km}^{ab} e_m^b \right) \right] \\ & + \left[f_k^a \left(G_{km}^{ac} e_m^c - B_{km}^{ac} f_m^c \right) - e_k^a \left(G_{km}^{ac} f_m^c + B_{km}^{ac} e_m^c \right) \right] \end{aligned} \tag{I.23}$$

And the generalized expressions for the reactive power injected into the phases of bus *k* are:

$$Q_k^\rho = \left[f_k^\rho \sum_{i=k,m} \sum_{j=a,b,c} \left(G_{km}^{\rho j} e_i^j - B_{km}^{\rho j} f_i^j \right) - e_k^\rho \sum_{i=k,m} \sum_{j=a,b,c} \left(G_{km}^{\rho j} f_i^j + B_{km}^{\rho j} e_i^j \right) \right] \tag{I.24}$$

As expected, the expressions for calculating the active and reactive powers injected into bus *m* are of the same form as (I.22) and (I.24), with the subscript *m* replacing *k* and *vice versa*:

$$P_m^\rho = e_m^\rho \sum_{i=k,m} \sum_{j=a,b,c} \left(G_{mk}^{\rho j} e_i^j - B_{mk}^{\rho j} f_i^j \right) + f_m^\rho \sum_{i=k,m} \sum_{j=a,b,c} \left(G_{mk}^{\rho j} f_i^j + B_{mk}^{\rho j} e_i^j \right) \tag{I.25}$$

$$Q_m^\rho = \left[f_m^\rho \sum_{i=k,m} \sum_{j=a,b,c} \left(G_{mk}^{\rho j} e_i^j - B_{mk}^{\rho j} f_i^j \right) - e_m^\rho \sum_{i=k,m} \sum_{j=a,b,c} \left(G_{mk}^{\rho j} f_i^j + B_{mk}^{\rho j} e_i^j \right) \right] \tag{I.26}$$

I.2 FACTS devices power equations

I.2.1 Polar co-ordinates

To illustrate the analytical process applied to VSC devices in order to derive its complex power equations the STATCOM is selected. Based on Figure 3.4, nodal power equations were derived in Section 3.3 for the STATCOM and at its connecting bus, say *k*,

$$\boldsymbol{S}_{\mathrm{vR}}^{\rho} = \boldsymbol{E}_{\mathrm{vR}}^{\rho}\boldsymbol{I}_{vR}^{*} = \boldsymbol{E}_{\mathrm{vR}}^{\rho}\boldsymbol{Y}_{vR}^{*}\left[\left(\boldsymbol{E}_{vR}^{\rho}\right)^{*} - \left(\boldsymbol{V}_{k}^{\rho}\right)^{*}\right] \tag{I.27}$$

$$\boldsymbol{S}_{k}^{\rho} = \boldsymbol{E}_{k}^{\rho}\boldsymbol{I}_{k}^{*} = \boldsymbol{E}_{k}^{\rho}\boldsymbol{Y}_{vR}^{*}\left[\left(\boldsymbol{V}_{k}^{\rho}\right)^{*} - \left(\boldsymbol{E}_{vR}^{\rho}\right)^{*}\right] \tag{I.28}$$

where the nodal voltages and source voltages are expressed in terms of a function with voltage magnitude and phase angle:

$$\begin{aligned}\boldsymbol{V}_{k}^{\rho} &= \left[V_{k}^{a}\angle\theta_{k}^{a} \quad V_{k}^{b}\angle\theta_{k}^{b} \quad V_{k}^{c}\angle\theta_{k}^{c}\right]^{T} \\ \boldsymbol{E}_{vR}^{\rho} &= \left[V_{vR}^{a}\angle\delta_{vR}^{a} \quad V_{vR}^{b}\angle\delta_{vR}^{b} \quad V_{vR}^{c}\angle\delta_{vR}^{c}\right]^{T}\end{aligned} \tag{I.29}$$

and the admittance matrix in complex form:

$$\boldsymbol{Y}_{vR}^{\rho} = \begin{bmatrix} \boldsymbol{Y}_{vR}^{aa} & 0 & 0 \\ 0 & \boldsymbol{Y}_{vR}^{bb} & 0 \\ 0 & 0 & \boldsymbol{Y}_{vR}^{cc} \end{bmatrix} \tag{I.30}$$

Nodal voltages (I.24) can be expressed as a diagonal matrix to compute the complex power, so that diagonal matrix and equation (I.27) are substituted into (I.28), the complex power at bus *k* becomes

$$\begin{bmatrix} \boldsymbol{S}_{k}^{a} \\ \boldsymbol{S}_{k}^{b} \\ \boldsymbol{S}_{k}^{c} \end{bmatrix} = \begin{bmatrix} \boldsymbol{V}_{k}^{a} & 0 & 0 \\ 0 & \boldsymbol{V}_{k}^{b} & 0 \\ 0 & 0 & \boldsymbol{V}_{k}^{c} \end{bmatrix} \left\{ \begin{bmatrix} \boldsymbol{Y}_{vR}^{aa} & 0 & 0 \\ 0 & \boldsymbol{Y}_{vR}^{bb} & 0 \\ 0 & 0 & \boldsymbol{Y}_{vR}^{cc} \end{bmatrix}^{*} \begin{bmatrix} \boldsymbol{V}_{k}^{a} \\ \boldsymbol{V}_{k}^{b} \\ \boldsymbol{V}_{k}^{c} \end{bmatrix}^{*} + \begin{bmatrix} \boldsymbol{Y}_{vR}^{aa} & 0 & 0 \\ 0 & \boldsymbol{Y}_{vR}^{bb} & 0 \\ 0 & 0 & \boldsymbol{Y}_{vR}^{cc} \end{bmatrix}^{*} \begin{bmatrix} \boldsymbol{E}_{vR}^{a} \\ \boldsymbol{E}_{vR}^{b} \\ \boldsymbol{E}_{vR}^{c} \end{bmatrix}^{*} \right\} \tag{I.31}$$

then

$$\begin{bmatrix} \boldsymbol{S}_{k}^{a} \\ \boldsymbol{S}_{k}^{b} \\ \boldsymbol{S}_{k}^{c} \end{bmatrix} = \begin{bmatrix} \boldsymbol{V}_{k}^{a}\boldsymbol{Y}_{vR}^{aa} & 0 & 0 \\ 0 & \boldsymbol{V}_{k}^{b}\boldsymbol{Y}_{vR}^{bb} & 0 \\ 0 & 0 & \boldsymbol{V}_{k}^{c}\boldsymbol{Y}_{vR}^{cc} \end{bmatrix}^{*} \begin{bmatrix} \boldsymbol{V}_{k}^{a} \\ \boldsymbol{V}_{k}^{b} \\ \boldsymbol{V}_{k}^{c} \end{bmatrix}^{*} + \begin{bmatrix} \boldsymbol{V}_{k}^{a}\boldsymbol{Y}_{vR}^{aa} & 0 & 0 \\ 0 & \boldsymbol{V}_{k}^{b}\boldsymbol{Y}_{vR}^{bb} & 0 \\ 0 & 0 & \boldsymbol{V}_{k}^{c}\boldsymbol{Y}_{vR}^{cc} \end{bmatrix}^{*} \begin{bmatrix} \boldsymbol{E}_{vR}^{a} \\ \boldsymbol{E}_{vR}^{b} \\ \boldsymbol{E}_{vR}^{c} \end{bmatrix}^{*} \tag{I.32}$$

Finally the three-phase complex power becomes:

$$\begin{bmatrix} S_k^a \\ S_k^b \\ S_k^c \end{bmatrix} = \begin{bmatrix} V_k^a Y_{vR}^{aa*} V_k^{a*} \\ V_k^b Y_{vR}^{bb*} V_k^{b*} \\ V_k^c Y_{vR}^{cc*} V_k^{c*} \end{bmatrix} + \begin{bmatrix} V_k^a Y_{vR}^{aa*} E_{vR}^{a\,*} \\ V_k^b Y_{vR}^{bb*} E_{vR}^{b\,*} \\ V_k^c Y_{vR}^{cc*} E_{vR}^{c\,*} \end{bmatrix} \tag{I.33}$$

It is clear now that the complex power for one phase, says *a* is expressed as:

$$S_k^a = V_k^a Y_{vR}^{aa*} V_k^{a**} + V_k^a Y_{vR}^{aa*} E_{vR}^{a\,*} \tag{I.34}$$

Expanding equation (I.32) with the nodal voltage, source voltage and admittances yields:

$$\begin{aligned} S_k^a &= V_k^a e^{j\theta_k^a} \left(G_{vR}^{aa} - jB_{vR}^{aa}\right) V_k^a e^{-j\theta_k^a} \\ &+ V_k^a e^{j\theta_k^a} \left(G_{vR}^{aa} - jB_{vR}^{aa}\right) V_{vR}^a e^{-j\delta_{vR}^a} \end{aligned} \tag{I.35}$$

then

$$\begin{aligned} S_k^a &= V_k^a V_k^a e^{j\left(\theta_k^a - \theta_k^a\right)} \left(G_{vR}^{aa} - jB_{vR}^{aa}\right) \\ &+ V_k^a E_{vR}^a e^{j\left(\theta_k^a - \delta_{vR}^a\right)} \left(G_{vR}^{aa} - jB_{vR}^{aa}\right) \end{aligned} \tag{I.36}$$

Applying the Euler identity in equation (I.34)

$$\begin{aligned} S_k^a &= V_k^a V_k^a \left(G_{vR}^{aa} - jB_{vR}^{aa}\right)\left[\cos\left(\theta_k^a - \theta_k^a\right) + j\sin\left(\theta_k^a - \theta_k^a\right)\right] \\ &+ V_k^a E_{vR}^a \left(G_{vR}^{aa} - jB_{vR}^{aa}\right)\left[\cos\left(\theta_k^a - \delta_{vR}^a\right) + j\sin\left(\theta_k^a - \delta_{vR}^a\right)\right] \end{aligned} \tag{I.37}$$

$$\begin{aligned} S_k^a &= V_k^a V_k^a G_{vR}^{aa} - jV_k^a V_k^a B_{vR}^{aa} \\ &+ V_k^a V_{vR}^a \left[G_{vR}^{aa} \cos\left(\theta_k^a - \delta_{vR}^a\right) + B_{vR}^{aa} \sin\left(\theta_k^a - \delta_{vR}^a\right)\right] \\ &+ jV_k^a V_{vR}^a \left[G_{vR}^{aa} \sin\left(\theta_k^a - \delta_{vR}^a\right) + B_{vR}^{aa} \cos\left(\theta_k^a - \delta_{vR}^a\right)\right] \end{aligned} \tag{I.38}$$

Separating real and imaginary parts leads to expression for the active and reactive power respectively. For the active power the expression for the active power injected at bus *k* phase *a* can be write as:

$$P_k^a = \left(V_k^a\right)^2 G_{vR}^{aa} - V_k^a V_{vR}^a \left[G_{vR}^{aa} \cos\left(\theta_k^a - \delta_{vR}^a\right) + B_{vR}^{aa} \sin\left(\theta_k^a - \delta_{vR}^a\right)\right] \quad (I.39)$$

Similar expressions can be obtained for phases *b* and *c*. A generalized expression for the three-phases at bus *k* can be write as:

$$P_k^\rho = \left(V_k^\rho\right)^2 G_{vR}^{\rho\rho} - V_k^\rho V_{vR}^\rho \left[G_{vR}^{\rho\rho} \cos\left(\theta_k^\rho - \delta_{vR}^\rho\right) + B_{vR}^{\rho\rho} \sin\left(\theta_k^\rho - \delta_{vR}^\rho\right)\right] \quad (I.40)$$

For the reactive power:

$$Q_k^a = -\left(V_k^a\right)^2 B_{vR}^{aa} + V_k^a V_{vR}^a \left[G_{vR}^{aa} \sin\left(\theta_k^a - \delta_{vR}^a\right) + B_{vR}^{aa} \cos\left(\theta_k^a - \delta_{vR}^a\right)\right] \quad (I.41)$$

And the generalized expressions for the reactive power injected into the phases of bus k are:

$$Q_k^\rho = -\left(V_k^\rho\right)^2 B_{vR}^{\rho\rho} + V_k^\rho V_{vR}^\rho \left[G_{vR}^{\rho\rho} \sin\left(\theta_k^\rho - \delta_{vR}^\rho\right) + B_{vR}^{\rho\rho} \cos\left(\theta_k^\rho - \delta_{vR}^\rho\right)\right] \quad (I.42)$$

As expected, the expressions to compute the active and reactive powers injected into the STATCOM are of the same form as (I.38) and (I.40), with the subscript *vR* replacing *k* and *vice versa*:

$$P_{vR}^\rho = \left(V_{vR}^\rho\right)^2 G_{vR}^{\rho\rho} - V_{vR}^\rho V_k^\rho \left[G_{vR}^{\rho\rho} \cos\left(\delta_{vR}^\rho - \theta_k^\rho\right) + B_{vR}^{\rho\rho} \sin\left(\delta_{vR}^\rho - \theta_k^\rho\right)\right] \quad (I.43)$$

$$Q_{vR}^\rho = -\left(V_{vR}^\rho\right)^2 B_{vR}^{\rho\rho} + V_{vR}^\rho V_k^\rho \left[G_{vR}^{\rho\rho} \sin\left(\delta_{vR}^\rho - \theta_k^\rho\right) + B_{vR}^{\rho\rho} \cos\left(\delta_{vR}^\rho - \theta_k^\rho\right)\right] \quad (I.44)$$

Active and reactive power expression in polar coordinates for SSSC, UPFC and HVDC-VSC controllers in the three-phase frame of reference are obtained in a same manner as the above process.

I.2.2 Rectangular co-ordinates

Rectangular co-ordinate analysis employs nodal voltage and source voltages expressed in their real and imaginary parts rather than in voltage magnitudes and phase angles as state variables:

$$\boldsymbol{V}_k^\rho = \left[e_k^a + \mathrm{j}f_k^a \quad e_k^b + \mathrm{j}f_k^b \quad e_k^c + \mathrm{j}f_k^c\right]^T \quad (I.45)$$

$$\boldsymbol{E}_{vR}^\rho = \left[e_{vR}^a + \mathrm{j}f_{vR}^a \quad e_{vR}^b + \mathrm{j}f_{vR}^b \quad e_{vR}^c + \mathrm{j}f_{vR}^c\right]^T \quad (I.46)$$

Expanding equation (I.32) with the nodal voltage, source voltage and admittances yields,

$$\begin{aligned} S_k^a &= \left(e_k^a + \mathrm{j}f_k^a\right)\left(G_{vR}^{aa} - \mathrm{j}B_{vR}^{aa}\right)\left(e_k^a - \mathrm{j}f_k^a\right) \\ &\quad -\left(e_k^a + \mathrm{j}f_k^a\right)\left(G_{vR}^{aa} - \mathrm{j}B_{vR}^{aa}\right)\left(e_{vR}^a - \mathrm{j}f_{vR}^a\right) \end{aligned} \tag{I.47}$$

then

$$\begin{aligned} S_k^a &= e_k^a\left(G_{vR}^{aa}e_k^a - B_{vR}^{aa}f_k^a\right) + f_k^a\left(G_{vR}^{aa}f_k^a + B_{vR}^{aa}e_k^a\right) \\ &\quad + \mathrm{j}\left[f_k^a\left(G_{vR}^{aa}e_k^a - B_{vR}^{aa}f_k^a\right) - e_k^a\left(G_{vR}^{aa}f_k^a + B_{vR}^{aa}e_k^a\right)\right] \\ &\quad - e_k^a\left(G_{vR}^{aa}e_{vR}^a - B_{vR}^{aa}f_{vR}^a\right) - f_k^a\left(G_{vR}^{aa}f_{vR}^a + B_{vR}^{aa}e_{vR}^a\right) \\ &\quad - \mathrm{j}\left[f_k^a\left(G_{vR}^{aa}e_{vR}^a - B_{vR}^{aa}f_{vR}^a\right) - e_k^a\left(G_{vR}^{aa}f_{vR}^a + B_{vR}^{aa}e_{vR}^a\right)\right] \end{aligned} \tag{I.48}$$

and

$$\begin{aligned} S_k^a &= e_k^a\left[\left(G_{vR}^{aa}e_k^a - B_{vR}^{aa}f_k^a\right) - \left(G_{vR}^{aa}e_{vR}^a - B_{vR}^{aa}f_{vR}^a\right)\right] + f_k^a\left[\left(G_{vR}^{aa}f_k^a + B_{vR}^{aa}e_k^a\right) - \left(G_{vR}^{aa}f_{vR}^a + B_{vR}^{aa}e_{vR}^a\right)\right] \\ &\quad + \mathrm{j}\left\{f_k^a\left[\left(G_{vR}^{aa}e_k^a - B_{vR}^{aa}f_k^a\right) - \left(G_{vR}^{aa}e_{vR}^a - B_{vR}^{aa}f_{vR}^a\right)\right] + e_k^a\left[-\left(G_{vR}^{aa}f_k^a + B_{vR}^{aa}e_k^a\right) + \left(G_{vR}^{aa}f_{vR}^a + B_{vR}^{aa}e_{vR}^a\right)\right]\right\} \end{aligned} \tag{I.49}$$

Separating real and imaginary parts leads to expressions that can be computed for the active and reactive powers respectively. For the active power, the expression becomes

$$\begin{aligned} P_k^a &= e_k^a\left[\left(G_{vR}^{aa}e_k^a - B_{vR}^{aa}f_k^a\right) - \left(G_{vR}^{aa}e_{vR}^a - B_{vR}^{aa}f_{vR}^a\right)\right] \\ &\quad + f_k^a\left[\left(G_{vR}^{aa}f_k^a + B_{vR}^{aa}e_k^a\right) - \left(G_{vR}^{aa}f_{vR}^a + B_{vR}^{aa}e_{vR}^a\right)\right] \end{aligned} \tag{I.50}$$

Similar expressions can be obtained for phases *b* and *c*. A generalized expression for the three-phases at bus *k* can be write as:

$$\begin{aligned} P_k^\rho &= e_k^\rho\left[\left(G_{vR}^{\rho\rho}e_k^\rho - B_{vR}^{\rho\rho}f_k^\rho\right) - \left(G_{vR}^{\rho\rho}e_{vR}^\rho - B_{vR}^{\rho\rho}f_{vR}^\rho\right)\right] \\ &\quad + f_k^\rho\left[\left(G_{vR}^{\rho\rho}f_k^\rho + B_{vR}^{\rho\rho}e_k^\rho\right) - \left(G_{vR}^{\rho\rho}f_{vR}^\rho + B_{vR}^{\rho\rho}e_{vR}^\rho\right)\right] \end{aligned} \tag{I.51}$$

For the reactive power:

$$\begin{aligned} Q_k^a &= f_k^a\left[\left(G_{vR}^{aa}e_k^a - B_{vR}^{aa}f_k^a\right) - \left(G_{vR}^{aa}e_{vR}^a - B_{vR}^{aa}f_{vR}^a\right)\right] \\ &\quad + e_k^a\left[-\left(G_{vR}^{aa}f_k^a + B_{vR}^{aa}e_k^a\right) + \left(G_{vR}^{aa}f_{vR}^a + B_{vR}^{aa}e_{vR}^a\right)\right] \end{aligned} \tag{I.52}$$

And the generalized expressions for the reactive power injected into the phases of the bus *k* are:

$$\begin{aligned} Q_k^\rho = f_k^\rho &\left[\left(G_{vR}^{\rho\rho} e_k^\rho - B_{vR}^{\rho\rho} f_k^\rho\right) - \left(G_{vR}^{\rho\rho} e_{vR}^\rho - B_{vR}^{\rho\rho} f_{vR}^\rho\right)\right] \\ + e_k^\rho &\left[-\left(G_{vR}^{\rho\rho} f_k^\rho + B_{vR}^{\rho\rho} e_k^\rho\right) + \left(G_{vR}^{\rho\rho} f_{vR}^\rho + B_{vR}^{\rho\rho} e_{vR}^\rho\right)\right] \end{aligned} \tag{I.53}$$

As expected, the expressions for calculating the active and reactive powers injected into the STATCOM are of the same form as (I.51) and (I.53), with the subscript *vR* replacing *k* and *vice versa*:

$$\begin{aligned} P_{vR}^\rho = e_{vR}^\rho &\left[\left(G_{vR}^{\rho\rho} e_{vR}^\rho - B_{vR}^{\rho\rho} f_{vR}^\rho\right) - \left(G_{vR}^{\rho\rho} e_k^\rho - B_{vR}^{\rho\rho} f_k^\rho\right)\right] \\ + f_{vR}^\rho &\left[\left(G_{vR}^{\rho\rho} f_{vR}^\rho + B_{vR}^{\rho\rho} e_{vR}^\rho\right) - \left(G_{vR}^{\rho\rho} f_k^\rho + B_{vR}^{\rho\rho} e_k^\rho\right)\right] \end{aligned} \tag{I.54}$$

$$\begin{aligned} Q_{vR}^\rho = f_{vR}^\rho &\left[\left(G_{vR}^{\rho\rho} e_{vR}^\rho - B_{vR}^{\rho\rho} f_{vR}^\rho\right) - \left(G_{vR}^{\rho\rho} e_k^\rho - B_{vR}^{\rho\rho} f_k^\rho\right)\right] \\ + e_{vR}^\rho &\left[-\left(G_{vR}^{\rho\rho} f_{vR}^\rho + B_{vR}^{\rho\rho} e_{vR}^\rho\right) + \left(G_{vR}^{\rho\rho} f_k^\rho + B_{vR}^{\rho\rho} e_k^\rho\right)\right] \end{aligned} \tag{I.55}$$

Active and reactive power expression in polar coordinates for SSSC, UPFC and HVDC-VSC controllers in the three-phase frame of reference are obtained in a same manner as the above process.

APPENDIX II: NETWORKS TEST DATA

Data are given in per unit on a 100 MW and 400 KV base values of active power and voltage respectively.

II.1 Five-bus System Test

Transmission lines

Bus code		Impedance	Line Charging
north	south	0.02 + j0.06	0.0 + j0.06
north	lake	0.08 + j0.24	0.0 + j0.05
south	lake	0.06 + j0.18	0.0 + j0.04
south	main	0.06 + j0.18	0.0 + j0.04
south	elm	0.04 + j0.12	0.0 + j0.03
lake	main	0.01 + j0.03	0.0 + j0.02
main	elm	0.08 + j0.24	0.0 + j0.05

Generation

Bus code	MW	MVAR	MVAR limits		Voltage magnitude
			min	max	
north*	-	-	-	-	1.06
south	40	0	-300	300	1.00

Loads

Bus code	MW	MVAR
south	40	0
lake	45	15
main	40	5
elm	60	10

II.2 New England Reduced System Test

Transmission lines

Bus code		Impedance			Line Charging		
from	to						
1	2	0.0035	+j	0.0411	0.0	+j	0.6987
1	39	0.0010	+j	0.0250	0.0	+j	0.7500
2	3	0.0013	+j	0.0151	0.0	+j	0.2572

2	25	0.0070	+j	0.0086	0.0	+j	0.1460
3	4	0.0013	+j	0.0213	0.0	+j	0.2214
3	18	0.0011	+j	0.0133	0.0	+j	0.2138
4	5	0.0008	+j	0.0128	0.0	+j	0.1342
4	14	0.0008	+j	0.0129	0.0	+j	0.1382
5	6	0.0002	+j	0.0026	0.0	+j	0.0434
5	8	0.0008	+j	0.0112	0.0	+j	0.1476
6	7	0.0006	+j	0.0092	0.0	+j	0.1130
6	11	0.0007	+j	0.0082	0.0	+j	0.1389
7	8	0.0004	+j	0.0046	0.0	+j	0.0780
8	9	0.0023	+j	0.0363	0.0	+j	0.3804
9	39	0.0010	+j	0.0250	0.0	+j	1.200
10	11	0.0004	+j	0.0043	0.0	+j	0.0729
10	13	0.0004	+j	0.0043	0.0	+j	0.0729
13	14	0.0009	+j	0.0101	0.0	+j	0.1725
14	15	0.0018	+j	0.0217	0.0	+j	0.3660
15	16	0.0009	+j	0.0094	0.0	+j	0.1710
16	17	0.0007	+j	0.0089	0.0	+j	0.1342
16	19	0.0016	+j	0.0195	0.0	+j	0.3040
16	21	0.0008	+j	0.0135	0.0	+j	0.2548
16	24	0.0003	+j	0.0059	0.0	+j	0.0680
17	18	0.0007	+j	0.0082	0.0	+j	0.1319
17	27	0.0013	+j	0.0173	0.0	+j	0.3216
21	22	0.0008	+j	0.0140	0.0	+j	0.2565
22	23	0.0006	+j	0.0096	0.0	+j	0.1845
23	24	0.0022	+j	0.0350	0.0	+j	0.3610
25	26	0.0032	+j	0.0323	0.0	+j	0.5130
26	27	0.0014	+j	0.0147	0.0	+j	0.2396
26	28	0.0043	+j	0.0474	0.0	+j	0.7802
26	29	0.0057	+j	0.0625	0.0	+j	1.0290
28	29	0.0014	+j	0.0151	0.0	+j	0.2490

Transformers

Bus code		Rs	Xs	Tv	Uv
from	to				
2	30	0.0	0.0181	1.025	1
6	31	0.0	0.025	1.07	1
10	32	0.0	0.02	1.07	1
12	11	0.0016	0.0435	1.006	1
12	13	0.0016	0.0435	1.006	1
19	20	0.0007	0.0138	1.06	1
19	33	0.0007	0.0142	1.07	1
20	34	0.0009	0.018	1.009	1
22	35	0	0.0143	1.025	1
23	36	0.0005	0.0272	1	1
25	37	0.0006	0.0232	1.025	1
29	38	0.0008	0.0156	1.025	1

Generation

Bus code	MW	MVAR	MVAR limits		Voltage magnitude
			min	max	
39*	-	-	-	-	1.0300

APPENDIX II: NETWORKS TEST DATA

Data are given in per unit on a 100 MW and 400 KV base values of active power and voltage respectively.

II.1 Five-bus System Test

Transmission lines

Bus code		Impedance	Line Charging
north	south	0.02 + j0.06	0.0 + j0.06
north	lake	0.08 + j0.24	0.0 + j0.05
south	lake	0.06 + j0.18	0.0 + j0.04
south	main	0.06 + j0.18	0.0 + j0.04
south	elm	0.04 + j0.12	0.0 + j0.03
lake	main	0.01 + j0.03	0.0 + j0.02
main	elm	0.08 + j0.24	0.0 + j0.05

Generation

Bus code	MW	MVAR	MVAR limits		Voltage magnitude
			min	max	
north*	-	-	-	-	1.06
south	40	0	-300	300	1.00

Loads

Bus code	MW	MVAR
south	40	0
lake	45	15
main	40	5
elm	60	10

II.2 New England Reduced System Test

Transmission lines

Bus code		Impedance			Line Charging		
from	to						
1	2	0.0035	+j	0.0411	0.0	+j	0.6987
1	39	0.0010	+j	0.0250	0.0	+j	0.7500
2	3	0.0013	+j	0.0151	0.0	+j	0.2572

30	250	0.0	-200	300	1.0475
31	573.2	0.0	-300	300	0.9520
32	650	0.0	-300	300	0.9831
33	632	0.0	-200	300	0.9972
34	508	0.0	-200	300	1.0123
35	650	0.0	-250	350	1.0493
36	560	0.0	-150	250	1.0635
37	540	0.0	-250	350	1.0278
38	830	0.0	-400	400	1.0265

* Slack bus

Loads

Bus code	MW	MVAR
3	322	2.4
4	500	184
7	233	84
8	522	176
12	8.5	88
15	320	153
16	329.4	32.3
18	158	30
20	680	103
21	274	115

Bus code	MW	MVAR
23	247.5	84.6
24	308.6	-92.2
25	224	47.2
26	139	17
27	281	75.5
28	206	27.6
29	283.5	26.9
31	9.2	4.6
39	1104	250

II.3 IEEE 57 Buses System Test

Transmission lines

Bus code		Impedance			Line Charging		
From	to						
1	2	0.0083	+j	0.028	0.0	+j	0.129
2	3	0.0298	+j	0.085	0.0	+j	0.0818
3	4	0.0112	+j	0.0366	0.0	+j	0.038
4	5	0.0625	+j	0.132	0.0	+j	0.0258
4	6	0.043	+j	0.148	0.0	+j	0.0348
6	7	0.02	+j	0.102	0.0	+j	0.0276
6	8	0.0339	+j	0.173	0.0	+j	0.047
8	9	0.0099	+j	0.0505	0.0	+j	0.0548
9	10	0.0369	+j	0.1679	0.0	+j	0.044
9	11	0.0258	+j	0.0848	0.0	+j	0.0218
9	12	0.0648	+j	0.295	0.0	+j	0.0772
9	13	0.0481	+j	0.158	0.0	+j	0.0406
13	14	0.0132	+j	0.0434	0.0	+j	0.011
13	15	0.0269	+j	0.0869	0.0	+j	0.023
1	15	0.0178	+j	0.091	0.0	+j	0.0988
1	16	0.0454	+j	0.206	0.0	+j	0.0546
1	17	0.0238	+j	0.108	0.0	+j	0.0286
3	15	0.0162	+j	0.053	0.0	+j	0.0544

5	6	0.0302	+j	0.0641	0.0	+j	0.0124
7	8	0.0139	+j	0.0712	0.0	+j	0.0194
10	12	0.0277	+j	0.1262	0.0	+j	0.0328
11	13	0.0223	+j	0.0732	0.0	+j	0.0188
12	13	0.0178	+j	0.058	0.0	+j	0.0604
12	16	0.018	+j	0.0813	0.0	+j	0.0216
12	17	0.0397	+j	0.179	0.0	+j	0.0476
14	15	0.0171	+j	0.0547	0.0	+j	0.0148
18	19	0.461	+j	0.685	0.0	+j	0
19	20	0.283	+j	0.434	0.0	+j	0
21	22	0.0736	+j	0.117	0.0	+j	0
22	23	0.0099	+j	0.0152	0.0	+j	0
23	24	0.166	+j	0.256	0.0	+j	0.0084
26	27	0.165	+j	0.254	0.0	+j	0
27	28	0.0618	+j	0.0954	0.0	+j	0
28	29	0.0418	+j	0.0587	0.0	+j	0
25	30	0.135	+j	0.202	0.0	+j	0
30	31	0.326	+j	0.497	0.0	+j	0
31	32	0.507	+j	0.755	0.0	+j	0
32	33	0.0392	+j	0.036	0.0	+j	0
34	35	0.052	+j	0.078	0.0	+j	0.0032
35	36	0.043	+j	0.0537	0.0	+j	0.0016
36	37	0.029	+j	0.0366	0.0	+j	0
37	38	0.0651	+j	0.1009	0.0	+j	0.002
37	39	0.0239	+j	0.0379	0.0	+j	0
36	40	0.03	+j	0.0466	0.0	+j	0
22	38	0.0192	+j	0.0295	0.0	+j	0
41	42	0.207	+j	0.352	0.0	+j	0
38	44	0.0289	+j	0.0585	0.0	+j	0.002
46	47	0.023	+j	0.068	0.0	+j	0.0032
47	48	0.0182	+j	0.0233	0.0	+j	0
48	49	0.0834	+j	0.129	0.0	+j	0.0048
49	50	0.0801	+j	0.128	0.0	+j	0
50	51	0.1386	+j	0.22	0.0	+j	0
29	52	0.1442	+j	0.187	0.0	+j	0
52	53	0.0762	+j	0.0984	0.0	+j	0
53	54	0.1878	+j	0.232	0.0	+j	0
54	55	0.1732	+j	0.2265	0.0	+j	0
44	45	0.0624	+j	0.1242	0.0	+j	0.004
56	41	0.553	+j	0.549	0.0	+j	0
56	42	0.2125	+j	0.354	0.0	+j	0
57	56	0.174	+j	0.26	0.0	+j	0
38	49	0.115	+j	0.177	0.0	+j	0.006
38	48	0.0312	+j	0.0482	0.0	+j	0

Transformers

Bus code		Rs	Xs	Tv
from	to			
4	18	0.555	0.97	1.0
4	18	0.43	0.978	1.0
21	20	0.7767	1.043	1.0
24	25	1.182	1	1.0
24	25	1.23	1	1.0
24	26	0.0473	1.043	1.0

Bus code		Rs	Xs	Tv
from	to			
41	43	0.412	1.0	1.0
15	45	0.1042	0.955	1.0
14	46	0.0735	0.9	1.0
10	51	0.0712	0.93	1.0
13	49	0.191	0.895	1.0
11	43	0.153	0.958	1.0

7	29	0.0648	0.967	1.0	40	56	1.195	0.958	1.0
34	32	0.953	0.975	1.0	39	57	1.355	0.98	1.0
11	41	0.749	0.955	1.0	9	55	0.1205	0.94	1.0

Generation

Bus code	MW	MVAR	MVAR limits		Voltage magnitude
			min	max	
1*	-	-	-	-	1.06
2	0	0.0	-17	50	1.01
3	40	0.0	-10	60	0.985
6	0	0.0	-8	25	0.98
8	450	0.0	-140	200	1.005
9	0	0.0	-3	9	0.98
12	310	0.0	-150	155	1.015

* Slack bus

Shunt compensation

Bus code	MW	MVAR
18	0	0.1
25	0	0.059
53	0	0.063

Loads

Bus code	MW	MVAR	Bus code	MW	MVAR	Bus code	MW	MVAR
1	55	17	20	2.3	1	47	29.7	11.6
2	3	88	23	6.3	2.1	49	18	8.5
3	41	21	25	6.3	3.2	50	21	10.5
5	13	4	27	9.3	0.5	51	18	5.3
6	75	2	28	4.6	2.3	52	4.9	2.2
8	150	22	29	17	2.6	53	20	10
9	121	26	30	3.6	1.8	54	4.1	1.4
10	5	2	31	5.8	2.9	55	6.8	3.4
12	377	24	32	1.6	0.8	56	7.6	2.2
13	18	2.3	33	3.8	1.9	57	6.7	2
14	10.5	5.3	35	6	3			
15	22	5	38	14	7			
16	43	3	41	6.3	3			
17	42	8	42	7.1	4.4			
18	27.2	9.8	43	2	1			
19	3.3	0.6	44	12	1.8			

APPENDIX III: JACOBIAN MATRIX ELEMENTS

POLAR CO-ORDINATES

III.1 Unified Power Flow Controller

Consider the UPFC connected between buses *k* and *m*, for which the linearised equation for polar co-ordinates is shown in Equation (3.88). The Jacobian matrix elements are explicitly given below, with the help of a phase superscript ρ used to denote *a*, *b* and *c*, respectively.

The Jacobian terms at sending node *k* are:

$$\frac{\partial P_k^\rho}{\partial \theta_k^\rho} = -Q_k^\rho - \left(V_k^\rho\right)^2 B_{kk}^{\rho\rho} \tag{III.1}$$

$$\frac{\partial P_k^\rho}{\partial V_k^\rho} V_k^\rho = P_k^\rho + \left(V_k^\rho\right)^2 G_{kk}^{\rho\rho} \tag{III.2}$$

$$\frac{\partial Q_k^\rho}{\partial \theta_k^\rho} = P_k^\rho - \left(V_k^\rho\right)^2 G_{kk}^{\rho\rho} \tag{III.3}$$

$$\frac{\partial Q_k^\rho}{\partial V_k^\rho} V_k^\rho = Q_k^\rho - \left(V_k^\rho\right)^2 B_{kk}^{\rho\rho} \tag{III.4}$$

$$\frac{\partial P_k^\rho}{\partial \theta_m^\rho} = V_k^\rho V_m^\rho \left[G_{km}^{\rho\rho} \sin\left(\theta_k^\rho - \theta_m^\rho\right) - B_{km}^{\rho\rho} \cos\left(\theta_k^\rho - \theta_m^\rho\right) \right] \tag{III.5}$$

$$\frac{\partial P_k^\rho}{\partial V_m^\rho} V_m^\rho = V_k^\rho V_m^\rho \left[G_{km}^{\rho\rho} \cos\left(\theta_k^\rho - \theta_m^\rho\right) + B_{km}^{\rho\rho} \sin\left(\theta_k^\rho - \theta_m^\rho\right) \right] \tag{III.6}$$

$$\frac{\partial P_k^\rho}{\partial \delta_{cR}^\rho} = V_k^\rho V_{cR}^\rho \left[G_{km}^{\rho\rho} \sin\left(\theta_k^\rho - \delta_{cR}^\rho\right) - B_{km}^{\rho\rho} \cos\left(\theta_k^\rho - \delta_{cR}^\rho\right) \right] \tag{III.7}$$

$$\frac{\partial P_k^\rho}{\partial V_{cR}^\rho} V_{cR}^\rho = V_k^\rho V_{cR}^\rho \left[G_{km}^{\rho\rho} \cos\left(\theta_k^\rho - \delta_{cR}^\rho\right) + B_{km}^{\rho\rho} \sin\left(\theta_k^\rho - \delta_{cR}^\rho\right) \right] \tag{III.8}$$

$$\frac{\partial P_k^\rho}{\partial \delta_{vR}^\rho} = V_k^\rho V_{vR}^\rho \left[G_{vR}^{\rho\rho} \sin\left(\theta_k^\rho - \delta_{vR}^\rho\right) - B_{vR}^{\rho\rho} \cos\left(\theta_k^\rho - \delta_{vR}^\rho\right) \right] \tag{III.9}$$

$$\frac{\partial P_k^\rho}{\partial V_{vR}^\rho} V_{vR}^\rho = V_k^\rho V_{vR}^\rho \left[G_{km}^{\rho\rho} \cos\left(\theta_k^\rho - \delta_{vR}^\rho\right) + B_{km}^{\rho\rho} \sin\left(\theta_k^\rho - \delta_{vR}^\rho\right) \right] \tag{III.10}$$

$$\frac{\partial Q_k^\rho}{\partial \theta_m^\rho} = -V_k^\rho V_m^\rho \left[G_{km}^{\rho\rho} \cos\left(\theta_k^\rho - \theta_m^\rho\right) + B_{km}^{\rho\rho} \sin\left(\theta_k^\rho - \theta_m^\rho\right) \right] \tag{III.11}$$

$$\frac{\partial Q_k^\rho}{\partial V_m^\rho} V_m^\rho = V_k^\rho V_m^\rho \left[G_{km}^{\rho\rho} \sin\left(\theta_k^\rho - \theta_m^\rho\right) - B_{km}^{\rho\rho} \cos\left(\theta_k^\rho - \theta_m^\rho\right) \right] \quad \text{(III.12)}$$

$$\frac{\partial Q_k^\rho}{\partial \delta_{cR}^\rho} = -V_k^\rho V_{cR}^\rho \left[G_{km}^{\rho\rho} \cos\left(\theta_k^\rho - \delta_{cR}^\rho\right) + B_{km}^{\rho\rho} \sin\left(\theta_k^\rho - \delta_{cR}^\rho\right) \right] \quad \text{(III.13)}$$

$$\frac{\partial Q_k^\rho}{\partial V_{cR}^\rho} V_{cR}^\rho = V_k^\rho V_{cR}^\rho \left[G_{km}^{\rho\rho} \sin\left(\theta_k^\rho - \delta_{cR}^\rho\right) - B_{km}^{\rho\rho} \cos\left(\theta_k^\rho - \delta_{cR}^\rho\right) \right] \quad \text{(III.14)}$$

$$\frac{\partial Q_k^\rho}{\partial \delta_{vR}^\rho} = -V_k^\rho V_{vR}^\rho \left[G_{km}^{\rho\rho} \cos\left(\theta_k^\rho - \delta_{vR}^\rho\right) + B_{km}^{\rho\rho} \sin\left(\theta_k^\rho - \delta_{vR}^\rho\right) \right] \quad \text{(III.15)}$$

$$\frac{\partial Q_k^\rho}{\partial V_{vR}^\rho} V_{vR}^\rho = V_k^\rho V_{vR}^\rho \left[G_{km}^{\rho\rho} \sin\left(\theta_k^\rho - \delta_{vR}^\rho\right) - B_{km}^{\rho\rho} \cos\left(\theta_k^\rho - \delta_{vR}^\rho\right) \right] \quad \text{(III.16)}$$

Where $B_{kk} = \left(B_{cR} + B_{vR}\right); G_{kk} = \left(G_{cR} + G_{vR}\right)$ and $B_{km} = B_{cR}$ and $G_{km} = G_{cR}$
The Jacobian terms at receiving node *m* are obtained by changing subscript *k* to *m* and *vice*. However it should be notice that now $B_{mm} = B_{mk} = B_{cR}$ and $G_{mm} = G_{mk} = G_{cR}$ and derivatives respect to shunt voltage source are zero.

From Equation (3.78) it should be notice that $P_{mk}^\rho = P_k^\rho$ and its derivatives are equals. Finally $P_{bb}^\rho = P_{vR}^\rho + P_{cR}^\rho$ derivatives correspondent to P_{bb}^ρ are show below.

The Jacobian matrix elements of series converter are:

$$\frac{\partial P_{cR}^\rho}{\partial \theta_k^\rho} = V_{cR}^\rho V_k^\rho \left[G_{km}^{\rho\rho} \sin\left(\delta_{cR}^\rho - \theta_k^\rho\right) - B_{km}^{\rho\rho} \cos\left(\delta_{cR}^\rho - \theta_k^\rho\right) \right] \quad \text{(III.17)}$$

$$\frac{\partial P_{cR}^\rho}{\partial \theta_m^\rho} = V_{cR}^\rho V_m^\rho \left[G_{km}^{\rho\rho} \sin\left(\delta_{cR}^\rho - \theta_m^\rho\right) - B_{km}^{\rho\rho} \cos\left(\delta_{cR}^\rho - \theta_m^\rho\right) \right] \quad \text{(III.18)}$$

$$\frac{\partial P_{cR}^\rho}{\partial V_k^\rho} V_k^\rho = V_{cR}^\rho V_k^\rho \left[G_{km}^{\rho\rho} \cos\left(\delta_{cR}^\rho - \theta_k^\rho\right) + B_{km}^{\rho\rho} \sin\left(\delta_{cR}^\rho - \theta_k^\rho\right) \right] \quad \text{(III.19)}$$

$$\frac{\partial P_{cR}^\rho}{\partial \delta_{cR}^\rho} = -Q_{cR}^\rho - \left(V_{cR}^\rho\right)^2 B_{mm}^{\rho\rho} \quad \text{(III.20)}$$

$$\frac{\partial P_{cR}^\rho}{\partial V_{cR}^\rho} V_{cR}^\rho = P_{cR}^\rho + \left(V_{cR}^\rho\right)^2 G_{mm}^{\rho\rho} \quad \text{(III.21)}$$

$$\frac{\partial P_{cR}^\rho}{\partial V_m^\rho} V_m^\rho = V_{cR}^\rho V_m^\rho \left[G_{km}^{\rho\rho} \cos\left(\delta_{cR}^\rho - \theta_k^\rho\right) + B_{km}^{\rho\rho} \sin\left(\delta_{cR}^\rho - \theta_k^\rho\right) \right] \quad \text{(III.22)}$$

The Jacobian elements of shunt-connected inverter are:

$$\frac{\partial P_{vR}^{\rho}}{\partial \theta_k^{\rho}} = V_{vR}^{\rho} V_k^{\rho} \left[G_{vR}^{\rho\rho} \sin\left(\delta_{vR}^{\rho} - \theta_k^{\rho}\right) - B_{vR}^{\rho\rho} \cos\left(\delta_{vR}^{\rho} - \theta_k^{\rho}\right) \right] \tag{III.23}$$

$$\frac{\partial P_{vR}^{\rho}}{\partial V_k^{\rho}} V_k^{\rho} = V_{vR}^{\rho} V_k^{\rho} \left[G_{vR}^{\rho\rho} \cos\left(\delta_{vR}^{\rho} - \theta_k^{\rho}\right) + B_{vR}^{\rho\rho} \sin\left(\delta_{vR}^{\rho} - \theta_k^{\rho}\right) \right] \tag{III.24}$$

$$\frac{\partial P_{vR}^{\rho}}{\partial \delta_{vR}^{\rho}} = -Q_{vR}^{\rho} - \left(V_{vR}^{\rho}\right)^{\rho} B_{vR}^{\rho\rho} \tag{III.25}$$

$$\frac{\partial P_{vR}^{\rho\rho}}{\partial V_{vR}^{\rho}} V_{vR}^{\rho} = P_{vR}^{\rho} + \left(V_{vR}^{\rho}\right)^{\rho} G_{vR}^{\rho\rho} \tag{III.26}$$

III.2 High-voltage Direct Current VSC-based

Jacobian matrix elements for the HVDC-VSC model are given as:

$$\frac{\partial P_k^{\rho}}{\partial \theta_k^{\rho}} = -Q_k^{\rho} - \left(V_k^{\rho}\right)^2 G_{vR1}^{\rho\rho} \tag{III.27}$$

$$\frac{\partial P_k^{\rho}}{\partial V_k^{\rho}} V_k^{\rho} = P_k^{\rho} + \left(V_k^{\rho}\right)^2 G_{vR1}^{\rho\rho} \tag{III.28}$$

$$\frac{\partial P_k^{\rho}}{\partial \delta_{vR1}^{\rho}} = -V_k^{\rho} V_{vR1}^{\rho} \left[G_{vR1}^{\rho\rho} \sin\left(\theta_k^{\rho} - \delta_{vR1}^{\rho}\right) - B_{vR1}^{\rho\rho} \cos\left(\theta_k^{\rho} - \delta_{vR1}^{\rho}\right) \right] \tag{III.29}$$

$$\frac{\partial P_k^{\rho}}{\partial V_{vR1}^{\rho}} V_{vR1}^{\rho} = -V_k^{\rho} V_{vR1}^{\rho} \left[G_{vR1}^{\rho\rho} \cos\left(\theta_k^{\rho} - \delta_{vR1}^{\rho}\right) + B_{vR1}^{\rho} \sin\left(\theta_k^{\rho} - \delta_{vR1}^{\rho}\right) \right] \tag{III.30}$$

$$\frac{\partial Q_k^{\rho}}{\partial \theta_k^{\rho}} = P_k^{\rho} - \left(V_k^{\rho}\right) G_{vR1}^{\rho\rho} \tag{III.31}$$

$$\frac{\partial Q_k^{\rho}}{\partial V_k^{\rho}} V_k^{\rho} = Q_k^{\rho} - \left(V_k^{\rho}\right)^2 B_{vR1}^{\rho\rho} \tag{III.32}$$

$$\frac{\partial Q_k^{\rho}}{\partial \delta_{vR1}^{\rho}} = V_k^{\rho} V_{vR1}^{\rho} \left[G_{vR1}^{\rho\rho} \cos\left(\theta_k^{\rho} - \delta_{vR1}^{\rho}\right) + B_{vR1}^{\rho\rho} \sin\left(\theta_k^{\rho} - \delta_{vR1}^{\rho}\right) \right] \tag{III.33}$$

$$\frac{\partial Q_k^{\rho}}{\partial V_{vR1}^{\rho}} V_{vR1}^{\rho} = -V_k^{\rho} V_{vR1}^{\rho} \left[G_{vR1}^{\rho\rho} \sin\left(\theta_k^{\rho} - \delta_{vR1}^{\rho}\right) - B_{vR1}^{\rho\rho} \cos\left(\theta_k^{\rho} - \delta_{vR1}^{\rho}\right) \right] \tag{III.34}$$

$$\frac{\partial P_{vR1}^{\rho}}{\partial \theta_k^{\rho}} = -V_{vR1}^{\rho} V_k^{\rho} \left[G_{vR1}^{\rho\rho} \sin\left(\delta_{vR1}^{\rho} - \theta_k^{\rho}\right) - B_{vR1}^{\rho\rho} \cos\left(\delta_{vR1}^{\rho} - \theta_k^{\rho}\right) \right] \tag{III.35}$$

$$\frac{\partial P_{vR1}^{\rho}}{\partial V_k^{\rho}} V_k^{\rho} = -V_{vR1}^{\rho} V_k^{\rho} \left[G_{vR1}^{\rho\rho} \cos\left(\delta_{vR1}^{\rho} - \theta_k^{\rho}\right) + B_{vR1}^{\rho\rho} \sin\left(\delta_{vR1}^{\rho} - \theta_k^{\rho}\right) \right] \tag{III.36}$$

$$\frac{\partial P^{\rho}_{vR1}}{\partial \delta^{\rho}_{vR1}} = -Q^{\rho}_{vR1} - \left(V^{\rho}_{vR1}\right)^2 B^{\rho\rho}_{vR1} \tag{III.37}$$

$$\frac{\partial P^{\rho}_{vR1}}{\partial V^{\rho}_{vR1}} V^{\rho}_{vR1} = P^{\rho}_{vR1} + \left(V^{\rho}_{vR1}\right)^2 G^{\rho\rho}_{vR1} \tag{III.38}$$

$$\frac{\partial Q^{\rho}_{vR1}}{\partial \delta^{\rho}_{vR1}} = P^{\rho}_{vR1} - \left(V^{\rho}_{vR1}\right)^2 G^{\rho\rho}_{vR1} \tag{III.39}$$

$$\frac{\partial Q^{\rho}_{vR1}}{\partial \theta^{\rho}_{k}} = V^{\rho}_{vR1} V^{\rho}_{k} \left[G^{\rho\rho}_{vR1} \cos\left(\delta^{\rho}_{vR1} - \theta^{\rho}_{k}\right) + B^{\rho}_{vR1} \sin\left(\delta^{\rho}_{vR1} - \theta^{\rho}_{k}\right) \right] \tag{III.40}$$

$$\frac{\partial Q^{\rho}_{vR1}}{\partial V^{\rho}_{k}} V^{\rho}_{k} = -V^{\rho}_{vR1} V^{\rho}_{k} \left[G^{\rho\rho}_{vR1} \sin\left(\delta^{\rho}_{vR1} - \theta^{\rho}_{k}\right) - B^{\rho\rho}_{vR1} \cos\left(\delta^{\rho}_{vR1} - \theta^{\rho}_{k}\right) \right] \tag{III.41}$$

$$\frac{\partial Q^{\rho}_{vR1}}{\partial V^{\rho}_{vR1}} V^{\rho}_{vR1} = Q^{\rho}_{vR1} - \left(V^{\rho}_{vR}\right)^2 B^{\rho\rho}_{vR1} \tag{III.42}$$

$$\frac{\partial P^{\rho}_{HVDC}}{\partial \theta^{\rho}_{k}} = -Q^{\rho}_{k} - \left(V^{\rho}_{k}\right)^2 G^{\rho\rho}_{vR1} \tag{III.43}$$

$$\frac{\partial P^{\rho}_{HVDC}}{\partial V^{\rho}_{k}} V^{\rho}_{k} = P^{\rho}_{k} + \left(V^{\rho}_{k}\right)^2 G^{\rho\rho}_{vR1} \tag{III.44}$$

$$\frac{\partial P^{\rho}_{HVDC}}{\partial \delta^{\rho}_{vR1}} = -V^{\rho}_{k} V^{\rho}_{vR1} \left[G^{\rho\rho}_{vR1} \sin\left(\theta^{\rho}_{k} - \delta^{\rho}_{vR1}\right) - B^{\rho\rho}_{vR1} \cos\left(\theta^{\rho}_{k} - \delta^{\rho}_{vR1}\right) \right] \tag{III.45}$$

$$\frac{\partial P^{\rho}_{HVDC}}{\partial V^{\rho}_{vR1}} V^{\rho}_{vR1} = -V^{\rho}_{k} V^{\rho}_{vR1} \left[G^{\rho\rho}_{vR1} \cos\left(\theta^{\rho}_{k} - \delta^{\rho}_{vR1}\right) + B^{\rho\rho}_{vR1} \sin\left(\theta^{\rho}_{k} - \delta^{\rho}_{vR1}\right) \right] \tag{III.46}$$

$$\frac{\partial P^{\rho}_{HVDC}}{\partial \delta^{\rho}_{vR2}} = -Q^{\rho}_{vR2} - \left(V^{\rho}_{vR2}\right)^2 B^{\rho\rho}_{vR2} \tag{III.47}$$

RECTANGULAR Co-ordinates

III.3 Unified Power Flows Controller

The Jacobian matrix elements in equation (4.86) are given below

$$\frac{\partial P^{\rho}_{k}}{\partial e^{\rho}_{k}} = 2\left(G^{\rho\rho}_{cR} + G^{\rho\rho}_{vR}\right) e^{\rho}_{k} - \left(G^{\rho\rho}_{cR} e^{\rho}_{m} - B^{\rho\rho}_{cR} f^{\rho}_{m}\right) \tag{III.48}$$

$$- \left(G^{\rho\rho}_{cR} e^{\rho}_{cR} - B^{\rho\rho}_{cR} f^{\rho}_{cR}\right) - \left(G^{\rho\rho}_{vR} e^{\rho}_{vR} - B^{\rho\rho}_{vR} f^{\rho}_{vR}\right)$$

$$\frac{\partial P^{\rho}_{k}}{\partial f^{\rho}_{k}} = 2\left(G^{\rho\rho}_{cR} + G^{\rho\rho}_{vR}\right) f^{\rho}_{k} - \left(G^{\rho\rho}_{cR} f^{\rho}_{m} + B^{\rho\rho}_{cR} e^{\rho}_{m}\right) \tag{III.49}$$

$$- \left(G^{\rho\rho}_{cR} f^{\rho}_{cR} + B^{\rho\rho}_{cR} e^{\rho}_{cR}\right) - \left(G^{\rho\rho}_{vR} f^{\rho}_{vR} + B^{\rho\rho}_{vR} e^{\rho}_{vR}\right)$$

$$\frac{\partial Q_k^\rho}{\partial e_k^\rho} = 2\left(B_{cR}^{\rho\rho} + B_{vR}^{\rho\rho}\right)e_k^\rho + \left(G_{cR}^{\rho\rho} f_m^\rho + B_{cR}^{\rho\rho} e_m^\rho\right) \tag{III.50}$$
$$+\left(G_{cR}^{\rho\rho} f_{cR}^\rho + B_{cR}^{\rho\rho} e_{cR}^\rho\right)+\left(G_{vR}^{\rho\rho} f_{vR}^\rho + B_{vR}^{\rho\rho} e_{vR}^\rho\right)$$

$$\frac{\partial Q_k^\rho}{\partial e_k^\rho} = -2\left(B_{cR}^{\rho\rho} + B_{vR}^{\rho\rho}\right)f_k^\rho - \left(G_{cR}^{\rho\rho} e_m^\rho - B_{cR}^{\rho\rho} f_m^\rho\right) \tag{III.51}$$
$$-\left(G_{cR}^{\rho\rho} e_{cR}^\rho - B_{cR}^{\rho\rho} f_{cR}^\rho\right)-\left(G_{vR}^{\rho\rho} e_{vR}^\rho - B_{vR}^{\rho\rho} f_{vR}^\rho\right)$$

$$\frac{\partial P_k^\rho}{\partial e_m^\rho} = -\left(G_{cR}^{\rho\rho} e_k^\rho + B_{cR}^{\rho\rho} f_k^\rho\right) \tag{III.52}$$

$$\frac{\partial P_k^\rho}{\partial f_m^\rho} = -\left(G_{cR}^{\rho\rho} f_k^\rho - B_{cR}^{\rho\rho} e_k^\rho\right) \tag{III.53}$$

$$\frac{\partial P_k^\rho}{\partial e_{cR}^\rho} = -\left(G_{cR}^{\rho\rho} e_k^\rho + B_{cR}^{\rho\rho} f_k^\rho\right) \tag{III.54}$$

$$\frac{\partial P_k^\rho}{\partial f_{cR}^\rho} = -\left(G_{cR}^{\rho\rho} f_k^\rho - B_{cR}^{\rho\rho} e_k^\rho\right) \tag{III.55}$$

$$\frac{\partial P_k^\rho}{\partial e_{vR}^\rho} = -\left(G_{vR}^{\rho\rho} e_k^\rho + B_{vR}^{\rho\rho} f_k^\rho\right) \tag{III.56}$$

$$\frac{\partial P_k^\rho}{\partial f_{vR}^\rho} = -\left(G_{vR}^{\rho\rho} f_k^\rho - B_{vR}^{\rho\rho} e_k^\rho\right) \tag{III.57}$$

$$\frac{\partial Q_k^\rho}{\partial e_m^\rho} = -\left(G_{cR}^{\rho\rho} f_k^\rho - B_{cR}^{\rho\rho} e_k^\rho\right) \tag{III.58}$$

$$\frac{\partial Q_k^\rho}{\partial f_m^\rho} = \left(G_{cR}^{\rho\rho} e_k^\rho + B_{cR}^{\rho\rho} f_k^\rho\right) \tag{III.59}$$

$$\frac{\partial Q_k^\rho}{\partial e_{cR}^\rho} = -\left(G_{cR}^{\rho\rho} f_k^\rho - B_{cR}^{\rho\rho} e_k^\rho\right) \tag{III.60}$$

$$\frac{\partial Q_k^\rho}{\partial f_{cR}^\rho} = \left(G_{cR}^{\rho\rho} e_k^\rho + B_{cR}^{\rho\rho} f_k^\rho\right) \tag{III.61}$$

$$\frac{\partial Q_k^\rho}{\partial e_{vR}^\rho} = -\left(G_{vR}^{\rho\rho} f_k^\rho - B_{vR}^{\rho\rho} e_k^\rho\right) \tag{III.62}$$

$$\frac{\partial Q_k^\rho}{\partial f_{vR}^\rho} = \left(G_{vR}^{\rho\rho} e_k^\rho + B_{vR}^{\rho\rho} f_k^\rho\right) \tag{III.63}$$

$$\frac{\partial P_m^\rho}{\partial e_k^\rho} = -\left(G_{cR}^{\rho\rho} e_m^\rho + B_{cR}^{\rho\rho} f_m^\rho\right) \tag{III.64}$$

The Jacobian terms of series converter are:

$$\frac{\partial P_{cR}^\rho}{\partial e_k^\rho} = \left(G_{cR}^{\rho\rho} e_{cR}^\rho + B_{cR}^{\rho\rho} f_{cR}^\rho\right) \tag{III.65}$$

$$\frac{\partial P_{cR}^{\rho}}{\partial f_k^{\rho}} = \left(G_{cR}^{\rho\rho} f_{cR}^{\rho} - B_{cR}^{\rho\rho} e_{cR}^{\rho}\right) \tag{III.66}$$

$$\frac{\partial P_{cR}^{\rho}}{\partial e_m^{\rho}} = -\left(G_{cR}^{\rho\rho} e_{cR}^{\rho} + B_{cR}^{\rho\rho} f_{cR}^{\rho}\right) \tag{III.67}$$

$$\frac{\partial P_{cR}^{\rho}}{\partial f_m^{\rho}} = -\left(G_{cR}^{\rho\rho} f_{cR}^{\rho} - B_{cR}^{\rho\rho} e_{cR}^{\rho}\right) \tag{III.68}$$

$$\frac{\partial P_{cR}^{\rho}}{\partial e_{cR}^{\rho}} = -2G_{cR}^{\rho\rho} e_{cR}^{\rho} + \left(G_{cR}^{\rho\rho} e_k^{\rho} - B_{cR}^{\rho\rho} f_k^{\rho}\right) - \left(G_{cR}^{\rho\rho} e_m^{\rho} - B_{cR}^{\rho\rho} f_m^{\rho}\right) \tag{III.69}$$

$$\frac{\partial P_{cR}^{\rho}}{\partial f_{cR}^{\rho}} = -2G_{cR}^{\rho\rho} f_{cR}^{\rho} + \left(G_{cR}^{\rho\rho} e_k^{\rho} - B_{cR}^{\rho\rho} f_k^{\rho}\right) - \left(G_{cR}^{\rho\rho} f_m^{\rho} - B_{cR}^{\rho\rho} e_m^{\rho}\right) \tag{III.70}$$

The Jacobian terms of shunt co inverter are:

$$\frac{\partial P_{vR}^{\rho}}{\partial e_k^{\rho}} = -\left(G_{vR}^{\rho\rho} e_{vR}^{\rho} + B_{vR}^{\rho\rho} f_{vR}^{\rho}\right) \tag{III.71}$$

$$\frac{\partial P_{vR}^{\rho}}{\partial f_k^{\rho}} = -\left(G_{vR}^{\rho\rho} f_{vR}^{\rho} - B_{vR}^{\rho\rho} e_{vR}^{\rho}\right) \tag{III.72}$$

$$\frac{\partial P_{vR}^{\rho}}{\partial e_{vR}^{\rho}} = 2G_{vR}^{\rho\rho} e_{vR}^{\rho} - \left(G_{vR}^{\rho\rho} e_k^{\rho} - B_{vR}^{\rho\rho} f_k^{\rho}\right) \tag{III.73}$$

$$\frac{\partial P_{vR}^{\rho}}{\partial f_{vR}^{\rho}} = 2G_{vR}^{\rho\rho} f_{vR}^{\rho} - \left(G_{vR}^{\rho\rho} f_k^{\rho} + B_{vR}^{\rho\rho} e_k^{\rho}\right) \tag{III.74}$$

For voltage magnitude control:

$$\frac{\partial \left(E_k^{\rho}\right)^2}{\partial e_k^{\rho}} = 2e_k^{\rho} \tag{III.75}$$

$$\frac{\partial \left(E_k^{\rho}\right)^2}{\partial f_k^{\rho}} = 2f_k^{\rho} \tag{III.76}$$

III.4 High-voltage Direct Current VSC-based

The relevant Jacobian elements are given below:

$$\frac{\partial P_k^\rho}{\partial e_k^\rho} = 2G_{vR1}^{\rho\rho} e_{vR1}^\rho - G_{vR1}^{\rho\rho} e_{vR1}^\rho + B_{vR1}^{\rho\rho} f_{vR1}^\rho \tag{III.77}$$

$$\frac{\partial P_k^\rho}{\partial f_k^\rho} = 2G_k^{\rho\rho} f_k^\rho - G_{vR1}^{\rho\rho} f_{vR1}^\rho - B_{vR}^{\rho\rho} e_{vR1}^\rho \tag{III.78}$$

$$\frac{\partial P_k^\rho}{\partial e_{vR1}^\rho} = -G_{vR1}^{\rho\rho} e_k^\rho - B_{vR1}^{\rho\rho} f_k^\rho \tag{III.79}$$

$$\frac{\partial P_k^\rho}{\partial f_{vR1}^\rho} = -G_{vR1}^{\rho\rho} f_k^\rho + B_{vR1}^{\rho\rho} e_k^\rho \tag{III.80}$$

$$\frac{\partial Q_k^\rho}{\partial e_k^\rho} = -2B_{vR1}^{\rho\rho} e_k^\rho + G_{vR1}^{\rho\rho} f_{vR1}^\rho + B_{vR1}^{\rho\rho} e_{vR1}^\rho \tag{III.81}$$

$$\frac{\partial Q_k^\rho}{\partial f_k^\rho} = -2B_{vR1}^{\rho\rho} f_k^\rho - G_{vR1}^{\rho\rho} e_{vR1}^\rho + B_{vR1}^{\rho\rho} f_{vR1}^\rho \tag{III.82}$$

$$\frac{\partial Q_k^\rho}{\partial e_{vR1}^\rho} = -G_{vR}^{\rho\rho} f_k^\rho + B_{vR}^{\rho\rho} e_k^\rho \tag{III.83}$$

$$\frac{\partial Q_k^\rho}{\partial f_{vR1}^\rho} = G_{vR1}^{\rho\rho} e_k^\rho + B_{vR1}^{\rho\rho} f_k^\rho \tag{III.84}$$

$$\frac{\partial P_{vR1}^\rho}{\partial e_k^\rho} = -G_{vR1}^{\rho\rho} e_{vR1}^\rho - B_{vR1}^{\rho\rho} f_{vR1}^\rho \tag{III.85}$$

$$\frac{\partial P_{vR1}^\rho}{\partial f_k^\rho} = -G_{vR1}^{\rho\rho} f_{vR1}^\rho + B_{vR1}^{\rho\rho} e_{vR1}^\rho \tag{III.86}$$

$$\frac{\partial P_{vR1}^\rho}{\partial e_{vR1}^\rho} = 2G_{vR1}^{\rho\rho} e_{vR1}^\rho - G_{vR1}^{\rho\rho} e_k^\rho + B_{vR1}^{\rho\rho} f_k^\rho \tag{III.87}$$

$$\frac{\partial P_{vR1}^\rho}{\partial f_{vR1}^\rho} = 2G_{vR1}^{\rho\rho} f_{vR1}^\rho - G_{vR1}^{\rho\rho} f_k^\rho - B_{vR1}^{\rho\rho} e_k^\rho \tag{III.88}$$

$$\frac{\partial Q_{vR1}^\rho}{\partial e_k^\rho} = -G_{vR1}^{\rho\rho} f_{vR1}^\rho + B_{vR1}^{\rho\rho} e_{vR1}^\rho \tag{III.89}$$

$$\frac{\partial Q_{vR1}^\rho}{\partial f_k^\rho} = G_{vR1}^{\rho\rho} e_{vR1}^\rho + B_{vR1}^{\rho\rho} f_{vR1}^\rho \tag{III.90}$$

$$\frac{\partial Q_{vR1}^\rho}{\partial e_{vR1}^\rho} = -2B_{vR1}^{\rho\rho} e_{vR1}^\rho + G_{vR1}^{\rho\rho} f_k^\rho + B_{vR1}^{\rho\rho} e_k^\rho \tag{III.91}$$

$$\frac{\partial Q_{vR1}^\rho}{\partial f_{vR1}^\rho} = -2B_{vR1}^{\rho\rho} f_{vR1}^\rho - G_{vR1}^{\rho\rho} e_k^\rho + B_{vR1}^{\rho\rho} f_k^\rho \tag{III.92}$$

$$\frac{\partial P_{\mathrm{HVDC}}^\rho}{\partial e_k^\rho} = 2G_{vR1}^{\rho\rho} e_{vR1}^\rho - G_{vR1}^{\rho\rho} e_{vR1}^\rho + B_{vR1}^{\rho\rho} f_{vR1}^\rho \tag{III.93}$$

$$\frac{\partial P^{\rho}_{\mathrm{HVDC}}}{\partial f^{\rho}_{k}} = 2G^{\rho\rho}_{vR1} f^{\rho}_{vR1} - G^{\rho\rho}_{vR1} f^{\rho}_{vR1} - B^{\rho\rho}_{vR1} e^{\rho}_{vR1} \tag{III.94}$$

$$\frac{\partial P^{\rho}_{\mathrm{HVDC}}}{\partial e^{\rho}_{vR1}} = -G^{\rho\rho}_{vR1} e^{\rho}_{k} - B^{\rho\rho}_{vR1} f^{\rho}_{k} \tag{III.95}$$

$$\frac{\partial P^{\rho}_{\mathrm{HVDC}}}{\partial f^{\rho}_{vR1}} = -G^{\rho\rho}_{vR1} f^{\rho}_{k} + B^{\rho\rho}_{vR1} e^{\rho}_{k} \tag{III.96}$$

$$\frac{\partial P^{\rho}_{\mathrm{HVDC}}}{\partial e^{\rho}_{vR2}} = -G^{\rho\rho}_{vR2} e^{\rho}_{m} - B^{\rho\rho}_{vR2} f^{\rho}_{m} \tag{III.97}$$

APPENDIX IV: IMPLICIT TRAPEZOIDAL INTEGRATION METHOD WITH NEWTOM ITERATION

IV.1 Implicit Trapezoidal Integration Method with Newton Iteration

An implicit trapezoidal integration method has been used in the three-phase dynamic power flow algorithm for large-scale power system with VSC-based FACTS controllers in the present research. The basic trapezoidal method is very well known, having been established as a useful method of integration before digital computers made hand calculation redundant. This method has gain recognition as being very powerful, having great advantages over other numerical methods.

The implicit trapezoidal method is based on the algebratization of a function with the assumption that the function is linear during and integration time step. The trapezoidal method is derived from a single-step method, where the solution of a set of differential equations is rewritten in the algebraic form of,

$$w_{j+1} = w_j + \frac{h}{2}\left[f\left(t_{j+1}, w_j\right) + f\left(t_j, w_j\right)\right], \qquad 0 \le j \le N-1, \tag{IV.1}$$

Having computed t_j, t_{j+1}, and w_j, we need to determine $w = w_{j+1}$, the solution to

$$F(w) = w - w_j + \frac{h}{2}\left[f\left(t_{j+1}, w_j\right) + f\left(t_j, w_j\right)\right] = 0 \tag{IV.2}$$

To approximate this solution, select $w_{j+1}^{(0)}$, usually as w_j, and generated $w_{j+1}^{(k)}$ by applying Newton-Raphson to (IV.2),

$$\begin{aligned} w_{j+1}^{(k)} &= w_{j+1}^{(k-1)} - \frac{F\left(w_{j+1}^{(k-1)}\right)}{F'\left(w_{j+1}^{(k-1)}\right)} = \\ &= w_{j+1}^{(k-1)} - \frac{w_{j+1}^{(k-1)} - w_j - \frac{h}{2}\left[f\left(t_j, w_j\right) + f\left(t_{j+1}, w_{j+1}^{(k-1)}\right)\right]}{1 - \frac{h}{2} f_y\left(t_{j+1}, w_{j+1}^{(k-1)}\right)} \end{aligned} \tag{IV.3}$$

Until $\left|w_{j+1}^{(k)} - w_{j+1}^{(k-1)}\right|$ is within a prescribe small tolerance (i.e. $1e^{-12}$); normally only four or five iterations per step are required.